Universidad de Buenos Aires

Facultad de Ciencias Exactas y Naturales

Departamento de Ciencias de la Atmósfera y los Oceános

Modelado climático en Sudamérica:

el valor agregado por los Modelos Climáticos

Regionales

Tesis presentada para optar al Título de Doctora de la Universidad de Buenos Aires en el Área
Ciencias de la Atmósfera y los Oceános

Lic. Magdalena Falco

Directores: Dra. Andrea F. Carril

　　　　　Dr. Laurent Li

Consejero de estudios: Dr. Claudio G. Menéndez

Lugar de trabajo: Centro de Investigaciones del Mar y la Atmósfera. CONICET-UBA

Fecha de defensa: 2019

Modelado climático en Sudamérica: el valor agregado por los Modelos Climáticos Regionales

Resumen

Este trabajo de tesis tiene como objetivo estudiar el valor agregado (VA) por los Modelos Climáticos Regionales (MCR) en simular el clima de Sudamérica. El VA se define como una medida de que tan hábil es el MCR en reproducir el clima observado en comparación al Modelo Climático Global (MCG) del que se obtuvieron las condiciones de borde. La tesis va más allá de la típica comparación entre el MCR y el MCG, ya que explora varios aspectos del VA recientemente propuestos en la literatura. También proponemos un enfoque innovador para comprender el papel del clima regional en Suadmérica en el modelado de la circulación extratropical. Por lo tanto, abordamos la cuestión del VA de los MCRs a través de diferentes perspectivas: primero a través de enfoques estadísticos, y luego a través de experimentos de sensibilidad que incluyen un estudio de resolución incrementada en un MCR y un experimento de anidamiento bidireccional.

La tesis muestra que los MCRs agregan valor con respecto a su forzante global de menor resolución, pero solo en algunos aspectos del clima. El valor agregado se encuentra principalmente asociado a la temperatura superficial del aire, ya que esta variable tiene una marcada componente estacionaria a escala regional en zonas de terreno complejo, como la cordillera de los Andes y las tierras altas de Brasil, y en las costas del continente.

Los resultados son más complejos al estudiar la precipitación. La respuesta a si el MCR agrega valor o no a la climatología de su forzante depende de varios factores, entre ellos el MCR utilizado y su configuración física, el MCG, la estación del año, la localidad, la métrica utilizada, entre otros. Sin embargo, los resultados sugieren que el aumento en la resolución tiene el potencial de mejorar la precipitación asociada a la fase activa del Monzón Sudamericano en los trópicos, producto de un incremento en la convergencia de humedad en niveles bajos y a un aumento en la frecuencia de ocurrencia de eventos de precipitación intensa. Por otro lado, no encontramos mejoras del MCR con respecto a su forzante global durante el invierno, probablemente debido a que las precipitaciones en esta estación del año están asociadas al pasaje de frentes de escala sinóptica.

La interacción bidireccional entre un MCR y un MCG resultó en una mejora en la circulación a niveles bajos del MCG dentro de SA e indujo efectivamente una mejora en la circulación extratropical del hemisferio sur. Las mejoras en el continente se identificaron en el transporte de energía asociado a la corriente en chorro en niveles bajos o "low-level jet" entre los trópicos y los extratrópicos. Esta mejora local efectivamente forzó la circulación de gran escala, especialmente durante el verano, reduciendo el desvío que presentaba el MCG en simular la ubicación de la corriente en chorro en la tropósfera superior. Por lo tanto, los datos climáticos de alta resolución sobre SA tienen el potencial de agregar valor no sólo localmente en el continente sino también de efectivamente favorecer la circulación extratropical.

Palabras claves: modelos climáticos globales, valor agregado, modelos climáticos regionales, Sudamérica, CORDEX, anidado unidireccional, anidado bidireccional.

Climate modeling in South America: the value added by Regional Climate Models

Abstract

This thesis work aims to study the value added by Regional Climate Models (RCMs) in simulating the climate of South America. The added value (AV) is defined as a measure of how skillful is the RCM in reproducing the observed climate compared to the Global Climate Model (GCM) from which the boundary conditions were obtained. The thesis goes beyond the typical comparison between the RCM and the GCM since it explores several aspects of AV recently proposed in the literature. We also propose an innovative approach to understand the role of the regional climate in South America in the modeling of the extratropical circulation. Therefore, we address the AV issue through different perspectives: first through statistical approaches, and then through sensitivity experiments that include an increased resolution study in an RCM and a two-way nesting experiment.

The thesis shows that RCMs add value regarding its lower resolution global forcing, but only in some aspects of climate. The added value is mainly associated with surface air temperature, since this variable has a marked stationary component at a regional scale in complex terrain areas, as the Andes mountain range and the Brazilian highlands, and also in the coasts.

The results are more complex when studying precipitation. The response to whether the RCM adds value or not to the GCM climatology depends on several factors, including the RCM and its physical configuration, the GCM, the season, the location, the metric used, among others. However, results suggest that the increase in resolution has the potential to improve local precipitation associated with the active phase of the South American Monsoon System in the tropics, as a result of an increase in moisture convergence at low levels and an increase in the frequency of occurrence of intense precipitation events. On the other hand, we did not find improvements of the RCM compared to its global forcing during winter, probably because rainfall in this season is associated with synoptic-scale frontal passages.

The two-way interaction between an RCM and a GCM resulted in an improvement in the circulation at low levels of the GCM within SA and effectively enhanced the extratropical cir-

culation of the southern hemisphere. The improvements in the continent were identified in the transport of energy associated with the low-level jet stream (LLJ) between the tropics and extratropics. This local improvement effectively forced large-scale circulation, especially during the summer, reducing the bias of the GCM in simulating the location of the eddy-driven jet stream in the upper troposphere. Therefore, high-resolution climate data on SA have the potential to add value not only locally in the continent but also to effectively enhance the extratropical circulation.

Agradecimientos

A mi maestra y directora, Andrea, por la dedicación y apoyo que le brindó a este trabajo, y por el respeto a mis sugerencias e ideas. Gracias por confiar en mí.

A mi director y a mi consejero, Laurent y Claudio, porque compartieron sus experiencias y conocimientos con mucha humildad, y porque cada vez que lo necesité me aconsejaron de forma amable y sincera.

A Rosmeri, Carlos Cabrelli, Ale Di Luca y Jan Polcher, que me dieron una mano cuando lo necesité y fueron de gran ayuda en esta tesis.

Al CONICET, que a través de su beca de Posgrado financió mis estudios. Al CIMA, el instituto que me ofreció un lugar de trabajo y que me brindó todo lo necesario para trabajar cómoda. A la UMI, por su gran apoyo en nuestra colaboración con Francia. Al DCAO y a la UBA, que me dió la oportunidad de llevar a cabo este doctorado. A LMD, por haberme recibido tantas veces con los brazos abiertos.

A mis amigos de la facu y compañeros de oficina que tuve a lo largo de estos años, de los que pude aprender muchas cosas y me alegraron los días.

A mi familia: Jorge, Fede y Pipi por haberme apoyado y por estar siempre presentes.

A Edu, mi coach, por sus tips en productividad.

A los jurados de esta tesis, que aceptaron la difícil tarea de leerla y evaluarla.

A todos, muchas gracias.

Contents

Chapter 1

Introduction (English)

1.1 Background

Global Climate Models (GCMs) emerged from the scientific need to understand the functioning of the Earth's climate system, being currently the primary tool for understanding and studying future climate changes. However, the low-resolution climate information provided by these models does not cover the demands of end users, such as impact modelers and decision makers, who require reliable regional and local climate information (Maraun et al., 2010). To solve the problem of spatial scale, the community of climate modeling developed statistical and dynamical techniques of scale reduction or downscaling that complement the GCMs. Among the methods of dynamic downscaling are those based on tools such as high-resolution GCMs, variable-resolution GCMs, and Regional Climate Models (RCMs).

RCMs are limited area models combined with a description of the lateral boundaries and are currently the most widely used dynamic downscaling tool. Their initial and lateral boundary conditions (LBC) are provided by GCMs or global reanalysis to ensure global consistency. The fundamental hypothesis of this technique, called "one-way nesting," is that while the GCM provides large-scale information to the RCM through the LBC, the RCM can reproduce sub-scale information within the limited domain (Laprise, 2008). As a result, RCMs generate physically-consistent regional to local climate information in scales that cannot be represented in the coarser-resolution driver (Giorgi and Gutowski, 2015). Some researchers give a twist by adding a "two-way nesting" coupling, where the RCM also forces the GCM within its domain. The hypothesis behind this approach is that the effects of enhanced small-scale from the RCM propagate to larger scales and this, in turn, improves the simulation of the large-scale

phenomena of the GCM.

Although the climate modeling community widely uses RCMs, there are a large number of research papers that question the capability and usability of these models (Dimitrijevic and Laprise, 2005, Hong and Kanamitsu, 2014, Laprise, 2008, Pielke and Wilby, 2012). This distrust is partly due to several inconsistencies between the RCM and its driver, together with issues regarding resolution inadequacies in the physics of the model. Some voices argue that the wide diffusion of this approach does not obey the goodness of the method but to its viability. The definition of a limited geographical area rather than the whole globe allows increasing the resolution without prohibitively increasing the computational cost of the experiments, but it does not necessarily improve the representation of climate. It is known that the GCM forcing has a first-order effect on the RCM, and thus, it remains that the limiting factor in the skill of the RCM is the quality of the lateral boundary forcing provided by the global model (Rojas and Seth, 2003, Seth and Rojas, 2003). In that sense, it is not expected that the RCM reduces the bias of the climatic signal introduced by the global model through the LBC; as this bias could even be amplified (Hong and Kanamitsu, 2014).

Therefore, one of the key debates associated with RCMs is whether they improve in the representation of climate when compared to their driving GCMs. In this context, added value (AV) is defined as a measure of the extent to which the downscaled climate is closer to the observation that the model from which the boundary conditions are obtained (IPCC, 2013). As explained by Rummukainen (2016), the 'added' word typically refers to information that is not directly present nor easily retrievable from the GCM, and the 'value' word signifies that the additional information is credible or has utility. There is no single best way to study the AV of RCMs (see Di Luca et al., 2015), and the approaches usually used are three: (a) through scale-aware AV metrics, (b) through experiments based on decomposition techniques of spatial scales, and (c) through sensitivity experiments. The first approach consists of new scale-aware AV metrics, proposed by several authors inspired by the problem of comparing data sets with very different resolution (Kanamitsu and DeHaan, 2011, Parker et al., 2015, Wang et al., 2015). The second approach focus on the fine-scale details present in the RCM but absent in its driver, and thus, propose different scale decomposition techniques to quantify the AV associated with high-resolution phenomena (Bettge and Baumhefner, 1980, Denis et al., 2002a, Di Luca et al., 2012, Errico, 1985, Feser and von Storch, 2005). These two approaches, i.e. (a) and (b), are many times combined (Parker et al., 2015, Di Luca et al., 2016). The third technique consists of performing sensitivity experiments to assess the AV issue ex-

plicitly. These experiments evaluate the role of surface forcing representation in climate simulation (Gao et al., 2006, De Sales and Xue, 2011) or the impact of increased resolution in the representation of climate (Curry et al., 2016, Gao et al., 2006, Karmacharya et al., 2016, among others).

The growing interest of the Regional Climate Model Community on assessing the AV of RCMs is accompanied by an important production of scientific articles focused on this issue in different parts of the world. The main conclusion drawn from the literature is that there is no clear result concerning the improvement/downgrading representation of the climate system when using RCMs. It depends on many factors, such as the study domain, the model evaluated, the reference used, the variable analyzed, the temporal scale, the specific application, the experiment configuration, along with others (Torma et al., 2015, Giorgi and Gutowski, 2015, Di Luca et al., 2015). Nevertheless, a general consensus is that AV signal is expected for mesoscale atmosphere phenomena (Feser et al., 2011, Di Luca et al., 2012, Karmacharya et al., 2016, Lucas-Picher et al., 2016), over regions with complex surface forcing (Gao et al., 2006, De Haan et al., 2014, Di Luca et al., 2012, Prömmel et al., 2010, Feser and von Storch, 2005, Lenz et al., 2017), and also for extreme events (Coppola et al., 2014, Giorgi, 2002, Di Luca et al., 2012, Rummukainen, 2016, Prein et al., 2016). Regarding "two-way nesting" technique the results are encouraging: not only does the RCM add value to the Global Model simulation, but also RCM/GCM simulations in a "two-way nesting" system improves when compared to the ones using a "one-way nesting" system (Chen et al., 2010, Inatsu and Kimoto, 2009, Inatsu et al., 2012, Lorenz and Jacob, 2005).

Therefore, if we make a review of the scientific works published in recent years, we fairly conclude that there is a high level of confidence that RCMs add value to their global forcing in simulating the present climate (IPCC, 2013), but this is true only in some aspects of climate. It is not easy to identify the main factors to which the AV signal is attributed, and applying the various and complementary approaches described before is necessary to fully understand how, when and where RCMs have the potential to improve the simulation of climate when compared to a lower-resolution global simulation.

1.2 Motivation and objectives

South America is a vast continent, with significant physiographic features of the land such as the Andes mountain range and the Brazilian Highlands. The South American climate is domi-

nated by the effects of its complex topography, and by regional processes such as mesoscale circulations that develop important convective systems (Velasco and Fritsch, 1987), the low-level jet (Vernekar et al., 2003), the Chaco Low (Seluchi and Marengo, 2000a), the surface-atmosphere interactions (Sörensson et al., 2010, Sörensson and Menéndez, 2011), among others. Thus, it is very challenging for GCMs and RCMs to replicate the multitude of physical processes and the complexity of their feedbacks, which span multiple temporal and spatial scales, over such a large and heterogeneous continent.

While GCMs are generally capable of reproducing the main large-scale circulation characteristics, their performance deteriorates when evaluating regional aspects of climate (Barros and Doyle, 2018, Gulizia et al., 2013, Rusticucci et al., 2010, Silvestri and Vera, 2008, Zazulie et al., 2017). The need to have high-resolution simulations is imperative to adequately represent regional processes that modulate the South American Monsoon System in the tropics and subtropics, and cyclone activities over mid-latitudes (Garreaud et al., 2009). However, the limitation in computational resources restricts the spatial scale of global simulations from GCMs or Reanalysis. The RCMs have a higher spatial resolution than that of the GCMs, which implies a clear advantage when reproducing regional climatic phenomena, and they are presented as the most viable option to address the problem of scale reduction over SA.

Previous works have assessed regional climate simulations over SA within the context of CLARIS Project (Menéndez et al., 2010), CLARIS-LPB Project (Carril et al., 2012, 2016, López-Franca et al., 2016, Sánchez et al., 2015, Solman et al., 2013, Solman, 2016, Zaninelli et al., 2015, 2018, Sanabria and Carril, 2018, Menéndez et al., 2016), and the CREMA Project (Coppola et al., 2014, da Rocha et al., 2009, 2014, Fernandez et al., 2006, Giorgi et al., 2014, Llopart et al., 2014, Reboita et al., 2014b, 2018a, Seth et al., 2007), indicating an overall good performance of RCMs in reproducing different aspects of the observed climate. However, none of these works focus entirely on the AV issue, and only a few of them (da Rocha et al., 2009, 2014, Llopart et al., 2014, Sánchez et al., 2015, Solman, 2016) only performs a general comparison of surface variables between the RCM and its forcing. Hence, until now, we have limited knowledge about how RCMs can add value over the continent, and it is largely based on seasonal validation. The availability of new and complementary methodologies enables us to revisit the AV issue in SA. Therefore, there is an urgent need for further AV studies over SA using state-of-the-art climate model simulations to understand the real value added by RCMs.

The thesis aims to study the AV of high-resolution climate data, usually obtained from RCM simulations, compared to lower-resolution data over South America. The thesis goes beyond

the frequently RCM/GCM comparison by exploring several aspects of AV recently proposed in the literature. We also propose an innovative approach to understand the role of regional climate in the modeling of the general circulation. Hence, we address the AV issue through different perspectives: first through statistical approaches, and then through sensitivity experiments that include an RCM resolution study and a two-way nesting experiment. Specific objectives include:

— To evaluate the capacity of CORDEX simulations in comparison with its global forcing to simulate the mean seasonal precipitation and the surface air temperature over SA.

— To propose a scale-aware methodology to study the error sources of model and observations to analyze the relative importance of each source.

— To identify those regions in the continent where RCMs have the potential to add value concerning their global forcing. These regions must have mesoscale characteristics in the climatological or extreme values of surface variables.

— To study the role of resolution in the simulation of the most relevant processes associated with the South American Monsoon System.

— To explore the effect of regional information in the simulation of the Southern Hemisphere extratropical circulation.

Introducción (Español)

1.3   Antecedentes

Los Modelos Climáticos Globales (MCGs) surgieron de la necesidad científica de comprender el funcionamiento del sistema climático terrestre, siendo actualmente la herramienta principal para comprender y estudiar los cambios climáticos futuros. Sin embargo, la información climática de baja resolución proporcionada por estos modelos no cubre las demandas de los usuarios finales, como los modeladores de impacto y los encargados de tomar decisiones, que requieren información climática regional y local confiable (Maraun et al., 2010). Para resolver el problema de la escala espacial, la comunidad de modelado climático desarrolló técnicas estadísticas y dinámicas de reducción de escala que complementan a los MCGs. Entre los métodos de reducción de escala dinámica se encuentran aquellos basados en MCGs de alta resolución, MCGs de resolución variable y modelos climáticos regionales (MCRs).

Los MCRs son modelos de área limitada que incluyen una descripción de los límites laterales y actualmente son la herramienta de reducción de escala dinámica más utilizada. Sus condiciones de borde iniciales y laterales son proporcionadas por MCGs o reanálisis global con el fin de asegurar una coherencia global. La hipótesis fundamental de esta técnica, llamada "anidamiento unidireccional", es que mientras que el MCG proporciona a través de la información de borde la información de gran escala, el MCR puede reproducir dentro de su dominio información de escala regional que se encuentra ausente en el forzante global (Laprise, 2008). Como resultado, el MCR provee información información climática físicamente consistentes en escalas que no pueden ser representadas por su forzante de baja resolución (Giorgi and Gutowski, 2015). Complementario a esta metodología, algunos investigadores han propuesto una alternativa que consiste en una "anidación bidireccional", donde el MCR también conduce al MCG dentro de su dominio. Esta hipótesis propone que los efectos de la mejora en la representación de los fenómenos de pequeña escala se propaga a las grandes escalas y

esto mejora, por lo tanto, la simulación de los fenómenos de gran escala reproducidos por el MCG.

A pesar de que los MCRs son ampliamente utilizados por la comunidad del modelado climático, hay algunos trabajos de investigación que cuestionan la capacidad y utilidad de estos modelos (Dimitrijevic and Laprise, 2005, Hong and Kanamitsu, 2014, Laprise, 2008, Pielke and Wilby, 2012). Esta falta de confianza se debe en parte a varias inconsistencias entre el MCR y su forzante global, junto con problemas relacionados con la incompatibilidad de la resolución y la física del modelo. Algunas voces argumentan que la amplia difusión de esta técnica no obedece a la bondad del método, sino a su viabilidad. La definición de un área geográfica limitada en lugar de todo el globo permite aumentar la resolución sin aumentar prohibitivamente el costo computacional de los experimentos, pero no necesariamente mejora la representación del clima. Se sabe que el MCG tiene un efecto de primer orden en el MCR y, por lo tanto, la calidad de la condición de borde lateral proporcionada por el MCG sigue siendo un factor limitante en la habilidad del MCR (Rojas and Seth, 2003, Seth and Rojas, 2003). En ese sentido, no es de esperar que el MCR pueda corregir el sesgo de la señal climática introducida por el modelo global a través de las condiciones de borde lateral; ya que este sesgo podría inclusive ser amplificado (Hong and Kanamitsu, 2014).

Por lo tanto, una de las cuestiones clave asociadas a los MCRs es si actualmente mejoran la representación del clima en comparación con su forzante global. En este contexto, el valor agregado (VA) de los MCRs se define como una medida de que tan hábil es el MCR en reproducir el clima observado en comparación al modelo del que se obtuvieron las condiciones de borde (IPCC, 2013). Como lo explica Rummukainen (2016), la palabra "agregado" generalmente se refiere a la información que no está directamente presente ni es fácilmente recuperable del MCG, y la palabra "valor" significa que la información adicional es creíble o tiene utilidad. No existe una única manera de estudiar el VA de los MCRs (consulte Di Luca et al., 2015), y los enfoques que se utilizan habitualmente son tres: (a) a través de métricas de VA que reconocen la escala del modelo, (b) a través de experimentos basados en técnicas de descomposición de escalas, y (c) mediante experimentos de sensibilidad. El primer enfoque consiste en nuevas métricas de VA que considera la escala, propuestas por varios autores inspirados en el problema de comparar conjuntos de datos de resolución muy diferente (Kanamitsu and DeHaan, 2011, Parker et al., 2015, Wang et al., 2015). El segundo enfoque se centra en los detalles de pequeña escala presentes en el MCR pero ausentes en su forzante, y por lo tanto, proponen diferentes técnicas de descomposición de escala para cuantificar el VA aso-

ciado con fenómenos de alta resolución (Bettge and Baumhefner, 1980, Denis et al., 2002a, Di Luca et al., 2012, Errico, 1985, Feser and von Storch, 2005) . Estos dos enfoques, es decir, (a) y (b), muchas veces son combinados (Parker et al., 2015, Di Luca et al., 2016). La tercera técnica consiste en realizar experimentos de sensibilidad para evaluar explícitamente algunas cuestiones relacionadas al VA. Estos experimentos evalúan el rol que cumple la representación de la superficie en la simulación del clima (Gao et al., 2006, De Sales and Xue, 2011) o el impacto de una mayor resolución en el modelo en la representación del clima (Curry et al., 2016, Gao et al., 2006, Karmacharya et al., 2016, entre otros).

El creciente interés de la Comunidad del Modelado Climático Regional en la evaluación del VA de los MCRs está acompañado por una importante producción de artículos científicos en diferentes partes del mundo centrados en este tema. La principal conclusión que se extrae de la literatura es que no hay un resultado claro con respecto a la mejora/degradación de la representación del sistema climático cuando se usa un MCR. Depende de muchos factores, como el dominio de estudio, el modelo evaluado, la condición de borde, la variable analizada, la escala temporal, la aplicación específica, la configuración del experimento, junto con otros (Torma et al., 2015, Giorgi and Gutowski, 2015, Di Luca et al., 2015). Sin embargo, hay un consenso general de que se espera una señal de VA para fenómenos atmosféricos de mesoescala (Feser et al., 2011, Di Luca et al., 2012, Karmacharya et al., 2016, Lucas-Picher et al., 2016), sobre regiones de topografía compleja (Gao et al., 2006, De Haan et al., 2014, Di Luca et al., 2012, Prömmel et al., 2010, Feser and von Storch, 2005, Lenz et al., 2017), y también para eventos extremos (Coppola et al., 2014, Giorgi, 2002, Di Luca et al., 2012, Rummukainen, 2016, Prein et al., 2016). En cuanto a la técnica de "anidación bidireccional", los resultados son alentadores: el MCR no solo agrega valor a la simulación del Modelo Global, sino que las simulaciones de MCR/MCG en un sistema de interacción bidireccional mejoran en comparación con las que usan un sistema de interacción unidireccional (Chen et al., 2010, Inatsu and Kimoto, 2009, Inatsu et al., 2012, Lorenz and Jacob, 2005).

Por lo tanto, si hacemos una revisión de los trabajos científicos publicados en los últimos años, llegamos a la conclusión de que existe un alto nivel de confianza en que los MCRs agregan valor respecto a su forzante global para simular el clima actual (IPCC, 2013), pero esto es cierto solo en algunos aspectos del clima. No es fácil identificar los principales factores a los que se atribuye la señal de VA, y es necesario aplicar los diferentes enfoques descriptos anteriormente para realmente comprender cómo, cuándo y dónde los MCRs tienen el potencial de mejorar la simulación del clima en comparación a una simulación global de baja resolución.

1.4 Motivación y objetivos

América del Sur es un vasto continente, con importantes características fisiográficas de la tierra, como la cordillera de los Andes y las tierras altas de Brasil. El clima de América del Sur está dominado por los efectos de su topografía compleja y por procesos regionales como las circulaciones de mesoescala que desarrollan importantes sistemas convectivos (Velasco and Fritsch, 1987), la corriente en chorro en niveles bajos (Vernekar et al., 2003), la baja del Chaco (Seluchi and Marengo, 2000a), las interacciones superficie-atmósfera (Sörensson et al., 2010, Sörensson and Menéndez, 2011), entre otros. Por lo tanto, es muy difícil para los MCGs y los MCRs replicar la multitud de procesos físicos y la complejidad de sus interacciones, que abarcan múltiples escalas temporales y espaciales, en un continente tan grande y heterogéneo.

Si bien los MCGs generalmente son capaces de reproducir las principales características de circulación a gran escala, su desempeño se deteriora cuando se evalúan aspectos regionales del clima (Barros and Doyle, 2018, Gulizia et al., 2013, Rusticucci et al., 2010, Silvestri and Vera, 2008, Zazulie et al., 2017). La necesidad de tener simulaciones de alta resolución es imperativa para representar adecuadamente los procesos regionales que modulan el Sistema Monzónico Sudamericano en los trópicos y subtrópicos, y la actividad ciclónica en latitudes medias (Garreaud et al., 2009). Sin embargo, la limitación en recursos computacionales restringe la escala espacial de simulaciones globales de MCGs o Reanalysis. Los MCR tienen una resolución espacial más alta que la de los MCGs, lo que implica una clara ventaja cuando se reproducen fenómenos climáticos regionales, y se presentan como la opción más viable para abordar el problema de la reducción de escala sobre SA.

Trabajos anteriores han evaluado las simulaciones de clima sobre SA en el contexto de los Proyectos CLARIS (Menéndez et al., 2010), CLARIS-LPB (Carril et al., 2012, 2016, López-Franca et al., 2016, Sánchez et al., 2015, Solman et al., 2013, Solman, 2016, Zaninelli et al., 2015, 2018, Sanabria and Carril, 2018, Menéndez et al., 2016), y CREMA (Coppola et al., 2014, da Rocha et al., 2009, 2014, Fernandez et al., 2006, Giorgi et al., 2014, Llopart et al., 2014, Reboita et al., 2014b, 2018a, Seth et al., 2007), indicando un buen comportamiento general de los MCRs en reproducir diferentes aspectos del clima observado. Sin embargo, ninguno de estos trabajos se enfoca completamente en estudiar el VA de estos modelos, y solo unos pocos de ellos (da Rocha et al., 2009, 2014, Llopart et al., 2014, Sánchez et al., 2015, Solman, 2016) realiza una comparación general de las variables en superficie entre el MCR y su forzante. Por lo tanto, hasta ahora, tenemos un conocimiento limitado sobre cómo los MCRs pueden agregar valor

en SA y se basan en gran medida en una validación estacional. Como resultado, existe una necesidad urgente de realizar estudios complementarios de VA sobre SA para comprender el valor real agregado por estas simulaciones climáticas de alta resolución.

El objetivo de la tesis es estudiar el VA de los MCRs en comparación con su forzante global en Sudamérica. La tesis va más allá de la típica comparación MCR/MCG, ya que explora varios aspectos del VA recientemente propuestos en la literatura. También proponemos un enfoque innovador para comprender el papel del clima regional en el modelado de la circulación general. Por lo tanto, abordamos el problema del VA a través de diferentes perspectivas: primero a través de enfoques estadísticos, y luego a través de experimentos de sensibilidad que incluyen un estudio de resolución en un MCR y un experimento de anidamiento bidireccional. Los objetivos específicos incluyen:

— Evaluar la capacidad de las simulaciones de CORDEX en comparación con su forzante global para simular la precipitación media estacional y la temperatura del aire en la superficie sobre SA.

— Proponer una metodología de reconocimiento de escala para estudiar las fuentes de error del modelo y las observaciones con el fin de analizar la importancia relativa de cada fuente.

— Identificar aquellas regiones en el continente donde los MCRs tienen el portencial de agregar valor con respecto a su forzante global. Estas regiones deben presentar características de mesoescala en los valores climatológicos o extremos de variables superficiales.

— Estudiar el papel de la resolución en la simulación de los procesos más relevantes asociados al Monzón Sudamericano.

— Explorar el efecto de información climática regional en la simulación de la circulación extratropical del hemisferio sur.

Chapter 2

Assessment of CORDEX simulations over South America: added value on seasonal climatology and resolution considerations

Resumen del capítulo

En este capítulo se evalúa un nuevo conjunto de simulaciones del Proyecto CORDEX en Sudamérica junto con su forzante global para investigar el valor agregado de los Modelos Climáticos Regionales (MCRs) en la representación de las condiciones climáticas medias en el continente. Se analizan simulaciones que presentan dos tipos diferentes de condición de borde lateral: cinco simulaciones de evaluación forzadas por el reanálisis ERA-Interim, y otras cinco simulaciones históricas forzadas por Modelos Climáticos Globales (MCGs). Las medias del conjunto de simulaciones, denominada ensembles, y las simulaciones individuales se evalúan comparándolas con dos o tres bases observacionales reticuladas de la temperatura del aire a 2 metros de la superficie y la precipitación total. El análisis se realiza para las estaciones de verano e invierno, durante un período común de 1990 a 2004. Los resultados indican que el valor agregado de los MCRs depende de diversos factores tales como la condición de borde, las propiedades de la superficie del área, la estación del año y la variable considerada. En el trabajo se encontró que los MCRs presentan un VA cuando se los compara con ERA-Interim en la simulación de la climatología de temperatura del aire en verano en latitudes tropicales

y subtropicales. Sin embargo, se encontraron resultados mixtos cuando se evalúa la climatología de la precipitación estival tanto en experimentos de evaluación como en los históricos. Para el invierno, no hay una mejora notable por parte de los MCRs en simular los campos climatológicos de precipitación y temperatura. Para comprender mejor el valor agregado de los MCRs, es necesario distinguir los diferentes términos que contribuyen a las desviaciones de aquellos datos provenientes de simulaciones climáticas con respecto a los datos provenientes de bases observadas. Se identificaron cuatro términos a considerar durante el proceso de evaluación: la incertidumbre de la observación, el error de representatividad, el error de interpolación y el error propio del modelo. En este capítulo proponemos una estimación de cada una de estas fuentes de error e identificamos algunas regiones dentro del continente en donde estos errores no son despreciables, tales como zonas con terreno complejo. Por lo tanto, concluímos que para comprender mejor el valor agregado real de los MCRs es necesaria una validación usando métricas complementarias que consideren la escala espacial de la simulación, los errores de remapeado y la incertidumbre en la observación.

Abstract

In this chapter, a new set of CORDEX simulations, together with their coarser-resolution driving Global Climate Models (GCMs), are used to investigate added value of Regional Climate Models (RCMs) in reproducing mean climate conditions over South America. Two types of simulations with different lateral boundary conditions are considered: five hindcast simulations use reanalysis as boundary conditions, and five other historical simulations use GCMs outputs. Multi-model ensemble means and individual simulations are evaluated against two or three observation-based gridded datasets for 2-meter temperature and total precipitation. The analysis is performed for summer and winter, over a common period from 1990 to 2004. Results indicate that added value of RCMs is dependent on driving fields, surface properties of the area, season and variable considered. A robust added value for RCMs driven by ERA-Interim is obtained in reproducing the summer climatology of surface air temperature over tropical and subtropical latitudes. Mixed results can be seen, however, for summer precipitation climatology in both hindcast and historical experiments. For winter, there is no noticeable improvement by the RCMs for the large-scale precipitation and surface air temperature climatology. To further understand the added value of RCMs, models deviations from observation are decomposed according to different terms that reflect the observational un-

certainty, the representativeness error, the interpolation error, and the actual performance of the model. Regions where these errors are not negligible, such as in complex terrain regions, among others, can be identified. There is a clear need for complementary assessment to understand better the real value added by RCMs.

2.1 Introduction

The limited computational resources currently available in local research institutions over South America (SA) makes RCMs the most viable tool for the production of high-resolution climate simulations. This has prompted the need to establishing common experimental frameworks in order to produce an ensemble of different RCM simulations, and understand regional climate modeling strengths and weaknesses. The first project that managed to create an ensemble of RCM simulations was the one from Roads et al. (2003), who analyzed an ensemble of four RCMs driven by the NCEP/NCAR I global reanalysis (Kalnay et al., 1996), followed by CREAS regional program (Marengo et al., 2009). The CLARIS (Menéndez et al., 2010) and CLARIS-LPB Projects (Boulanger et al., 2016) succeeded to create a large ensemble of regional simulations, involving different RCMs driven by ERA-Interim reanalysis (Dee et al., 2011) and CMIP3 Global Climate Models (GCMs; Meehl et al., 2007). More recently, the CREMA experiment (Coppola et al., 2014) succeeded to produce several simulations of RegCM4 RCM forced by different GCMs and reanalysis over SA. Within the CORDEX framework (Giorgi and Gutowski, 2015), several simulations with updated model versions have been recently incorporated to the CORDEX SA domain (Fig. 2.1), enabling the availability of state-of-the-art nested RCMs at a horizontal resolution of $\sim$0.44°x$\sim$0.44°.

The CORDEX Project comprehend two types of simulations for the recent past concerning the boundary forcing: the hindcast simulations and the historical simulations. Hindcast simulations, also known as evaluation simulations, are those where reanalysis forces the RCM. These simulations have a reasonable representation of the mean climate, and they are usually used for model validation as they have a high year-to-year correlation with the observed climate. On the other hand, historical simulations belong to climate change projection simulations and differentiate from the hindcast ones in being forced by GCMs instead of reanalysis. These simulations also allow a good reproduction of the mean climate when integrated over long periods, but they are not synchronized with the observed climate. Validating this type of simulations is complicated, as their deviations from observation can be associated to the

RCM itself or as an inherited bias from the GCM. Yet, it is important to evaluate and understand the RCM-GCM chain behavior, as they also allow future climate change projections.
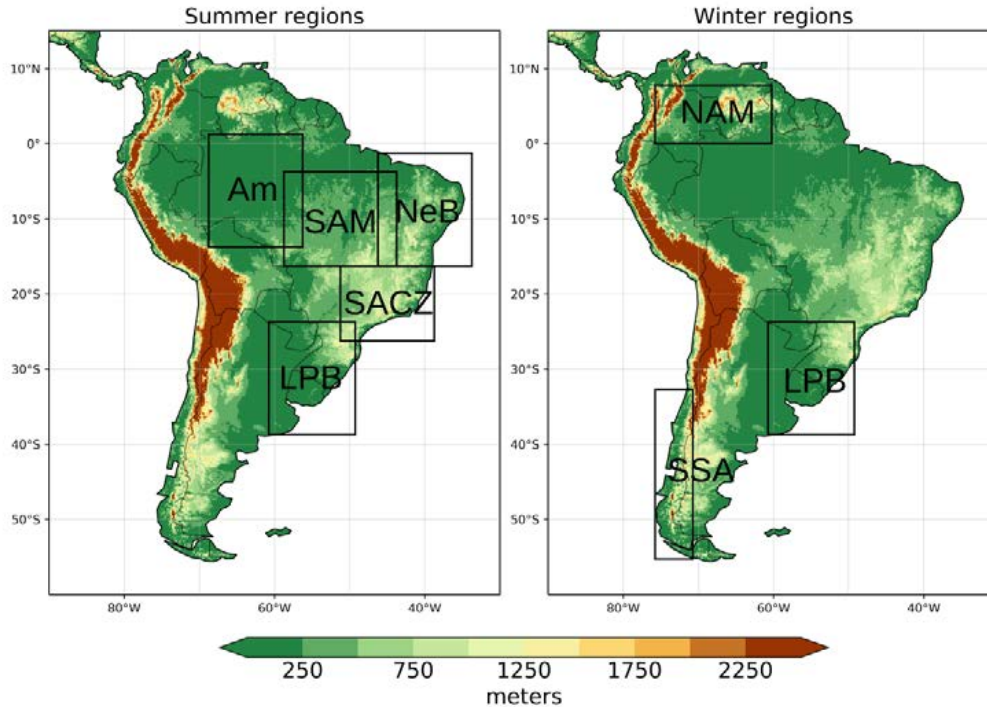
Fig. 2.1. CORDEX region 1 domain, with ETOPO2 (National Geophysical Data Center, 2006) terrain height (m) indicated in shading. Boxes in solid-black lines denote areas selected for area-mean assessment.

One of the main debates is whether RCMs can add value in the simulation of mean seasonal features and rainfall over SA. While some works find an improvement on representing the mean features (Chou et al., 2002, 2005, da Rocha et al., 2009, 2014, De Sales and Xue, 2006, Llopart et al., 2014, Misra et al., 2002, Nobre et al., 2001, Pesquero et al., 2009, Solman et al., 2008, Vernekar et al., 2003), others find a deterioration (Coppola et al., 2014, Feser, 2006, Giorgi et al., 2014, Roads et al., 2003). In the context of the CREMA experiment, when comparing RegCM4 simulations with their driving data, the results suggest an added value in reproducing extreme events over SA (Coppola et al., 2014, Giorgi et al., 2014). Also, the model partly reduces the dry bias of precipitation in the Amazon Basin when comparing to different CMIP5 GCMs (Llopart et al., 2014, da Rocha et al., 2014). Some few more works have addressed the added value in seasonal climate over SA, and there are no matching results: Roads et al.

(2003) assessed the capabilities of RCMs compared to its forcing data, finding no noticeable improvement in precipitation when assessing the large-scale fields; Seth et al. (2007) studied the performance of RCMs forced by reanalysis for different regions on tropical and extratropical latitudes in SA. In their work they concluded that regions where remote influences are strong (Northeast SA, Southeast SA, and Amazon regions) the AV of RCMs is low; by contrast, where local processes dominate and remote influences are weak (maximum monsoonal precipitation region) there is some potential for the regional model to add value. Pesquero et al. (2009) assessed the AV of the ETA Model compared to its driver HadAM3P, and found that the regional model reproduced many of the South American mesoscale climate features and together added new value to the driver model.

When it is to identify the added value of an RCM, it is important to note that not all available metrics are optimal for its calculation. The methodology selected should not only assess model performance but should also consider in some way the difference between the resolution of the RCM and its driving data. For example, Gilleland et al. (2009) argue that most traditional verification metrics are based on a point-to-point validation without any consideration of the spatial information. Kanamitsu and DeHaan (2011) illustrate this problem by showing that the identification of high skill regions is lost when averaging over large areas. They also raised the idea of differentiating relevant terms in the deviations between RCM and its driving GCM, including terms related to model resolution or model error. They conclude that the deviations of the model from the validating observations can not only be associated with the model performance but also with model resolution, interpolation, and observational uncertainty. For these reasons, many authors proposed new AV metrics to assess model performance (Denis et al., 2002a, Feser and von Storch, 2005, Kanamitsu and DeHaan, 2011, Di Luca et al., 2012, Wang et al., 2015, among others).

Therefore, motivated by the availability of new simulations from CORDEX and the lack of studies about AV over the continent, this chapter aims to assess the AV of RCM simulations compared to its coarser-resolution driver in South America. As a first step, we evaluate the capacity of climate models to simulate seasonal mean precipitation and surface air temperature through its comparison with observed gridded datasets. We believe this is a fundamental step, not only for RCM evaluation but also due to the discrepancies in the literature whether RCMs can add value or not over large-scale mean values (Llopart et al., 2014, Roads et al., 2003).

The chapter is organized as follows: in section 2 we first describe the observed and sim-

ulated data used in this study, followed by the introduction of model errors and observed uncertainties. In section 3 we assess the general and regional performance of individual and multi-model ensemble data in simulating the seasonal spatial patterns of the mean state, including a regional assessment of model errors and observational uncertainties. Finally, in section 4, we present a discussion of the most relevant results together with our main conclusions.

2.2 Data and methods

2.2.1 CORDEX simulations and observed data

For our analysis, we selected the common time period of the integrations, covering from 1990 to 2004, to keep the same time-scale variability. The seasons considered were austral summer (December, January, and February) and winter (June, July, and August). All RCMs use roughly the same domain and horizontal resolution ($\sim$0.44$°$x$\sim$0.44$°$), but different grid types. For a direct assessment and intercomparison of RCM simulations, we interpolated all original monthly precipitation and 2-meter-temperature data onto a regularly spaced latitude/longitude grid of 0.5$°$x0.5$°$. ERAi and CMIP5 GCM fields were also interpolated into a common regularly spaced grid of 1.5$°$x1.5$°$. Both variables were interpolated using a bilinear interpolation procedure, and a height correction was applied to the surface air temperature fields. The height correction consisted of adding the difference between the model native height (interpolated into the regular grid) and the observed height, multiplied by a standard lapse rate of -6,5$°$/km.

Different gridded data for precipitation and surface air temperature were used to evaluate the simulations. With the goal of measuring the uncertainty among observation data sets, we consider three station-based monthly data for precipitation (CRU, UDEL and CPC-UNI), over land on a 0.5$°$x0.5$°$ resolution. We also considered two of the above data sets (CRU and UDEL) for surface air temperature. Complementary to the interpolation of model simulations, the observed datasets were also interpolated using the same procedure to the same 0.5$°$x0.5$°$ regular grid, and also, to the 1.5$°$x1.5$°$ grid to allow GCM evaluation. Throughout the work, the set of observed datasets is denoted as Obs, and the reference field for the assessment is calculated as the average across all the observed datasets.

Table 2.1. Overview of Regional Climate Models used in the present study and their boundary conditions.

Experiment Acronym	RCM id / Reference	Resolution / Number of grid points	Boundary condition id / Reference	Boundary resolution
HadRM3P-fERAi	MOHC-HadRM3P Gordon et al. (2000)	0.44°x0.44° 146x167	ECMWF-ERAINT Dee et al. (2011)	1.5°x1.5°
REMO2009-fERAi	MPI-CSC-REMO2009 Jacob et al. (2012)	0.44°x0.44° 143x167	ECMWF-ERAINT	1.5°x1.5°
RCA4-fERAi	SMHI-RCA4 Kupiainen et al. (2014)	0.44°x0.44° 146x167	ECMWF-ERAINT	1.5°x1.5°
RegCM4-fERAi	ICTP-RegCM4-3 Giorgi et al. (2012)	0.44°x0.44° 189x199	ECMWF-ERAINT	1.5°x1.5°
WRF341I-fERAi	UCAN-WRF341I Skamarock et al. (2005)	0.44°x0.44° 146x167	ECMWF-ERAINT	0.75°x0.75°
RCA4-fEC-EARTH	SMHI-RCA4 Kupiainen et al. (2014)	0.44°x0.44° 146x167	EC-EARTH Hazeleger et al. (2010)	1.25°x1.25°
REMO2009-fMPI	MPI-CSC-REMO2009 Jacob et al. (2012)	0.44°x0.44° 143x167	MPI-ESM-LR Stevens et al. (2013)	1.875°x1.875°
WRF341I-fCanESM2	UCAN-WRF341I Skamarock et al. (2005)	0.44°x0.44° 146x167	CCCma-CanESM2 Chylek et al. (2011)	1.875°x1.875°
RegCM4-fHadGEM2	ICTP-RegCM4-3 Giorgi et al. (2012)	0.44°x0.44° 189x199	MOHC-HadGEM2-ES Collins et al. (2011)	1.875°x1.25°
LMDZ4-fIPSL-CM5A	IPSL-LMDZ4 Hourdin et al. (2006)	∼0.48°x∼0.48° 184x180	IPSL-CM5A Hourdin et al. (2012)	3.75°x1.9°

2.2.2   Model error and observational uncertainties

The main advantage of RCMs is they are integrated with a higher spatial resolution than their boundary-condition providers and, therefore, add to the latter information on a regional scale. Thus, one can distinguish between two different spatial scales: the small scales that can be reproduced only by the RCM and the large scales reproduced by both simulations. However, when it comes to consciously comparing an RCM with its driving data, there is no optimal methodology to follow (Prein et al., 2016). On the one hand, if we choose to interpolate the RCM and the observations to the resolution of the GCM, we would benefit the GCM, since we

are removing the small-scale variability of the RCM. But if we interpolate the global model to the resolution of the regional model and the observations, then the GCM is disfavored since the reduction of the grid will generate non-consistent physical information. In this chapter, we performed the evaluation of the experiments in their resolution, that is, in a 0.5° grid for the regional simulations and a 1.5° grid for the global simulations. However, for the evaluation to be adequate, we considered other sources of error associated with grid interpolation, resolution and observational uncertainty.

Kanamitsu and DeHaan (2011) introduced a clear picture of model error or deviation from the observed reference by describing the whole process of model validation. Firstly, each grid point value in model represents an entire area of the field, and therefore the model will not be able to reproduce the sub-grid variability. This error or limitation can be called representativeness error and is a function of resolution of the model and variability of the field. Secondly, interpolation error can be identified as those changes of a field when interpolated from the model grid into a validation grid. The magnitude of this error is also influenced by the model's resolution and the variability of the field. Finally, the observations used for the evaluation are not perfect, and generally have errors associated with instrumental and data acquisition imperfections. Interpolation and representativeness errors should also be counted when using station-based gridded datasets. The concept of Kanamitsu and DeHaan (2011), expressed as an apparent deviation between the model and observation for a single location, can be qualitatively formulated as

$$Model\ Error = [\varepsilon_M] + [\varepsilon_R] + \varepsilon_I + \varepsilon_{obs}, \tag{2.1}$$

where $[\ ]$ is a spatial interpolation operator, ε_M is the model deviation from observations, ε_R is the representativeness error of model grid value, ε_I is the interpolation error, and ε_{obs} is the error associated with observation. Eq. (1) shows that model deviation seen in a validation operation is directly related to the performance of the model, i.e., the true model error, if and only if ε_R, ε_I, and ε_{obs} are negligible. In real world, they are generally not negligible, and they need an appropriate evaluation, which allows us to have just an appreciation for the true performance (or error) of a model.

In our chapter, we revisit Eq. (1) and adapt it to our experimental design. Our reference observations for evaluation are station-based gridded datasets, so the grid spacing of the observational dataset defines the finest scale on which the comparisons are meaningful (Prein et al., 2016). All observed datasets have a resolution of 0.5°x0.5°. This entails that it is impos-

sible to quantify the sub-grid representativeness error of RCMs, as they have a finer resolution. Following Eq. (1), the deviation of both RCM experiments from the reference field will be affected by the following terms:

$$\varepsilon_{RCM}^{m} = f(\varepsilon_{M}^{m}, \varepsilon_{R}^{0.5°}, \varepsilon_{I}^{0.5°}, \varepsilon_{obs}), \tag{2.2}$$

where m can be RCMs-fERAi or RCMs-fCMIP5, $\varepsilon_{R}^{0.5°}$ is the representativeness error at a resolution of 0.5°, that is neglected hereafter since its resolution is close to that of the observations, and $\varepsilon_{I}^{0.5°}$ is the interpolation error at a resolution of 0.5°. In the same way, the errors associated with GCMs will include the same terms but for a coarser resolution grid. Therefore, the deviation of both GCM experiments from the reference field will be affected by the following terms:

$$\varepsilon_{GCM}^{m} = f(\varepsilon_{M}^{m}, \varepsilon_{R}^{1.5°}, \varepsilon_{I}^{1.5°}, \varepsilon_{obs}), \tag{2.3}$$

again, m can be ERAi or CMIP5, $\varepsilon_{I}^{1.5°}$ is the interpolation error at a resolution of 1.5°, and $\varepsilon_{R}^{1.5°}$ is the representativeness error between the resolutions of 0.5° and 1.5°. In this case, the term associated with the representativeness error is not negligible, as degrading the observed field into the GCM resolution for evaluation implies losing details in the process of filtering.

In this chapter, we present a methodology that accounts for the different terms involved in the process of model evaluation. Despite strong constraints and difficulties in calculating precisely each term in Eqs. (2) and (3), we try to estimate their order of magnitude. We aim to find regions with significant contributions in order to determine if the model's deviations from observation are genuinely associated with model performance or not.

Starting with the model error, ε_{M}, we cannot execute a temporal validation as historical simulations are not synchronized with the observed variability. Consequently, we perform a multi-model evaluation of the seasonal climatology by using the root-mean square (RMS) error metric. We define ε_{M} as the RMS deviations of all individual members of an ensemble m from the reference data, that is

$$\varepsilon_{M}^{m} = \sqrt{\frac{1}{N_m} \sum_{i=1}^{N_m} ([\overline{F_{m,i}}]^{res} - [\overline{F_{ref}}]^{res})^2} \tag{2.4}$$

with N_m the number of associated simulations, and $[\,]^{res}$ the interpolation of the simulation and station-based observed datasets to a regular grid of resolution res (0.5° for both RCMs and 1.5° for both GCMs). It is worthy to note that the reference field is calculated as an average among available datasets in the resolution of each experiment.

The degradation of the observed field from 0.5° to 1.5° is done by aggregating the reference field at 0.5° into a coarser-resolution grid of 1.5°x1.5°. The aggregation is performed by averaging all original sub-grid values inside each of the coarser grid boxes (Di Luca et al., 2012). The aggregated values are then re-distributed into the original resolution, which will give an estimation of the details lost in the process of filtering. The error ε_R is calculated as the RMS difference between the degraded and reconstructed fields

$$\varepsilon_R^{1.5°} = \sqrt{(\overline{F_{ref}^{0.5°}} - \overline{F_{ref}^{1.5°}})^2} = \mid \overline{F_{ref}^{0.5°}} - \overline{F_{ref}^{1.5°}} \mid . \tag{2.5}$$

Eq. (6) permits to measure the information contained in the range of resolutions from $0.5°$ to $1.5°$.

Unlike Kanamitsu and DeHaan (2011), we won't neglect ε_I and ε_{obs} as both terms can be significant over some regions. While there is no easy way to calculate the interpolation error, we estimate it by interpolating the mean observed climatological field into a regularly-spaced but staggered grid, and then interpolating it back to the original grid. For the 0.5°x0.5° resolution we consider a displacement of 0.25° in both latitude and longitude directions and for the 1.5°x1.5° a displacement of 0.75°. The interpolation error is then estimated as half the difference between the double interpolated field and the original field

$$\varepsilon_I^{res} = \frac{\sqrt{([\overline{F_{ref}^{res}}]] - \overline{F_{ref}^{res}})^2}}{2} = \frac{\mid [[\overline{F_{ref}^{res}}]] - \overline{F_{ref}^{res}} \mid}{2}. \tag{2.6}$$

Finally, we need to point out that a main part of observation errors comes from the representativeness error and interpolation error when station-based information is converted into a regular grid. But its estimation is out of the scope of our study. Nevertheless, we can estimate the observational uncertainty as the spreading among individual datasets. For that, we substitute m by Obs and res by $0.5°$ in Eq. (4), and obtain

$$\varepsilon_{obs} = \sqrt{\frac{1}{N_{Obs}} \sum_{i=1}^{N_{Obs}} ([\overline{F_{Obs,i}}]^{0.5} - [\overline{F_{ref}}]^{0.5})^2}. \tag{2.7}$$

2.3   Results

### 2.3.1   Seasonal spatial patterns of the mean state

The challenge for regional climate modelers in representing the South American climate comes from the extent of the computational domain and the complexity of the physical phenomena

involved. During the austral summer, precipitation maximizes over tropical and subtropical latitudes and is largely associated to the SAM System (Fig. 2.2a). All multi-model ensemble climatologies can reproduce large-scale features of the summer precipitation, but the presence of deviations from the reference indicates some systematic biases (Figs. 2.2b-2.2e). There are some common biases in all experiments, such as an overestimation of precipitation intensity along the Andes Cordillera, a dry bias in northern and central Brazil and a wet bias in Northeast Brazil (NeB). This last behavior is accentuated in historical experiments, especially in RCMs-fCMIP5. All the three ensembles, RCMs-fERAi, RCMs-fCMIP5 and CMIP5, show a wet bias over the South Atlantic Convergence Zone (SACZ) and a dry bias over La Plata Basin (LPB). On the contrary, ERAi has opposite biases in these two regions. The spatial distribution of surface air temperature biases (Figs. 2.2g-2.2j) reveals a cold bias over most of the continent in all experiments. This is not true over the Amazon basin, where RCMs-fERAi and CMIP5 ensembles show small positive values. Also, over LPB, most ensembles except ERAi product have a warm bias.

Given that results are presented as ensemble mean, it is important to assess the multi-model dispersion over each ensemble. Following Rinke et al. (2006) and Solman et al. (2013), we can highlight those areas where the dispersion among datasets is larger than the interannual variability of the field (hatched areas in Fig. 2.2). In the case of summer precipitation, all three ensemble mean climatologies have large inter-model spread over most of tropical and subtropical SA (Fig. 2.2b, 2.2d, and 2.2e), suggesting that the ensemble climatology is not very representative of individual climatologies. The absence of hatched areas for observed climatologies (Fig. 2.2a) indicates that the inter-dataset spread is small over most of SA. Regarding surface air temperature, only CMIP5 ensemble has large hatched areas that denote a large dispersion among simulations over most of the continent.

Winter precipitation climatology (Fig. 2.3a) exhibits two maxima: the first over the northern part of the continent, north of the equator, associated to the North American Monsoon (NAM) System; and the other one over the meridional Andes, south of $40°$S, associated to baroclinic activities. While all experiments show the northern precipitation maximum associated to the NAM System (not shown), they fail to capture the observed intensity by largely underestimating it (Figs. 2.3b-2.3e). Even ERAi fails to simulate the southward extension of the NAM influence, which is noticed by the wet bias at the southern edge of the region. All ensembles present a significant multi-model spread over the tropics, indicating a wide variation in the representation of the NAM. In the extratropics, all multi-model ensembles overestimate
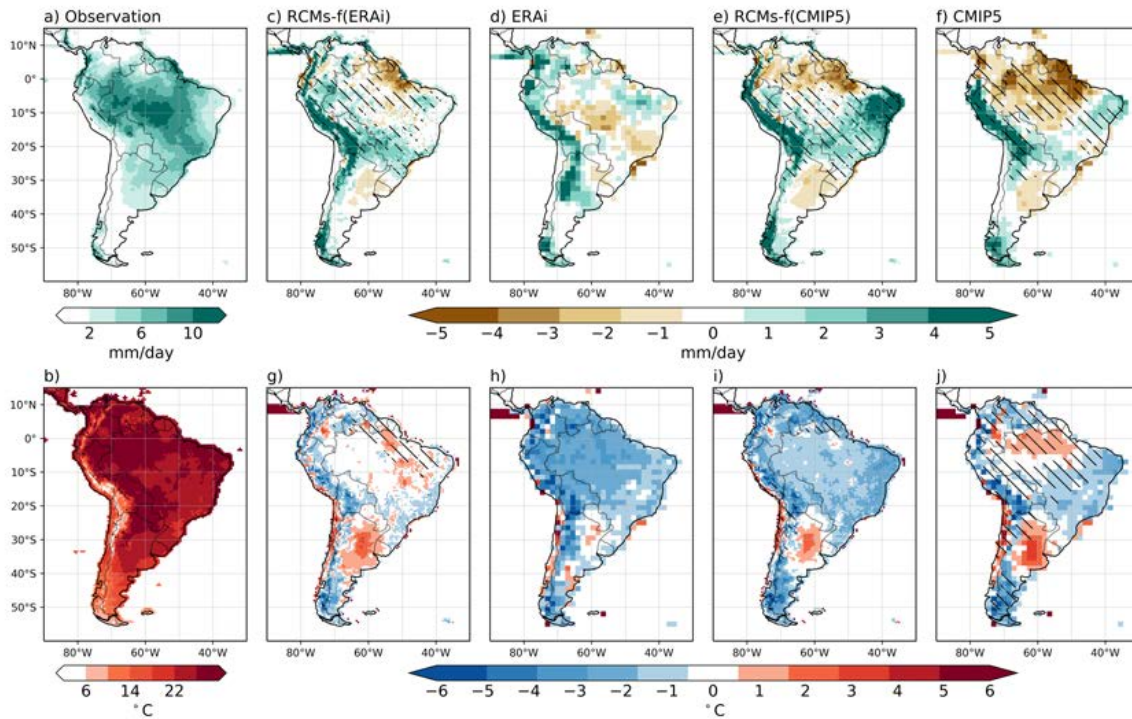
Fig. 2.2. Summer mean precipitation (mm/day; top panels) and 2-meter surface air temperature (°C; bottom panels) of the observed fields and the multi-model ensembles. The first column is the average of observed datasets and the second, third, forth and fifth columns are the climatologies of RCMs-fERAi, ERAi, RCMs-fCMIP5, and CMIP5, respectively. Hatched areas indicate regions where the inter-model standard deviation is larger than the natural variability, represented by the mean interannual standard deviation of all simulations involved.

precipitation over the western slope of the Andes. The bias is maximal in RCMs, as they also present an unrealistic extension over northern Chile. Regarding 2-meter temperature (Fig. 2.3, bottom panels), we note again that most experiments have a cold bias over most of the continent, except RCMs-fERAi multi-model ensemble over the southern Amazon basin and CMIP5 multi-model ensemble over northern Brazil and LPB. During this cold season, unlike in summer, both RCM ensembles have large inter-model spread for surface-air temperature climatology over the tropical and subtropical latitudes, and also over Patagonia in the case of RCMs-fCMIP5. CMIP5 simulations continue to show large inter-model spread over the same latitudes as in summer.

Taylor diagrams (Taylor, 2001) are multi-parameter-based diagrams that allow intercomparison of models performance in reproducing a reference pattern. They are a useful and
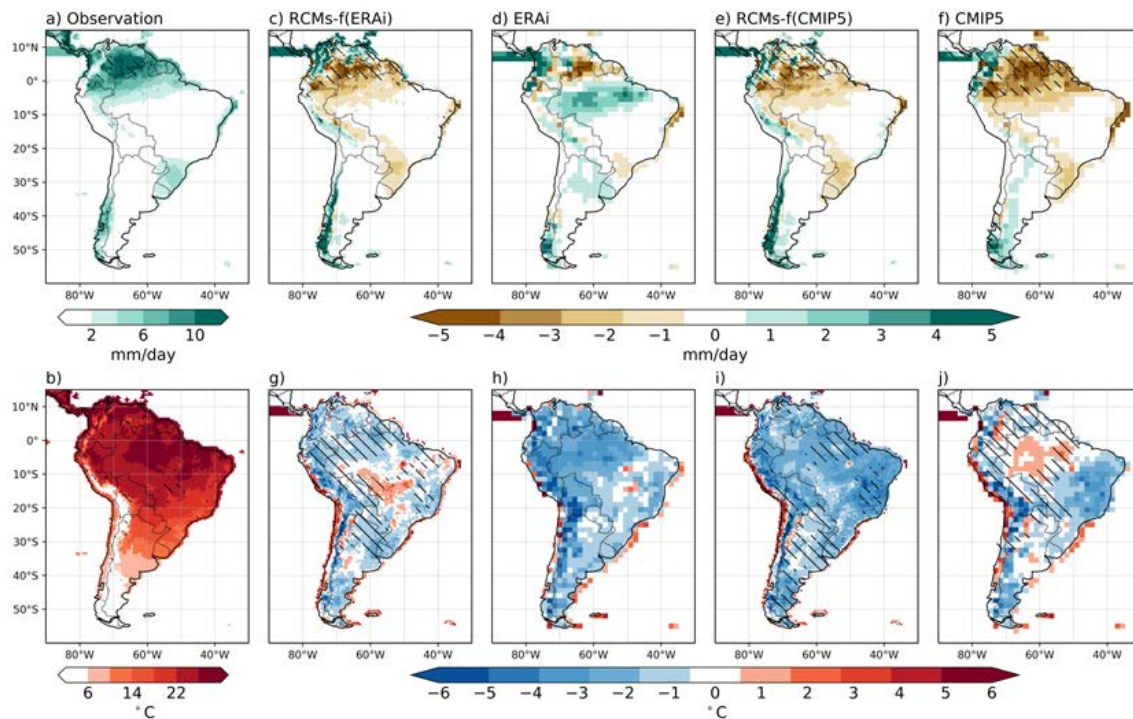
Fig. 2.3. As in Fig. 2.2 but for the winter season.

visual tool to summarize how well climate models reproduce the observed climate. We first assess models performance over the South American low-level terrain (lower than 1500m) in Fig. 2.4. Results suggest that there is a clear distinction between model's ability to reproduce 2-meter temperature climatology and precipitation climatology (Fig. 2.4). The spatial correlation between observed and modeled climatology is always higher for 2-meter temperature (ranging from 0.9 to 0.99) than for precipitation (from 0.5 to 0.9). It is interesting to note that in all cases the ensemble mean improves the field when comparing to each individual simulation, as suggested by other authors (Carril et al., 2012, López-Franca et al., 2016). Surface air temperature tends to be closer from each other in the Taylor diagrams compared to precipitation points, which indicates a larger inter-model spread for precipitation.

During summer, ERAi reanalysis and RCMs-fERAi multi-model ensemble have both the best performance in reproducing the observed summer precipitation climatology (Fig. 2.4a). Their overall performance is similar in terms of correlation but not in terms of normalized standard deviation (nSTD). When compared with the reference, ERAi has lower spatial variability (nSTD<1) and RCMs has higher spatial variability (nSTD>1). These characteristics are also valid when evaluating the ensemble of RCMs-fCMIP5 and their driving data ensemble.
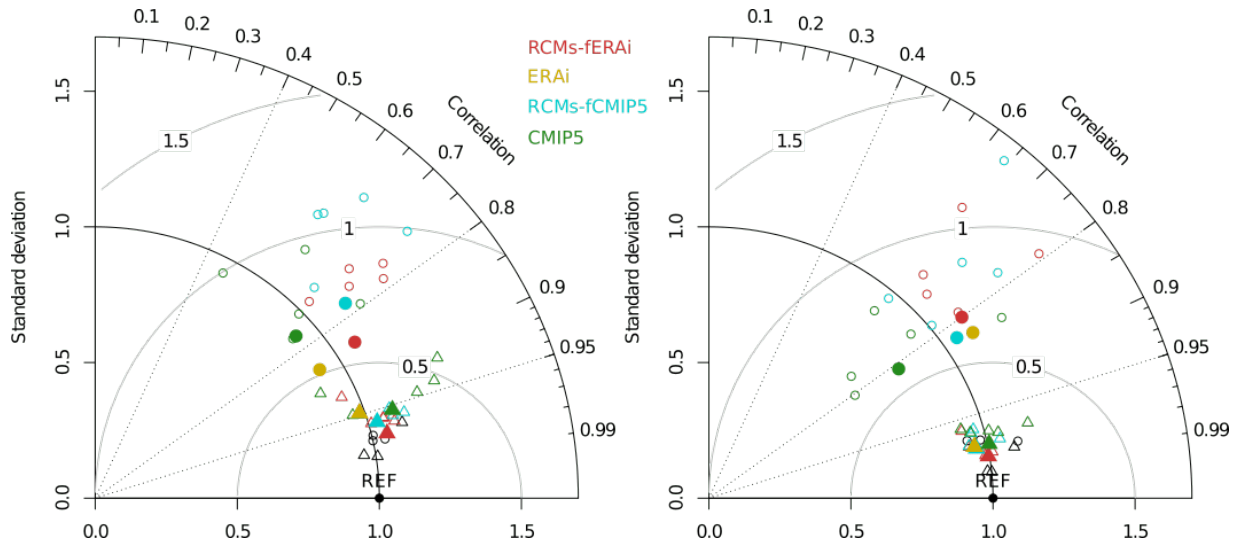
Fig. 2.4. Taylor diagrams showing the correlation, normalized standard deviation and centered RMSE for individual simulations (empty markers) and for multi-model ensembles (full markers). The left panel corresponds to summer and the right one to winter. The observation ensemble is considered as the reference data. Red, yellow, light-blue and green colors represent the RCMs forced by reanalysis, the reanalysis itself, RCMs forced by CMIP5 and CMIP5 models themselves, respectively. Black markers represent individual observed datasets. Circles correspond to seasonal precipitation climatology and triangles to seasonal surface air temperature climatology. The calculation excludes grid points with topography higher than 1500m.

During this season, all RCMs-fCMIP5 individual simulations show worse performance, compared to RCMs-fERAi individual simulations, probably due to the quality of the different boundary conditions. Nevertheless, all RCM individual simulations have larger nSTD when compared to their driving data, suggesting there is an excessive spatial variability. Regarding surface air temperature, the ensemble of RCMs-fERAi is the one showing the best match with the observed climatology pattern by presenting the highest spatial correlation coefficient. In both experiments, there is an added value from RCM ensembles in reproducing the referenced surface air temperature, each individual simulation being also the case. Again, as noted in Fig. 2.2, CMIP5 simulations tend to have a significant spread during this season.

RCMs-fCMIP5 ensemble is the most skillful multi-model ensemble in simulating the winter precipitation climatology (Fig. 2.4b). RCMs-fERAi has similar nSTD than its driving data but lower spatial correlation. In the historical experiments, RCMs-fCMIP5 has higher correlation and a spatial variability nearer the observed when comparing to its driving data. Alike sum-

mer, RCMs-fERAi continue having the best performance in reproducing the winter 2-meter temperature climatology, but all ensemble and individual simulations have high correlation values and near to 1 nSTD, suggesting an overall good performance.

2.3.2 Regional performance of individual simulations and multi-model ensembles

Regional-scale climate assessment is fundamental for understanding the potential added value of RCMs since AV is expected only over those regions where stationary climatic features are associated to small-spatial scale processes (Di Luca et al., 2012). For this reason, we emphasize on the evaluation of regional performance by selecting several key areas over the whole continent (Fig. 2.1). It is clear that RCMs ensembles can add value to the simulated climate when compared to their driving data (Figs. 2.2 and 2.3), but it is worthy to note that there is a large spread among simulations (Figs. 2.2, 2.3 and 2.4). We need to evaluate the performance of individual RCM simulations against their driving data, which can reveal the robustness of results. To do so, we use an AV index defined as the ratio between the absolute error (AE) of the RCM and the AE of the GCM. The AE is calculated as the absolute difference between the simulation climatology with the reference, followed by an average over each individual region. Hence, if the index is smaller than one, the RCM has a lower AE than its driving data, suggesting a better representation of the mean climatology over a region. The index is also calculated for the multi-model ensemble climatology to see how representative it is.

When analyzing the AV index over all summer regions (table 2), we find that even though the ensemble of RCMs-fERAi represents the mean value of precipitation better than its driver does, individual simulations show different statistics. Over the five regions, only three of them (SAM, SACZ and LPB) show added value within at least one individual simulation: three simulations (over five) in the case of SAM region, two in the case of SACZ and only one in LPB. For RCMs driven by CMIP5, the RCMs add value over the CMIP5 driver only in Am region, coincident with results in Fig. 2.9, since 3 of 5 individual simulations have lower bias than its driver. Other regions where individual simulations add value in precipitation are SAM with two simulations, NeB with one simulation, SACZ with one simulation and LPB with three simulations.

Summer surface air temperature shows a more positive outlook for the RCMs-fERAi ensemble, as in Am (5 simulations), SAM (5 simulations), NeB (3 simulations) and SACZ (4 simulations) almost all simulations, together with the ensemble mean, show a lower AE than ERAi. RCMs-fCMIP5 adds value over two regions: Am (4 simulations) and LPB (3 simulations). For Am, the ensemble mean did not represent individual performance. This counter-intuitive

Table 2.2. Added Value Index (AVI) of individual regional climate simulations against their driving data for austral summer (DJF) and for each study region. The index is calculated as the ratio of the area-averaged absolute error (AE) of RCM over that of GCM. Bold figures highlight cases with AVI smaller than 1, indicating added value in RCM.

Experiment	Am		SAM		NeB		SACZ		LPB	
Acronym	pr	tas	pr	tas	pr	tas	pr	tas	pr	tas
RCMs-fERAi	**0.80**	**0.10**	**0.52**	**0.21**	**0.84**	**0.37**	**0.81**	**0.65**	**0.83**	2.06
HadRM3P-fERAi	1.55	**0.45**	1.42	**0.45**	1.08	**0.41**	**0.71**	**0.44**	**0.61**	3.91
REMO2009-fERAi	1.67	**0.25**	**0.97**	**0.92**	1.45	1.59	**0.97**	**0.53**	1.12	1.47
RCA4-fERAi	1.44	**0.13**	1.47	**0.27**	3.04	**0.98**	1.13	**0.99**	1.91	3.16
RegCM4-fERAi	1.36	**0.21**	**0.93**	**0.36**	1.21	**0.36**	1.35	**0.90**	1.64	2.90
WRF341I-fERAi	3.19	**0.67**	**0.98**	**0.75**	1.07	1.02	1.12	1.17	1.15	1.77
RCMs-fCMIP5	**0.56**	1.75	1.23	1.63	2.46	1.44	1.82	1.37	1.15	**0.72**
RCA4-fEC-EARTH	1.05	**0.60**	2.49	**0.70**	3.31	**0.92**	1.56	1.05	2.17	1.17
REMO2009-fMPI	**0.74**	**0.89**	2.08	1.26	2.21	1.23	1.85	**0.99**	**0.95**	**0.52**
WRF341I-fCanESM2	**0.58**	**0.19**	**0.79**	1.16	2.44	3.44	3.72	2.80	**0.84**	1.43
RegCM4-fHadGEM2	1.51	1.67	1.22	**0.80**	**0.96**	1.26	1.22	1.06	1.22	**0.92**
LMDZ4-fIPSL-CM5A	**0.81**	**0.94**	**0.89**	1.32	1.07	1.66	**0.72**	1.50	**0.43**	**0.61**

result is probably caused by the large spreading among CMIP5 models over this region (Fig. 2.2j).

For winter precipitation, Table 3 shows that AV can only be found in some individual simulations over NAM region (2 simulations of CMIP5-driving RCMs and one of ERAi-driving RCMs), four simulations in LPB (two in each experiment) and only one simulation in SSA. Regarding surface air temperature, most models show an improvement over NAM region for both experiments (5 in ERAi-driving RCMs and 3 in CMIP5-driving RCMs), but in the case of CMIP5-driving RCMs the higher skill is not represented by the ensemble mean. For RCMs-fERAi, there are two individual simulations showing added value in LPB and also two simulations in SSA with an AV index of 1.

Box-and-whisker plots are an excellent non-parametric tool for evaluating quartile distribution, allowing us to visually analyze and compare various L-estimators beyond the mean value. Assessing the distribution of rainfall and surface air temperature allows us not only to assess the biases in the mean climate but also to evaluate the interannual variability of

Table 2.3. Same as in Table 2 but for austral winter (JJA).

| Experiment | NAM | | LPB | | SSA | |
Acronym	pr	tas	pr	tas	pr	tas
RCMs-fERAi	1.05	**0.41**	1.25	1.06	1.69	**0.94**
HadRM3P-fERAi	1.26	**0.37**	**0.70**	**0.70**	2.25	1.00
REMO2009-fERAi	**0.77**	**0.27**	**0.93**	**0.65**	2.34	1.03
RCA4-fERAi	1.61	**0.50**	2.73	1.42	1.64	1.00
RegCM4-fERAi	1.24	**0.41**	1.08	1.20	1.26	1.27
WRF341I-fERAi	1.64	1.08	1.58	2.68	1.58	1.17
RCMs-fCMIP5	**0.71**	1.73	1.08	2.08	2.23	1.08
RCA4-fEC-EARTH	1.08	**0.84**	1.94	1.98	1.62	1.04
REMO2009-fMPI	**0.65**	**0.71**	1.11	1.37	2.31	**0.84**
WRF341I-fCanESM2	**0.69**	1.20	**0.74**	3.89	1.55	1.35
RegCM4-fHadGEM2	1.73	1.04	1.53	1.43	**0.82**	**0.91**
LMDZ4-fIPSL-CM5A	1.10	**0.94**	**0.70**	2.09	2.43	1.18

the simulations. Generally speaking, models are far from correctly reproducing the observed variability (Figs. 2.5 and 2.6). However, in most regions, data sets broadly reproduce the observed statistical distribution by intersecting at least part of the inter-quartile range (IQR; that is 25th-75th quartile distance) with the corresponding observed one.

Most of the experiments tend to have a systematic cold bias over most regions during summer (Fig. 2.5). This is especially true for ERAi reanalysis and RCMs-fCMIP5 ensemble. Precipitation is well simulated in all experiments and over most regions, an exception is RCMs-fCMIP5 ensemble which has a systematic wet bias over SAM, NeB and SACZ. Concerning the AV of RCMs in precipitation, there is a little improvement compared to its driving data. RCMs-fERAi improves ERAi by better reproducing the observed median value and the interannual variability over Am region. There are also some improvements over LPB and SACZ for the median value but not so much for the interannual variability. RCMs-fCMIP5 only slightly improve its driving data for precipitation distribution over LPB. Regarding surface air temperature, the added value is more evident, especially for the case of hindcast simulations. RCMs-fERAi improves the reproduction of the observed distribution over Am, SAM, NeB and SACZ region. On the other hand, RCMs-fCMIP5 ensemble does not seem to reduce the bias of CMIP5 sim-
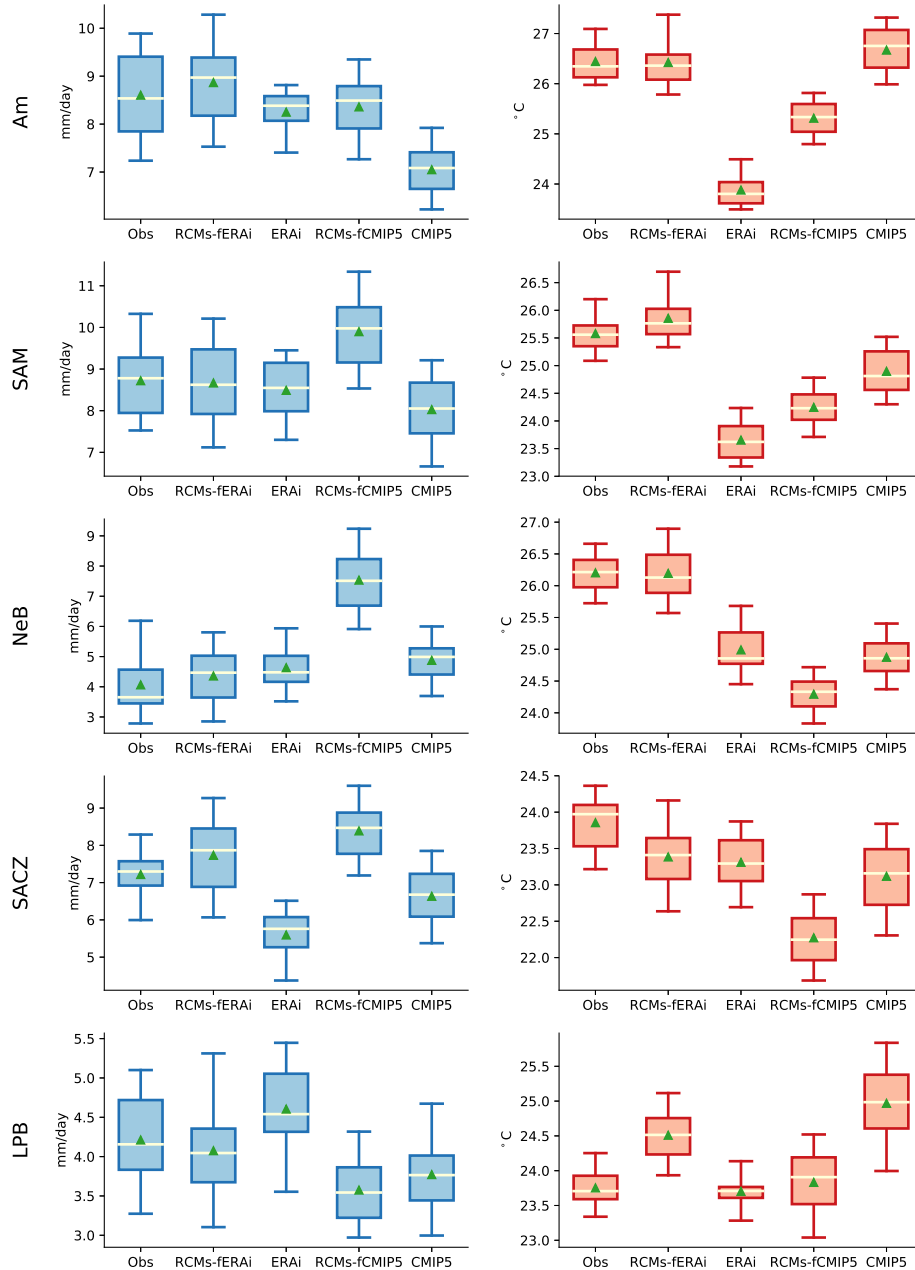
Fig. 2.5. Box-and-whisker plots showing the mean temporal summer distribution statistics in each study region. Every box represents the inter-quartile range (25th-75th percentile), the median is indicated with a white line and the mean with a green triangle. The whiskers indicate the 95th and 5th percentiles. The regional time series of each simulation is obtained by spatially averaging all values within the region in every time step. Also, all percentiles of the multi-model ensembles are calculated as the average of individual percentiles. The left panels correspond to precipitation (mm/day; blue) and the right panels to 2-meter temperature (°C; red).

ulations, but they rather improve the representation of the interannual variability; this is the case for Am, SAM, SACZ and LPB regions.
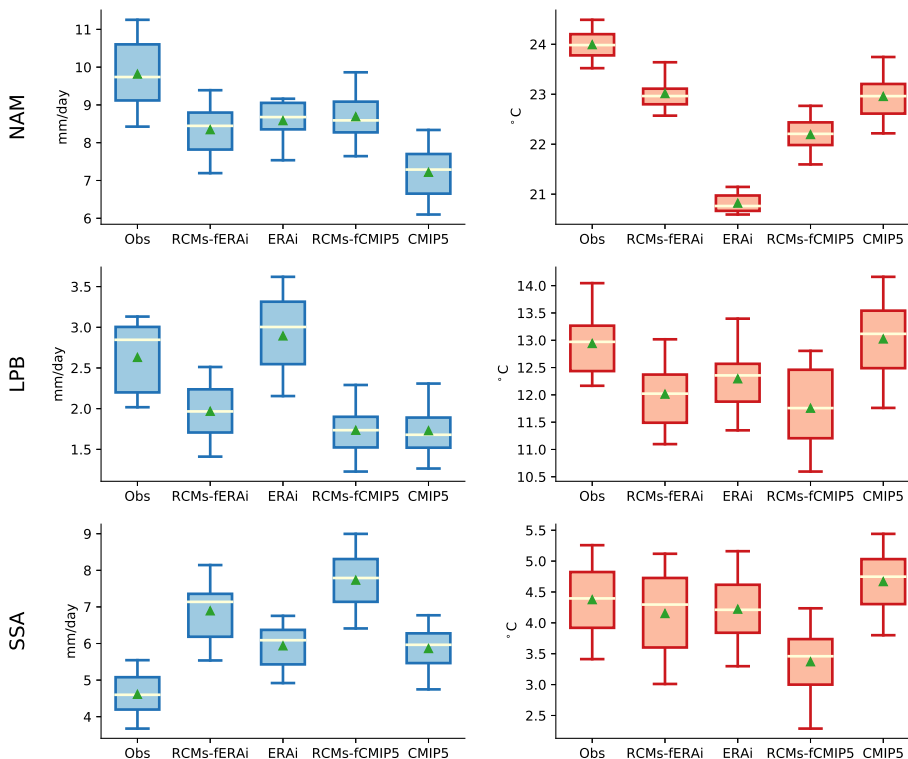
Fig. 2.6. As in Fig. 2.5 but for the winter season.

During winter, there is a general disability of climate models in reproducing the observed statistics over NAM, by systematically underestimating both temperature and precipitation (Fig. 2.6). AV hardly manifests, but RCMs-fERAi reduces the large cold bias that ERAi has over the NAM region and the same region sees an improvement in RCMs-fCMIP5 which reduces the dry bias of CMIP5 simulations. Winter precipitation statistics over SSA indicate a general systematic overestimation of rainfall by all models. This is especially true for both RCM ensembles, which lowers its performance when comparing to their driving data.

2.3.3 Assessment on model errors and observational uncertainties

The assessment performed in the previous sections combines different types of error, which makes difficult to understand how the RCM simulations add value (or not), compared to its coarser-resolution driver. We follow the resolution-aware methodology described in the methods section to identify the type of error that should not be neglected during the assessment. A regional comparison of all the terms presented in Eqs. (2) and (3) is performed over each

region for both temperature and precipitation. We present the average value of each term over each region for DJF and JJA respectively (Fig. 2.7). The observational uncertainty, ε_{obs}, is considered as a reference value, as no assessment can be done when errors are smaller than this term. Results show that model error (ε_M) is usually the largest one. We recall that it generally represents the model performance that we actually want to evaluate. However, ε_R, and ε_I are not always negligible. The spatial distribution of these errors (see supplementary material) shows they are particularly large over complex terrain regions, especially for surface air temperature. This result is also evident in the regional diagram (Fig. 2.7), where the coarse-resolution errors, i.e., $\varepsilon_I^{1.5}$ and $\varepsilon_R^{1.5}$, are relatively large over SACZ in summer and NAM and SSA in winter. ε_R is usually larger than ε_I, being the latter the one that presents the smallest values when comparing to the other terms. ε_I is also dependent of resolution, being the interpolation error associated to a grid of 1.5° resolution ($\varepsilon_I^{1.5}$) larger than the one from a grid of 0.5° resolution ($\varepsilon_I^{0.5}$)

In summer, all $\varepsilon_R^{1.5}$ and $\varepsilon_I^{1.5}$ are of a similar order of magnitude, close to ε_{obs} for both temperature and precipitation. $\varepsilon_R^{1.5}$ often exceeds ε_{obs} value, as is the case in NeB and SACZ for precipitation and in NeB, SACZ and LPB for surface air temperature (Fig. 2.7, left panels). When analyzing the regional performance of models, ERAi has the best performance in reproducing regional precipitation climatology, since ε_M^{ERAi} has the lowest values compared to $\varepsilon_M^{RCMs-fERAi}$, $\varepsilon_M^{RCMs-fCMIP5}$ and ε_M^{CMIP5} over most regions. This is the case over Am, SAM, NeB and LPB regions. For surface air temperature, the experiment with lower values is $\varepsilon_M^{RCMs-fERAi}$, mainly over Am, SAM, NeB and SACZ region. The results are not very encouraging for RCM historical simulation ensemble for precipitation, but improve for surface air temperature: $\varepsilon_M^{RCMs-fCMIP5}$ is lower than ε_M^{CMIP5} only in Am region for precipitation and in Am, SAM, and LPB for surface air temperature. In addition to this, $\varepsilon_M^{RCMs-fCMIP5}$ presents an outlier in precipitation over NeB, with a value of 4.7 mm/day.

During winter, ε_{obs} is large for precipitation over the NAM region (Fig. 2.7, right panels), as was already seen with the spread among datasets in Fig. 2.3a. The uncertainty is also relatively large (larger than 0.5 °C) over NAM and SSA for surface air temperature, probably because of the selection of domains placed over complex terrain regions. $\varepsilon_R^{1.5}$ is larger than the observational uncertainty for surface air temperature, by exceeding it over all three winter regions (i.e., NAM, LPB and SSA). $\varepsilon_I^{1.5}$ is also larger than ε_{obs} in NAM for surface air temperature. Regarding ε_M, RCMs usually have similar or larger RMSE in precipitation than its driving data; except for the case of NAM region where $\varepsilon_M^{RCMs-fCMIP5}$ has a lower value than ε_M^{CMIP5}.

The aforementioned also represents the case for 2-meter temperature, except for RCMs-fERAi over LPB.
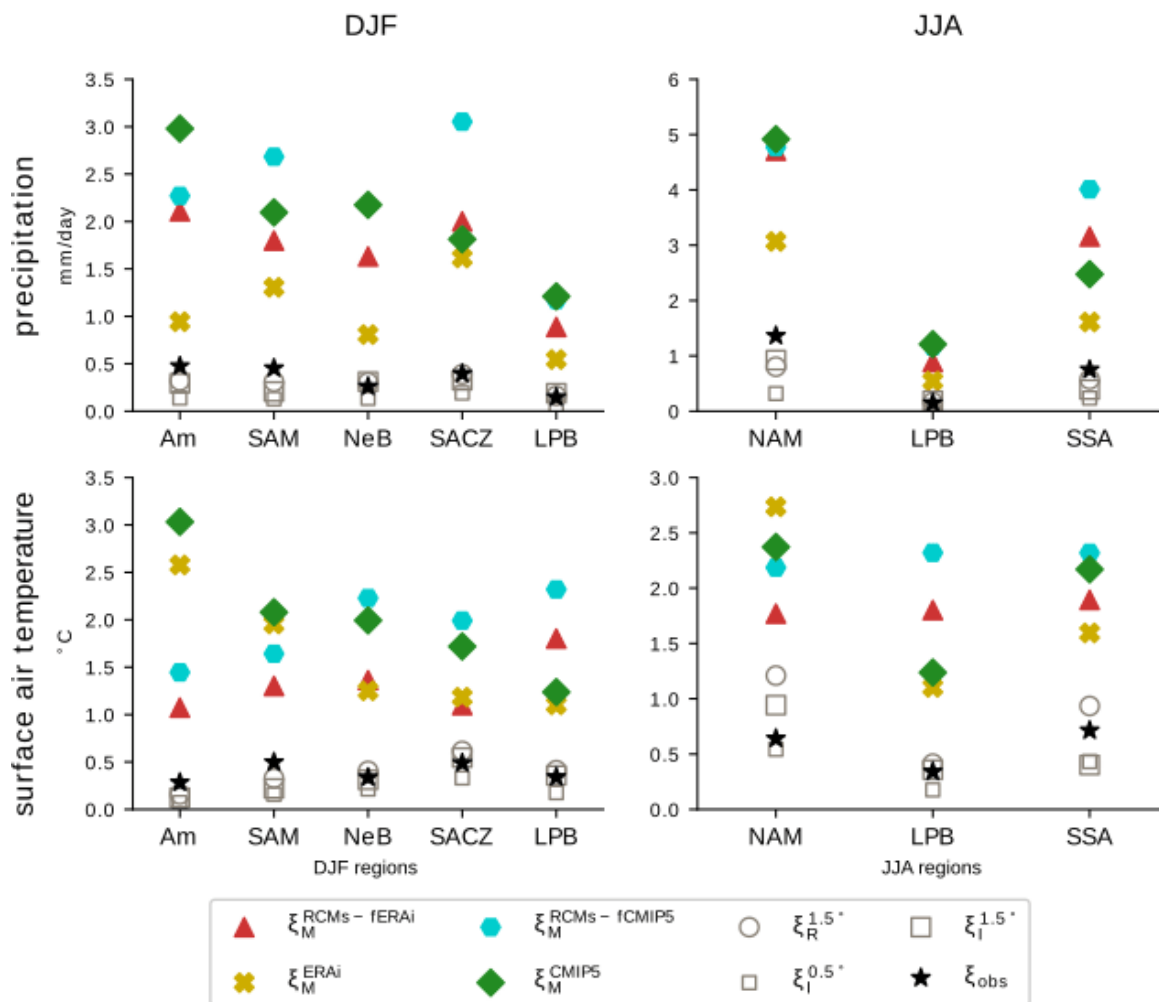
Fig. 2.7. Diagrams summarizing different errors or deviations obtained with our best estimation for each of our regions of interest. Left panels are for austral summer DJF, and right ones for austral winter JJA. Values plotted in the form of different symbols represent the spatial average of different terms in Eqs. (2) and (3). Top panels are for precipitation (mm/day), and bottom panels for 2-meter temperature (°C). Red, yellow, light-blue and green colors represent our estimations in RCMs forced by reanalysis, reanalysis, RCMs forced by CMIP5 and CMIP5, respectively. Black markers represent our estimation for observational uncertainty. Grey empty markers correspond to interpolation (square markers) and representativeness (circle markers) errors.

2.4 Conclusions and discussion

Although many CORDEX simulations over SA became available recently, there was a general lack of works investigating the AV of RCMs over the continent. It is thus very relevant for us to assess these regional simulations, which can provide a useful guide for researchers or end users of these simulations. The particularity of our approach was in the joint evaluation of RCM simulations and their coarser-resolution driving data. We first evaluated their capability in reproducing mean climate conditions over the continent. We used two types of RCM experiments with different nature in lateral boundary conditions: hindcast simulations with RCMs driven by ERA-Interim re-analysis and historical simulations with RCMs driven by CMIP5 global models. Our database included five hindcast simulations and five other historical simulations, as well as their driving data. The multi-model ensembles and individual simulations were evaluated against two or three observed gridded datasets for 2-meter temperature and total precipitation, respectively. We performed the analysis on a seasonal basis, for austral summer and winter, over a common period ranging from 1990 to 2004.

Generally speaking, all multi-model ensembles can reproduce main features of summer and winter climatologies. However, individual simulations exhibit a large inter-model spread, especially for precipitation, suggesting the need for assessing models individually. The ensembles also have some common model biases, as it is the overestimation of precipitation intensity along the Andes Cordillera. An important bias is found during the warm season since the ensembles differ substantially in their representation of location and intensity of the maximum monsoon rainfall. Regarding surface air temperature, models tend to simulate lower temperatures than the observed, as shown by in the bias fields and the box-and-whisker plots. This cold bias is maximized by ERAi and RCMs-fCMIP5 over the Amazon Basin region. Over the tropical and subtropical latitudes, CMIP5 models show a large spread among simulations in reproducing the surface air temperature climatology for both winter and summer seasons.

Solman et al. (2013) assessed the capability of a set of 7 hindcast RCMs, performed in the framework of the CLARIS-LPB Project, in reproducing the mean climate conditions over the South American continent. If we compare the CLARIS-LPB simulations with the ones shown here for CORDEX, we find that the distribution and intensity of biases are very similar (see Figs. 2 and 3 from Solman et al.). However, some improvements are found for CORDEX such as a reduction of the precipitation bias over LPB during winter, and a reduction of the warm bias over central SA in the same season. Also, our results are consistent with Solman et al.

(2013) in terms of spread among simulations, both showing that the inter-model uncertainty is larger than the observational uncertainty.

We performed a regional assessment in several key areas of the whole continent in summer and winter. In summer, RCMs-fERAi ensemble shows a better reproduction of observed precipitation and surface air temperature when compared to ERAi. However, some opposite results can be found for precipitation when conducting the comparison individually. There is a clear warning message on the practice of only analyzing the multi-model ensemble, especially over regions with large inter-model spread. Surface air temperature exhibits some encouraging results, with a general improvement when compared to ERAi. Regarding historical simulations with RCMs driven by CMIP5, results are inconclusive, since added value is only found in certain regions and in limited simulations. It is important to highlight that the complexity to be considered is increased when assessing the AV of RCMs in their historical simulations, as it should include GCM/RCM physical compatibility. We need to consider different GCM/RCM configurations to understand if biases are inherited from GCM through boundary conditions. During winter, RCMs do not noticeably improve the representation of precipitation or surface air temperature. As a matter of fact, they even tend to degrade the winter climatology.

We are aware that the direct comparison between the modeled field and the observed field include some additional sources of error independent of model performance. Thus, model error is associated to model performance only in those regions where ε_R, ε_I, and ε_{obs} are negligible. In general, model error, ε_M, is the largest one over full SA continent, allowing a direct evaluation of climate models. However, we have identified some areas where other sources of error are not at all negligible. ε_R has its highest values over regions with strong surface forcing, such as the Andes Cordillera. ε_I also showed the same behavior. ε_{obs} is also large over complex-terrain regions, especially for surface air temperature. This last result is probably due to the scarcity of surface meteorological stations over isolated mountainous regions and to different interpolation techniques used in each dataset.

There is a general disagreement over literature regarding added value of RCMs for large-scale mean values, as some works find an improvement on representing the mean climatic features (Kerkhoff et al., 2014, Llopart et al., 2014, Nikulin et al., 2012, Torma et al., 2015, Fotso-Nguemo et al., 2017, Veljovic et al., 2010, Prein et al., 2016), while others find a deterioration (Coppola et al., 2014, Feser, 2006, Giorgi et al., 2014, Roads et al., 2003, Mishra et al., 2017). Our results are consistent with this general uncertainty since they suggest that added value

of RCMs depends on the different driving fields (i.e., hindcast or historical), the surface properties of the area, the season and the variable analyzed. The dependency of AV to diverse factors was already noted by Torma et al. (2015). The methodology used throughout this chapter leaves an important message about comparing RCMs with its coarser-resolution driving data, as the model assessment should not only consider model performance but also the resolution of the model and the uncertainty in observations. As stated in the Introduction, the present chapter is a first step to assessing the AV of state-of-the-art RCMs over SA. However, to understand the potential added value of RCMs, further investigation should include the analysis of high-frequency temporal scales and small-scale spatial scales.

Chapter 3

The potential added value of Regional Climate Models in South America using a Multiresolution Approach

Resumen del capítulo

El objetivo de este capítulo es identificar aquellas regiones dentro del Continente Sudamericano en donde el clima observado presenta características regionales. Nos interesa particulamente aquellas escalas que pueden ser explícitamente simuladas por un Modelo Climático Regional (MCR) y no por su forzante global de menor resolución. De esta forma, se define el potencial valor agregado de los MCRs como aquella señal climática de mesoescala presente tanto en los datos observados como en las simulaciones regionales. Para ello, se propone un método de separación de escalas espaciales basado en la teoría wavelet. Una vez filtradas las longitudes de onda más gruesas, nos centramos en analizar la variabilidad espacial de la lluvia extrema y la variabilidad espacio-temporal de la temperatura máxima y mímina en base diaria. Además, evaluamos la manera en que 6 MCRs pertenecientes al Proyecto CORDEX representan el clima en dichas escalas. Los resultados confirman que los MCRs tienen el potencial de agregar valor en la representación de la precipitación extrema y la temperatura media superficial en Sudamérica. Sin embargo, esta condición no es aplicable en todo el continente, sino que es relevante en aquellas regiones terrestres que presentan una topografía compleja, en zonas de alta montaña y en las costas del continente. Los MCRs fueron capaces de simular la variabilidad de mesoescala presente en los datos observados, pero presentan una gran dis-

persión entre sí. Esta dispersión se identificó principalmente en los campos de precipitación extrema y en la componente transiente de la variabilidad de mesoescala de la temperatura máxima y mínima.

Abstract

The objective of this chapter is to identify those regions within the South American continent where the observed climate has regional characteristics. We are particularly interested in those scales that can be explicitly simulated by a Regional Climate Model (RCM) and not by its coarser-resolution global forcing. In this way, the potential added value of RCMs is defined as the mesoscale climatic signal present in both the observed data and regional simulations. For this, a spatial-scale filtering method based on wavelet theory is proposed. Once the longer wavelengths were filtered, we focused on analyzing the spatial variability of extreme rainfall and the spatiotemporal variability of maximum and minimum temperature on a daily basis. In addition, we evaluated how 6 MCRs belonging to the CORDEX Project represent climate in these scales. The results confirm that the RCMs have the potential to add value to the representation of extreme precipitation and average surface temperature in South America. However, this condition is not applicable throughout the continent but is relevant in those terrestrial regions that have a complex topography, in high mountain areas and on the coasts of the continent. The RCMs were able to simulate the mesoscale variability present in the observed data, but they showed a large spread between them. This dispersion was identified mainly in the extreme precipitation fields and the transient component of the mesoscale variability of maximum and minimum temperature.

3.1 Introduction

Regional Climate Models (RCMs) were developed in the 1960s as a downscaling technique to obtain regional climate information that could not be obtained from Global Climate Models (GCMs). Current computational resources allow the production of some limited high-resolution GCM simulations, but they are still costly and in most cases unpractical for data transfer and regional studies. For these reasons, RCMs continue being the most used tool by the community to produce high-resolution climate simulations. The benefits of increasing the resolution of the simulations are huge, and they include a better representation of landforms (e.g., to-

pography or land-sea mask), better spatial representativeness of the field (regional informa-tion) and a wider range of atmospheric processes explicitly simulated (Hong and Kanamitsu, 2014, Lucas-Picher et al., 2016).

However, many authors have concluded that increasing the resolution of the simulation do not always improves the representation of climate, but sometimes they even tend to de-grade it (Carril et al., 2002, Coppola et al., 2014, Feser, 2006, Giorgi et al., 2014, Menéndez et al., 2001, Roads et al., 2003, Mishra et al., 2017). Their results suggest that high-resolution is not required over some regions, and attribute it to the lack of small-scale physiographic forc-ings or mesoscale climate processes. Also, the use of RCMs comes with several drawbacks, such as issues concerning the simulation spin-up time, model physics, domain size and lat-eral boundary conditions (Giorgi and Mearns, 1999). Therefore, the key question associated to RCMs is whether they improve the representation of climate compared to its driving data. In this context, the added value (AV) definition arises as the ability of RCMs in simulating finer scale details than the driving data while reproducing the large-scale fields correctly (Feser et al., 2011, Di Luca et al., 2012, Laprise, 2003, Prömmel et al., 2010, IPCC, 2013).

A popular approach for addressing the AV of RCMs is through a spatial-decomposition of climate statistics into different resolution ranges. On the basis of this approach, there are three meaningful spatial ranges: the small-scales (SS) that can be resolved by the RCMs only, the large-scales (LS) resolved by both RCMs and GCMs, and the planetary scales (PS) resolved only by the GCMs which are transferred to the RCM by the lateral driving (Bresson and Laprise, 2009). Many works focus on the SS features, arguing that the RCM is not intended to improve the large-scale circulation of the driving data but is intended to add regional detail in response to regional scale forcing (Giorgi, 2006, Di Luca et al., 2012, Hong and Kanamitsu, 2014, Laprise, 2008, Denis et al., 2002a). Their findings suggest that the enhanced resolution of RCMs allows for a better description of mesoscale atmospheric dynamics and fine-scale surface forcing. The added value in SS is found especially where surface forcing is strong, such as near moun-tains or coastal regions with a sharp variation of surface properties (Feser, 2006, Feser et al., 2011, Di Luca et al., 2012, 2013a,b, Lo et al., 2008, Bresson and Laprise, 2009, Bielli and Laprise, 2007, Parker et al., 2015, Lenz et al., 2017, Di Luca et al., 2016).

When coming to spectral filtering to separate spatial scales, the Discrete Fourier Trans-form (DFT) is the most known technique. Fourier showed that any periodic function could be expressed as an infinite sum of periodic complex exponential functions. The problem of using the DFT in limited area fields is that they are usually aperiodic and present trends that

are probably associated with larger waves than the domain size (Feser et al., 2011). Hence, along with the study of AV arises the need for an adequate technique that separates different spatial scales in meteorological limited area fields.

Discussions regarding the best scale-separation technique to meteorological fields have dominated research in recent years. Errico (1985) proposed a variant of the DFT technique by previously removing the linear trend; however, this preprocessing of the field removes the large-scale gradient across the domain affecting the large-scale components of the spectrum. Denis et al. (2002a) suggested a better solution to the DFT problem by making a spectral transformation using the Discrete Cosine Transform (DCT). This technique uses a symmetrization process, which involves taking a mirror image of the original function before the application of the DFT, to solve the problem of aperiodic boundary conditions. The DCT was used by several researchers for scale separation (Denis et al., 2002b, Feser, 2006, Parker et al., 2015, Bresson and Laprise, 2009), due to the improvement of applying the DCT as a preprocessing procedure to eliminate spatial trends. However, using this technique has its disadvantages as it is not efficient working on singular perturbations and it may generate artificial wavy contributions.

Numerous works focus on finding the optimal weights for applying digital filters in meteorological limited area fields (Bettge and Baumhefner, 1980, Feser and von Storch, 2005, Shapiro et al., 1970, Shuman, 1957). These filters are effective and easy to use, but they require the election of coefficients that are obtained empirically with no mathematical background. In that regard, the discrete wavelet decomposition technique can be seen as a discrete filter technique but with one major advantage: it has a solid mathematical background. Mallat (1989) presented the Multiresolution Approach (MRA), a method that decomposes a signal into different resolutions through discrete wavelet transformations. The decomposition is simply obtained by successive highpass and lowpass filtering of the field. The wavelet approach applied in meteorological fields was used in several studies (Domingues et al., 2005, Liu et al., 2007, Desrochers and Yee, 1999, Jameson and Waseda, 2000, Yano et al., 2001, Di Luca et al., 2012), but only Di Luca et al. (2012) did it in the context of AV.

Di Luca et al. (2012) propose a slightly different version of the MRA presented by Mallat (1989). In their work, they aggregate the original high-resolution field into coarse-resolution ones of decreasing resolutions. After this aggregation, the results on the original grid and the virtually created coarser grids are analyzed to calculate the benefit of the higher resolution for different meteorological parameters. This way, the potential AV (PAV) of RCMs is assessed by

studying the SS variability of some climate statistics that would be absent on a coarser grid. The word "potential" accounts for the fact that no direct validation is performed between observations and the RCMs.

It is a fact that RCMs will be able to simulate high-resolution information over South America that is absent in a coarser-resolution GCM simulation. But we first need to evaluate if the observed climate statistics exhibit regional features. And then, if this features are well represented by the RCMs in the whole domain. We follow the methodology proposed by Di Luca et al. (2012) and Di Luca et al. (2013a) to answer the questions posted above.

We study the PAV of RCMs in SA to identify those land areas over the continent where observations meet a necessary condition: the presence of mesoscale features. We also evaluate the representation of this variability by RCM simulations from the Coordinated Regional Climate Downscaling Experiment (CORDEX). For this, we use the MRA as a scale-decomposition technique to isolate the SS variability of climate statistics obtained from observed and modeled daily precipitation and surface air temperature data.

This chapter is structured in five sections. The next one describes the RCM simulations and the gridded observations used in this study. Section 3 introduces the MRA for scale-separation of a field and the general framework used to evaluate the PAV of RCMs. An analysis of the MRA applied to atmospheric fields, together with the results of the PAV study are presented in Section 4. Our conclusions are drawn in the final section.

3.2 Database

This study includes six RCM simulations from the CORDEX Project and three gridded observed datasets. A brief description of the simulations is presented in Table 1. All RCMs were integrated over the region 1 domain of CORDEX (Fig. 3.1). They are hindcast simulations with their initial and boundary conditions provided by ERA-Interim (ERAi) reanalysis. The RCMs were driven with a coarse version of ERAi on a $1.5°$x$1.5°$ resolution, except for LMDZ4 and WRF341I that were driven by ERAi on a resolution of $0.75°$x$0.75°$. We use only hindcast simulations to minimize the effects of errors in the boundary driving fields, since we are evaluating the ability of RCMs in simulating the SS variability. We selected three strategic areas for a regional assessment (black boxes in Fig. 3.1): Tropical South America (TSA), Andes Cordillera (AC), and La Plata Basin (LPB). The first region, TSA, was selected since the monsoon system presents mesoscale phenomena, being therefore a potential region for AV. The grid points used are

those with heights between sea level and 1500 m above sea level. AC region was selected due to its surface properties, characterized by complex physiographic features. To understand PAV over high-terrain regions we consider only grid points with heights above 1500 m. LPB is a complex region, known for its large land-atmosphere interactions and the complex dynamic processes that modulate its variability. For this region, we consider only land grid points between sea level and 1500 m.
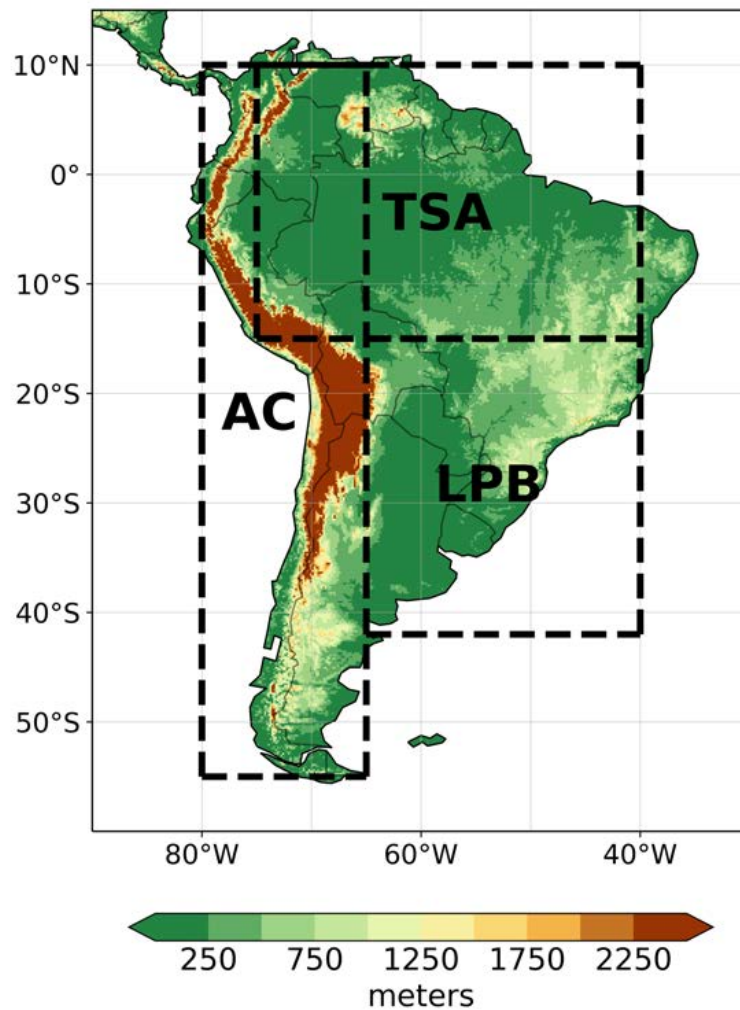
Fig. 3.1. CORDEX region 1 domain, with ETOPO2 (National Geophysical Data Center, 2006) terrain height (m) indicated in shading. Boxes in dotted-black lines denote areas selected for regional assessment.

The referece data include two daily gridded climate datasets from the Climate Prediction

Center (CPC; https://www.esrl.noaa.gov/psd/) and the TRMM_3B42 product (Huffman et al., 2007). For precipitation, we used CPC-UNI from CPC, that is a global daily unified gauge-based analysis (Xie et al., 2010). The dataset is constructed on a 0.125° lat/lon grid over the entire global land areas and released on a 0.5° lat/lon grid over the global domain for a period from 1979 to the present. Also, we include the maximum and minimum 2-meter temperature station-based analysis from CPC. The dataset is constructed alike the precipitation data. Finally, we consider the 7th version of the TRMM_3B42 product, from now on TRMM, that is a satellite-based and gauge-based gridded dataset. The product has a 3-hourly temporal resolution and a 0.25°x0.25° spatial resolution, starting in 1998 to the present. The spatial coverage extends from 50°N to 50°S.

The analysis is performed on a daily basis, for the period covering from 1990 to 2008, except for TRMM that is considered since 1998. Our chapter focuses on three surface variables, which are precipitation (pr), maximum 2-meter temperature (tasmax) and minumum 2-meter temperature (tasmin). The study seasons are austral summer (December, January, and February) and winter (June, July, and August). The RCMs and the observations are on different grids, and a propper RCM evaluation would require a remapping on a common grid. However, no direct comparison is performed and the statistics are calculated in their native grid. Our decision is based on the fact that an interpolation procedure affects the final field by smoothing it, especially for extreme events or over regions with complex surface forcing (see Falco et al. (2018) and Diaconescu et al. (2015)). We evaluate the RCM statistics considering a perfect model approach, i.e. no direct comparison with their driving data is performed, by following the PAV concept defined by Di Luca et al. (2012). We consider that the RCM simulations and CPC data have approximately the same resolution, near 50 km, regardless they are actually slightly different. The same applies to a downscaled version of TRMM when downgraded to a 0.5° resolution.

3.3 Methods

3.3.1 The Multiresolution Approach

References and modeled fields are decomposed into the sum of components on different spatial scales by performing a discrete 2D Haar wavelet decomposition. Wavelets, rather than Fourier transforms, were chosen because they are locally defined, and therefore more suit-

Table 3.1. Overview of Regional Climate Models used in the present study and their boundary conditions.

Experiment Acronym	RCM id / Reference	Type of grid	Resolution / Number of grid points
HadRM3P	MOHC-HadRM3P Gordon et al. (2000)	Rotated lat/lon	0.44°x0.44° 146x167
REMO2009	MPI-CSC-REMO2009 Jacob et al. (2012)	Rotated lat/lon	0.44°x0.44° 143x167
RCA4	SMHI-RCA4 Kupiainen et al. (2014)	Rotated lat/lon	0.44°x0.44° 146x167
RegCM4	ICTP-RegCM4-3 Giorgi et al. (2012)	Rotated Mercator	0.44°x0.44° 189x199
WRF341I	UCAN-WRF341I Skamarock et al. (2005)	Rotated lat/lon	0.44°x0.44° 146x167
LMDZ4	IPSL-LMDZ4 Hourdin et al. (2006)	Irregular rectangular lat/lon	~0.48°x~0.48° 184x180

able for representing discontinuous spatial fields characterized by the presence of mesoscale features. Wavelet transformations have a similar format to Fourier transformations, in the sense that the function/field is decomposed in several orthonormal basis functions. The main difference with Fourier is that the functions are wavelets, which are local, slightly smooth and non-periodic (Sifuzzaman et al., 2009). In this section, we present a brief overview of the MRA that consists on a pyramidal algorithm based on successive convolutions of a field with a discrete wavelet. For our purposes here we will confine our discussion to the Haar wavelet, but more details on this topic can be found in Desrochers and Yee (1999), Domingues et al. (2005), Jameson and Waseda (2000) and Mallat (1989).

As the name suggests, wavelets are small wave-like oscillations with an amplitude that begins at zero, increases, and then decreases back to zero. Wavelets are given by scaling functions ϕ, which play the role of average function or low-pass filter. The complementary details of the field will be given by an orthogonal wavelet, ψ, that play the role of high-pass filter. In our chapter, we use the Haar wavelet because it is conceptually simple, exactly reversible

and computationally cheap. Also, the Haar transform does not have overlapping windows, and reflects only changes between adjacent grid pairs. Therefore, this wavelet has the great advantage of being able to isolate very fine details in a field. For one dimension, x, Haar's scaling function $\phi(x)$ can be described as

$$\phi(x) = \begin{cases} 1 & \text{if } 0 \leq x < 1, \\ 0 & \text{otherwise.} \end{cases} \tag{3.1}$$

$\phi(x)$ is a lowpass filter with coefficients $\left[\frac{1}{2}, \frac{1}{2}\right]$, and its convolution with a function will produce a less detailed approximation of the latter. In practice, each grid-point of the field in the dimension x will be averaged with the adjacent one. In two dimensions, x and y, a two-dimensional scaling function $\phi(x, y)$ is required for field decomposition. The 2D wavelet can be constructed as the product of separable scaling function

$$\phi(x, y) = \phi(x)\phi(y). \tag{3.2}$$

The complementary details can also be obtained by convoluting the field with a two-dimensional orthogonal wavelet function $\psi(x, y)$, constructed as $\psi(x)\psi(y)$, together with the covariances terms $\phi(x)\psi(y)$ and $\psi(x)\phi(y)$.

Decomposition starts in the highest resolution, and the convolution between $\phi(x, y)$ and the original field will result in an average of the field in both directions (Fig. 3.2b). Following Nyquist's rule, it is clear that taking a grid each two results in no loss of information (Fig. 3.2c). Therefore, the process leads to a sub-sampling from 50 km resolution (level 0) to a 100 km resolution (level 1). Also, from a practical viewpoint, the complementary details can be obtained simply by calculating the difference between the original field and the approximated field (fig 2d). The process of sub-sampling can be repeated recursively. Each new level of approximation will result in a dyadic degradation of the resolution, e.g. from 50 km to 100 km, from 100 km to 200 km, and so on.

3.3.2 AV and PAV indices

The metrics used in this chapter compare the simulation fields at different resolutions by using different climate statistics that are variable-dependent. Their formulation is determined on the basis of a comprehensive analysis of the expected AV in high-resolution simulations and the results found in previous works. All proposed metrics are calculated within the PAV concept, meaning no quantitative validation with observations is performed. The reasons to
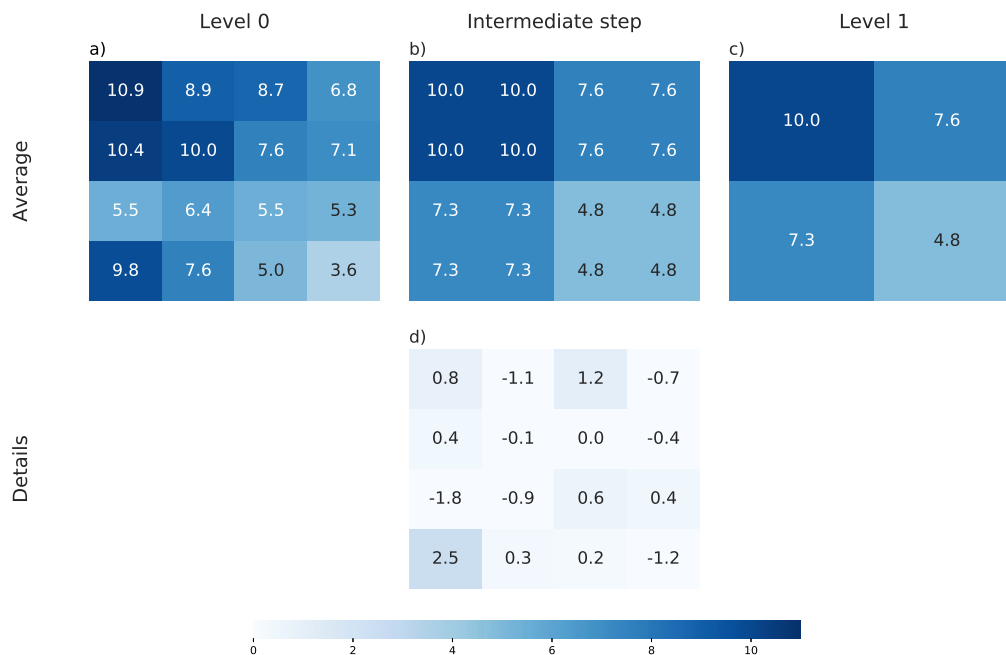
Fig. 3.2. Conceptual example of a sub-sampling technique from level 0 to level 1. Each column represents a different step in the degradation process, starting from the original field to a downscaled one (a to c). The first row depicts the average fields, while the second row depicts the sum of the vertical, horizontal and diagonal details (d).

consider only the PAV are two: i) because we use the raw grid of each model and dataset, and ii) because we analyze spatial scales smaller than the effective resolution (Skamarock, 2004). Resolutions smaller than the effective resolution are those where the model's kinetic energy spectra has a deviation to the observed one. This deviation from observations is due to energy removal by the model's dissipation mechanisms. Hence, a direct comparison with observations should also account for the effect of model's dissipation in the SS energetics, and is beyond the scope of this chapter. The following subsections present a detailed approach of the metrics used for each variable.

Precipitation

There is a general consensus in literature that the AV of RCMs in simulating precipitation is expected in high-order statistics, such as more intense or localized weather events (Bielli and Laprise, 2006, Gibba et al., 2018, Giorgi et al., 2014, Laprise, 2008). The empirical probability density function (EPDF) is a good example to illustrate the AV of RCMs in precipitation (Giorgi
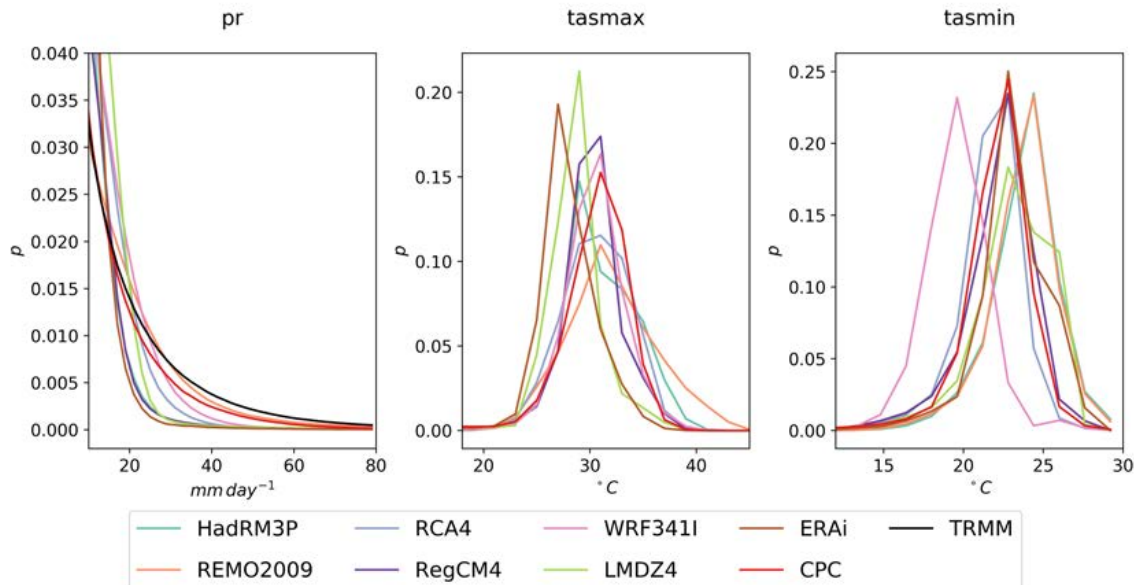
Fig. 3.3. Empirical distribution of daily intense precipitation events (left panel) and maximum and minimum daily surface air temperatures (central and right panels, respectively) for Tropical South America during the austral summer. The selected region is depicted in Fig. 3.1.

et al., 2014, Coppola et al., 2014). Hence, we present the EPDF of pr (pr>10 mm day^{-1}) for all individual RCM simulations, together with ERAi reanalysis and observation datasets (Fig. 3.3, left panel). The EPDF was calculated using summertime daily data of all grid points over the TSA region (Fig. 3.1). We show only the tail of the EPDF (pr intensities larger than 10 mm day^{-1}). We find that all RCMs have a higher-skill in reproducing the observed precipitation distribution tail compared to ERA-Interim. Similar results were found in other works (Coppola et al., 2014, Giorgi et al., 2014), and can be related to the representativeness error of the field, meaning the inability of a model to reproduce the sub-grid variability (see Falco et al. (2018) and Kanamitsu and DeHaan (2011)).

Any climate statistic X processed through the MRA will give several coarser-resolution versions of it, from a level 1 decomposition with a resolution of 100 km to a level N_0 decomposition with a resolution of $50 * 2^{N_0}$. Each field is identified as X_r with r the level of decomposition; hence, X_0 is the original field on a 50 km resolution, X_1 is the degraded field on a 100 km resolution, and so on. N_0 is the coarsest grid, close to the size of the domain (e.g. X_{N_0} is a constant field). Therefore, the MRA enables us to have a multi-scale dataset with $N_0 + 1$ simulations for each model. We limit the downscaling to a level 3, meaning we have a total of four simulations for each model: 50 km, 100 km, 200 km, and 400 km resolutions. TRMM has

a higher resolution than the RCMs, so the MRA is applied until level 4, with the level 1 degradation simulating the original field. We follow Di Luca et al. (2012) methodology and define the $pr_{95,r}$ statistic to analyze the dependence of precipitation on resolution. $pr_{95,r}$ is calculated as the 95th percentile of daily precipitation data at each spatial scale r by considering only wet events, meaning days with intensities larger that 1 mm day^{-1}. To directly compare the statistic between the original resolution and a downscaled one, we recalculate $pr_{95,0}$ statistic including precipitation values of all the grid points inside the downscaled grid. We define the PAV index for precipitation as

$$PAV(r) = pr_{95,0} - pr_{95,r} = pr_{95,r}^{SS} \tag{3.3}$$

where $pr_{95,r}^{SS}$ are the details of pr_{95} from 50 km to $50 * 2^r$ km. Assuming that $50 * 2^r$ km is the resolution of a GCM, the PAV index can be interpreted as the SS variability of extreme precipitation that is resolved only by the RCM and, thus, can be seen as the PAV of RCMs over a coarser-resolution GCM. We also define the relative PAV, rPAV, in order to normalize the index

$$rPAV = \frac{PAV}{pr_{95,0}}. \tag{3.4}$$

rPAV vary between 0 and 1, and measures the percentage of the total extreme precipitation variablity explained by the small scales. A value of rPAV near zero means that the SS are negligible over the area, and a value near one indicates that all extreme precipitation intensity is determined by SS.

Surface air temperature

The mean climatology of surface air temperature variables are highly influenced by surface forcings, as exhibited by the EPDFs of tasmax and tasmin (Fig. 3.3). ERAi's tasmax EPDF suggests a systematic cold bias compared to CPC in reproducing the daily maximum temperatures over the tropics (Fig. 3.3, central panel). Also, the distribution is narrower than the observed, suggesting differences in the variability. The representation of the distribution peak is rectified by all RCMs, indicating a better representation of the median observed value for tasmax. The improvement is not so evident when analyzing the spread of the distribution, in that some have a narrower distribution than the observed, while others have a wider range. Therefore, AV in tasmax can either be associated to stationary or transient characteristics of mesoscale processes, as suggested by other authors (Feser, 2006, Laprise, 2008, Lee

and Hong, 2013, Prömmel et al., 2010). Finally, ERA-Interim has a good representation of the observed tasmin distribution and no apparent AV of RCMs is found (Fig. 3.3, right panel).

Associated to each level of decomposition r, X can be separated in two components, the SS and the LS, that is

$$X_r = X_r^{SS} + X_r^{LS}. \tag{3.5}$$

$50 * 2^r$ is the cutoff resolution that divides the SS with the LS, X_r^{SS} is the detail field from 50 km to $50 * 2^r$ and X_r^{LS} is the lower-resolution field from $50 * 2^r$ to $50 * 2^N$. Following Di Luca et al. (2013a), we decompose the temporal dimension of tasmax and tasmin through a Reynolds decomposition of Eq. (5) and obtain

$$X_r = \overline{X_r^{LS}} + X_r^{LS\prime} + \overline{X_r^{SS}} + X_r^{SS\prime} \tag{3.6}$$

where the overline represents the temporal mean and the prime the temporal fluctuation of each term. By assuming that the temporal fluctuations of the large-scales are independent of the spatio-temporal fluctuations, i.e. the co-variances terms are negligible, and noticing that the variance of the mean large-scales is zero, then the variance of Eq. (6) can be expressed as,

$$\sigma^2 = Var\left(X\right) = Var\left(X_r^{LS\prime}\right) + Var\left(\overline{X_r^{SS}}\right) + Var\left(X_r^{SS\prime}\right) = \sigma_{r,t}^{LS2} + \sigma_{r,s}^{SS2} + \sigma_{r,t}^{SS2} \tag{3.7}$$

with $\sigma_{r,t}^{LS2}$ denoting the temporal variance of the LS, $\sigma_{r,s}^{SS2}$ the spatial variance of the SS, and $\sigma_{r,t}^{SS2}$ the temporal variance of the SS. Let's remember that the scale division into LS and SS depend of the cutoff resolution r. The first term, $\sigma_{r,t}^{LS2}$, can be interpreted as the temporal variability resolved by a GCM of resolution $50 * 2^r$. The other two terms, $\sigma_{r,s}^{SS2}$ and $\sigma_{r,t}^{SS2}$ represent the stationary and transient components of the variability originated from the SS. Hence, the potential added value of an RCM can be defined as

$$PAV(r) = \sigma_{r,s}^{SS2} + \sigma_{r,t}^{SS2}, \tag{3.8}$$

and the contribution of the SS variability to the total variability is

$$rPAV = \frac{PAV}{\sigma^2}. \tag{3.9}$$

3.4 Results

3.4.1 The Multi-resolution approach applied to meteorological fields

The scale-separation of a limited-area field is sensible to the filtering technique used. Because wavelet methods have only relatively recently been used in climatology (Domingues et al.,

2005), we first need to evaluate if this method is appropriate for spatial decomposition. In this section we assess the MRA from a mathematical perspective to glean a better understanding of the proposed method.
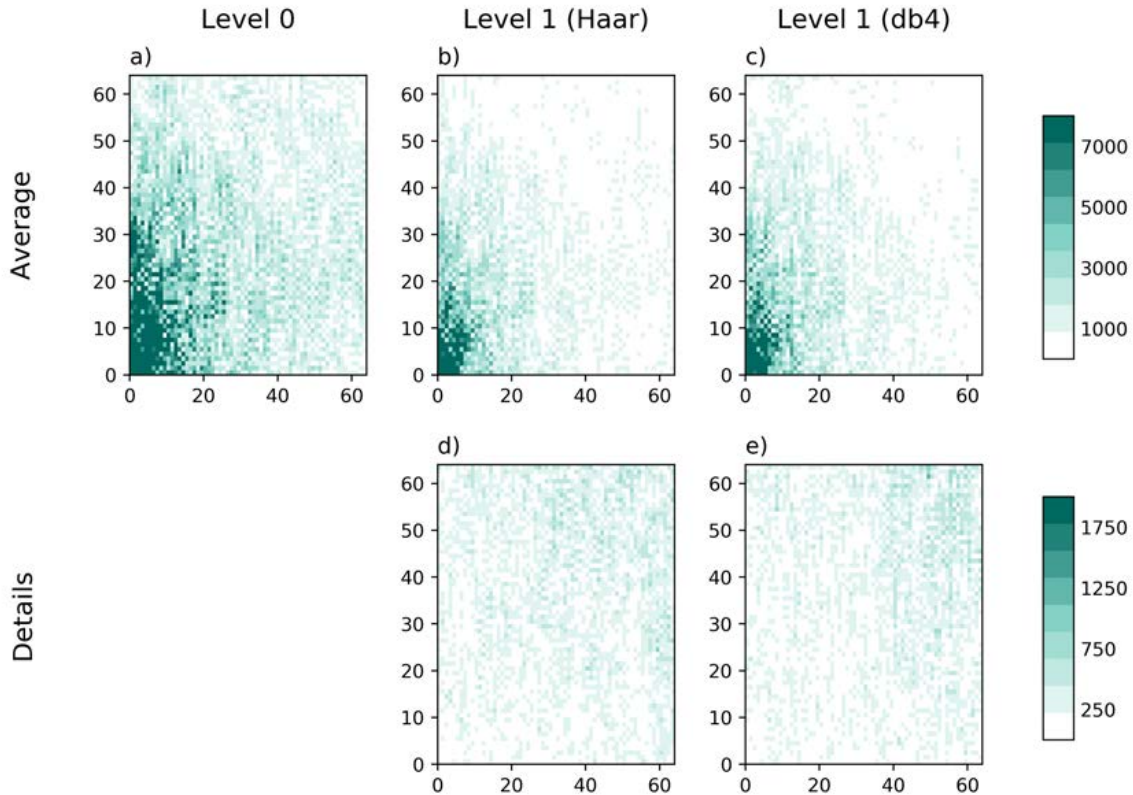
Fig. 3.4. Two-dimensional Fast-Fourier-Transform spectral analysis of a precipitation field subsampling from level 0 to level 1 using two different wavelets. The field selected is from TRMM for the day 20/01/1998. The spectrum are shown for the original field (a), the approximation field using Haar wavelet (b), the approximation field using db4 wavelet (c), the detail field using Haar wavelet (d), and the detail field using db4 wavelet (e). The axes show the zonal wavenumbers k (x axis) and the meridional wavenumbers l (y axis) corresponding to the limited domain.

A two-dimension spectral analysis of the original and filtered fields can give an insight of changes in the wavelength content after the processing. This analysis allows us to understand how wavelets separate the small-scales from the largest ones. There is also a need to analyze the characteristics of different wavelet filters and determine how they compare to one another (Figs. 4 and 5). Therefore, the spectral transformation of a daily accumulated pr field after the convolution with two different wavelets, Haar wavelet and Daubechies 4 wavelet (db4; Daubechies, 1988), is presented (Fig. 3.4). The original power spectra have an

anisotropic nature, with the largest variability present in the meridional direction (Fig 4a). The spectrum also has a significant spread to the whole range of the horizontal scales, indicating not only the presence of large-scale features but also of small-scales. This result is expected, as the pr field of one particular day has a very different structure than the mean climatology, showing sparse relative maximum values throughout the continent (not shown). The spectra of the approximated fields after convoluting with both wavelets are very similar, indicating that the scale function wavelets have a similar effect on the field (Figs. 4b and 4c). The same happens to the detail spectra (Figs. 4d and 4e).
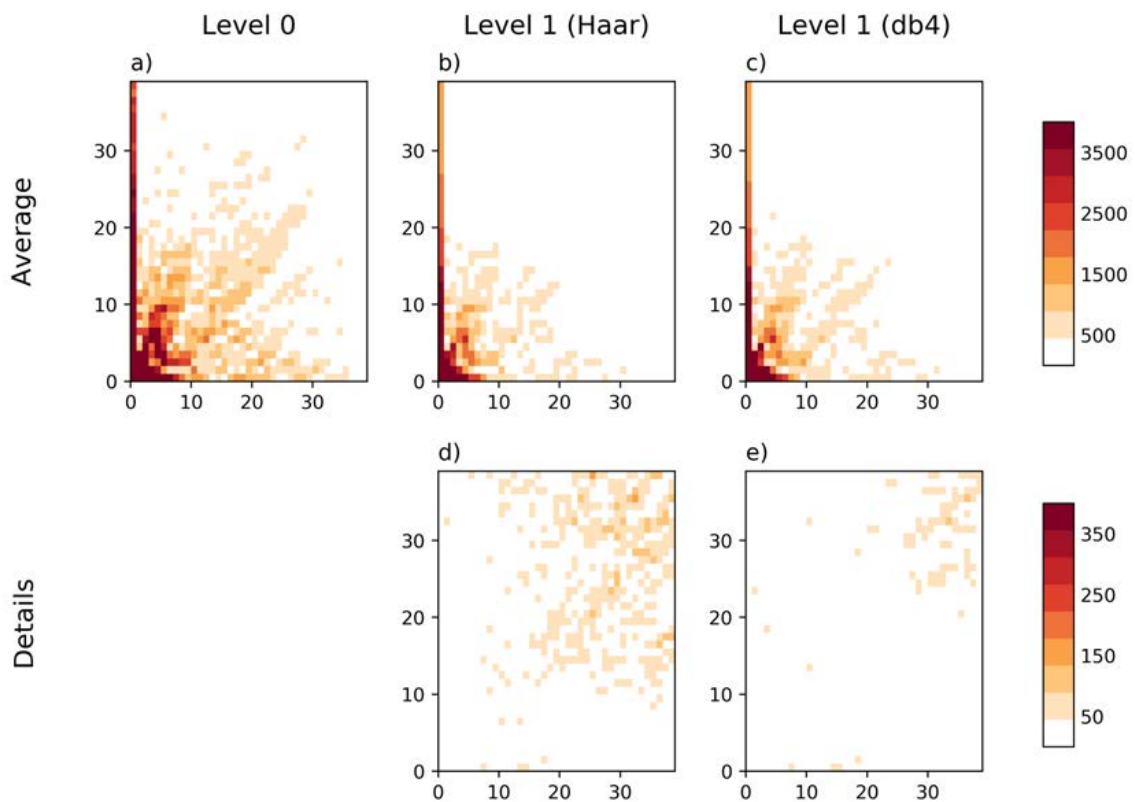
Fig. 3.5. The same as Fig. 3.4 but using a maximum 2-meter temperature field from WRF341I for the day 10/01/1990.

The spectrum of a daily tasmax field is very different from the pr one since it is strongly confined to the largest scales (Fig. 3.5). The power of the original field decreases quasi-radially from the largest scale (small wavenumbers) components to the smallest scale (large wavenumbers) components. A very large anisotropy is also detected, corresponding to large scales in the zonal direction and all scales in the meridional direction. This anisotropy is related to the expected large meridional gradient of the field. The wavelet transformation

spectrum shows an even more concentrated spectrum in the lowest wavenumbers (Figs. 5b and 5c). Contrary to pr, the transformation differs when using different wavelets, being Haar wavelet able to separate better the small-scales from the largest ones (Figs. 5d and 5e). Because of this property, together with the ones listed in the methods section, we conclude that the Haar wavelet decomposition is an appropriate filtering technique to distinguish the mesoscale features of a field from the larger-scale ones.

3.4.2 Potential for added value in South America

All PAV indices proposed in the methods section vary with resolution. The downscaling of the field to coarser resolutions will smooth the field in every new level of decomposition, and new details will be added to the SS variability. However, these indices depend also on other factors such as the season, region, model, and variable.

We first study how these indices change with resolution, region and season (Figs. 6 and 7). Independently of the season and variable, all index increase as the resolution decreases, as expected, but some regional differences are seen. In the warm season, the differences in PAV are usually maximal for the degradation between 50 km and 100 km, whereas they decrease when downscaling to a very coarse grid from 200 km to 400 km (Fig. 3.6, left panels). If we consider TRMM as the reference, CPC-UNI together with REMO2009 are both the datasets with the best skill in representing the values and shapes. An exception is over AC region, where REMO2009 highly overestimates the SS variability of extreme pr. All other models, except for LMDZ4, have the same deviations. On the contrary, all models misrepresent the spatial variability of SS extreme precipitation in TSA and LPB by underestimating it.

The shape of summer tasmax PAV curves differs significantly with the region (Fig. 3.6, central panels). The stationary PAV seems to have a maximum increase between 50 km and 100 km in the tropics and the Andes, but not in LPB where the relation with resolution appears to be linear. Also, the transient term appears to have a linear relationship with resolution in all regions studied, and its contribution to PAV are modest. In TSA and AC, the transient tasmax PAV is always smaller than the stationary term, and the differences maximize in the AC region. When comparing the RCMs with CPC data, we see that the most substantial differences in PAV are found in the AC region, where many models overestimate the spatial SS variance. Similar results to the ones found for tasmax are valid also for tasmin PAV (Fig. 3.6, right panels). An exception is LPB, where the stationary term is always larger than the transient term.

Generally speaking, winter results are very similar to summer ones (Fig. 3.7). The shapes
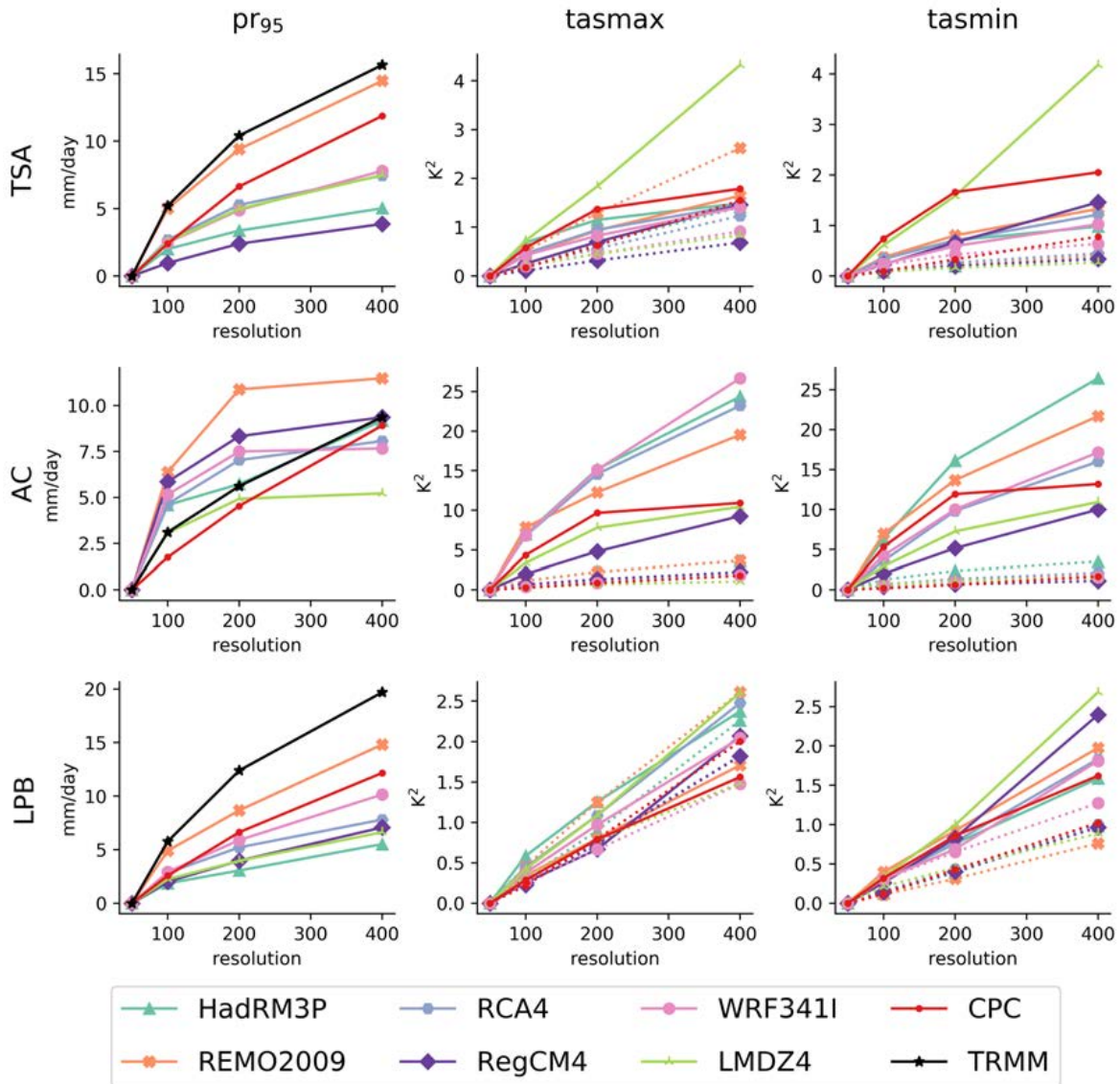
Fig. 3.6. Regional-mean values of PAV measure in summer (DJF) as a function of resolution. Each column correspond to a different variable, pr_{95} (left panels), tasmax (middle panels) and tasmin (right panels), and each row to a different region. The tasmax and tasmin PAV index are split into the stationary term (full lines) and the transient term (dotted lines).

of the pr_{95} curves are very similar to summer, and model deviations from TRMM also. However, in this season, the LMDZ4 appears to be the one between the RCMs with the best skill in reproducing the PAV index, especially over LPB. Regarding tasmax and tasmin curves, the stationary component continues being larger than the transient component for TSA and AC regions, with the difference maximizing in this last region. Also, when compared to CPC, all

models underestimate the SS stationary variability of tasmax and tasmin over the tropics except LMDZ4 model that largely overestimate it.
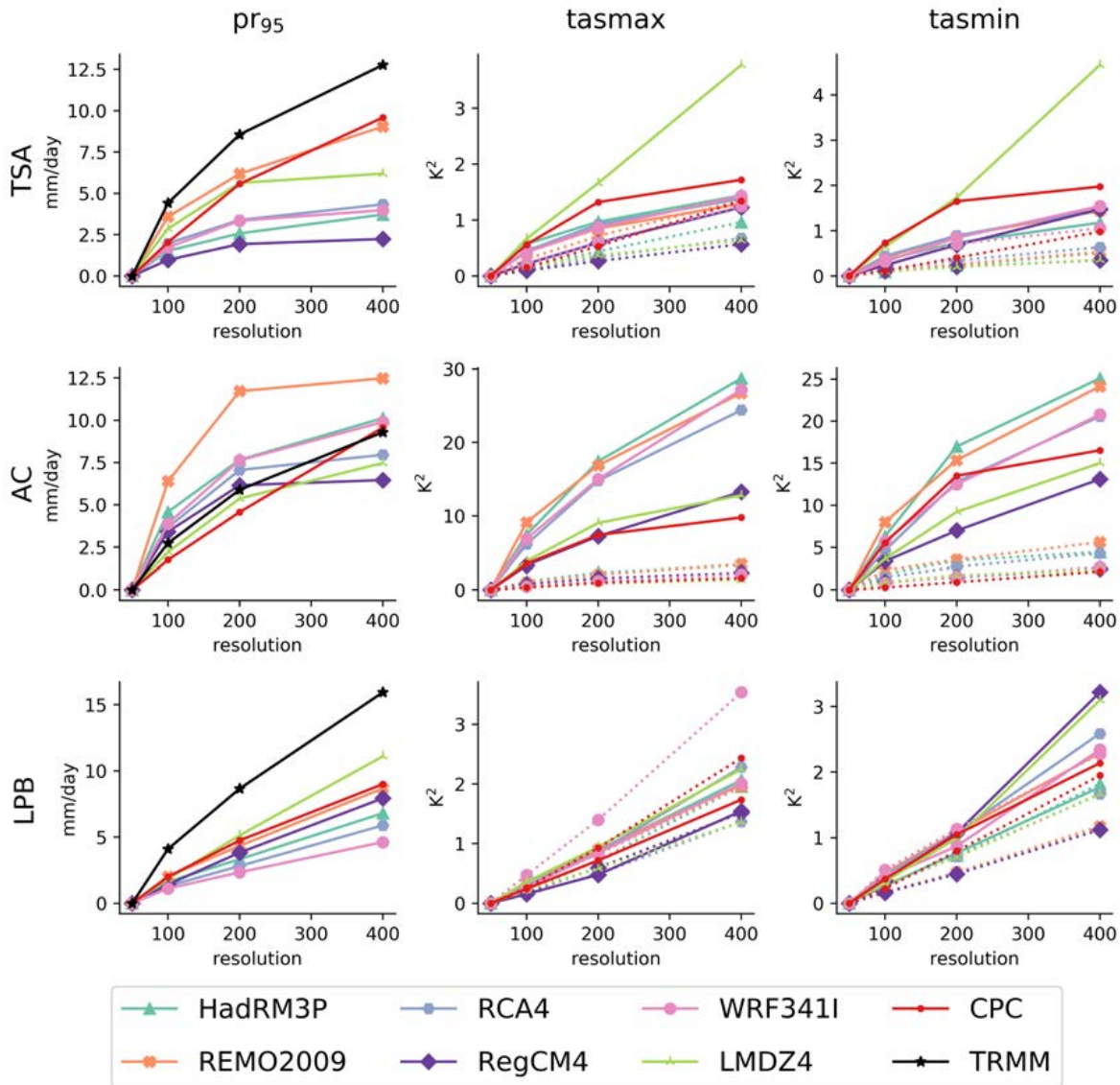
Fig. 3.7. The same as in Fig. 3.6 but for the winter (JJA) season.

As seen in the previous figures, the largest differences between the original field and the downscaled versions are in the highest resolutions. We select a level 2 of downscaling to calculate the PAV indices, meaning that the forthcoming analysis will focus on the scales between 50 km and 200 km. We continue our investigation by studying the spatial distribution of the PAV indices for both seasons, calculated following Eq. (3) for pr_{95} and Eq. (8) for tasmax and tasmin (Figs. 8, 9 and 10).

The spatial distribution of PAV derived from pr_{95} indicates a significant inter-dataset spread (Fig. 3.8). The PAV differences are more sensitive to the model or dataset used than the season considered and therefore hinders the understanding of this index. Focusing on TRMM, PAV values are large over the whole domain studied, except over the southern Pacific Ocean. Also, PAV maximizes over LPB for both seasons and the tropics in summer. The majority of the RCMs do not capture the SS variability observed over LPB; they do, however, exhibit higher PAV values in the tropics during summer (e.g., Brazil) than in winter. This seasonal difference may be associated with the existence of small-scale convection systems during the active phase of the SAMS. On the other hand, when comparing to TRMM, all RCMs and CPC data underestimate the PAV values, except over the Andes Cordillera where models tend to overestimate its magnitude.

The spatial distribution of the SS stationary variance ($\sigma_{2,s}^{SS}$) indicate that most of the variability is located over regions with complex topography and coasts (first and third rows in Figs. 9 and 10). On the contrary, SS is negligible over the oceans. These results are independent of the season and coincide with Di Luca et al. (2013a) when analyzing the same term over the United States with other RCMs. The variability over regions with complex high-mountain topography is associated to an altitude effect that induces large mean horizontal temperature gradients between adjacent grid pairs. On the other hand, the $\sigma_{2,s}^{SS}$ signal over the coasts is related to a thermal contrast between the continent and adjacent oceanic grid points. Unfortunately, this last effect cannot be evaluated using CPC, as it is constructed only over land areas. These stationery features are well represented by all RCMs, with similar values and spatial variability. LPB is another region with $\sigma_{2,s}^{SS}$, identified for both variables (tasmax and tasmin) and both seasons. The presence of SS stationary variance over southeast Brazil is probably due to the presence of the Brazilian Highlands (Fig. 3.1), but its magnitude is small and is not equally represented by all RCMs. In that sense, while some models show considerable SS variability, such as the HadRM3P model, others show almost no signal, such as the RegCM4 model.

The spatial distribution of the SS transient variance ($\sigma_{2,t}^{SS}$) is more complicated than the stationary one, in the sense that many processes can introduce this type of variability. We can also identify substantial inter-model differences, intra-seasonal differences and differences between tasmax and tasmin statistics associated to this term (second and last rows in Figs. 9 and 10). However, broadly speaking, the transient SS variability is smaller than its stationary counterpart, and it can usually be found in the extratropics, especially over the AC and

sometimes over Patagonia. The large inter-model spread makes it difficult to gain insight into the dominant processes, but they may be related to frontal passages. This last statement is more evident for tasmin variable, where $\sigma_{2,t}^{SS}$ in winter over the extratropics are usually larger than in summer for all models (Fig. 3.10). Also, the signal is found over the coasts for all RCMs and suggests the influence of land-sea contrast again. As was found for the stationary term, the SS transient variability is also negligible over the oceans. Using CPC as a reference, the RCMs are not able to reproduce the spatial distribution of $\sigma_{2,t}^{SS}$ (Fig. 3.9). However, tasmax SS variability in middle-latitudes during winter (e.g., 20°S-40°S) is maximum for both CPC data and the RCMs. Regarding tasmin SS transient variability, CPC has negligible values over all the continent during summer and small values in the winter. All models show larger values than the reference, especially over central and southern Andes and over Patagonia.
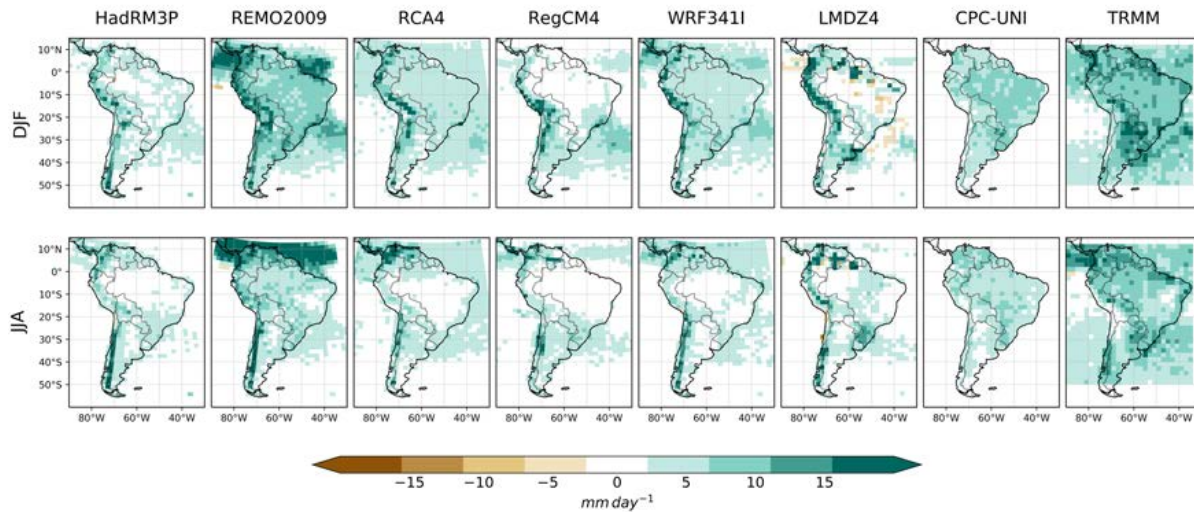
Fig. 3.8. Spatial distribution of pr PAV ($pr_{95,200}^{SS}$) for summer (DJF; top panels) and winter (JJA; bottom panels). Each column correspond to a different dataset.

The results presented above consider the absolute values of the PAV indices, which are also related to the total variability of the field. The normalization of the index allows to compare the PAV values between different regions and summarize the contribution of the SS variability to the total variability of the field. Therefore, we calculate the spatial-mean rPAV indices over each region and season following Eq. (4) for pr_{95} and Eq. (9) for tasmax and tasmin (Fig. 3.11). The following analysis is also carried out for a level 2 of decomposition, meaning the SS corresponds to the spatial scales between 50 km and 200 km.

During summer, results for the pr_{95} rPAV metric show that the median contribution of the
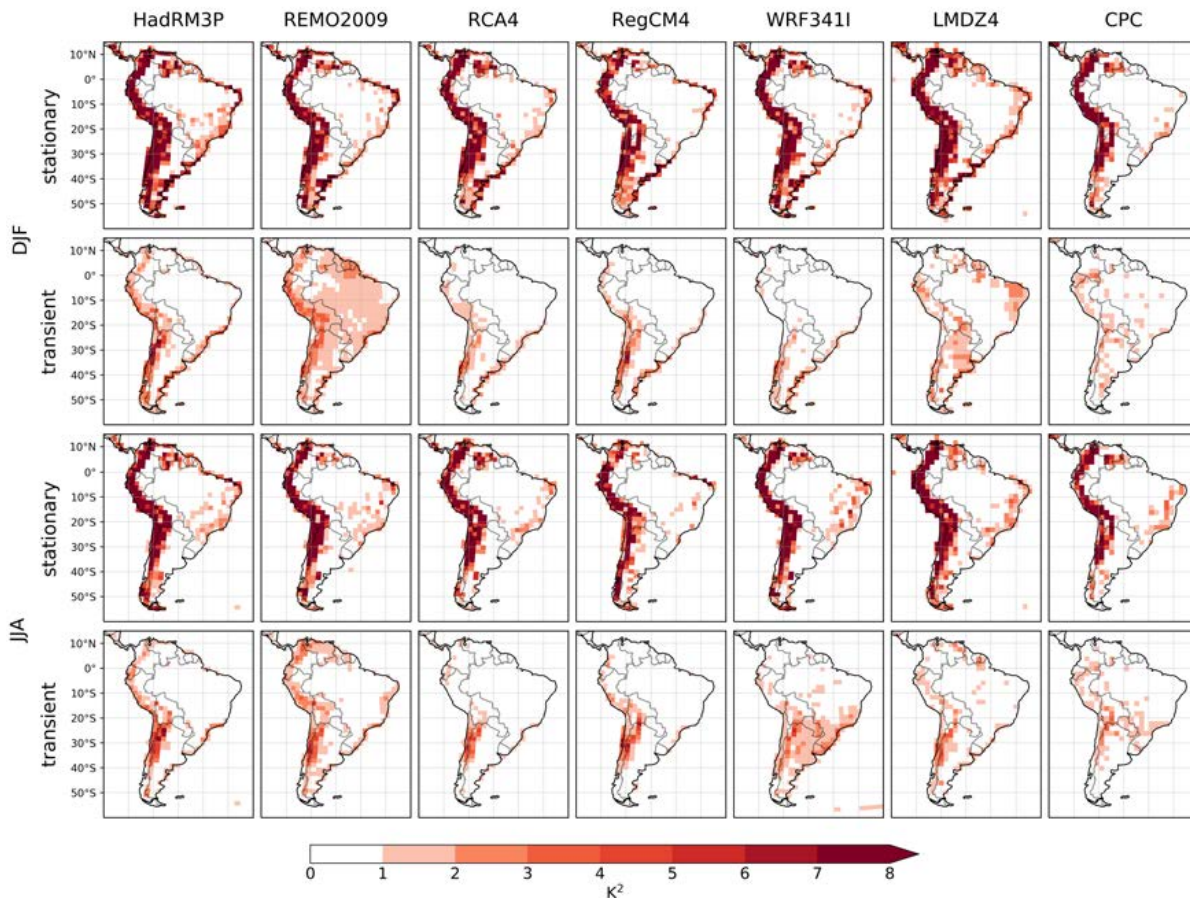
Fig. 3.9. Spatial distribution of the stationary ($\sigma_{200,s}^{SS}{}^2$; first and third row) and transient ($\sigma_{200,t}^{SS}{}^2$; second and third row) SS variance of tasmax in summer (first two rows) and winter (last two rows). Each column correspond to an individual model, except for the last column that correspond to CPC.

SS variability to the total pr_{95} variability is of approximately 20%, 31% and 17% for TSA, AC and LPB regions, respectively. This implies that high resolution is relatively important for simulating the spatial structure of extreme precipitation, especially over areas with complex topography. However, TRMM and CPC data suggest that the rPAV index for extreme rainfall is not very sensitive to the region studied. Contrarily, RCMs tend to have large rPAV values over the AC region, overestimating the observed pr_{95} variability, while having small amounts over TSA and LPB, underestimating the observed SS relative contribution. Results for the cold season indicate that the rPAV mean value for pr_{95} is approximately of 25%, 32% and 18% for TSA, AC and LPB regions, respectively. Thus, the relative contribution of the SS is slightly higher in winter than in summer. Again, the RCMs tend to overestimate the SS variability over the Andes and underestimate it elsewhere. Also, TRMM data suggest that the relative contribution
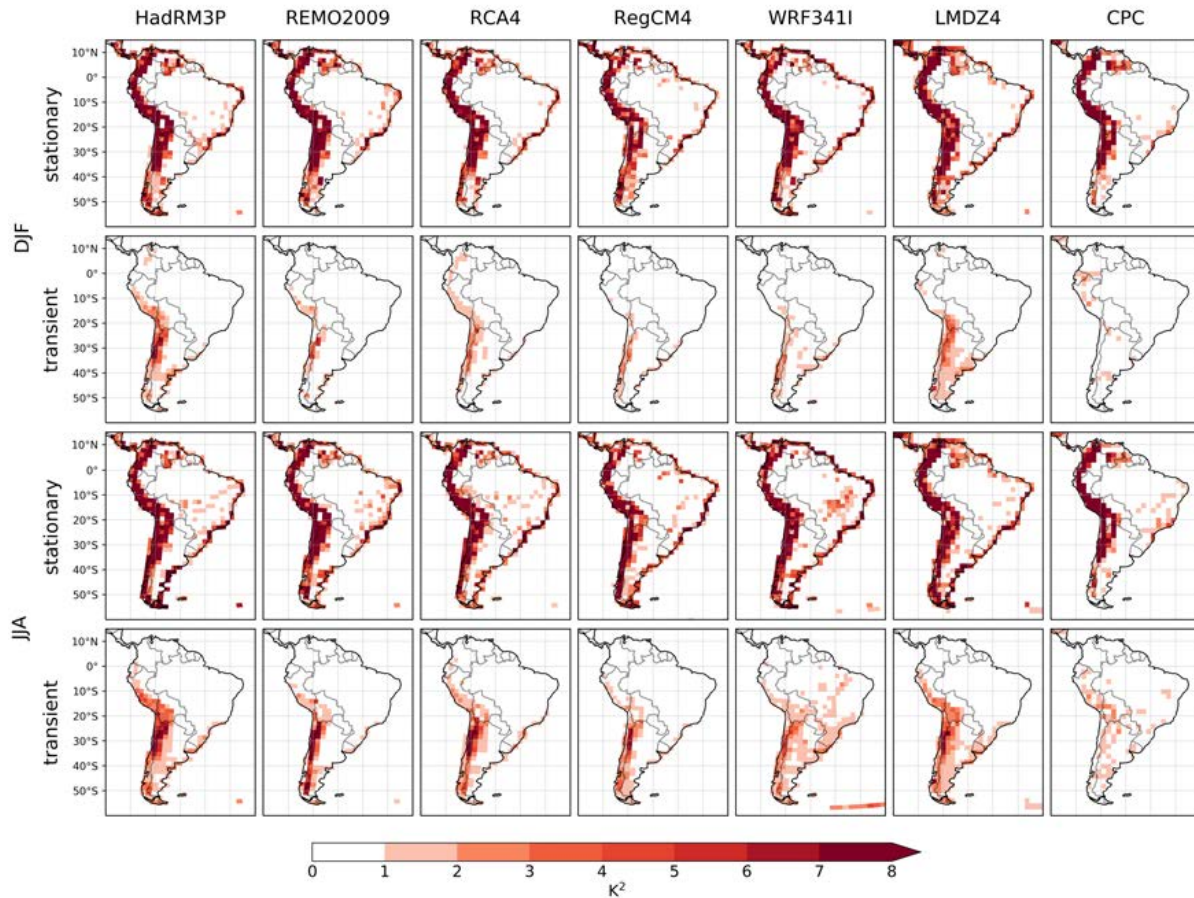
Fig. 3.10. The same as in Fig. 3.9 but for tasmin variable.

of the SS variability is more important in the tropics than in high altitudes and over LPB.

For the tasmax variable, the rPAV metric during summer shows that the SS variability contribution (the total contribution of the stationary and transient terms) is of a 28%, 71% and 15% to the total variability for the TSA, AC and LPB regions, respectively. The largest spread between models is found over the AC region, ranging from about 50% to 80%. However, all data show large percentages over the area, indicating the huge importance of the SS in representing the total tasmax variability over high-terrain areas. According to previous results, most of the signal is associated with the stationary component of the SS. On the contrary, rPAV percentages over TSA and LPB regions are small. In LPB, this is partly because the total variability over the region is large in both seasons (not shown), and that the stationary component is small. Compared to CPC data, models tend to underestimate the SS variability over TSA except for LMDZ4 that overestimate it, and overestimate the SS variability over the AC region. During winter, the SS contribution to the total variability is smaller than in summer,

showing median values of 18%, 65% and 7% for the TSA, AC, and LPB, respectively.

The median contribution of tasmin SS variability to the total one is of 50%, 76% and 20% for the TSA, AC, and LPB, respectively. Hence, rPAV from tasmin is much higher than from tasmax in the tropics (i.e., TSA). This result is related to the fact that the total tasmin variability is much smaller than the total tasmax variability (not shown), whereas the PAV values are in the same order of magnitude. The representation of rPAV by the RCMs when comparing with CPC is similar to the results found for tasmax. Again, the SS contribution to the total variability is smaller during the winter, with median rPAV values of 37%, 71% and 11% for TSA, AC, and LPB, respectively.
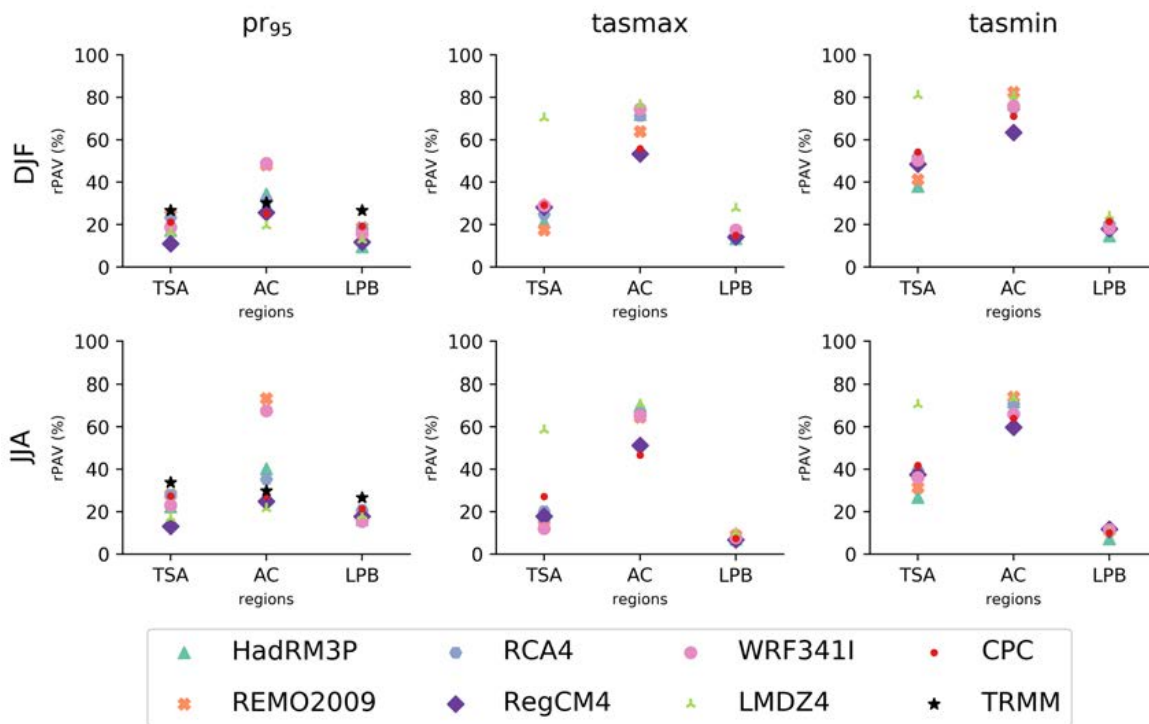
Fig. 3.11. Regional-mean values of rPAV for summer (DJF; top panels) and winter (JJA; bottom panels).

3.5 Concluding remarks

The purpose of this study was to evaluate the potential for added value of Regional Climate Models in simulating mesoscale features present in the observed climate of South America. To this end, we followed the methodology proposed by Di Luca et al. (2012) for daily precipitation data and Di Luca et al. (2013a) for daily maximum and minimum surface air temperature

data. The domain covered the South American continent, and the analysis was performed using six RCM simulations from the CORDEX Project, together with TRMM and CPC as observations for evaluation purposes. The seasons selected were austral summer and winter, covering a time period from 1990 to 2008 except for TRMM that was considered since 1998.

Our filtering technique was slightly different from the one used by Di Luca et al. since we followed the traditional Multiresolution Approach proposed by Mallat (1989). The methodology appears to be stable regardless of the wavelet used. We selected the Haar wavelet for our analysis because it is conceptually simple and reflects only changes between adjacent grid pairs, making it suitable for isolating very fine details in a field.

Mesoscale variability associated with precipitation is usually expected for high-order statistics such as extreme precipitation. The results showed that PAV associated to extreme pr is contained in all CORDEX simulations and observed datasets presented. For each data, the PAV increased when decreasing the resolution of the field. The gain of PAV appeared to follow an exponential relation with resolution, being higher when decreasing from 50 km to 100 km than from 200 km to 400 km. When considering the spatial distribution of PAV index from TRMM, results indicate a small spatial and seasonal sensitivity. However, careful attention must be paid in generating conclusions with TRMM as some studies suggest that satellite-retrieved products have some limitations in detecting extreme events (AghaKouchak et al., 2011, Scheel et al., 2011, Su et al., 2008). Contrarily to TRMM results, most of RCMs have high PAV values over the Andes Cordillera and all of them smaller than TRMM values elsewhere. The overall results indicate that PAV associated with extreme precipitation is located over land areas, especially over regions with complex topography or areas with meso-scale phenomena. Our findings are in line with the ones of Di Luca et al. (2012) by showing a little variation of PAV between different regions, and with larger values of PAV during summer.

The potential for the added value associated with maximum and minimum surface air temperature was assessed differently from precipitation. The PAV index was defined as the sum of two terms: the small-scale stationary variance and the small-scale transient variance. Except over LPB, the PAV index showed a similar sensitivity to resolution for both variables and seasons by presenting larger PAV values from 50 km to 100 km than from 200 km to 400 km, which is coincident with the results found by Lenz et al. (2017). Also, the variability associated with stationary small-scale features is always higher than the one related to transient features. LPB show very different results compared with the other regions since PAV appears to have a linear relationship with resolution and the transient PAV is not always smaller than

its stationary counterpart. When assessing the spatial distribution of PAV, results were very similar to the ones found by Di Luca et al. (2013a) in the United States, and by Lenz et al. (2017) in Europe. The PAV fields revealed that most of the stationary signal could be seen over regions with complex topography and land-sea contrast. The transient signal is usually small compared to the stationary counterpart, and its large inter-model dispersion hinders its understanding. However, transient PAV is generally found over those latitudes where the surface temperature has large meridional gradients, suggesting the signal is related to frontal passages. Also, a land-sea contrast is detected by all RCMs.

rPAV results suggest that the most considerable contribution of high-resolution can be expected over regions with complex topography such as the Andes Cordillera for all three variables. The results for TRMM indicate that the contribution of SS to the total extreme precipitation variability is in the order of 30% and have little regional sensitivity. Also, in contradiction with Di Luca et al. (2012), rPAV for extreme pr is higher in winter than in summer. However, we consider a broad range of latitudes while Di Luca et al. considers only subtropical latitudes. Contrarily to pr, the contribution of the SS to the total tasmax and tasmin variables range from 10% to 70% and vary depending upon the surface properties of the area. rPAV values are huge over high-terrain regions with percentages that exceed the 70% of the total variability. rPAV values are also relatively large over the tropics for tasmin, and the differences with tasmax can be linked to differences in the magnitude of the total variability, and not necessarily in the magnitude of the PAV index. Results found for PAV and rPAV are in good agreement, and they indicate that the potential for added value of high-resolution simulations in South America is generally maximum over complex-terrain regions, followed by tropical areas with mesoscale phenomena and finally over la Plata Basin.

While RCMs generally have a good performance in simulating the observed mesoscale variability, the spatial distribution of PAV revealed the presence of large inter-model spread on simulating extreme precipitation and the transient tasmax and tasmin variance of the small scales. Hence, a more exhaustive evaluation concerning model performance is suggested. Regarding the rPAV mean values, the models generally present deviations more minor than a 25%. We stress the LMDZ4 model because of the different behavior when compared to the other RCMs, sometimes improving the skill in representing the observed climate and sometimes degrading the results, which may be associated to differences in the nature of the model (i.e., Stretch-grid model).

Our research has confirmed that high-resolution simulations have the potential to add

value in the representation of extreme precipitation and mean surface temperature. However, this condition is not necessary everywhere but particularly in those regions characterized by important surface forcings, such as complex high-mountain topography or land-sea contrasts. The results found are in good agreement with previous findings in literature for other RCMs and regions of the globe (Gao et al., 2006, Di Luca et al., 2012, 2013a, 2016, Falco et al., 2018, Güttler et al., 2015, Lenz et al., 2017, Rojas, 2006, Dirmeyer et al., 2012), increasing the likelihood that high-resolution is a necessary condition to a better representation of the surface climate. However, our methodology has some important limitations such as the inability of the methodology to measure the dynamic effect of high resolution and to assess the true value added by RCMs through its direct validation with observations and their drivers. Also, our chapter considers spatial scales smaller than the model's effective resolution (Skamarock, 2004), and although we believe it is a fundamental issue that is yet to be clearly understood, understanding how model's diffusion influence the variability of surface variables is beyond the scope of this chapter. Our results are encouraging and should be validated by experiments involving increasing-resolution simulations and metrics that fairly compare the RCMs with their coarser-resolution driver.

Chapter 4

Sensitivity of the RegCM4 model to increased horizontal resolution in the simulation of the South American Monsoon System

Resumen del capítulo

En este capítulo, se investiga el papel de la resolución horizontal en la simulación del Sistema Monzónico Sudamericano (SMSA) con RegCM4, un modelo climático de área limitada. RegCM4 se integró en Sudamérica durante el período 2005-2016 con una configuración idéntica, pero con diferente espaciamiento horizontal de retícula con una resolución de 25, 50 y 100 km, respectivamente. Las tres simulaciones fueron conducidas por el reanálisis ERA-Interim. Los patrones de circulación, junto con la precipitación, se examinaron críticamente en términos de promedios de verano, variabilidad interanual a estacional y distribución de frecuencia. El modelo RegCM4 fue capaz de simular los principales patrones espaciales de lluvia y circulación atmosférica, junto con una buena representación de la variabilidad interanual a intraestacional del monzón. Sin embargo, el modelo regional mostró un déficit de lluvia en toda el área monzónica en comparación con las estimaciones observadas durante la fase activa del SMSA, como consecuencia de una convergencia de humedad demasiado débil. Este sesgo seco se redujo al aumentar la resolución del modelo, debido a un aumento en la convergencia de humedad y a una mejor representación de lluvias intensas. Además, se en-

contró un valor agregado al aumentar la resolución en la delineación del dominio monzónico, y la simulación de 25 km mostró un transporte de humedad más realista en los subtrópicos. En resumen, está claro que aumentar la resolución en RegCM4 tiene un efecto positivo en la simulación de los procesos dinámicos/termodinámicos dominantes del SMSA. Sin embargo, las diferencias entre las tres simulaciones son relativamente pequeñas, y la simulación de 25 km sigue teniendo importantes sesgos que creemos que deben tratarse con mejores y más apropiados esquemas físicos.

Abstract

In this chapter, the role of horizontal resolution in the simulation of the South American Monsoon System (SAMS) is investigated with RegCM4, a limited-area climate model. RegCM4 was integrated into South America during the 2005-2016 period with an identical configuration, but different horizontal grid spacing at a resolution of 25, 50 and 100 km, respectively. All the three simulations were driven by the ERA-Interim reanalysis. Circulation patterns, together with precipitation, were examined critically in terms of summer averages, interannual to seasonal variability, and frequency distribution. The RegCM4 model was capable of simulating spatial patterns of rainfall and main circulations, together with a good representation of the interannual to intraseasonal variability of the monsoon. However, the regional model showed insufficient rainfall amount in all the monsoon area compared to observed estimates during the active phase of the SAMS, as a consequence of too weak moisture convergence. This dry bias was reduced with higher resolution of the model, associated with an improvement in the low-level circulation, an increase in moisture convergence and a better representation of intense rainfall. Moreover, an added value of high resolution was found in the delineation of the monsoon domain, and the 25 km simulation showed a more realistic moisture transport in the subtropics. In summary, it is clear that increasing the resolution in RegCM4 has a positive effect in the simulation of the dominant dynamic/thermodynamic processes of the SAMS. However, differences among the three simulations are relatively small, and the 25 km simulation continues having important biases that we believe should be treated with improved and appropriate physical schemes.

4.1 Introduction

The South American Monsoon System (SAMS) is the dominant climatic feature of tropical and subtropical South America. In its most active stage in summer (December–January–February, DJF), climatic precipitation features include a maximum core over central Brazil, mostly associated with diurnal thermodynamic instability and topographic convergence (Vera et al., 2006b). North-eastern Brazil (NeB) has relatively dry characteristics and is identified as a transition zone with large inter-annual variability (Harzallah et al., 1996). In the subtropics, monsoonal precipitation is modulated by the low-level circulation, where the moisture pathways are a low-level northerly flow along the eastern flank of the Andes, called the South American Low-level Jet (LLJ), and a northerly flow into the South Atlantic Convergence Zone (SACZ) associated to the South Atlantic anticyclone (SAA). The SACZ is a region of enhanced convection that extends diagonally across central South America from the northwest to the southeast into the South Atlantic Ocean and represents the core of the monsoon dynamics. The SACZ exhibits intraseasonal variability with distinct dry and wet periods that are complemented by wet and dry periods over La Plata Basin (LPB), denoted as SACZ-LPB dipole (Nogués-Paegle et al., 1997). In LPB, mesoscale convective systems are the dominant sources of summer precipitation and a particular challenge for climate models and convection schemes (Salio et al., 2007). It is also a region with high coupling strength between soil moisture and evapotranspiration (Sörensson and Menéndez, 2011).

Current Coupled Model Inter-comparison Project Phase 5 (CMIP5) Global Climate Models (GCMs) misrepresent some important aspects of the SAMS, since they do not have the sufficient horizontal and vertical resolution to resolve features that are important at regional scales (Abadi et al., 2018, Barros and Doyle, 2018, Jones and Carvalho, 2013, Zazulie et al., 2017). For example, Zazulie et al. (2017) found that CMIP5 GCMs failed to simulate the LLJ. This finding was further confirmed by Barros and Doyle (2018), who evaluated 18 CMIP5 model simulations and found that all simulations, except one, underestimated the northern flow associated to the LLJ, causing weaker-than-observed precipitation over Southeastern South America (SESA). Increase the horizontal resolution of a model has interesting potential advantages such as a more accurate representation of surface forcings, and regional processes and interactions (Rauscher et al., 2010). There is evidence that the simulation of monsoon systems in GCMs can improve with increased horizontal resolution (Anand et al., 2018, Bacmeister et al., 2014, Custodio et al., 2012, 2017, Jung et al., 2012, Mizuta et al., 2012, Raj et al., 2018,

Sakaguchi et al., 2015, Shaffrey et al., 2009). For example, according to Custodio et al. (2017), increasing the resolution in the HadGEM1 model family results in a more realistic representation of climate patterns over South America and the adjacent oceans. Yet, a key limiting factor in simulating fine-scale regional climate information from GCMs is its computational cost, and therefore Regional Climate Models (RCMs) are currently the most popular tool used with this aim.

Contemporary RCMs have higher resolution compared to their global driver, and thus there is much potential for RCMs to add value to the former in the representation of regional climate. However, it is not straightforward that higher resolution means better representation of climate, as there are several issues associated with resolution such as parametrization inadequacies. RCM resolution studies are the best approach to explore the role of resolution in climate representation, and they are popular over different regions of the world. Many works show some encouraging results (Chan et al., 2013, De Sales and Xue, 2011, Fantini et al., 2018, Gao et al., 2006, Güttler et al., 2015, Karmacharya et al., 2016, 2017, Leung and Qian, 2003, Prein et al., 2016, Rauscher et al., 2010, Rojas, 2006, Sinha et al., 2013, Torma et al., 2015, van Roosmalen et al., 2010, Walther et al., 2013), and confirm that increasing resolution of a model improve the model performance in capturing both the spatial patterns and variability of mean climate and climate extremes. Contrarily, many other works find little-to-no added value (AV; Angélil et al., 2018, Casanueva et al., 2016, Dirmeyer et al., 2012, Gao et al., 2017, Jin et al., 2016, Kotlarski et al., 2014, Panitz et al., 2014, Panthou et al., 2018, Pryor et al., 2012, Shi et al., 2018, Singh et al., 2016, Tian et al., 2017), suggesting increasing resolution alone has little impact on climate representation.

Not surprisingly, several studies indicate that RCMs can reproduce many of the SAMS mesoscale climate features and together add value upon coarse-scale GCMs used for boundary condition by providing a more realistic representation of climate (Chou et al., 2002, 2005, da Rocha et al., 2009, 2014, De Sales and Xue, 2006, Llopart et al., 2014, Misra et al., 2002, Nobre et al., 2001, Pesquero et al., 2009, Solman et al., 2008, Vernekar et al., 2003). The higher skill may be related to the higher resolution of the RCM. In this regard, some sensitivity experiments with the Andes heights suggest that an accurate representation of the Andes is a necessary condition for climate models to correctly simulate the low-level circulation of the SAMS (De Sales and Xue, 2011, Figueroa et al., 1995, Insel et al., 2010, Junquas et al., 2015). For example, Insel et al. (2010) tested the role of the Andes through a sensitivity experiment, and concluded they are critical to the development of the LLJ. Their results suggest that the absence of the

Andes reduces moisture export from the Amazon into LPB, and leads to enhanced low-level convergence and increased convection and precipitation in parts of the Amazon Basin.

The Regional Climate Model (RegCM) is a well-known limited-area model, and its simulations were extensively evaluated over SA (da Rocha et al., 2009, 2014, Fernandez et al., 2006, Llopart et al., 2014, Reboita et al., 2014a,b, 2018a, Seth et al., 2007). Most works indicate that the model captures the basic features of the SAMS, including the variability in space and time, but the model also has some nonnegligible deficiencies, such as the underestimation of rainfall in the SA tropical and subtropical domain (see da Rocha et al., 2012). This dry bias usually occurs during the summer in the Amazon and SACZ. To understand the impacts of change in several RegCM model configurations, sensitivity experiments over SA have been performed using different land surface schemes (da Rocha et al., 2012, Llopart et al., 2014, 2017, Reboita et al., 2014a), cumulus convective schemes (da Rocha et al., 2012, Llopart et al., 2014, Reboita et al., 2014a), planetary boundary layer schemes (Reboita et al., 2014a) and domain sizes (Erfanian and Wang, 2018, Rojas and Seth, 2003, Seth and Rojas, 2003). However, so far, a comprehensive evaluation of the RegCM model sensitivity towards its horizontal resolution to simulating the SAMS has not been carried out. A higher horizontal resolution should lead to a better representation of the surface forcings, and thus to an improvement in the simulation of the low-level circulation over tropical and subtropical SA. Furthermore, an adequate spatial resolution to resolve the physical and dynamical processes of the SAMS should also improve its representation (Gao et al., 2006). Both factors should eventually lead to an improvement in the simulation of surface variables and reduce the biases with observations.

Historically, the default resolution of an RCM simulation over SA was of 50 km. A few long RCM runs at 25 km resolution have only recently been available within the CORDEX framework, and it is still unclear whether the increased resolution adds value when compared to a standard 50 km simulation. Despite the interest, there are very few works that explicitly distinguish the benefits of finer resolution in the simulation of the SAMS (Custodio et al., 2012, 2017). As computing resources continue to grow at an accelerated pace, a tendency is seen in climate research to increase the RCM resolution; this prompts the need to investigate the role that horizontal resolution plays in the simulation of the South American climate. While the comparison of multiple RCMs such as those available from CORDEX is helpful, analyzing sensitivity experiments with a single model in detail is also necessary. This study takes the latter approach and represents one of the first efforts to study the added value of increasing resolution in the representation of the SAMS while using the RegCM model.

This chapter aims to study the role of resolution in the simulation of various aspects of the SAMS, with emphasis on low-level circulation and surface variables, including intraseasonal features, summertime means of dynamic and thermodynamic variables, and extreme events. The experimental design and datasets used in this chapter are described in Section 2, and the methodology is described in Section 3. The results and concluding remarks are presented, respectively, in Sections 4 and 5.

4.2   Datasets and experimental design

4.2.1   RegCM4 simulation setup

The RegCM model is a limited area model developed in the International Centre for Theoretical Physics (ICTP). RegCM Version 4 (RegCM4) is its latest version, and the description of the model together with upgrades from older versions can be found in Giorgi et al. (2012). In this chapter, we study the simulations performed with the hydrostatic version of the RegCM4.6.1 branch, for the period from 2005 to 2016 and with one month of spin-up time. The simulation domain is slightly larger than the one recommended by CORDEX (Fig. 4.1; Giorgi et al., 2014), and includes part of the South Atlantic Ocean. As explained by Erfanian and Wang (2018), the expansion of the domain has some interesting potential benefits, as it enables the RCM to resolve the atmospheric processes over the influential remote oceans explicitly and enhances the representation of large-scale drivers in the RCM. The initial and boundary conditions were provided by ERA-Interim reanalysis (ERAi; Dee et al., 2011) with a horizontal grid spacing of $1.5°\times1.5°$. The model uses the Emanuel convection scheme over the land and oceans (Emanuel, 1991) and the Holtslag scheme for the planetary boundary layer (Holtslag et al., 1990). The land surface scheme used is the Community Land Model V4.5 (CLM4.5; Bonan et al., 2011).

RegCM4 was run at three different horizontal resolutions: 25 km, 50 km, and 100 km. All three simulations share identical configurations and were integrated on an 18-layer sigma-pressure vertical coordinate, using a Rotated Mercator cartographic projection. The 25 km resolution simulation, from now on named as RegCM4 25km, represents the highest spatial resolution current RCM simulations have over SA (Giorgi and Gutowski, 2015). On the other hand, the 50 km resolution (RegCM4 50km) represents the default historical resolution of RCMs (Boulanger et al., 2016), and the 100 km resolution (RegCM4 100km) represents the res-
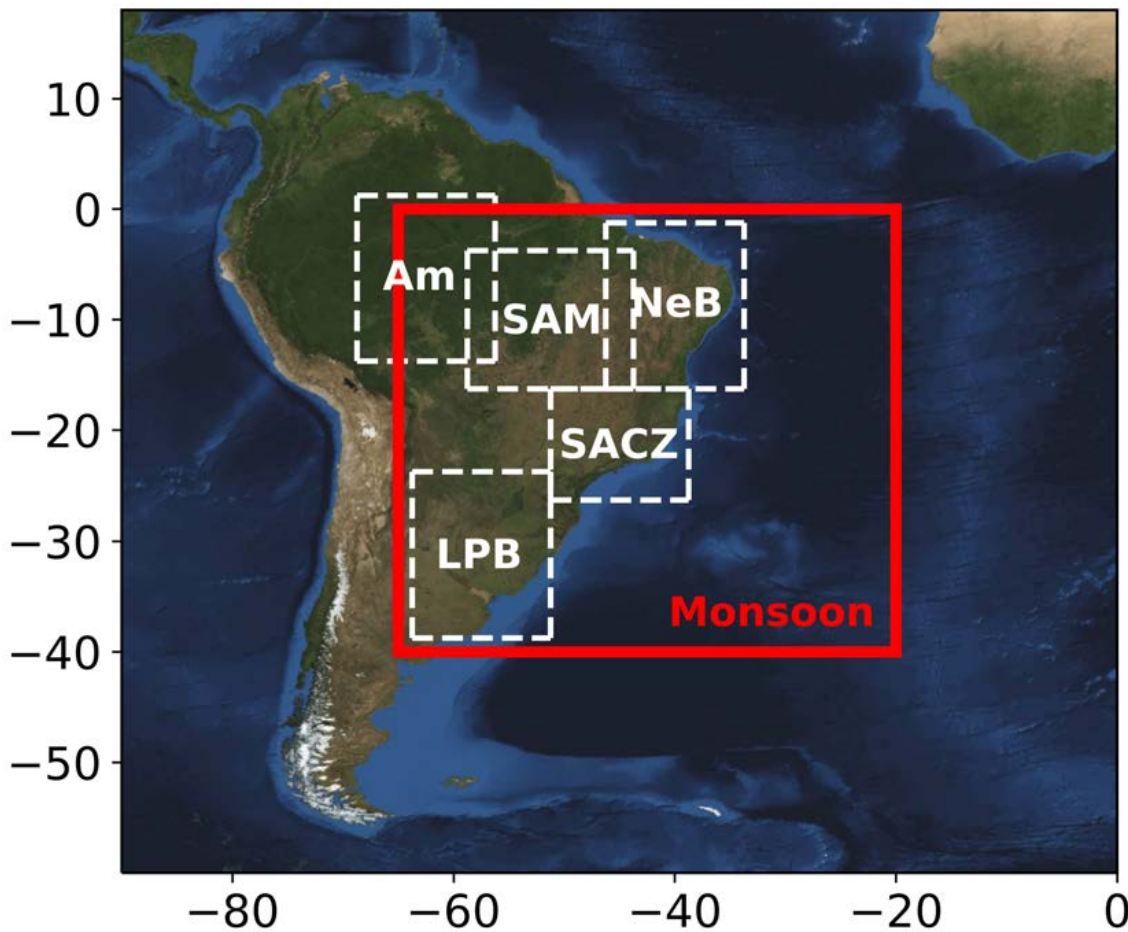
Fig. 4.1. RegCM4 integration domain, with ESRI World Imaginery in the background. White boxes in dashed lines denotes key sub-domains selected for assessment: Amazon (Am), South American Monsoon (SAM), Northeast Brazil (NeB) and La Plata Basin (LPB). The solid-red box denote the monsoon area.

olution of current high-resolution GCM simulations (IPCC, 2013).

4.2.2 Datasets for validation

Different gridded data for precipitation were used to evaluate the simulations. With the goal of measuring the uncertainty among observation data sets, we consider a station-based daily data from the Climate Prediction Center (CPC; Xie et al., 2010), a monthly station-based data from the Climatic Research Unit (CRU; New et al., 2002), and the satellite-based and gauge-based 3-hourly gridded dataset from TRMM_3B42 product (Huffman et al., 2007). The first two

datasets, i.e., CPC and CRU, are on a horizontal grid spacing of 0.5° over land. On the other hand, TRMM dataset is on a 0.25° grid resolution, and thus, is the best dataset to validate the 25km resolution simulation.

Montini and Jones (2017) validated the description of the LLJ by comparing five different reanalyses against observations from the South American Low-Level Jet Experiment (SALL-JEX; Vera et al., 2006a). Results show that ERAi was found as the best-performing reanalysis at pressure levels in representing the structure and intensity of the LLJ. In this chapter, ERAi is used as the reference when studying the general circulation and other atmospheric features of the SAMS.

The RegCM4 simulations, reanalysis, and observed gridded datasets are on different grids and spatial scales. All analyses are performed in the native data grid unless remapping is necessary. This is the case for the vertical cross-section figures and the spatial correlation table with TRMM. The remapping of variables is performed using a bilinear interpolation onto a regularly spaced latitude/longitude grid of 0.25°, 0.50° and 1°, for the 25km, 50km, and 100km, respectively.

4.3   Methods

Several diagnostics were used to evaluate the sensitivity of the RegCM4 model in the simulation of the most important features of the SAMS. The assessment is performed considering three extensions of the domain: the whole tropical and subtropical continental area (15°N-40°S), the monsoon area in the active phase of the SAMS [0°N-40°S]x[65°W-20°W]; red box in Fig. 4.1), and 5 key sub-regions of the SAMS: Amazon (Am), South American Monsoon (SAM), Northeast Brazil (NeB) and La Plata Basin (LPB), which are depicted as white boxes in Fig. 4.1.

4.3.1   Monsoon area and intensity

From a global perspective, monsoon systems are dominant in the tropics. Their main feature consists of a strong seasonal variation in both wind and precipitation, in response to the annual declination of solar radiation. Monsoon precipitation is characterized by wet and dry seasonal contrast, with the most significant percentage of rainfall concentrated in the local summer. Wang and Ding (2006) used this distinctive feature to define a simple precipitation index to determine the monsoon area and calculate the monsoon intensity. They delineate the monsoon area by identifying those regions in which the seasonal range, i.e., local summer-

minus-winter rainfall, exceeds 180 mm and the summer-to-annual rainfall ratio is higher than 35%. In the Southern Hemisphere, the summer is defined as December to February (DJF) and the winter as June to August (JJA). Some modifications of this index were proposed by other authors, as extending the length of local summer and winter, but they found that the index is little sensitive to the criteria used (Hsu, 2016, Wang and Ding, 2008). In this chapter, we keep the initial definition of global monsoon proposed by Wang and Ding (2006). We also consider the monsoon precipitation intensity, calculated as the seasonal range (DJF-JJA) divided by the annual mean rainfall (IPCC, 2013).

4.3.2   The LISAM index

On the basis of the strong seasonal variation of the SAMS circulation, da Silva and de Carvalho (2007) proposed an index, called the Large-Scale Index for South American Monsoon (LISAM) to characterize the large-scale features of the monsoon at intraseasonal to interannual time scales. The index can reveal important dynamical mechanisms of the SAMS. It is a Combined Empirical Orthogonal Functions (EOFc) performed on pentad (five-day average) means of precipitation, and low-level (850 hPa) specific humidity, air temperature, zonal and meridional wind components. The spatial domain covers the monsoon area (red box in Fig. 4.1). The LISAM index is simply the time coefficients of the first EOFc mode. The temporal evolution of the index has a distinctive interannual variability, with positive (negative) values associated with the active (passive) phase of the monsoon. Thus, the onset/demise of the SAMS can be derived from the transition phases of the LISAM. The index also allows studying the intraseasonal variability of the SAMS by analyzing high-frequency variations.

4.4   Results

4.4.1   Simulation of intraseasonal to interannual variability

The austral summertime monsoon precipitation domain over SA extends from the equator to 35°S, and from the Andes Mountain Range to the Atlantic coast, excluding LPB and NeB (Fig. 4.2, see regions in Fig. 4.1). All datasets show a maximum monsoon precipitation intensity centered in 50°W and 15°S, and a second relative maximum on the eastern slope of the Andes in the subtropics. In general, all RegCM4 model simulations and ERAi reanalysis resemble the observed spatial domain of the monsoon. However, ERAi has an extended monsoon area

over Buenos Aires province and a southward-than-observed domain over Am. The RegCM4 simulations also overestimate the extension and intensity of the monsoon area over LPB. In this sense, the 25km simulation adds value compared to the coarser resolution ones by better delineating the monsoon area over the subtropics. The monsoon intensity is reasonably well reproduced by all simulations and by the reanalysis, with maximum values extending over the SACZ area.
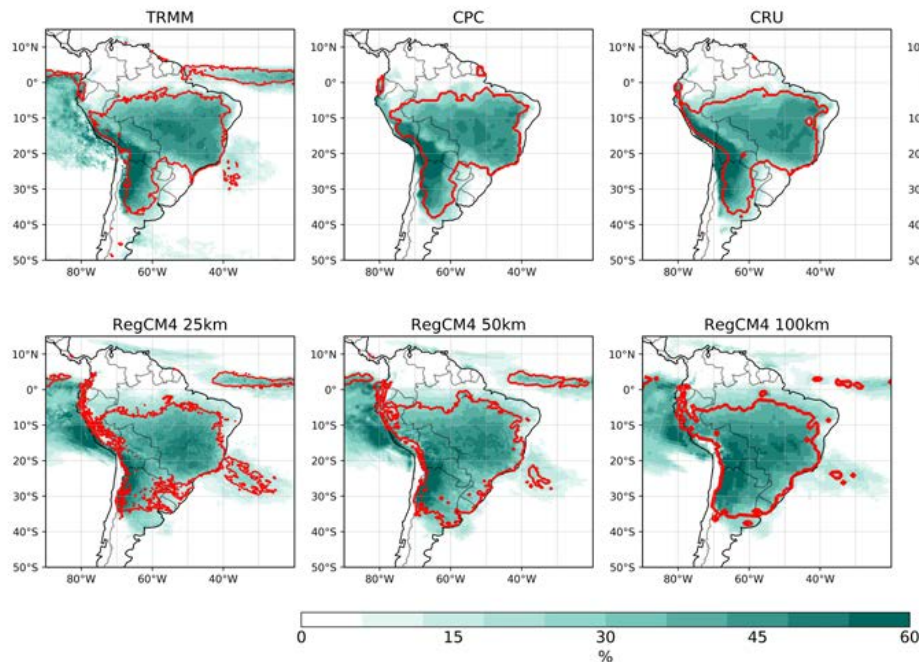
Fig. 4.2. Monsoon precipitation intensity (shading) and monsoon precipitation domain (red lines) are shown for TRMM, CPC, CRU, ERAi, RegCM4 25km, RegCM4 50km, and RegCM4 100km. The monsoon precipitation domain is defined where the seasonal range (i.e., accumulated precipitation in December-January-February - June-July-August) is >180 mm and the summer to annual rainfall ratio is >35%. The monsoon precipitation intensity is the seasonal range divided by the annual mean.

The LISAM index was calculated for ERAi reanalysis and the RegCM4 simulations over the monsoon area (red box in Fig. 4.1). LISAM clearly shows an annual cycle with fluctuations on short time-scales (Fig. 4.3). All three RegCM4 indices follow the year-to-year variation of ERAi and are strongly correlated with their driver (the three of them with a 0.93 correlation coefficient). This suggests that ERAi has a first-order effect in the interannual variability of the simulations. The largest differences between simulations can be identified in the higher frequencies, related to the intraseasonal variability of the SAMS. The mean onset of the SAMS

active phase for all data is at the end of October and the mean demise at the beginning of May. The demise of the monsoon is later than the one estimated by da Silva and de Carvalho (2007), but the analyzed periods do not overlap (they consider 1979–2005). This difference is consistent with the results of Jones and Carvalho (2013), who found a tendency of the SAMS to late demises.
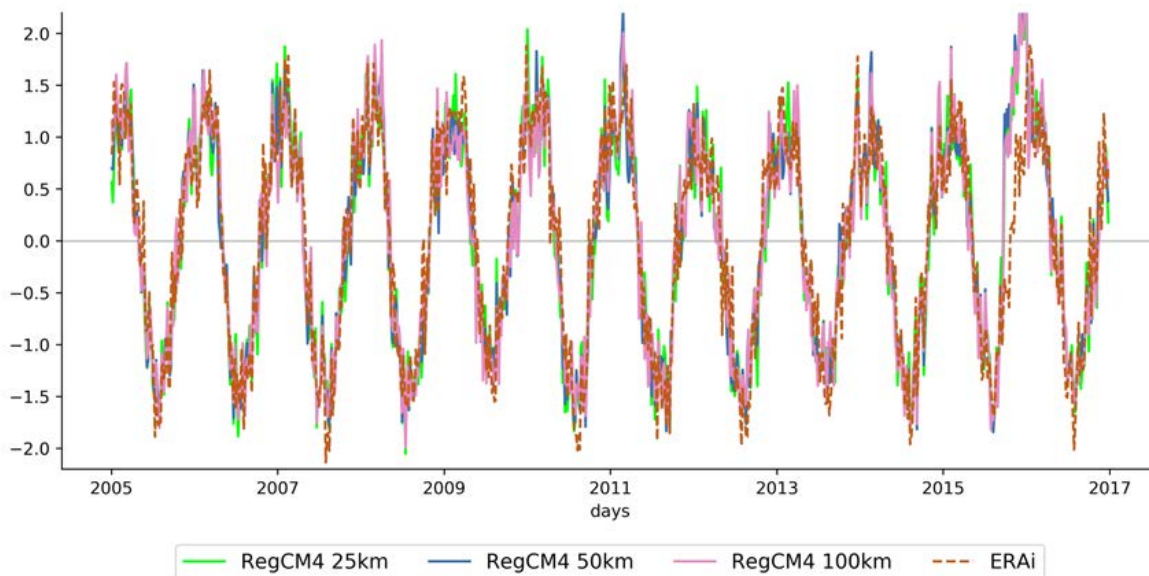
Fig. 4.3. Time evolution of the LISAM index, obtained as the first principal component of the combined empirical orthogonal function of precipitation, and low-level (850 hPa) zonal wind, meridional wind, specific humidity and temperature. The onset/demise of the SAMS can be derived from the transition phases of the LISAM: from negative (positive) values to positive (negative) values mark the onset (demise). The index is calculated for ERAi (brown), RegCM4 25km (green), RegCM4 50km (blue) and RegCM4 100km (violet) over the monsoon area (red box in Fig. 4.1).

The LISAM indices variability showed some large high-frequency differences between simulations and ERAi, indicating some differences in the intraseasonal time scales. Thus, the question that naturally arises is how different is the annual cycle among datasets. We consider the area averaged seasonal cycles of precipitation for different key sub-regions of the SAMS (white boxes in Fig. 4.1), following the cycle of the monsoon, i.e., from October to September. All datasets present clear annual cycle over Am, SAM and SACZ regions with most rainfall falling from October to April, as expected (Fig. 4.4). The seasonal cycle of precipitation over NeB has a delayed onset compared to the other regions, and most rainfall falls from January to June. Finally, LPB has different behavior than the other regions by not presenting

a marked annual cycle, precipitation during winter is relatively large and is associated with frontal passages.
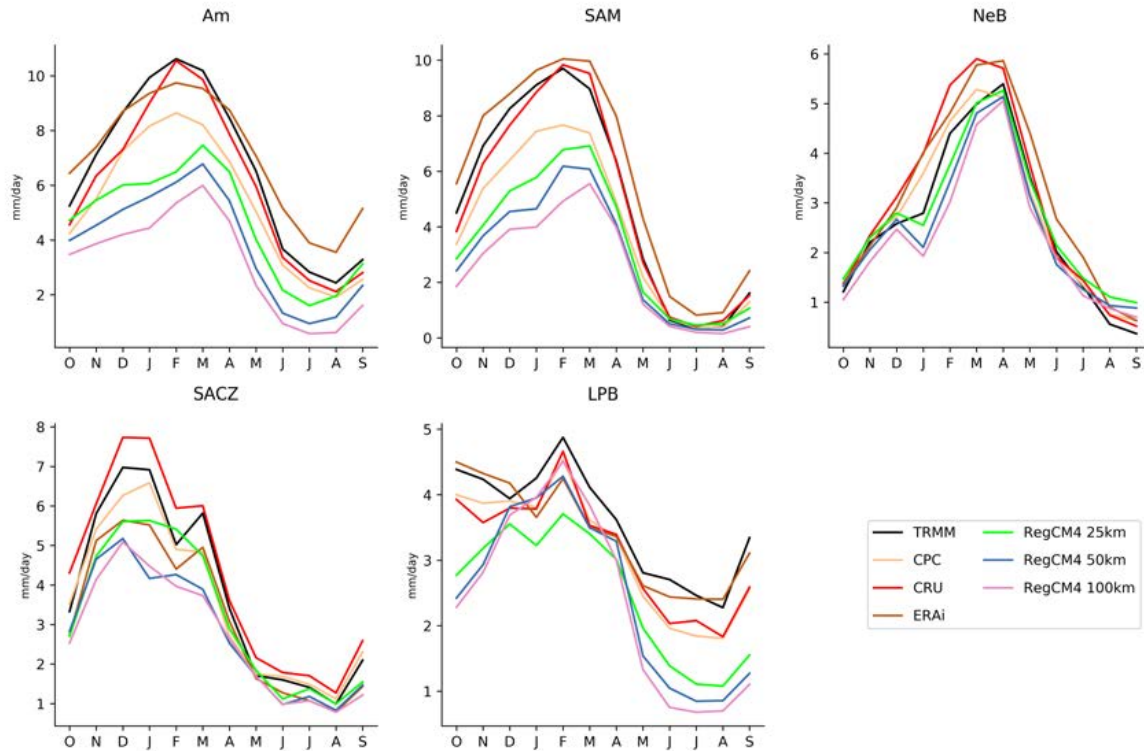
Fig. 4.4. Annual precipitation cycle (mm/day) for TRMM (black), CPC (orange), CRU (red), ERAi (brown), RegCM4 25km (green), RegCM4 50km (blue) and RegCM4 100km (violet) over the five sub-regions defined in Fig. 4.1: Am, SAM, SACZ, NeB and LPB.

The RegCM4 simulations and ERAi are capable of simulating the observed annual cycle of precipitation in all regions, including the abrupt seasonal change over Am, SAM and SACZ and the delayed monsoon rain over NeB (Fig. 4.4). An exception is LPB, where the simulations underestimate the precipitation during whole year, but especially during winter and thus have a larger annual-range than the observed data. This dry bias over LPB is a typical error in all climate models (e.g., Falco et al., 2018, Carril et al., 2016 and references therein). The three RegCM4 simulations have a common weakness, that is, they do not capture the rainfall intensity faithfully over the local convective areas which are the Am, SAM, and SACZ sectors, especially during the active phase of the SAMS. However, rain intensity over these areas is sensitive to resolution by showing increased values when increasing resolution. Hence, there is an added value of higher resolution simulations in the representation of rainfall over

local convective areas. The 25km simulation also shows a reduction of the dry bias during the austral winter in LPB, but it underestimates summertime precipitation while the coarser-resolution simulations do not. ERAi generally outperforms the RegCM4 simulations, but some deviations are also noticed, as a wet bias during winter over Am and a dry bias during summer over SACZ.

4.4.2 Summertime circulation and rainfall

Prominent regional characteristics of the atmospheric circulation at low and high layers accompany the seasonal changes of convection over SA. Thus, we need to study model sensitivity in the representation of monsoon dynamics. The summertime upper-level circulation as described by the reanalysis includes a well-defined anticyclonic gyre over Bolivia, centered near 15°S and 65°W, and an upper-level trough in the coast of northeast Brazil (Fig. 4.5; left panels). These characteristics are properly simulated by the RegCM4 model in both position and intensity. However, the anticyclonic gyre is located westward when compared to ERAi, and its position is slightly sensitive to resolution. The anticyclone is a response to diabatic heating released by the regional deep convection in Amazonia (Lenters and Cook, 1997), so model biases may be related to the underestimation of precipitation over Am or to a westward shift in the Chaco-Low (not shown). It is clear that increasing model resolution results in a more pronounced trough over NeB which, in turn, increases the southerly upper-level transport over the SACZ. In this regard, a closed cyclone can be detected in the 25km simulation, which is absent in the other two simulations. These changes in the upper-levels may be a consequence of changes in land-ocean thermal contrast (Zhou et al., 1998).

The divergent circulation over SA in the upper-levels is accompanied by significant rising motions (not shown), a low-level cyclonic circulation over the Chaco-Low (Salio et al., 2002), and an anticyclonic circulation associated to the SAA (Fig. 4.5; right panels). The low-level circulation in the tropics is dominated by the equatorial easterly trade winds which, after crossing the equator, become a northwesterly flow on the eastern slope of the Andes. Winds furthermore turn clockwise around the Chaco-Low and are embedded in the westerly flow at midlatitudes. The northern flow along the eastern slope of the Andes is the LLJ, which is responsible for transporting humid air masses from the tropics into the subtropics (Fig. 4.5, shaded). The poleward meridional humidity transport is at maximum over the foothills of the Andes from the tropics until 35°S, and there is a second maximum transport associated to the SAA, which feeds moisture directly into the SACZ. The RegCM4 simulation represents well the
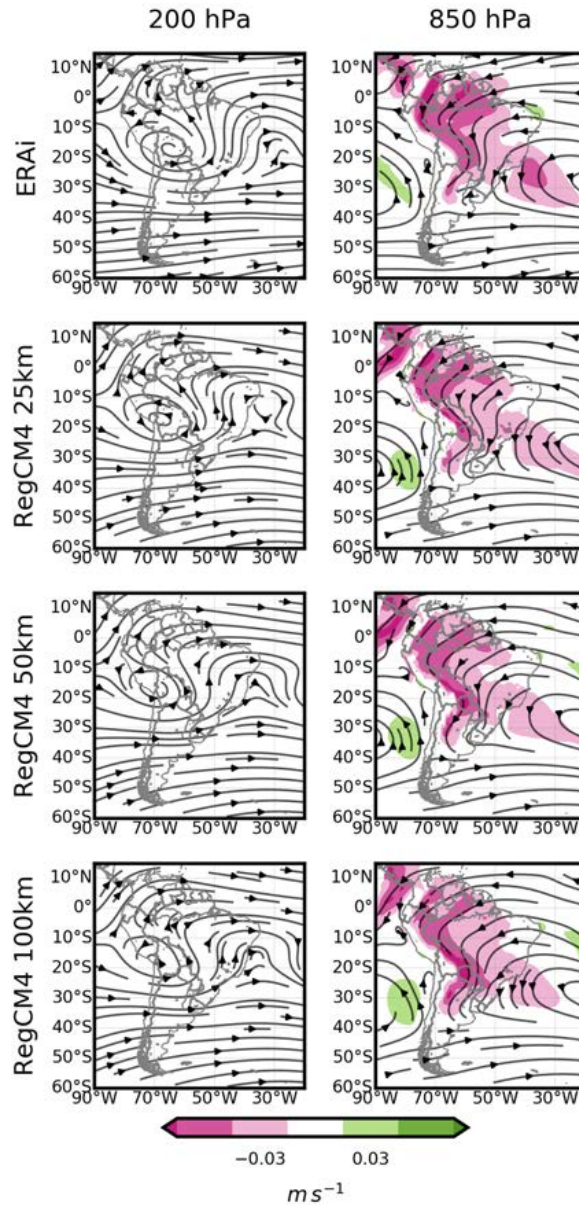
Fig. 4.5. Summer mean wind streamlines at 200 hPa (DJF; left panels) and 850 hPa (right panels) for ERAi, RegCM4 25km, RegCM4 50km and RegCM4 100km. Also shown is the summer mean meridional humid flux at 850 hPa (shading, right panels). Regions with topography higher than 1500 m are masked in the low-level fields.

low-level circulation and the meridional humidity transport, but the intensity of the transport is underestimated in the tropics and overestimated in the subtropics. The 25 km simulation is the only one able to represent the magnitude of the meridional transports in the tropics, and also shows a decreased transport in the subtropics, being closer to ERAi. This deceleration of

moisture flux in the subtropics may be a consequence of mass convergence over Amazonia.

The warm and humid air mass intrusion into the subtropics is an important characteristic of the SAMS, as it is one of the mechanism responsible of increasing the convective instability over the continent, resulting in the development of convective clouds. These mesoscale convective systems initiated in the exit region of the LLJ are the dominant sources of summer precipitation over LPB. We now further examine the vertical structure of the summertime meridional wind at 21°S latitude (Fig. 4.6). There are three sources of heat and moisture into the subtropics: at the foothills of the Andes associated with the LLJ, an oceanic one associated with the SAA and a small third one over the Brazilian Highlands. The pattern is in good agreement with the one obtained by Marengo et al. (2004) when using NCEP/NCAR Reanalysis II (Kalnay et al., 1996), but the LLJ intensity in the ERAi reanalysis is stronger. The LLJ has a deep structure, extending from 950 hPa to 700 hPa. The core of the LLJ is centered at 900 hPa. The reanalysis also shows an intense and shallower low-level northerly flow over the Atlantic Ocean, associated with an active SACZ, which is larger than the LLJ at this latitude. All RegCM4 simulations can represent the three major fluxes in the subtropics, but show a stronger (weaker) transport associated with the LLJ (SAA) than the reanalysis. The response of the RegCM4 model to increased resolution is to decrease (increase) the LLJ (SAA) flux intensity, with values closer to the reanalysis. The vertical structure of the LLJ is also sensitive to resolution, with the extension increasing while the resolution decreases. This way, the 100km simulation shows a deep and more intense LLJ with large values reaching almost the 500 hPa level. The simulation of a stronger LLJ by the RCM compared to its driver was already noticed by other works (De Sales and Xue, 2006, Vernekar et al., 2003) and relate the weak transport of the reanalysis to its coarse resolution. However, the LLJ intensity decreases when increasing the resolution in the model. This result, in principle anti-intuitive, may be explained by the enhanced convection found over Amazonia (see Fig. 4.4). The increased rainfall is a consequence of an increase in mass convergence, which would result in a deceleration of the flow in the tropics. Thus, the 25km simulation is the one that best resembles the poleward moisture flux when compared to ERAi.

After exploring the atmospheric circulation, we now examine the RegCM4 model sensitivity to resolution in terms of summertime rainfall. The observed precipitation climatology during summer presents large values over Am, SAM and SACZ regions, which exceed the 12 mm day^{-1} (Fig. 4.7). There is also an oceanic maximum over the equator associated to the ITCZ. All observed gridded datasets have similar rain intensities and distributions, indicating a good
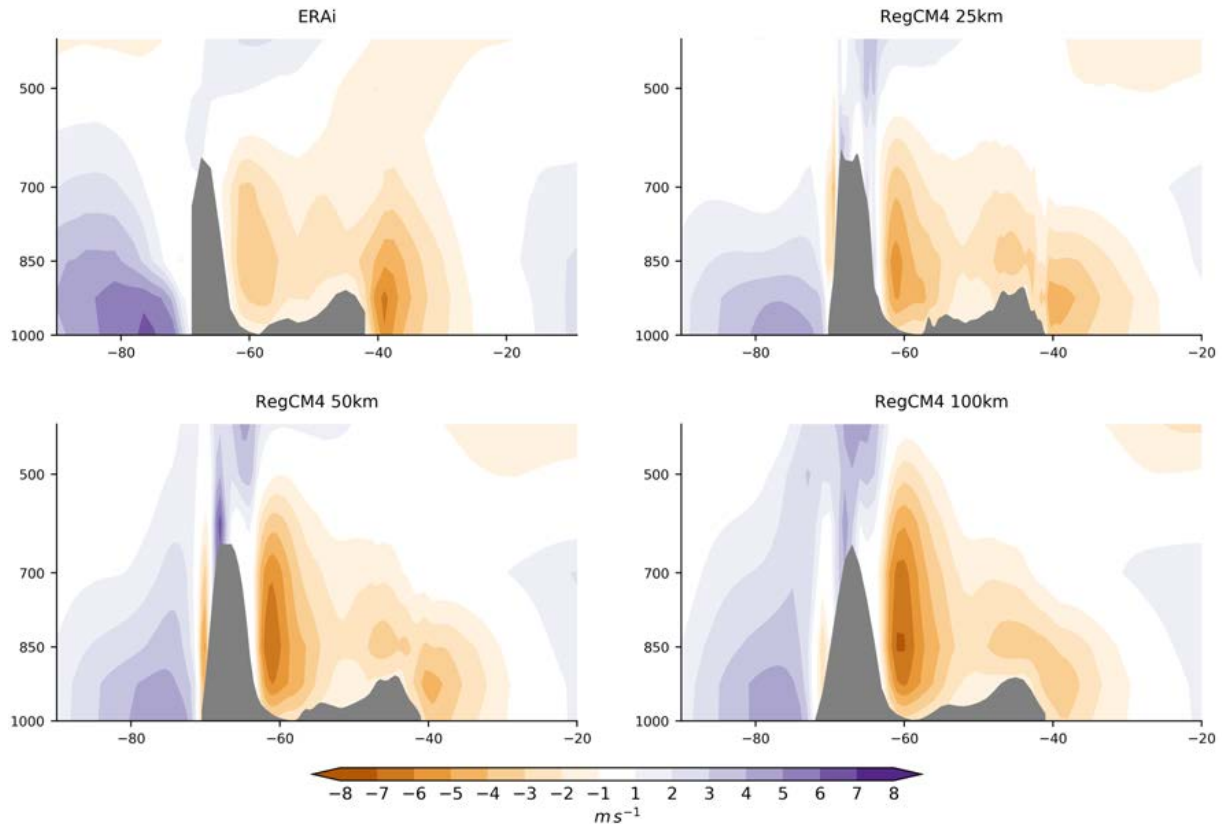
Fig. 4.6. Height-longitude section of summer mean meridional wind (m/s; DJF) from ERAi, RegCM4 25km, RegCM4 50km and RegCM4 100km along 21°S. Model topography is grey colored.

coherence among observed spatial patterns. ERAi is also capable of simulating the observed rainfall climatology, but it overestimates the intensity over the Andes mountain range. The RegCM4 model simulations show drier than observed conditions over the whole SAMS area, especially over Am and SAM regions, except in northwest Argentina and Bolivia where it has wetter than observed values. The results are consistent with those found when analyzing the annual cycle of precipitation. Other works in literature also reported this model deficiency (e.g., da Rocha et al., 2012, Erfanian and Wang, 2018, Llopart et al., 2014, Reboita et al., 2014a, Seth et al., 2007). In particular, Erfanian and Wang (2018) found very similar results, using the same model configuration at 50 km resolution but with another branch version (RegCM4.3.4). The 25km simulation shows a somewhat higher intensity of rain over convective areas (Am, SAM and SACZ). Precipitation over the oceanic SACZ and ITCZ regions also seems enhanced when increasing the resolution.

It is necessary to take the spatial scale into account to be able to faithfully compare datasets
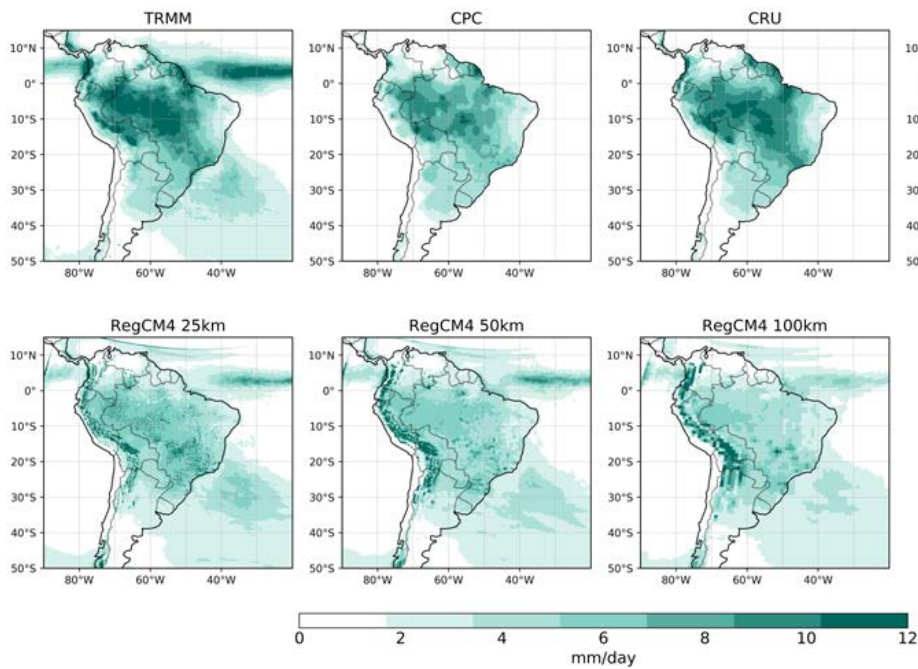
Fig. 4.7. Summer mean precipitation (mm/day; DJF) from TRMM, CPC, CRU, ERAi, RegCM4 25km, RegCM4 50km and RegCM4 100km. Each panel corresponds to a different dataset.

Table 4.1. Spatial-pattern correlation coefficients of individual regional climate simulations and the reanalysis against TRMM for austral summer rainfall (DJF) over the Monsoon area. The monsoon area can be identified as the red box in Fig. 4.1. Each column corresponds to the resolution of the common grids used for validation, and each row to an individual dataset.

	0.25°	0.5°	1.0°	1.5°
RegCM4 25km	0.80	0.83	0.84	0.83
RegCM4 50km		0.81	0.81	0.83
RegCM4 100km			0.74	0.73
ERAi				0.93

with different horizontal resolution (Hong and Kanamitsu, 2014, Kanamitsu and DeHaan, 2011). In that regard, Hong and Kanamitsu (2014) recommended that all comparisons need to be done on the coarsest resolution among the observations and models. Thus, we performed a comparison of the three RegCM4 simulations together with ERAi by interpolating high-resolution simulations onto the coarser resolution grids. TRMM is also remapped for validation purposes. We evaluate the performance of each model simulation in the representation of the summertime monsoon rainfall by calculating the spatial correlation coefficient and the spa-

79

tial root mean square error (RMSE) at different scales over the monsoon region (Tables 1 and 2). The 25km simulation shows an added value compared to the 50km and 100km simulations in the representation of the spatial pattern of precipitation when aggregated to the coarser grids (i.e., 0.5° and 1°). The 50km simulation also shows an added value compared to the 100km simulation when upscaled. However, none of the simulations outperform ERAi, being the reanalysis the one with the highest coefficient. These results are valid for both metrics, indicating a better skill when increasing resolution in representing the spatial pattern and intensity of the observed summertime precipitation.

Table 4.2. As in Table 1, but using a root mean square error (RMSE) metric.

	0.25°	0.5°	1.0°	1.5°
RegCM4 25km	1.98	1.92	1.87	1.94
RegCM4 50km		2.15	2.15	2.14
RegCM4 100km			2.46	2.50
ERAi				1.15

We further perform an analysis of the rainfall frequency distribution, which may be helpful to understand the origin of the biases in the mean summertime rainfall of RegCM4. These biases can be related to a misrepresentation of either wet day frequency or extreme events. A daily frequency distribution over the sub-regions helps to get insight into the simulation of the mean climate and extreme events during the most active phase of the monsoon (Fig. 4.8). The frequency distributions reveal that all RegCM4 simulations tend to overestimate light precipitation and underestimate extreme rainfall, especially over NeB, SACZ and LPB regions. The 25km simulation has an increase in the frequency of heavy events over local convective regions, i.e., Am, SAM, and SACZ, but the difference with the coarser-resolution simulations is small. It is interesting to notice that ERAi also have some important biases, and are opposed to the biases of the RegCM4 simulations, as there is an overestimation in the frequency of events in the middle of the distribution and an underestimation in the frequency of light precipitation events, especially over Am and SAM. CPC has a very similar distribution with TRMM, increasing the consistency among observed data.

Convection over the SAMS requires low-level convergence and uprising motion of moist air. Thus, humid transport together with mass convergence are both the main ingredients for tropical rainfall. Results indicate that the dry bias of the RegCM4 simulations is not related to a misrepresentation of the humidity transport flux, but because of weak low-level convergence
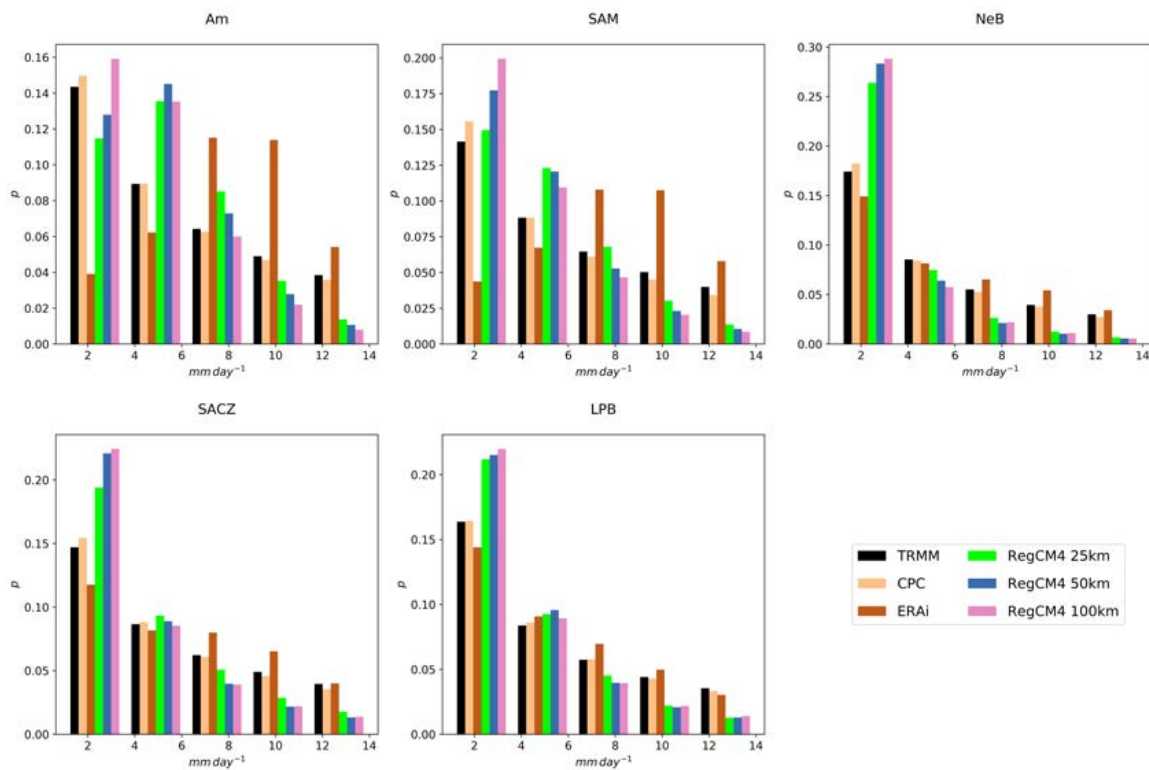
Fig. 4.8. Normalized frequency distribution of summertime daily precipitation (DJF) for TRMM (black), CPC (orange), ERAi (brown), RegCM4 25km (green), RegCM4 50km (blue) and RegCM4 100km (violet) over the five sub-regions defined in Fig. 4.1: Am, SAM, SACZ, NeB and LPB.

(Fig. 4.9). The model shows a divergent circulation along the whole subtropical coast, followed by convergence in the SACZ, that is probably associated with a sea-breeze circulation on the east coast of Brazil. This pattern is not present in the ERAi low-level divergence. The model also underestimates divergent flow in the subtropics and all divergence/convergence over the oceans. Erfanian and Wang (2018) found a similar pattern when analyzing the horizontal wind divergence using a similar version of the model. Increasing the resolution of the model results in a stronger convergence over convective areas, especially over Amazonia, which may be the ingredient to enhanced convection.

We finally analyze low-level circulation and sea level pressure deviations from ERAi. When downgrading the resolution, the model shows some biases compared to the reanalysis (Fig. 4.10). The differences suggest a misrepresentation of the Chaco-Low, with anticyclonic anomalies over the area. These anomalies induce an easterly circulation over the Amazon that may suppress rainfall and accelerates the LLJ. There is also an anticyclonic bias over the SACZ
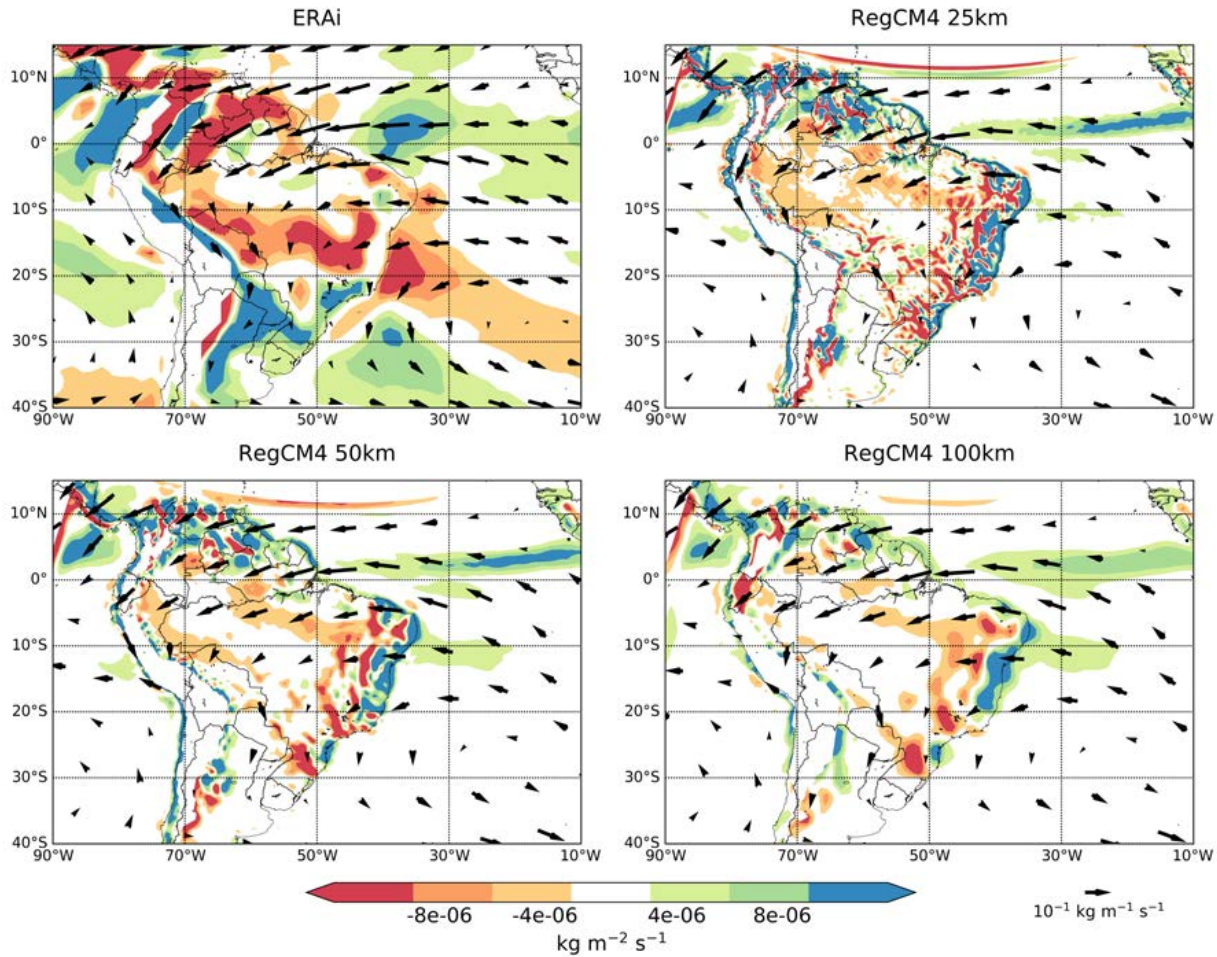
Fig. 4.9. Summer climatology of vertically-integrated moisture flux (arrows), and moisture flux divergence at 850 hPa (shading) for ERAi, RegCM4 25km, RegCM4 50km and RegCM4 100km. Moisture flux is integrated from 1000 hPa to 500 hPa. Regions with topography higher than 1500 m are masked.

oceanic area, with anomalous continental inflow over the continental SACZ. This sea-breeze circulation on the east coast of Brazil may be the reason for coastal convergence present in the RCM, but absent in the reanalysis. The improved low-level convergence in the 25km simulation found earlier is associated with a more accurate simulation of the Chaco-Low and low-level wind vectors. The anticyclonic bias over the subtropics is largely reduced when the model resolution is increased, as well as the low-level circulation over Amazonia. Therefore, the enhanced convection and humid convergence found over the SAMS for increased model resolution is a consequence of a better representation of the low-level circulation in the tropics and subtropics.
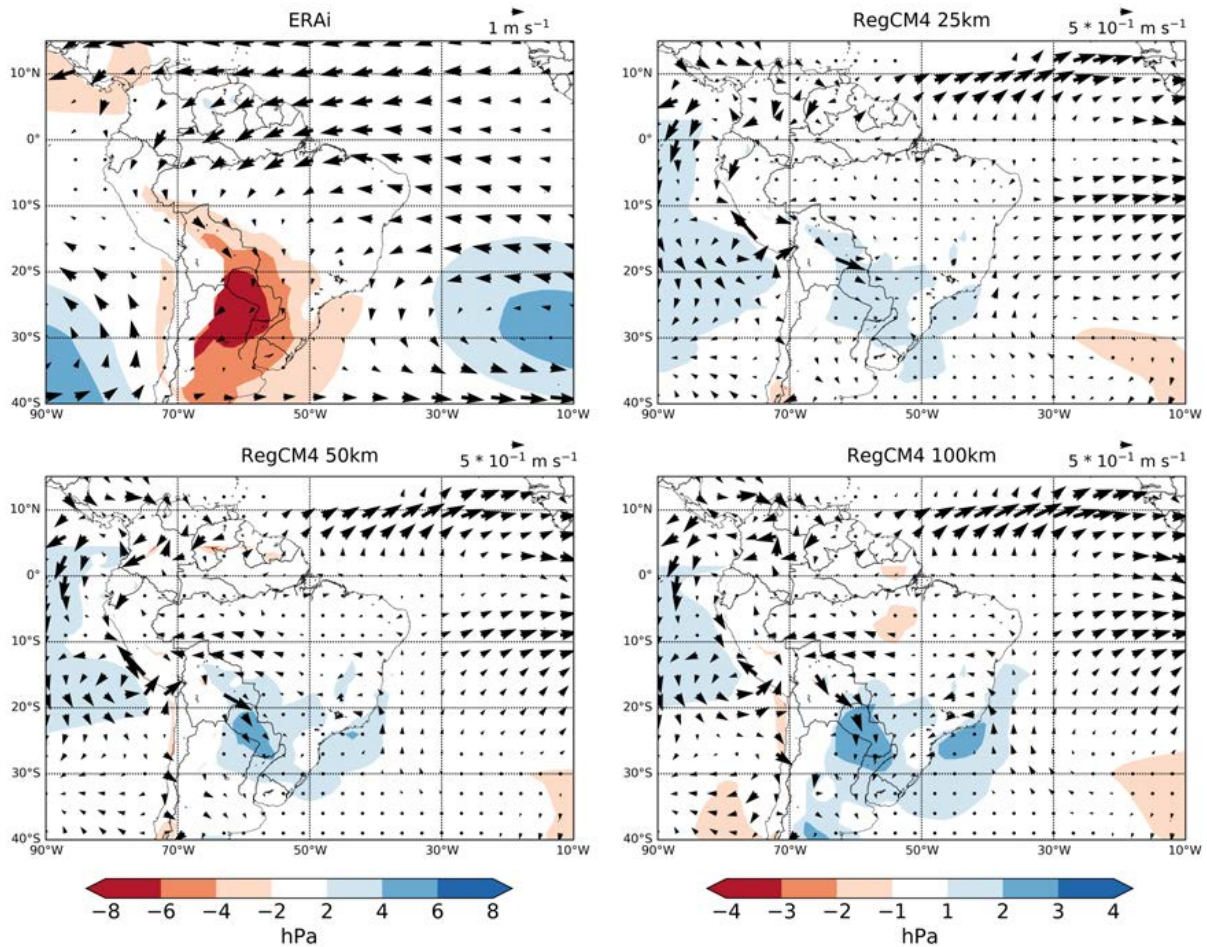
Fig. 4.10. Summer climatology of sea level pressure and circulation (arrows) at 850 hPa for ERAi (top-left panel), and bias for RegCM4 25km, RegCM4 50km and RegCM4 100km. Arrow scale is shown in the top-right of each panel. Color bar in the left corresponds to ERAi and in the right to model bias. Regions with topography higher than 1500 m are masked.

4.5 Concluding remarks

In this chapter we investigated the added value of high-resolution regional climate modeling in simulating various characteristics of the SAMS using the RegCM4 model at 25 km, 50 km, and 100 km grid spacing. The resolution study evaluated the RegCM4 sensitivity in the representation of the SAMS with all its most relevant characteristics such as inter-annual to intraseasonal variability, annual cycle, summertime rainfall patterns, upper and lower-level circulation, meridional flux, and precipitation frequency distribution.

RegCM4 simulations were able to capture the extension and intensity of the large-scale

monsoon characteristics, together with a correct representation of the interannual to intraseasonal variations of the SAMS. In agreement with Seth and Rojas (2003), we found that ERAi has a first-order effect in the interannual variability, suggesting that the onset/demise of the active phase of the SAMS is more sensitive to the driving data than to resolution. The most significant differences between simulations were found in fluctuations at intraseasonal time-scales, as well as the annual cycle of precipitation over central regions of the continent. The added value of increased resolution was found mainly over local convective areas, where the 25 km simulation reduced the dry bias in the annual cycle during the active phase of the SAMS, and also in the delimitation of the regional monsoon domain, where the 25km simulation was the only one that recognized part of LPB region does not have tropical monsoon characteristics.

We also evaluated the RegCM4 representation of the main summertime features of the SAMS. Results indicate that the model is capable of simulating the circulation and rainfall during this season, including the representation of the lower and upper-level circulation, the tropical-subtropical meridional wind, and the spatial pattern and frequency distribution of rainfall. However, the most important deficiency exhibited by all simulations while using the current physical configuration is in its inability to represent the intensity of convective precipitation by largely underestimating it. With a very similar version of the model and the same configuration, Erfanian and Wang (2018) attribute the bias to its inability to effectively capture the impact of forcings and processes acting outside the RCM domain. They proved that explicitly including the tropical and subtropical Atlantic and Pacific Oceans improves the simulation of the location, intensity, and seasonal migration of the ITCZ and SACZ, as key large-scale drivers of the regional climate, and resulted in a more accurate representation of the mean precipitation. The dry bias may also be reduced by selecting the appropriate physical scheme (Reboita et al., 2014a, Solman and Pessacg, 2012), or by increasing the resolution to convection-permitting scales (Prein et al., 2015).

Increasing the resolution in the RegCM4 model led to an improvement in the circulation/precipitation regime over the monsoon area and, as a consequence, it reduced the dry bias over convective regions. The enhanced rainfall can be related to a a better representation of the low-level circulation, an increase in moisture convergence and to better representation in the frequency of heavy events. The added value of increased resolution in the spatial correlation coefficients between simulated and observed summertime precipitation patterns was found not only on their original resolution but also when upscaling into the coarser resolution grid cells. The upper-level circulation also showed a sensitivity to resolution by presenting a stronger upper-

level cyclone over NeB, increasing the vertical wind shear. This result may be a consequence of an increase in the continent-ocean thermal contrast, which may be driven by the additional latent heat release with enhanced precipitation. Thus, increasing the resolution may have a positive influence in the dominant dynamic/thermodynamic process driving the SAMS.

It is interesting to notice the particular case of the summertime rainfall over LPB, where the 25km simulation has a dry bias that is reduced in the coarser-resolution simulations. The dry bias was identified in the regional annual cycle and the mean seasonal field. The increased precipitation in the 50km and 100km simulations is correlated with the enhanced moisture export from the Amazon into the subtropics associated with the LLJ. The results, thus, reiterates the importance of tropical-subtropical exchange in the simulation of regional climate over LPB. However, the results are in contradiction to the statement that a better representation of the Andes is a necessary condition to increase the moisture transport driven by the LLJ and suggest that this issue is more complex than originally thought.

ERAi outperformed RegCM4 integrations in the representation of rainfall, as was already reported by Falco et al. (2018). However, even though the reanalysis has a much coarser resolution than the RCM simulations, the RegCM4 is not expected to add value. This is partly associated with the fact that ERAi uses a data assimilation system that incorporates observed data. Thus, comparing ERAi with station-based gridded observations can somewhat be seen as an incestuous verification, since the reanalysis and observed datasets are not independent of each other.

Summarizing the results of this chapter, we found that increasing the resolution of the RegCM4 model effectively enhances the simulation of regional characteristics associated with the SAMS. We found that improvements in higher resolution are achieved mostly through reducing the dry bias of the RegCM4 model over convective areas and by improving the low-level circulation. However, differences between model resolutions were not outstanding for any diagnostic used, concluding that the RegCM model is not very sensitive to resolution. It is for this reason that we believe increasing the resolution alone is not enough for a better simulation of the SAMS, and improving the RCM physical parameterizations is also encouraged.

Chapter 5

The influence of regional nudging over South America on the simulation of the Southern Hemisphere extratropical circulation

Resumen del capítulo

Este capítulo presenta un nuevo enfoque para estudiar el valor agregado de proveer informa-ción climática regional sobre Sudamérica (SA) en un Modelo Climático Global en la simulación de la circulación extratropical del Hemisferio Sur (HS). Para ello, analizamos y comparamos los resultados del modelo LMDZ anidado sobre SA a diferentes forzantes de resolución mayor que proveen información regional sobre el continente. Los experimentos incluyen una simu-lación control, una simulación de anidamiento bidireccional (TWN) del LMDZ anidado inter-activamente a una versión regional de mayor resolución del modelo y una simulación per-fecta, en donde el modelo es conducido por ERA-Interim. Los resultados indican que la res-olución incrementada sobre SA mejora la representación de la circulación en la tropósfera baja dentro del continente y, por lo tanto, mejora la simulación del transporte meridional de energía desde los trópicos hacia los extratrópicos. Dicho flujo podría generar una fuente adicional para la ciclogénesis, acompañada por un aumento de la convergencia de calor y humedad hacia el ciclón. Esto aumentaría a su vez la inestabilidad condicional y conduciría a la intensificación y desarrollo del ciclón. La mejora local de la circulación en la tropósfera

baja dentro del continente es acompañada por una mejor representación de la circulación extratropical global, especialmente durante el verano. La información regional provista sobre SA tiene una respuesta positiva en la simulación de la posición de la corriente en chorro de latitudes medias durante el verano, ya que reduce significativamente el sesgo de la energía cinética zonal media fuera de la zona anidada. La mejora está acompañada por una mejor representación de los flujos transientes de calor y momento de las perturbaciones, junto con una mejor descripción de la convergencia del transporte de momento, mientras que el incremento en la energía cinética de las perturbaciones es menos pronunciado. Por otro lado, la circulación general durante el invierno fuera de la zona anidada muestra una reducción limitada del sesgo en la posición de la corriente en chorro cuando es conducido por diferentes bases regionales, especialmente en el caso del sistema TWN. Sin embargo, se encontraron mejoras del sistema TWN en comparación con el experimento control en las primeras etapas del ciclo de vida del ciclón. Los resultados del presente estudio sugieren, por lo tanto, que la provisión de información regional sobre SA excita de manera efectiva la simulación de la circulación atmosférica extratropical en el HS.

Abstract

This chapter presents a new approach to studying the added value of high-resolution information over South America (SA) in the simulation of the Southern Hemisphere (SH) extratropical circulation. For this, we analyze and compare the results of the LMDZ model nudged over SA to different forcing information. The experiments include a control simulation, a two-way nesting (TWN) simulation of the LMDZ interactively nested to a higher-resolution zoomed version of the model, and a perfect boundary simulation of the model nudged to ERA-Interim. The results indicate that enhanced resolution over SA improves the representation of the low-level circulation in the continent and, thus, simulates better the meridional transport of energy from the tropics into the extratropics. Such flow could imply an extra source for cyclogenesis, accompanied by the transport of heat and moisture into the cyclone, increasing conditional instability and leading to cyclone development. The local improvement of the low-level circulation is followed by a better representation of the global extratropical circulation, especially in the summertime season. The regional nudging over SA has positive feedback on the simulation of the midlatitude jet position during the austral summer by significantly reducing the bias deviation of the mean zonal kinetic energy outside the nudged zone. The improvement

is accompanied by a better representation of the transient eddy heat and momentum fluxes, together with a better description of momentum transport convergence, while the increment in eddy kinetic energy is less pronounced. On the other hand, the wintertime general circulation outside the nudged-zone shows a limited bias-reduction for the regional-driven simulations, especially in the case of the TWN system. However, improvements of the TWN system compared to the control experiment are noticed in the early stages of cyclone lifecycle. The findings of the present study suggest, thus, that improvements in resolution over SA effectively excites the simulation of the mean atmospheric circulation in the SH.

5.1 Introduction

Atmospheric eddies have a crucial role in the general circulation as they are responsible for large meridional transports of heat, moisture, and momentum. Transient eddies are migratory cyclones and anticyclones, with timescales of about 1 to 10 days, which propagate through baroclinic waveguide regions called storm tracks. Despite the progress achieved by the constant development of state-of-the-art General Circulation Models (GCMs) and Earth System Models, climate models still misrepresent some fundamental aspects of midlatitude atmospheric circulation and eddy activity. As an example, in the latest IPCC report (IPCC, 2013) it was concluded that GCMs present some biases in reproducing the observed location and intensity of storm tracks and jet-streams, as they tend to simulate weaker storm tracks and equatorward jet-streams than the observed for both hemispheres (Chang et al., 2012, Ceppi et al., 2012, Wilcox et al., 2012, Bracegirdle et al., 2013, Zappa et al., 2013, Pithan et al., 2016, Iqbal et al., 2018, Müller et al., 2018).

Much effort has been made to understand large-scale circulation sensitivity to different configurations of a model. Answers to this issue differ, going from an influence of the coupling with the Sea Surface Temperature (SST) ocean/ice model (Bracegirdle et al., 2013), the representation of the stratospheric ozone depletion in the Southern Hemisphere (SH) (Grise et al., 2014), the representation of shortwave cloud forcing (Ceppi et al., 2012), and an increased resolution of the model (Boville, 1991, Berckmans et al., 2013, Sakaguchi et al., 2016, Müller et al., 2018). Regarding this last factor, many authors associate the improvement in the general circulation to a better representation of orography at high resolutions, rather than a better simulation of other processes such as Rossby wave breaking or sub-synoptic scale eddies (Inatsu and Kimoto, 2009, Berckmans et al., 2013). For example, through a two-way nest-

ing sensitivity experiment, Inatsu and Kimoto (2009) found that the large-scale circulation was effectively-forced by an improvement in the representation of the mesoscale features of orography over northeast Asia. The research also concluded that a better description of mesoscale features in cyclones had a regional effect but did not affect the large-scale circulation. More recently, Sakaguchi et al. (2016) studied the impact of regional grid refinement on the large-scale circulation. The authors analyzed several variable-resolution mesh simulations with local refinement at 30 km over different regions of the world embedded in a quasi-uniform domain at 120 km elsewhere. When increasing the resolution over tropical Americas, the model simulated a descending branch of the Hadley cell shifted poleward from the position its coarser resolution version had, which also pushed the baroclinically unstable regions, momentum flux convergence, and the eddy-driven jet poleward.

Apart from Antarctica, South America (SA) is the largest and most southernmost continental landform in the SH, and the Andes Cordillera (from now on the Andes) plays a significant role in the life cycle of extratropical cyclones. A cyclolysis region is located upstream of the Andes and is mainly related to a blocking effect of the flow (Hoskins and Hodges, 2005). Furthermore, southeastern SA is one of the central regions in the SH of cyclone formation and owe its existence to the presence of the Andes (Gan and Rao, 1994, Sinclair, 1995, Hoskins and Hodges, 2005, Madonna et al., 2014, Reboita et al., 2010, 2018b, Krüger et al., 2012). The cyclogenesis region, together with its associated Warm Conveyor Belt, is present throughout the year and is controlled by the SA low-level jet (Mendes et al., 2007, Madonna et al., 2014). The SA low-level jet is established by the Andes through mechanical forcing and is responsible for large southern heat and moisture transports from Amazonia to the Subtropics (Campetella and Vera, 2002, Vera et al., 2006a). This low-level jet provides the main ingredients to cyclone intensification/formation over the Continent (Madonna et al., 2014, Mendes et al., 2007, Gozzo et al., 2014), and is thus responsible for transporting energy from the tropics into the extratropics (Trenberth and Stepaniak, 2003). Another effect of the Andes on transient disturbances is associated with an induced cyclonic circulation in its lee side when upper troughs that are traveling eastwards move over the mountain range at midlatitudes (Mendes et al., 2007).

Improvement in model resolution over SA results in a better representation of the Andes, together with a better simulation of mesoscale processes associated to surface forcing. Therefore, a higher model resolution should improve the simulation of transient and stationary eddy activity and, assuming a positive effect in the large-scales, an improvement of the simulation of the general circulation in the SH. However, for most research institutions, per-

forming a very high-resolution global simulation that represents the regional aspects of climate is computationally expensive or even unviable. Regional climate models (RCMs) are usually used with this aim, but their limited domain restricts them in simulating planetary-scale circulation. Inspired by the Limited Area Model approach (Laprise, 2008), we propose a solution to this problem by forcing a GCM over South America with regional information provided by an RCM or a reanalysis. We hypothesize that while the RCM or a Reanalysis provides the regional information through the nudging of the GCM over the continent, the GCM can reproduce the large-scale information elsewhere. This way, we study the added value of regional information over South America in the representation of the SH circulation.

The LMDZ model (Hourdin et al., 2006) is a GCM that has the particularity of allowing zooming and nudging. Both configurations of the model were widely used in other researches, over different regions of the world, reporting in general a good performance of the model (Zhou and Li, 2002, Goubanova and Li, 2007, Chen et al., 2010, Yang et al., 2016). In the SH, the model reproduces the main large-scale aspects of the circulation satisfactorily (Carril and Nuñez, 2000, Menéndez et al., 2001, Carril et al., 2002). However, Menéndez et al. (2001) reported significant biases of the model in representing some regional aspects of the SA climate. Carril et al. (2002) also studied the ability of the LMDZ over the Southern Ocean, finding that the model underestimates some transient properties of the general circulation. The authors attribute these biases in the underestimation of the baroclinic conversion term in middle latitudes.

This chapter presents a new approach to studying the added value of high-resolution information over SA in the simulation of the SH extratropical circulation. For this, we analyze and compare the results of the LMDZ model nudged over SA to different forcing information. The experiments include a control simulation, a two-way nesting simulation of the LMDZ nudged over SA to a higher-resolution zoomed version of the model, and a perfect boundary simulation of the model nudged to ERA-Interim. Our main purpose is to understand the effect of subsynoptic-scale regional information in SA on the general circulation. The layout of this paper is as follows. In section 2, we begin by describing the LMDZ model and the experiments analyzed in this chapter. We also introduce the methods of analysis. The following section, section 3, evaluates the LMDZ general circulation and its sensitivity to different regional forcings, emphasizing in the assessment of eddy activity. Section 4 is a discussion of the most relevant results found in this chapter. In section 5 we present the concluding remarks.

5.2 Experiments and methods

5.2.1 Model and experiment description

We use the LMDZ4 general circulation model, developed in the Laboratoire de Météorologie Dynamique (LMD). LMDZ4 is the atmospheric component of the IPSL-CM5A, and the description of the model's physical parametrizations can be found in Hourdin et al. (2006) and Dufresne et al. (2013). The key to our methodology is that LMDZ4 is nudged over the whole domain to a driving field by applying the following exponential relaxation procedure to different prognostic fields:

$$\frac{\partial X}{\partial t} = \frac{\partial X}{\partial t}_{GCM} + \frac{X_f - X}{\tau}, \tag{5.1}$$

where the prognostic fields, X, are the zonal wind, meridional wind, temperature and specific humidity. X_f is the driving field, and τ is the relaxation time. The shorter the relaxation time, the stronger the nudging.

An interesting aspect of the model is that it allows a stretching scheme (the letter Z of LMDZ denotes for Zoom), so the model can be used as a typical global model or as a regional model by using a variable resolution grid. In this chapter, we use the two versions of the LMDZ4 and distinguish them as LMDZ-Global and LMDZ-Regional. Despite having different resolutions, the configuration of both versions shares an identical physical parameterization to keep the physical compatibility between simulations.

LMDZ-Global integrations have 72 x 96 latitude and longitude grids and 19 sigma layers in the vertical. The grid of LMDZ-Global has a globally uniform resolution of 2.55° in latitude and 3.75° in longitude. The regional version of the LMDZ4, LMDZ-Regional, was used in an interactive mode with LMDZ-Global for a two-way nesting (TWN) experiment (see sect. 5.2.1.2). LMDZ-Regional has a zoom over South America (Fig. 5.1c), with the zoom centered at 21°S and 56°W and with a spatial coverage of 15°N-60°S, and 20°W-90°W. LMDZ-Regional has 150 x 152 latitude and longitude grids and 19 sigma levels. The resolution is high over the zoomed region, ranging between 0.55° and 0.5°, and very coarse elsewhere. As described for LMDZ-Global, LMDZ-Regional also allows a nudging of the simulation over the whole domain by following the relaxation procedure shown in Eq. (1).

The relaxation technique allowed us to perform several experiments of the LMDZ-Global nudged over South America to different drivers. In this chapter, we present and analyze three experiments (Table I). The simulations were evaluated against ERA-Interim reanalysis (Dee et al., 2011), from now on identified as ERAi. Results were presented only for summer (Decem-
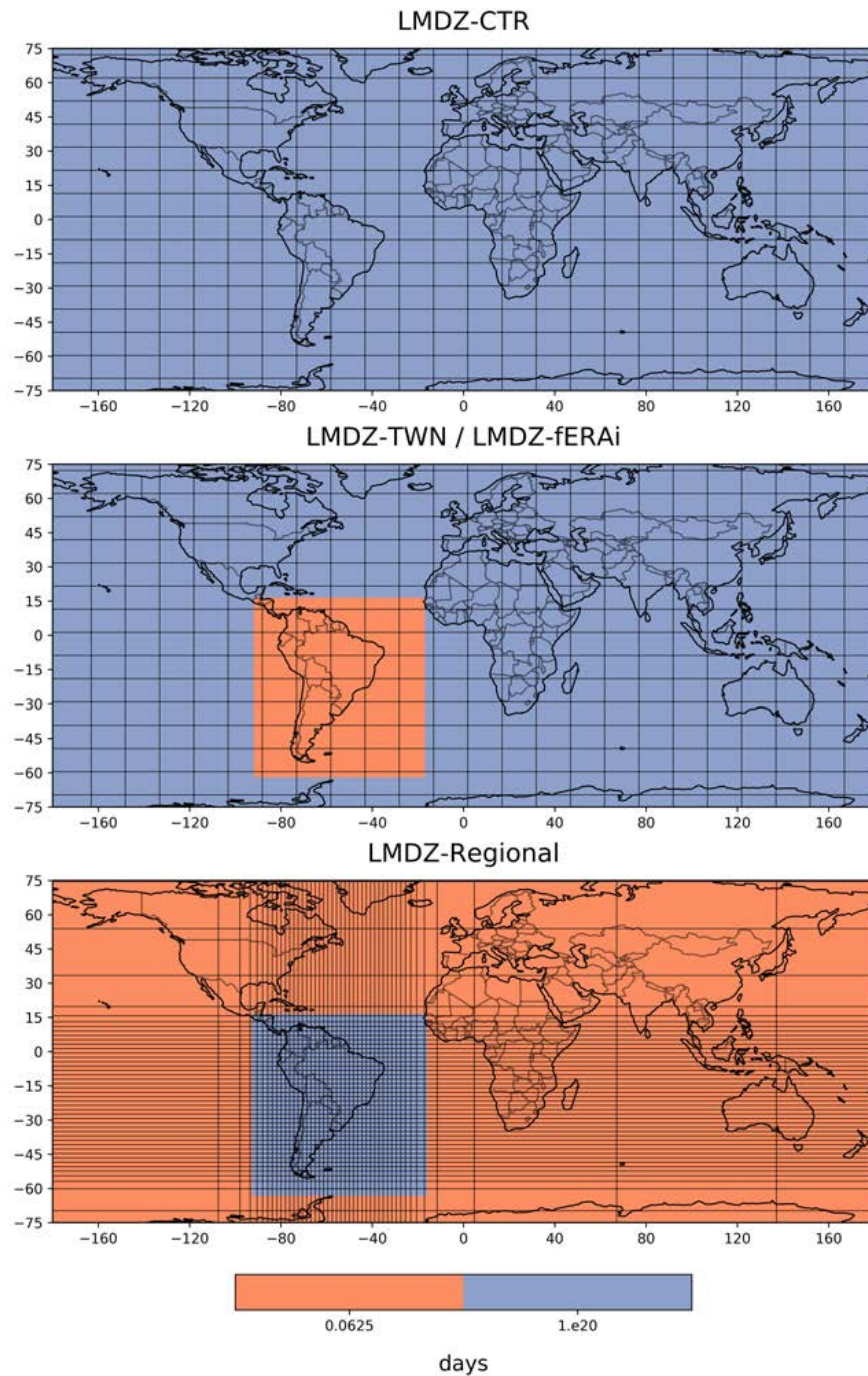
Fig. 5.1. Relaxation times of the experiments (shaded). A schematic representation of the grid is also displayed, where each line represents one of four latitudes/longitudes.

ber, January, and February; or DJF) and winter (June, July, and August; or JJA), as they are representative of the two seasonal extremes for the SH. Further details of the experiment set

up are presented below.

Table 5.1. List of simulations conducted. All simulations have a globally uniform resolution of $2.55°$ in latitude and $3.75°$ in longitude.

Simulation	Period	Boundary Conditions
LMDZ-CTR	80 years	Climatological SST and sea ice, without nudging
LMDZ-TWN	80 years	Climatological SST and sea ice, with a two-way-nudging with LMDZ-Regional
LMDZ-fERAi	32 years from 1979 to 2010	Climatological SST and sea ice, nudged to ERA-Interim over the whole SA continent

LMDZ-CTR

The control experiment is an AMIP LMDZ-Global run in a control climatological SST mode (sst-Clim), identified as LMDZ-CTR. The distributions of sea-surface temperature and sea ice are climatological ones, obtained from observations for the period 1979–XXXX. The integration was run for 80 years, with the model nudged over South America to LMDZ-Regional. However, the relaxation time scale is very long (i.e., several years) in the whole globe (Fig. 5.1a), meaning the nudging is negligible, and the simulation runs freely.

LMDZ-TWN

We performed a similar version of the experiment described above but considering an interactively nested system between LMDZ-Global and LMDZ-Regional. The interactive version of LMDZ-Global, named LMDZ-TWN, differentiates from LMDZ-CTR in the relaxation times (Fig. 5.1b). LMDZ-TWN is now nudged over South America to LMDZ-Regional by having a small relaxation time of 0.0625 days. The exponential relaxation procedure is applied with a time scale of 30 minutes, enabling the LMDZ-Regional to provide the regional information over SA in every step but allowing the GCM to run freely in the whole domain outside the zoom.

Regarding LMDZ-Regional, the relaxation times are long inside the zoom and small outside (Fig. 5.1c), implying that the model runs almost freely inside the zoom, whereas it follows the forcing outside the zoom. The approach is very similar to the one of a limited area model, with the grid points outside the zoom working as the buffer zone that receives the global in-

formation.

The overall view of the experiment LMDZ-TWN is that the relaxation procedure allows an interactive exchange of information every 30 minutes between LMDZ-Global and LMDZ-Regional. While LMDZ-Global provides the boundary information to LMDZ-Regional, LMDZ-Regional provides the regional information over the whole SA continent.

LMDZ-fERAi

We also performed a perfect boundary experiment to test the methodology proposed in this chapter. The experiment is a one-way nesting simulation of LMDZ-Global nudged over South America to ERAi, named LMDZ-fERAi. The relaxation times are the same ones as LMDZ-TWN (Fig. 5.1b). The time integration is 32 years long, starting in 1979 and ending in 2010. Because we consider ERAi reanalysis as the reference data, this simulation should be our best-case scenario.

5.2.2 Methodology for eddy analysis

We follow the traditional theory of baroclinic instability to evaluate migration systems. Eddies are defined as deviations from the time or longitudinally averaged flow. Stationary eddies in the SH are usually small compared with their transient counterpart, so they will not be considered. In this chapter, we focus on high-frequency transient eddies in midlatitudes with timescales shorter than ten days. The transient fields are calculated by processing daily global data through a fifth-order band-pass Butterworth filter that retains temporal fluctuations between 2.5 and 10 days.

The notations to define the time mean of any quantity Q is $\overline{Q}$, and the transient term of perturbations shorter than ten days is Q'. We have evaluated the exchange of energy between eddies and the zonal flow by separating the kinetic energy into components associated with eddy and mean motions. That way, the climatology equations of zonal kinetic energy (KZ) and transient eddy kinetic energy (TKE) are:

$$\overline{KZ} = \frac{1}{2}\overline{u}^2 \tag{5.2}$$

and

$$\overline{TKE} = \frac{1}{2}\left(\overline{u'^2} + \overline{v'^2}\right), \tag{5.3}$$

respectively. The poleward flux of heat and momentum associated to migratory eddies was evaluated through the daily covariance terms $\overline{u'T'}$ and $\overline{u'v'}$, respectively. We also include the

vertical heat transport $\overline{\omega' T'}$, due to its importance in the conversion from eddy available potential energy to TKE.

The eddy influence in the mean flow was summarized by the Eliassen-Palm flux (EP_{flux}). The EP_{flux} is a diagnostic of atmospheric motions that work as an indicator of eddy activity and eddy forcing of the zonal mean flow. Following Trenberth (1986), the EP_{flux} in the meridional and vertical directions can be defined as

$$EP_{flux} = \left(-\overline{u'v'}, \frac{f\overline{v'\theta'}}{\frac{\partial \theta_R(p)}{\partial p}} \right)^t \cos\phi, \tag{5.4}$$

where the subscript t is the vector transpose, ϕ the latitude, f the Coriolis parameter, θ' the transient potential temperature and $\theta_R(p)$ the reference potential temperature at a given pressure. If we neglect the eddy vertical transport of momentum (Trenberth, 1991), then the effect of the eddies on the zonal-mean flow is

$$\frac{\partial \overline{u}}{\partial t} = \frac{1}{\cos\phi} \nabla \cdot EP_{flux}. \tag{5.5}$$

5.3   Results

5.3.1   Assessment of the LMDZ-CTR general circulation

Before comparing the different experiments, we tested the ability of the LMDZ-CTR model in simulating the observed large-scale circulation of the SH through a set of energy diagnostics associated to the mean and transient flows. The Subtropical Jet (STJ) in winter and the Subpolar Jet (SPJ), also known as the eddy-driven jet, are dominant features of the extratropical climate; therefore, an accurate representation of the jet positions and intensities is necessary for climate models to correctly simulate the extratropical general-circulation. Also, TKE together with its related transports are considered due to its strong interaction with the mean flow.

The ERAi summer climatology of KZ at 300 hPa shows that the SPJ core axis is located around 50°S (Fig. 5.2a). LMDZ-CTR experiment simulates well KZ climatology during summer (Figs. 2b and 2c). However, it fails to reproduce its latitudinal position by simulating it northward from the reanalysis. The location of the maximum intensities is correctly simulated over the Atlantic and the Indian Ocean. Also, the wide area over the South Pacific suggests a double jet, but the model reproduces a weaker SPJ than the reanalysis.
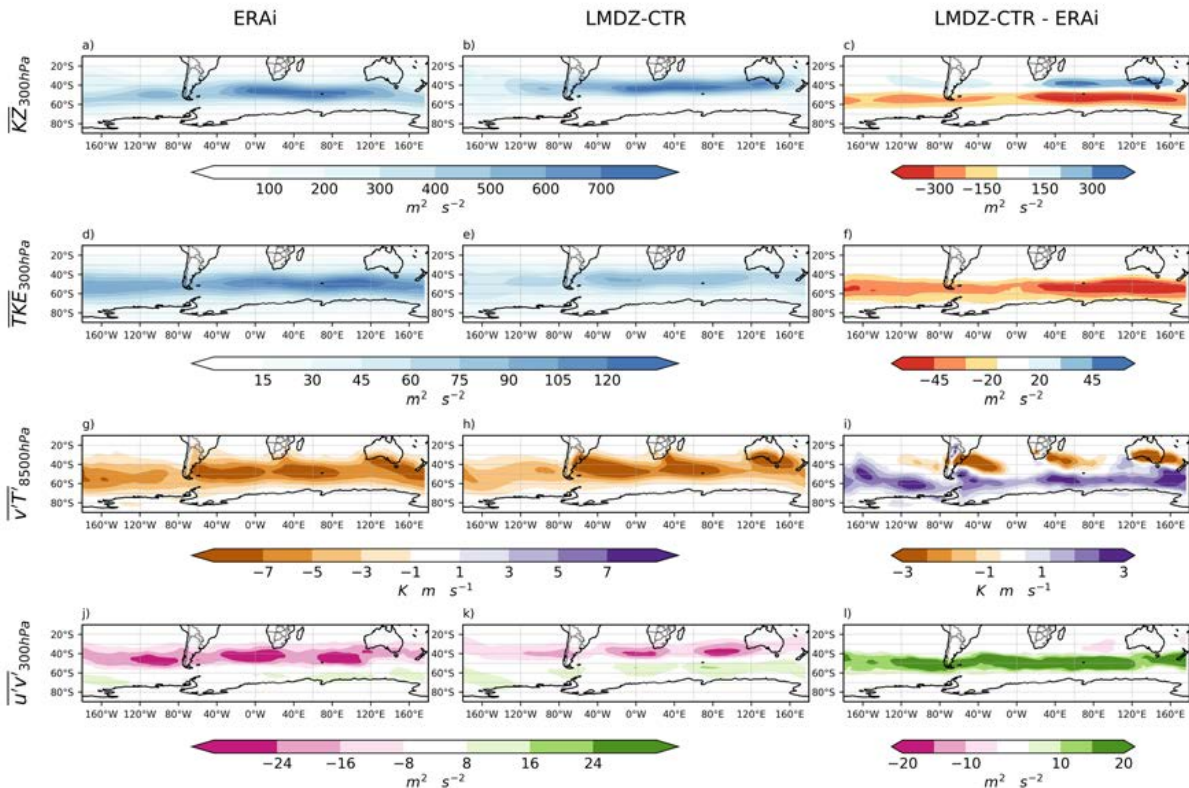
Fig. 5.2. Summer climatologies of the zonal kinetic energy at 300 hPa (a-c), transient eddy kinetic energy at 300 hPa (d-f), transient meridional heat flux at 850 hPa (g-i) and transient meridional momentum flux at 300 hPa (j-l). The left panels display the mean fields of ERAi, the central panels the mean fields of the LMDZ-CTR experiment and the right panels the biases of LMDZ-CTR with ERAi.

As described in the methods section, high-frequency eddy kinetic energy (TKE) is a proxy of the storm tracks, and represents the mean position and amplitude of transient eddies. In summer, the core of the storm tracks is located in the same latitude position as the jet core axis (Fig. 5.2d). The LMDZ-CTR model underestimates the intensity of the storm tracks, suggesting a misrepresentation of the migratory eddies (Figs. 2e and 2f). The result is partly associated with the idealized SST used to force the model, and also due to the low-resolution of the model over the oceans that soften the SST gradients Carril and Nuñez (2000), Inatsu and Hoskins (2004). Also, the position of maximum intensities is misrepresented, by locating it in the Atlantic Ocean, instead of the Indian Ocean.

In midlatitudes, transient eddies carry the mayor part of energy poleward. Fluxes of heat and momentum associated with migratory eddies are also considered due to their relevance

in the eddy/mean-flow interactions. The summer-mean ERAi maximum heat fluxes in the lower troposphere are located over the Warm Conveyor Belt regions (Shaw et al., 2016), preferentially in the western ocean basins between 40°S and 60°S (Fig. 5.2g). On the other hand, large poleward momentum fluxes are located at the upper levels of the troposphere, further downstream the location of heat fluxes, maximizing in the eastern sector of the ocean basins (Fig. 5.2j). Small positive values in momentum transport at high latitudes indicate a convergence of momentum near 60°S. LMDZ-CTR simulation captures the large-scale and most of the detailed features of the ERAi eddy heat and momentum transports (Figs. 2h and 2k). However, the intensity of the momentum transports are smaller than the reanalysis. On the other hand, LMDZ-CTR represents the maximum heat fluxes equatorward the reanalysis, especially in the western basins in the vicinity of the continents around 35°S.
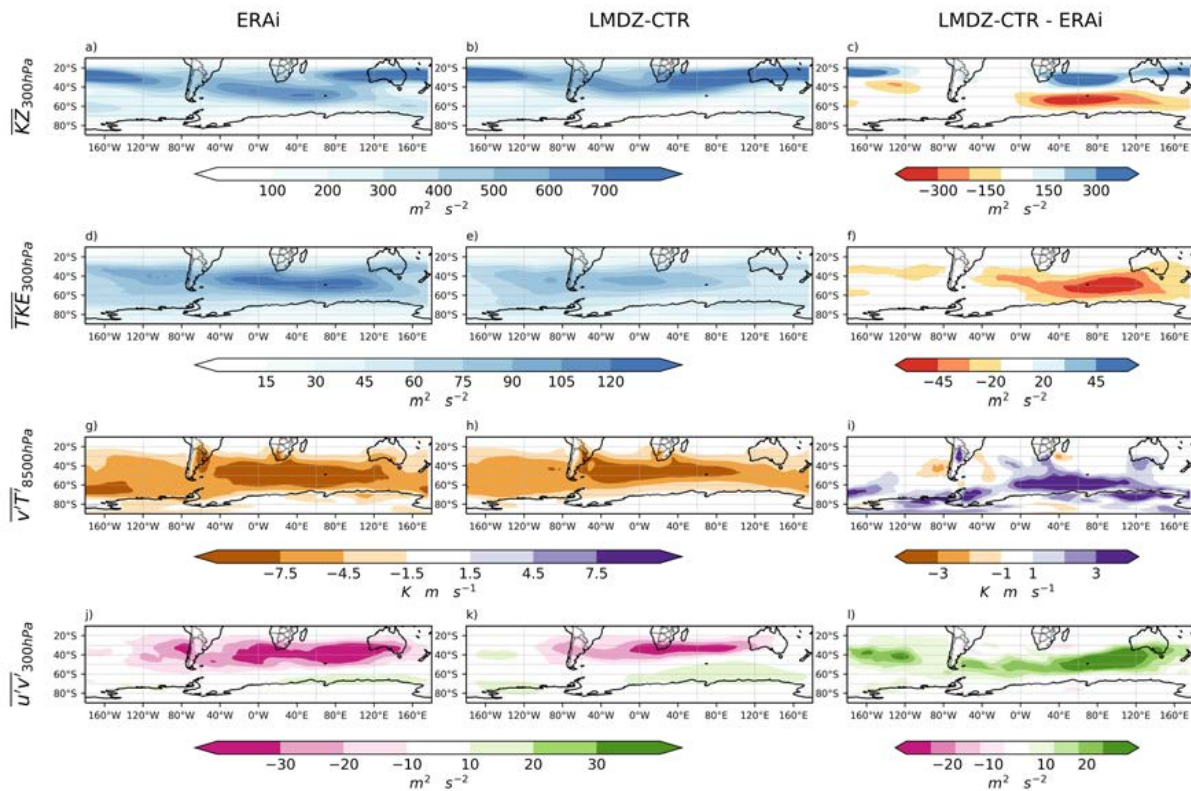
Fig. 5.3. Same as in Fig. 5.2 but for the winter season.

During winter, the mean position of the jet core axis is located equatorward its position in summer (Fig. 5.3a). The ERAi KZ presents a spiral structure around high latitudes with the entrance and exit of the jet located in the Indian Ocean. The double jet in the Pacific Ocean

is more evident than in summer, with the STJ as the dominating branch at the 300 hPa level. LMDZ-CTR experiment can reproduce this double-jet structure (Fig. 5.3b), but simulates a more (less) intense STJ (SPJ) than the reference. The LMDZ major deficiency is in its inability to simulate the jet entrance and exit regions located over the Indian Ocean by presenting a single continuous core. The bias, thus, is seen as positive (negative) values northern to (southern to) 40°S associated to the jet entrance (exit).

Temperature gradients in mid-latitudes are strongest in the winter hemisphere due to the seasonal changes of insolation. Therefore, storm tracks usually reach its maximum intensity during winter, maximizing the transport of heat and momentum (Figs. 5.3d, 5.3g and 5.3j). Alike summer, LMDZ-CTR has a weaker storm track activity than the reanalysis (Fig. 5.3f). This deviations from reanalysis was already noticed by Carril et al. (2002) when using a different configuration of the model. Differences with ERAi eddy fluxes are also noticeable, with the model simulating smaller heat and momentum transports (Figs. 3i and 3l). In particular, the southward extension of the eddy momentum transport and the eddy heat transport are mis-represented by the model (Figs. 3h and 3k), and the simulated maximum is only identified in the jet's equatorward flank.

5.3.2 Validating the nudging experiments

Despite the presence of regional characteristics in the general circulation of the SH, we no-ticed that most of LMDZ-CTR deviations from the reanalysis climatology in the diagnostics presented above vary principally with latitude. We therefore consider that the zonal-mean cross section outside the nudged region can be a good way to summarize the sensitivity of the LMDZ model to regional forcing in SA.

In summer, the vertical sections of zonal kinetic energy show a well defined SPJ core, with its center located in 50°S and extending from 40°S to 60°S (Fig. 5.4a). The vertical structure of the jet is deep, extending throughout the troposphere. In good agreement with the results presented in the previous section, LMDZ-CTR experiment has an equatorward shift in the po-sition of the jet core, as indicated by the dipole bias with positive values in the subtropics and negative values in the extratropics (Fig. 5.4b). The response of the LMDZ model to regional information nudged over SA indicate a substantial reduction of the KZ biases for both of the experiments, LMDZ-fERAi and LMDZ-TWN (Figs. 4c and 4d).

The ERAi TKE has a similar structure to KZ, with maximum values around 300 hPa and with a deep vertical structure (Fig. 5.4e). The underestimation of cyclone intensity by LMDZ-CTR
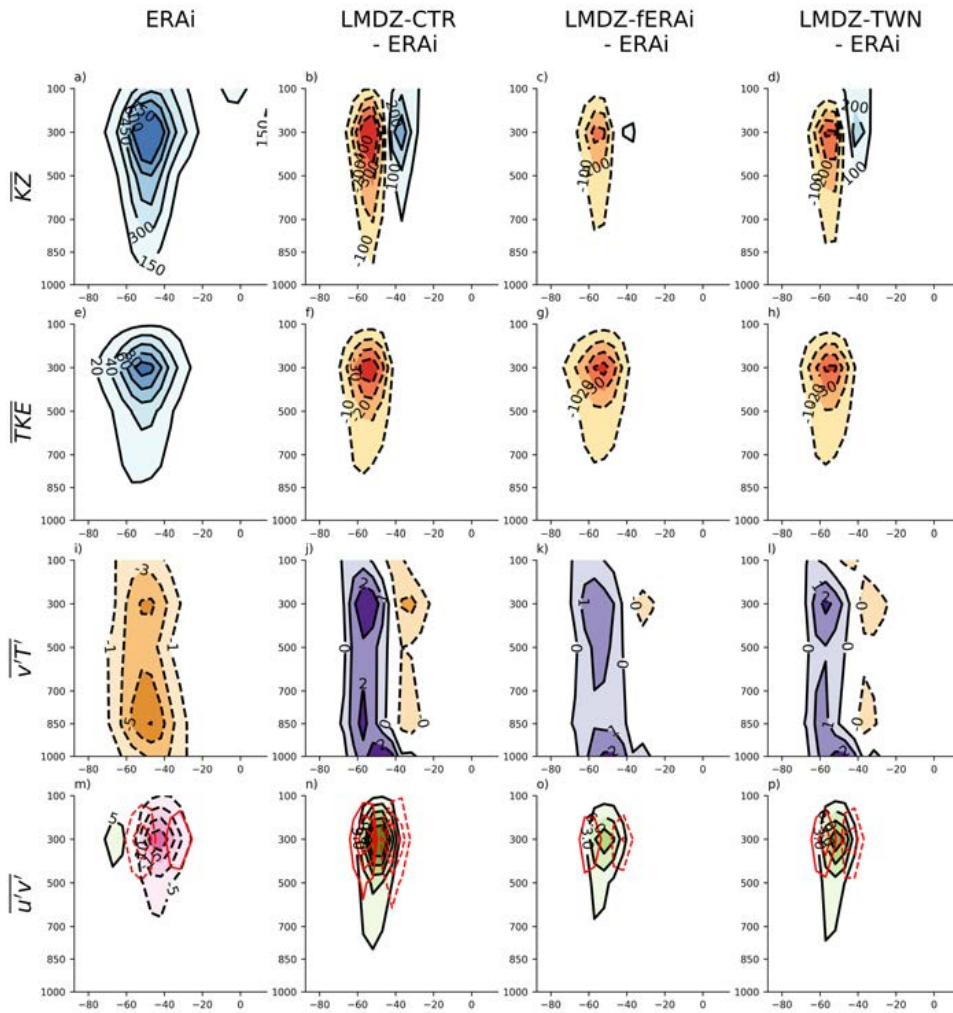
Fig. 5.4. Summer-mean latitude-pressure cross sections of zonal kinetic energy (a-d), with mean and bias contour intervals of 150 and 100 $m^2 s^{-2}$, transient eddy kinetic energy (e-h) with mean and bias intervals of 20 and 10 $m^2 s^{-2}$, transient meridional heat fluxes (i-l) with mean and bias intervals of 2 and 0.75 Kms^{-1} and transient meridional momentum fluxes (m-p) with mean and bias intervals of 5 and 3 $m^2 s^{-2}$, respectively. The mean values are calculated outside the nudged zone (180°W-90°W&20°W-180°E). Dashed contours show negative values. The figure also displays the meridional component of the Eliassen–Palm flux divergence (m-p, red lines), with mean and bias intervals of 5×10^{-6} and 3×10^{-6} ms^{-2}. The left panels display the climatology fields of ERAi, and the second, third and forth columns the difference between ERAi and LMDZ-CTR, LMDZ-fERAi and LMDZ-TWN, respectively.

is still perceived in the zonal-mean sections by presenting a TKE 40% smaller than reanalysis. Differences between experiments are quite subtle (Figs. 4f to 4h), suggesting the bias-

reduction in the mean-flow is not directly related to an improvement of the storm track mean position and intensity. It also suggests that the storm-track simulation is mostly influenced by the representation of the SST gradients rather than to a better representation of the regional information over SA (Inatsu and Hoskins, 2004).

During summer, the poleward eddy heat fluxes are maximum in the lower troposphere in the midlatitudes (Fig. 5.4i). Their role is to reduce the large equator-to-pole temperature gradient by transporting heat to higher latitudes, and consequently to reduce upper level westerlies and maintain the thermal wind balance. LMDZ-CTR tends to overestimate the transport in the subtropics and underestimate it in the extratropics (Fig. 5.4j). Both sensitivity experiments reduce this bias throughout the troposphere (Figs. 4k and 4l). In the vertical level of 850 hPa, the latitude with maximum transports is near 50°S, and the maximum LMDZ-CTR biases are located southward with deviations up to a 40% of the reference values. The bias is reduced to a 10% and a 24% for the LMDZ-fERAi and the LMDZ-TWN, respectively.

The summertime transient momentum fluxes are negligible in the lower troposphere, increasing its value with height until it reaches its maximum near the tropopause (Fig. 5.4m). The negative values in midlatitudes indicate that the dominant effect is a poleward momentum transport, that is followed by positive values near the poles. The meridional convergence (divergence) of momentum is, thus, maximum near 50°S (30°S) and is responsible for accelerating the zonal-mean flow (Trenberth, 1991). LMDZ-CTR simulates a weaker momentum transport than reanalysis, as indicated by the positive deviations in the climatology (Fig. 5.4n). The deviations in the upper troposphere are large, reaching a 60%, and are reduced to a 36% and 28% for the LMDZ-TWN and LMDZ-fERAi, respectively (Figs. 4o to 4p). All three LMDZ experiments simulate a weaker eddy influence on the mean flow than the reference, showing positive deviations in the position of convergence and negative deviations in the position of divergence. However, the response in the nudging experiments shows a reduction of the EP-flux convergence/divergence bias, which accounts for the strengthen of the SPJ near its observed position and a deceleration of the flow equatorward.

KZ in winter has very different zonal-mean features to summer, presenting a double structure of maximum intensities (Fig. 5.5a). The SPJ is located in the extratropics, with its center in the tropopause (∼100 hPa) near 60°S, and large values reaching the whole troposphere. On the other hand, the mean position of the STJ core is 30°S near the 300 hPa level, and its influence is confined to the upper troposphere. Both LMDZ-CTR and LMDZ-TWN fail to reproduce the SPJ, by presenting large negative KZ biases in the whole troposphere in the extratropics
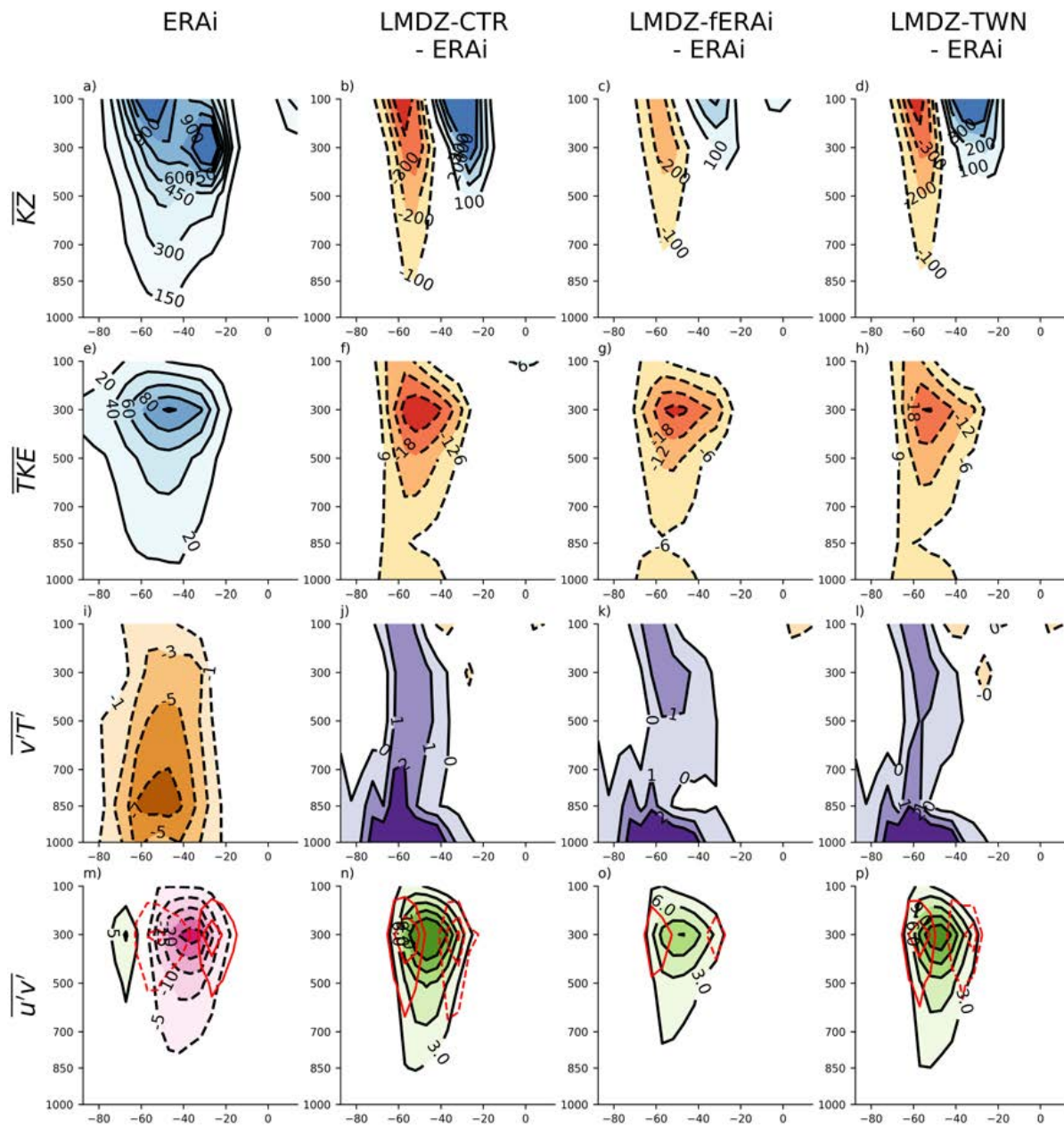
Fig. 5.5. Same as in Fig. 5.4 but for the winter season.

and large positive biases near the tropopause in the subtropics (Figs. 5b and 5d). Regarding the STJ, the LMDZ-CTR tend to simulate a stronger jet than the reanalysis, with positive deviations over the maximum core region. Contrary to the SPJ, the LMDZ-TWN improves significantly the deviations associated to the intensity of the STJ (Fig. 5.5d), especially in the Pacific Ocean (see Fig. S5.2 in supplementary material). The LMDZ-fERAi experiment improves sub-

stantially the simulation of both jets (Fig. 5.5c), suggesting that a "perfect" representation of SA have a positive effect in the structure of the mean flow throughout the SH.

The zonal-mean structure of winter TKE is similar to summer, with its maximum values located near 45°S and 300 hPa (Fig. 5.5e). However, wintertime eddy activity presents a stronger TKE and a broader latitudinal extension than in summer, with significant values from 20°S to the pole and until the lower troposphere. LMDZ-CTR continue simulating weaker storm tracks than the reanalysis, with deviations up to a 30% (Fig. 5.5f). Contrary to the results found in summer, the TKE deviations are somewhat reduced, especially for the LMDZ-TWN experiment (Figs. 5g and 5h).

Zonally-averaged eddy transports of heat and momentum are stronger in winter than in summer, as expected due to the intensification of the temperature gradient between the equator and the poles, and the consequent intensification of the storm tracks (Figs. 5i and 5m). From the transient heat flux standpoint, the poleward fluxes during winter are largest in the lower troposphere, near the 850 hPa level (Fig. 5.5i). Still, significant transport is found in the whole troposphere in midlatitudes (between 70°S and 30°S). All three experiments tend to underestimate the poleward heat transport throughout the troposphere, maximizing the deviations in the lower troposphere (Figs. 5j-5l). As in summer, at a level of 850 hPa, the maximum positive deviations are located southward the maximum transport, with biases in the core region of 25% for the LMDZ-CTR experiment. Both sensitivity experiments, LMDZ-fERAi and LMDZ-TWN, reduces the heat transport bias in mid-troposphere, especially between 850 hPa to 500 hPa, and by 15% and 20% in the core region, respectively. Together with the improvement in the simulation of the TKE, the results indicate that both sensitivity experiments simulate better the growing phase of baroclinic perturbations during winter.

The transient eddy momentum transport are maximum southerly of the STJ, near 35°S, with its core in 300 hPa. The eddy momentum flux convergence is located in the SPJ latitudes, near 50°S, and momentum divergence is present in the subtropics, where the STJ is located (Fig. 5.5m). The eddies, thus, are the ones responsible for transporting energy from the STJ to the SPJ. LMDZ-CTR simulation of momentum transport is much weaker than ERAi, with deviations that reach a 70% of the total magnitude (Fig. 5.5n). The transports improve significantly in the perfect-boundary experiment, LMDZ-fERAi, with deviations of a 45% (Fig. 5.5o), but the improvements are quite small in the LMDZ-TWN experiment (Fig. 5.5p). This is reflected in the conservative bias-reduction of the LMDZ-TWN convergence of the momentum flux deviations. The result is consistent with the fact that no improvement was found in the

simulation of the SPJ by the LMDZ-TWN experiment. However, an improvement in the momentum divergence is noticed for this interactive experiment, in agreement with the better representation of the STJ.

5.3.3   Regional analysis of the LMDZ-TWN experiment

The improvement of LMDZ-TWN in simulating some extratropical circulation features when compared to the control experiment is a direct consequence of its interaction with a higher-resolution regional version of the model in SA. Yet, it is not straightforward that LMDZ-Regional adds value to LMDZ-CTR experiment as it can even degrade the model's climate representation. To understand the results presented above, we need to understand better how the TWN experiment adds value, or not, to the control experiment in SA.

Poleward heat and moisture transports from the tropics to the extratropics are essential for cyclone formation and cyclone intensification. As discussed in the introduction, the warm and moist low-level jet in the lee side of the Andes plays a crucial role in the cyclogenesis in southern SA. We, therefore, start the analysis by evaluating the pathways of low-level heat $(\overline{vT})$ and moisture $(\overline{vq})$ transports over the continent.

Summer-mean climatology of meridional low-level (900 hPa) transports (Figs. 6a and 6d) shows two sources of northerly flow from Amazonia into the subtropics, one starting in Venezuela and crossing the continent in the lee of the Andes and another starting in northern Brazil and converging with the former at 10°S. The fields also distinguish a northerly flow from the South Atlantic Convergence Zone (SACZ) region to the subtropics. Both LMDZ experiments, LMDZ-CTR and LMDZ-TWN, fail to reproduce the moisture intrusion from northern Brazil into Amazonia by locating it to the south of the reanalysis (Figs. 6e and 6f). The northern branch is well simulated, but transports are overestimated. However, the LMDZ-TWN experiment have smaller biases when compared to the control experiment, indicating that it improves the meridional transport of air masses between the tropics and the subtropics. Focusing on the subtropics, in northern Argentina, LMDZ-CTR presents strong biases of heat and moisture that are mainly associated to an anticyclonic anomaly in the western flank of the Chaco-Low and an intense Chaco-Low (Fig. 5.6h), (Seluchi and Marengo, 2000b). Thus, the model overestimate the transport into the SACZ region and underestimate the transport into midlatitudes. The LMDZ-TWN experiment represents better the low-level steady circulation (Fig. 5.6i), whereby in this case too the energy transport is improved from the subtropics into the extratropics. LMDZ-CTR presents a positive bias in heat and moisture transport
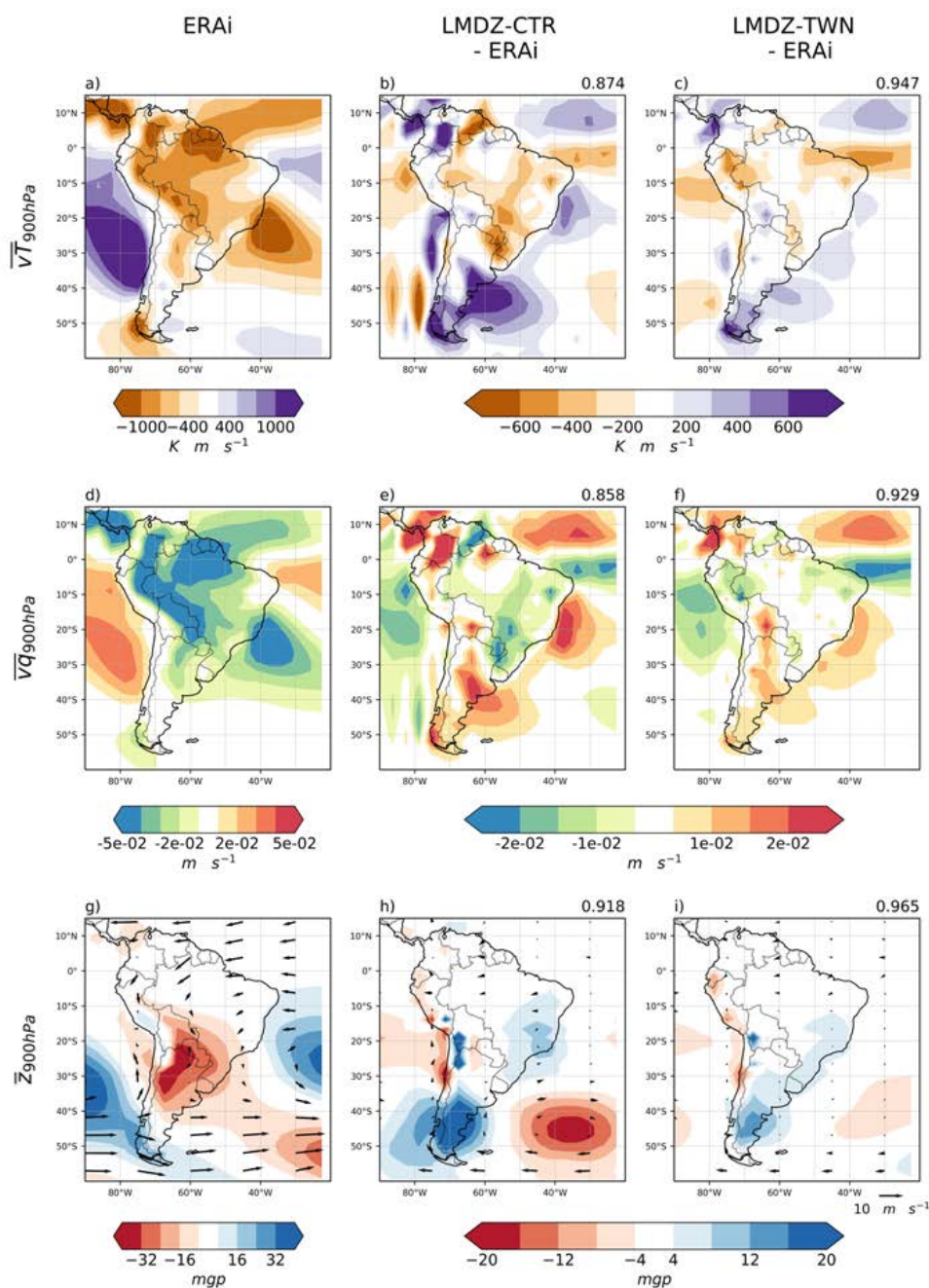
Fig. 5.6. Summer-mean heat (a-c) and moisture (d-f) daily meridional transports and zonal anomaly of geopotential height (g-i) in the lower troposphere (900 hPa). The figure also displays the 850 summer-mean winds (g-i). The left panels correspond to ERAi climatology, and the central and right panels the deviation from ERAi of LMDZ-CTR and LMDZ-TWN, respectively. Spatial-pattern correlation coefficients between ERAi and the simulated fields are given in the upper-right side of each panel.

over Patagonia and its surrounding ocean, which is associated to a stationary anticyclonic anomaly misrepresented by the model over the extratropics. The bias is largely reduced by the LMDZ-TWN approach, due to a better representation of the low-level circulation through reducing the anticyclonic anomaly over Patagonia.

The former comparison reveals the effect of high resolution on the better representation of the low-level circulation. Since results indicate that the interactive experiment improves the energy transport between the subtropics and the extratropics, then it should also favour the onset and intensification of cyclones in the region of maximum cyclogenesis near South America. We explore this theory by analyzing the transient transports of heat and momentum over the continent (Fig. 5.7).

The poleward transient heat flux during summer is largest in the mid-latitudes, south of $30°$S, and it intensifies immediately to the east of the Andes, peaking at $50°$S (Fig. 5.7a). The LMDZ-CTR experiment misrepresent the location of the maximum transport by locating it northward the reanalysis, with large negative deviation over eastern SA and the Atlantic Ocean between $30°$S and $40°$S (Fig. 5.7b). These deviations are significantly reduced in the LMDZ-TWN experiment (Fig. 5.7c).

Vertical heat transport and meridional transports of heat and momentum arising from migratory cyclones are intimately related, and the former is crucial for vertical energy transports and the conversion from eddy available potential energy to TKE. The summer-mean climatology of transient vertical heat transport has a strong resemblance in its pattern with the meridional transport, and thus, model biases are also alike (Figs. 7d to 7f). The LMDZ shows a larger than the reference eddy activity leeward of the Andes, from $20°$S to $40°$S, and extending into the Atlantic Ocean near $40°$S. The TWN experiment presents similar deviation signals, but with a significant bias-reduction and a higher pattern correlation coefficient.

The migratory eddies transport momentum poleward in midlatitudes during the summer period (Fig. 5.7g). Neither of the experiments capture well the intensity of the fluxes by simulating weaker transports than in the observational climatology (Figs. 5.7h and 5.7i). However, during this season, the deviation of the LMDZ-TWN simulation is significantly reduced compared to the control experiment. The correlations also reflect the better representation of the fluxes by going from a spatial correlation coefficient of 0.63 in the LMDZ experiment to 0.86 in the LMDZ-TWN experiment. The major improvements are found after the passage of the flow through the continent, seeming like a rectification of the flow. This suggests that the transient eddies in the LMDZ-TWN experiment are more vigorous and/or have an more realistic tilt of
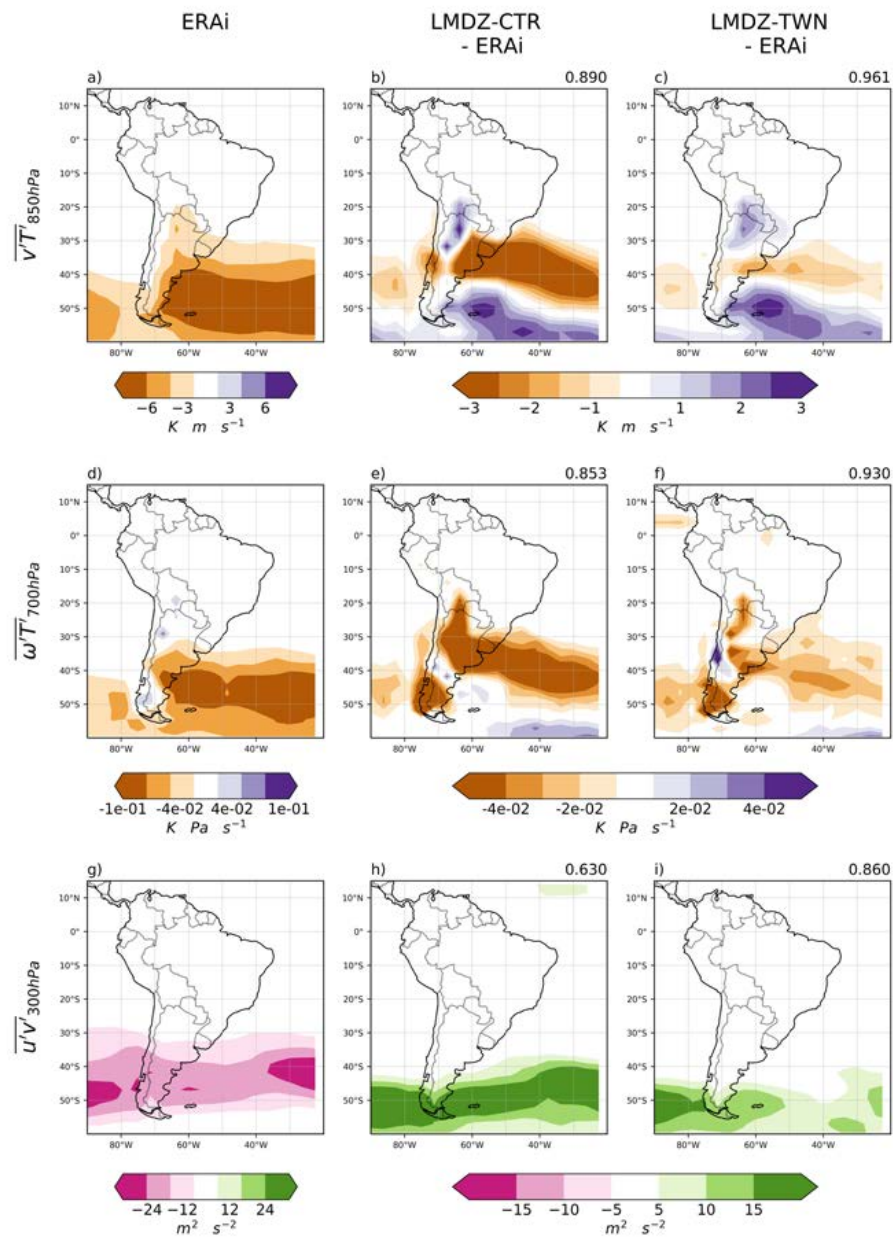
Fig. 5.7. Summer-mean transient eddy heat meridional fluxes (a-c), vertical heat fluxes (d-f) and horizontal momentum fluxes (g-i). The left panels correspond to ERAi climatology, and the central and right panels the deviation from ERAi of LMDZ-CTR and LMDZ-TWN, respectively. Spatial-pattern correlation coefficients between ERAi and the simulated fields are given in the upper-right side of each panel.

the axes of wedges and troughs in the South-Western Atlantic.

During winter, the poleward low-level transport of heat and moisture are only in a con-
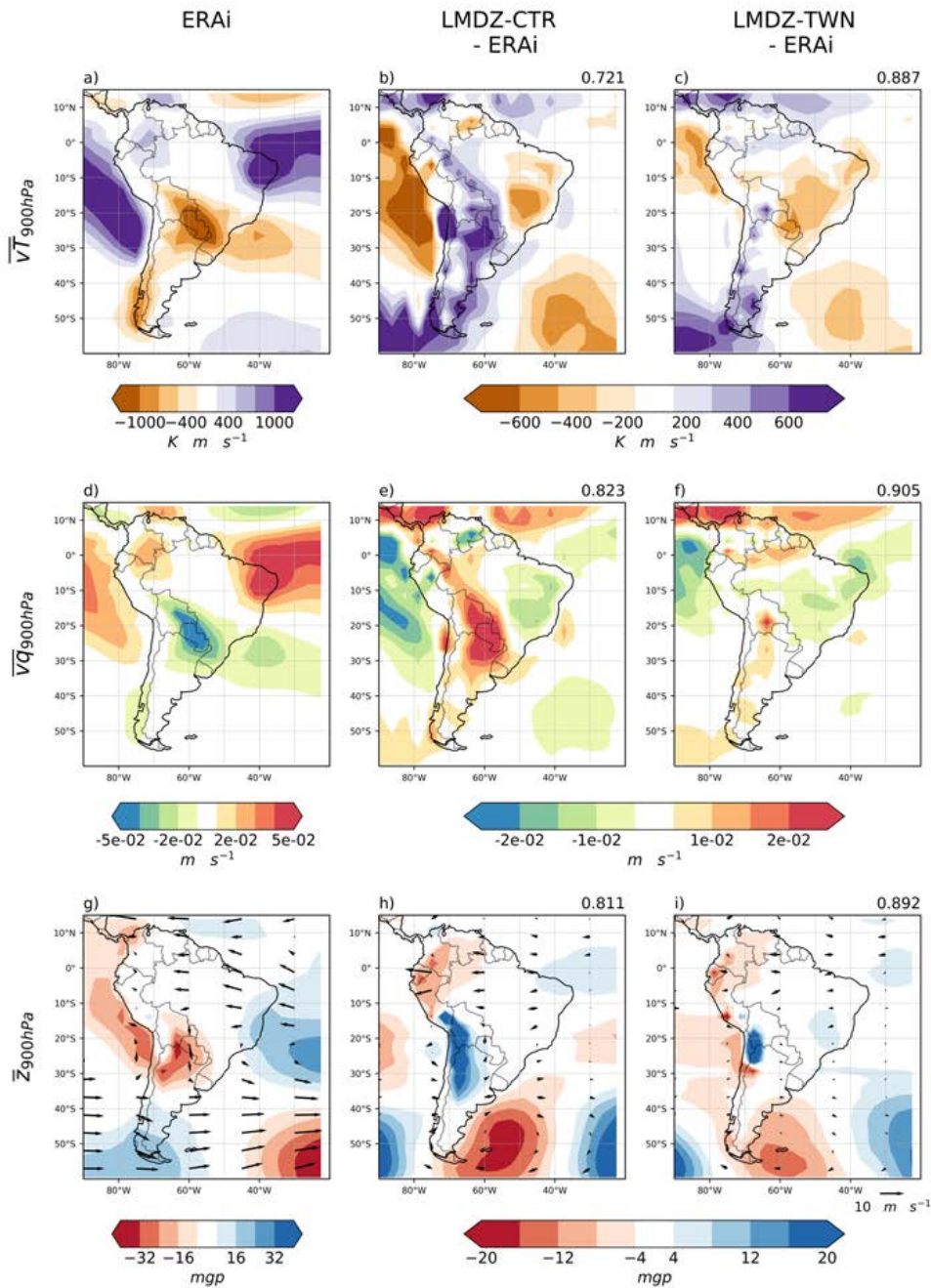
Fig. 5.8. Same as in Fig. 5.6 but for the winter season.

fined area in the subtropics centered at 25°S and with a southward extension up to 30°S, where the low-level jet flows out (Figs. 8a and 8d). The low-level jet is a regional feature of the South American climate and is present throughout the year (Seluchi and Marengo, 2000b, Berbery and Barros, 2002, Menéndez et al., 2001, Knippertz et al., 2013). During winter, this

phenomenon is related to events of tropical moisture exports within the warm sector of extratropical cyclones or ahead of upper-level troughs (Knippertz et al., 2013). The LMDZ experiment presents a weak skill in representing the low-level temperature advection over the whole continent, especially in the exit region of the low-level jet (Fig. 5.8b), with a correlation coefficient of 0.72. Consistent with a stationary geopotential bias over the Andes (Fig. 5.8h), the bias in the low-level flux of heat and momentum is largest over subtropical latitudes. The LMDZ-TWN results show a significant improvement in representing the observed low-level transports, especially over the northern and central sector of Argentina (Fig. 5.8c). The spatial correlation coefficient is also higher, presenting a value of 0.89. Moisture transports are better represented than heat transports by both experiments, but LMDZ-CTR experiment continue having large biases over the subtropics (Fig. 5.8e). Again, the LMDZ-TWN experiment has a better performance, reducing the bias by a 40% over the area (Fig. 5.8f).

As revealed in ERAi climatology, the winter-mean high-frequency eddy heat flux in the lower troposphere is maximized leeward of the Andes, with a continental maximum over northeast Argentina (Fig. 5.9a). LMDZ-CTR experiment has a good representation of the flux, with a high spatial correlation of 0.97. However, it underestimates the transport in the continent, especially over northern to central Argentina (Fig. 5.9b). The interactive experiment reduces the transport bias over northern Argentina (Figs. 5.9b and 5.9c).

Alike summer, the wintertime eddy vertical heat flux in the low midtroposphere is highly correlated with its meridional counterpart (Fig. 5.9d). However, downflow regions with positive values are identified, probably due to the mechanical forcing of the Andes. LMDZ-CTR model underestimates the downward flux over the Andes and the upward flux in its lee side, over central Argentina (Fig. 5.9e). The TWN experiment cannot show a clear successful result on the bias-reduction problem (Fig. 5.9f). The improvement is found only locally, over central Argentina and its surrounding continental shelf, but does not propagate farther.

Momentum transport in winter is larger than in summer, and has a poleward shift after the crossing the Andes (Fig. 5.9g). This poleward shift of the transport is not well represented by the simulations (Figs 5.9h and 5.9i). The LMDZ-TWN experiment subtly improves its representation, especially after the passage through the continent, as noted again by the increased correlation from 0.81 in the control experiment to 0.88 in the TWN experiment. However, the rectification of the flow is only regional, and the biases return to be comparable in the Atlantic Ocean.
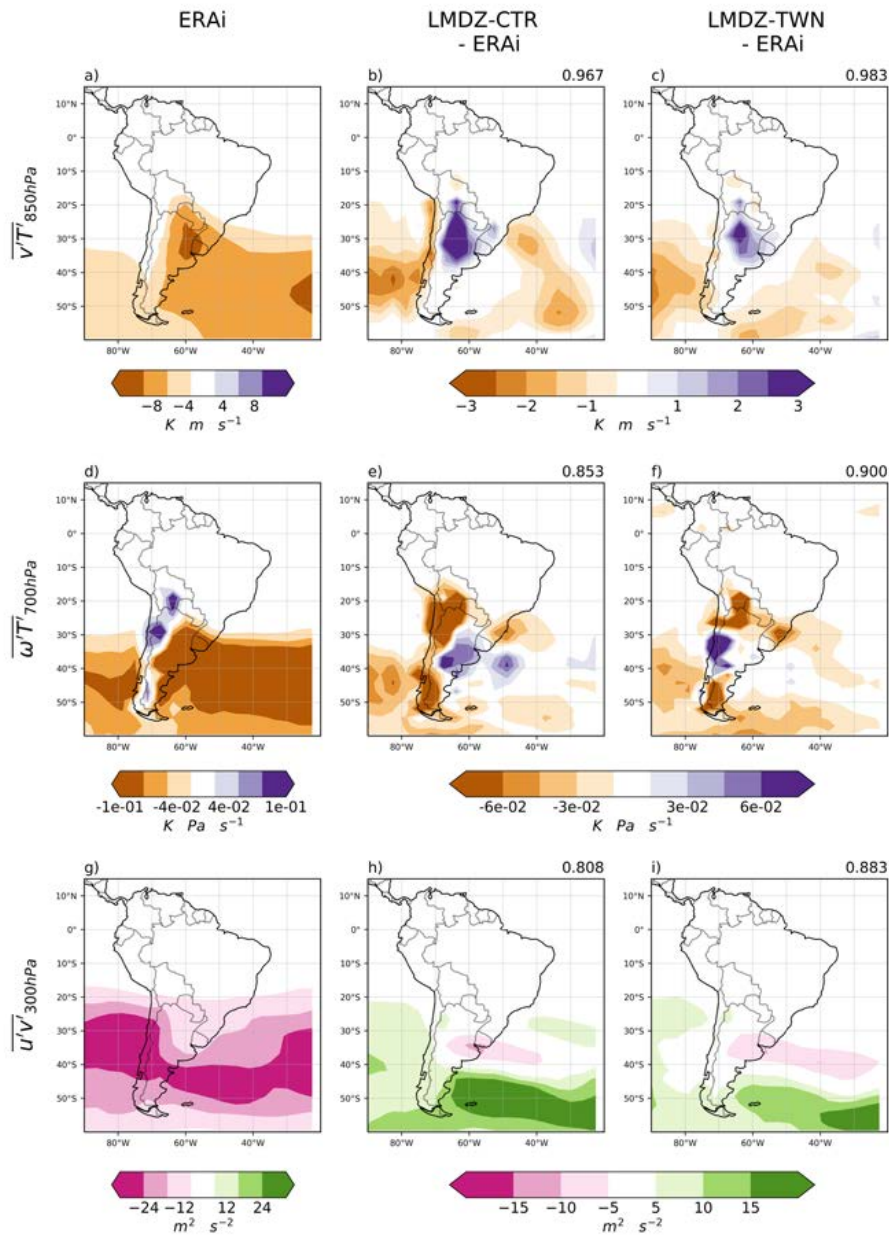
Fig. 5.9. Same as in Fig. 5.7 but for the winter season.

5.4 Final remarks

Despite the advances in their resolution and complexity, the state-of-the-art climate models continue failing to reproduce the intensity of eddy activity and the mean location of the jet streams in the Southern Hemisphere (Chang et al., 2012, Ceppi et al., 2012, Wilcox et al., 2012, Bracegirdle et al., 2013, IPCC, 2013, Pithan et al., 2016). A part of the deviations is due to the

rather coarse-resolution of the models, which fail to represent sub-synoptic mountain features and mesoscale weather phenomena. In the SH, the complex regional topography of the Andes has strong influences on the local climate and plays a major role in the cyclolysis and cyclogenesis of migratory eddies. In fact, the presence of the Andes control the storm track activity through mountain torque and also through moist and heat transport from the tropics to the extratropics by channeling the low-level jet.

In this chapter, we explored how the quality of the simulation of the South American climate affected the simulation of the general circulation of the southern hemisphere. For this, we studied the added value of high-resolution information over South America in the simulation of the SH extratropical circulation by nudging the LMDZ4 over the continent to different forcing information. Our approach is equivalent to the RCM's: while the higher-resolution simulations provided the regional information through the nudging of the GCM over SA, the GCM could reproduce the large-scale information elsewhere. The added value was explored under three setups: 1) An AMIP-type control simulation forced by climatological SST and sea ice distributions (LMDZ-CTR), 2) The same than the former but including an interactive nudging over SA to a regional and higher resolution version of the model (LMDZ-TWN), and 3) The same than the control simulation but including a nudging over SA to ERA-Interim (LMDZ-fERAi). We hypothesized that a better representation of the Andes, together with a better description of the mesoscale features and surface processes over SA, should improve the simulation of the general circulation in two ways: first, through enhancing the mountain torque exerted to the westerly flow, and second through improving the energy transports between the tropics and the extratropics.

The performance of all three experiments was assessed by studying a wide range of model fields and comparing them with ERA-Interim. Despite the relatively low resolution of LMDZ-CTR, this global model could reasonably well simulate the more significant large-scale circulation patterns over the SH. However, the model showed some typical climate model biases in simulating the storm track and the Southern Hemisphere jet latitude. One of the most significant deviations from the ERAi climate was its underestimation of the horizontal eddy momentum flux. An appropriate representation of this flux and its convergence is crucial due to its role in controlling the mean jet-stream position.

Mendes et al. (2007) found that the Andes plays a crucial role in the mean circulation over SA by channeling warm and moist tropical air from the Amazon basin into east subtropical South America. A summertime characteristic of the low-level circulation is the Chaco-Low,

that is known to regulate the incursion of that tropical air into the midlatitudes (Seluchi and Marengo, 2000b, Salio et al., 2002). Cyclogenesis is then accompanied by the transport of heat and moisture into the cyclone, increasing conditional instability and leading to cyclone development. Our results suggests that the enhanced resolution experiment has a better representation of the low-level circulation over SA and, thus, simulates better the meridional transport of moist enthalpy from the tropics into the extratropics. This confirms previous findings in literature when analyzing the impact of increased resolution in the simulation of the low-level jet Vernekar et al. (2003), De Sales and Xue (2011), Sakaguchi et al. (2015). The biases of the control experiment were partly explained by its simulation of a too-weak Chaco-Low, which reduced the transport of energy into midlatitudes and enhanced the transport into the South Atlantic Convergence Zone. The interactive experiment rectified these deviations from the ERAi flow and improved the eddy transports locally and over the adjacent Atlantic Ocean.

The local improvement of the summertime low-level circulation was followed by a better representation of the global extratropical circulation. When compared with the control experiment, the regional nudging over SA had a positive feedback on the simulation of the midlatitude jet position by significantly reducing the bias deviation of the mean KZ outside the nudged zone. The improvement was accompanied by a better representation of the transient eddy heat and momentum fluxes, together with a better description of momentum transport convergence, while the increment in eddy kinetic energy was less pronounced.

In winter, the penetration of tropical air towards higher latitudes is associated with Tropical Moisture Events (Seluchi and Marengo, 2000b, Knippertz et al., 2013). Compared to summer, wintertime improvements in the low-level circulation in SA were more subtle. A better representation of the low-tropospheric heat and momentum transport was identified, together with amelioration of eddy transports. However, the effect of the Andes had a limited reach, and only contributed to the synoptic-scale activity around the nested area, resulting in biases of similar magnitude in the eastern flank of the Atlantic Ocean.

The evaluation of all three experiments in simulating the wintertime general circulation outside the nudged-zone showed a limited bias-reduction for the regional-driven simulations, especially in the case of the TWN system. In fact, improvements of the TWN system compared to the control experiment were noticed only in the early stages of cyclone lifecycle (Lorenz, 1955), as it was perceived in the simulation of the eddy heat transport and eddy transient kinetic energy. Both of the experiments had large and comparable biases in simulating the SPJ, in line with the large deviations of eddy momentum transport and its convergence over

higher latitudes. A better representation of the STJ is, though, observed for the interactive nesting system, together with a bias-reduction of the maximum divergence equatorward the momentum convergence. Regarding the ERA-Interim driven simulation, we found an amelioration of the representation of the general circulation outside the nudged-zone, highlighting the importance of a correct representation of the SA climate in the simulation of the SH extratropical circulation.

The results from the present study demonstrated that improvements in resolution over SA effectively excites the simulation of the mean atmospheric circulation in the SH. The work, thus, emphasized how substantial improvements in representing the large-scale atmospheric circulation may be accessible with just increasing horizontal resolution over key areas of the globe. The current set-up, however, had some limitations such as the inability to investigate the high-resolution effect of SSTs. Also, our interpretations are based uniquely on the ERA-Interim reanalysis as the reference, and a more comprehensive analysis requires further assessment based on independent datasets. We believe this research has raised many questions in need of further investigation and future studies on the influence of the Andes on the simulation of the extratropical circulation are therefore recommended.

Chapter 6

Conclusions (English)

6.1 What we've learned

In the thesis, we studied the added value (AV) of regional climate models (RCMs) in South America (SA) from different perspectives and with different methodologies. Our main goal was to identify the AV signal to gain a deeper understanding of the strengths and weaknesses of RCMs in SA. Throughout the thesis, we explored several aspects of AV and reached the following conclusions:

6.1.1 Added value on seasonal climatology

The first question that arises when studying the AV of RCMs is whether they improve in the representation of the mean climate regarding the Global Climate Model (GCM) or global reanalysis used as initial and boundary condition. Because of its higher resolution, there are many reasons to suppose that the regional model can improve the simulation with respect to its driving data, such as its better representation of the surface forcing, a better simulation of regional processes and interactions, and a smaller time step interval. But there are also many other reasons to believe they cannot: their inability to simulate scales larger than their limited domain, the inconsistencies in the dynamics and physics among the RCM and its driver, the error propagated from the GCM to the RCM through the lateral condition, among others.

Our main conclusion when going through literature and from our own assessment is that there is no unique answer to this question. Sometimes the RCM will add value when compared to its driver, sometimes not. The most important issue here is to identify key factors to which most AV signal is attributed, where these factors can be the variable, region, statistic,

season of the year, RCM, boundary condition, among others. Results indicate that the AV signal is larger for surface air temperature than for precipitation, due to the sensitivity of this first variable to surface forcing; and over regions where regional processes dominate over remote forcings, such as summertime circulation in the tropics.

6.1.2 Selecting the right metric for the assessment

There is no doubt that it is very important to evaluate if the RCM can add value compared to a GCM in large-scale climate characteristics, that is, by interpolating into the coarser grid or through area averaging. But performing a spatial upscale of the RCM fields result in losing the main potential advantage the RCM has: its ability to simulate small-scale information. Thus, if the GCM has a much coarser resolution than the RCM, then a scale-aware metric is recommended. In the second chapter of the thesis, we were inspired by the work from Kanamitsu and DeHaan (2011), who discussed the possible reasons why a grid point value of a climate model is different from an observed one. They concluded that the reasons are four: due to observed uncertainty, the true model inability to simulate climate, interpolation errors and representativeness error. We proposed a way to estimate the magnitude of each source of error, and drawn the following conclusions:

— The uncertainty arising from the spread among gridded observed datasets is small for surface air temperature and precipitation. However, we found the uncertainty is reasonably high in surface air temperature over the Andes.

— Representativeness error, i.e., the error associated with upscaling the observed data into a coarser resolution grid, increases with resolution, meaning the largest the difference in resolution between observation and GCM, the higher this term is. It is also sensitive to the characteristics of the land, being largest over complex-terrain regions.

— The interpolation error has the lowest magnitude, and its behavior is very similar to the representativeness error.

— Model error is larger for precipitation than for surface air temperature. Also, it is generally the largest term when compared to the others, except over complex terrain regions where the other sources of error are not negligible.

6.1.3 Identifying those regions where high-resolution simulations have the potential to add value

In the last section, we highlighted the importance of taking into consideration the small-scale variability of RCMs. A necessary condition for the RCM to potentially add value is that both the observations and RCMs show a climatic signal in those spatial scales that can be explicitly reproduced by the regional model but not by its lower resolution driver. This small-scale climatic signal is defined as the PAV signal. A slightly more demanding condition is the ability of the RCMs to represent the observed small-scale variability.

For surface air temperature, we followed the methodology proposed by Di Luca et al. (2013a) and found that the largest PAV signal was associated with stationary features. The signal was located over complex terrain regions, which are the Andes mountain range and the Brazilian Highlands, due to an altitude effect that induces large mean horizontal gradients between adjacent grid pairs. PAV signal was also identified over coastal regions, due to the thermal contrast between the continent and the adjacent oceans. It is important to notice this is probably the reason why RCMs usually add value compared to their driver on the representation of surface air temperature seasonal means, especially over coastal and complex terrain areas. The temporal variance of small-scale surface air temperature was small, and models presented a large spread among themselves in representing this type of variability.

For precipitation, we followed the methodology proposed by Di Luca et al. (2012) and focused on the small-scale spatial variability of extreme events, depicted as the 95th percentile. TRMM_3B42 product (Huffman et al., 2007) showed little spatial sensitivity, identifying large grid point differences over the whole continent. The RCMs presented a large inter-model spread in representing the spatial variability of extreme rainfall, but they also tended to have large PAV values over the whole continent with the largest PAV signal intensities over the Andes mountain range.

6.1.4 Sensitivity of model to increased resolution in the representation of climate

The primary motivation for using RCMs is the possibility of being integrated at high resolutions. Therefore, it is important to understand the role played by the resolution in the simulation of the climate system. In this thesis, we performed two types of sensitivity experiments, one focused in studying the effect of increased resolution in the representation of the South American Monsoon System, and another one focused in understanding the role of regional

climate in the simulation of the extratropical circulation.

The RegCM4 model showed a positive response to the increased resolution by improving the simulation of the South American Monsoon System (SAMS). The model fails to simulate the intensity of convective rainfall during the active phase of the SAMS, but this dry bias is reduced when the resolution is increased. The enhanced precipitation is partly due to an increase in moisture convergence in the lower troposphere. Also, the highest resolution simulation represented better the large-scale features of the monsoon.

We also studied the influence of regional nudging over South America on the simulation of the Southern Hemisphere extratropical circulation. For this, we nudged the LMDZ GCM to ERA-Interim and to a higher resolution regional version of the model. Our results showed that forcing the GCM with regional climate information influences positively in the representation of the extratropical circulation, especially during the summertime season, by reducing the bias in the position of the jet in the upper troposphere. The improvement is caused by a better representation of the transient eddy heat and momentum fluxes, together with a better description of the latitude where momentum transport converge.

6.1.5 Final remarks

The thesis shows that RCMs add value regarding their global forcing, but only in some aspects of climate. The added value is mainly found for surface air temperature since this variable has large regional stationary characteristics. The highest AV signal can be detected in complex terrain regions, such as the Andes mountain range and the Brazilian Highlands, and over coasts.

The results are more complex when studying precipitation, and the response will depend on several factors, such as the RCM and its physical configuration, the boundary information, the domain, the season, among others. However, our results suggest that an increase in resolution has the potential to improve local precipitation in the tropics and subtropics during the active phase of the SAMS. On the other hand, no added value was found for rainfall during the wintertime, probably because synoptic-scale frontal systems originate it.

We also found that regional-scale information over the SA continent effectively excites the extratropical circulation in the southern hemisphere, especially during the austral summer. The improvement is associated with increased energy transport from the tropics into the subtropics driven by the low-level jet, which intensifies/develop cyclones over the eastern part of the Continent. This positively excites eddy disturbances in midlatitudes, and thus, reduces the mean bias in the position of the upper-level jet.

While this thesis considers several aspects associated with the AV of RCMs, other issues remained to be studied. Some of them are discussed below.

6.2 Other relevant aspects of climate assessment we have not considered

6.2.1 Comparing model sensitivity to resolution and different physical configurations

Despite having found a sensitivity of the RegCM4 model to the resolution, the differences between simulations were relatively small. The same happened when comparing the LMDZ model without any forcing and forced by regional information.

We believe that sensitivity studies to different physical configurations associated with land surface schemes, convection schemes, and boundary layer schemes are very important. In the framework of the CREMA project, the sensitivity of RegCM4 to different configurations in physics was evaluated, and the results suggest that the model is strongly influenced by the setting chosen. Therefore, we believe that it is essential to continue with this type of analysis for different regional models.

6.2.2 Diurnal cycle

The summer precipitation over tropical South America exhibits an afternoon rainfall maximum as a consequence of diurnal convective instability. In the case of Southeastern South America (SESA) the precipitation peak is found during the night and is associated with diurnally eastward propagating mesoscale convective systems (MCSs) originating over the Andes mountain in the afternoon. This MCSs owe their existence to the hot and moist air transported by the low-level jet, which as we know is not very well represented by GCMs.

We believe it is interesting to study the added value of RCMs compared to their driver in the simulation of the diurnal cycle in the tropics and the subtropics, focusing particularly over SESA. It is also important to understand diurnal cycle simulation sensitivity to resolution and convective parameterization. Unfortunately, a huge limitation for this assessment is the lack of hourly data in the CORDEX ESGF portal. Considering the future of regional climate modeling is to simulate convection explicitly, we believe it is fundamental to include the highest possible frequency in this database, at least for precipitation.

6.2.3 RCM-GCM chain behaviour

The assessment of RCM/GCM chain behavior is fundamental for climate change studies (Sørland et al., 2018). Impact models generally use RCM information, and even though we know the RCM represents well the climate system when forced by a reanalysis, the statement is not necessarily true when forced by a GCM. We believe there is a need for further assessment on how RCMs respond to different boundary conditions, and to identify those regions over the continent where the large-scale forcing has a first-order effect on the RCM.

For the reasons described above, we encourage the modeling community to perform more RCM/GCM sensitivity experiments. One work that partly addresses this issue is the one from Solman (2016) while using simulations belonging to CLARIS-LPB Project. Solman documented that the systematic model errors were more dependent on the RCMs than on the driving GCMs. Also, the CREMA experiment enabled several simulations of the RegCM4 model driven by different CMIP5 GCMs. However, there is currently no RCM/GCM assessment, nor the availability of simulations, to perform this type of analysis within the CORDEX framework.

6.2.4 The potential added value in climate change projections

As we know, RCMs were developed with the aim of generating regional climate information, not only for the present climate but also for climate change (CC) projections. We highlight again the importance of jointly validating RCM/GCM historical simulations, and we add the importance of comparing RCM/GCM projection differences. There are also some works that propose a way to study the potential for AV of RCMs on climate change projections (Di Luca et al., 2013b, Racherla et al., 2012). For example, Di Luca et al. (2013b) quantify the fine-scale part of the RCM-derived CC signal and evaluate its relative importance compared to either the large-scale CC part or to present climate statistics. Racherla et al. (2012) explore whether a correlation exists between the quality of the downscaled historical climate and the quality of the CC signal.

6.3 Future challenges

6.3.1 At project level: CORDEX Flagship Pilot Studies

The CORDEX Flagship Pilot Studies (CORDEX-FPS) emerged from the need to develop more targeted experimental setups than the standard experiment protocol proposed by CORDEX.

These FPS experimental setups should enable the CORDEX communities to better address many current challenges such as a more rigorous and quantitative assessment of the added value of regional downscaling, or a broader and more process-based evaluation of downscaling techniques and model, among others. There are currently several endorsed FPS setups, but probably the most challenging one is the one that seeks to move towards very high resolution, convection-permitting model long-run simulations over Europe and the Mediterranean. This recently launched project from CORDEX-FPS is on its testing phase to create the first multi-model convection permitting ensemble for investigating convective phenomena (Coppola et al., 2018). Three test cases of extreme precipitation were selected to obtain a first look at the ensemble performance, and preliminary results are encouraging.

In South America, the CORDEX-SESA FPS is being coordinated, which aims to study multiscale processes and interactions (convection, local, regional and remote processes, including the co-behavior of processes) that result in extreme precipitation events over southeastern South America. The project also aims to develop actionable climate information from multiple sources (statistical and dynamical downscaling products) based on co-production with the impact and user community (Huth et al., 2017).

6.3.2   At modeling level: Into the grey zone

The default resolution of current climate model simulations range from hundreds to tens of km, and parametrisations that represent sub-grid physical processes are required. During the last decades, there have been considerable advances in the development of physical schemes for these spatial scales. However, if we increase the resolution to 1-10km, then the convection scheme parametrisation is no longer required, but new challenges arise such as the need for non-hydrostatic models with new processes parametrisations (Sakradzija et al., 2016). The development of adequate parametrizations within this range of resolutions, called "the grey zone," is the current challenge for the Model Development Community (Frassoni et al., 2018). As models have transitioned to simulate deep convection explicitly, the already mentioned convection-permitting models, it has been found that modifying the existing convection parametrization can be preferable to just switch it off (Stirling and Lock, 2017). The problem behind is the impossibility of simulating cloud energy conversions from kinetic energy into heat, being heating the source that drives the dynamics of the cloud.

Experts in the grey zone modeling suggest that the best resolution to simulate the grey zone processes is up to 1km, intending to simulate deep convective updraughts, but new

problems arise at these scales because important circulations within the convective boundary layer also enter a grey zone regime.

Given the challenges and costs involved in running dynamical models at convection permitting scales, test cases are currently being performed to provide a first assessment of these simulation characteristics (Prein et al., 2015). However, runs at a climate and continental scale are currently unattainable and are expected for the next decades.

Land surface models are also advancing in the representation of land dynamics, especially when used for climate change projections. Land models started as a boundary condition of atmospheric models presenting static vegetation. These models soon evolved to include dynamic vegetation, then dynamic ecosystems (plant succession), and are currently expanding into a complex component that simulates biogeochemical cycles with CO_2-based photosynthesis in interaction with dynamic ecosystems that include different crops, land dust aerosols, among other land data sets.

6.3.3 At social level: Impact studies and more user-friendly information

Climate change is now undeniable and a risk to human and natural systems. The assessment of impacts, adaptation, vulnerability and the way in which it can be reduced and managed through adaptation and mitigation is imperative.

The first step is to identify those areas that are locally vulnerable and exposed to extreme weather events, as well as the adaptive responses that have occurred to date. Currently, there is a gradual change in the way of addressing disaster risks, since it combines the scientific knowledge of extreme events coming from specialists in different areas, such as meteorologists, hydrologists, engineers, anthropologists, geographers, among others, and the local knowledge of the neighbors of the most affected areas (Hidalgo et al., 2018). This transdisciplinary approach, which involves the participation of decision makers and the community involved, helps develop a common vision of risk and allows more problem-oriented impact studies at a local level, together with the co-production of user-friendly information (Vera, 2018).

In the context of urban and rural areas, CC will affect these areas with increasingly frequent and dangerous events. Therefore, the next step is to examine future risks and potential benefits in all sectors and regions, highlighting which are the most important strategies to reduce risks through mitigation and adaptation.

Conclusiones (Español)

6.1　Lo que hemos aprendido

En este trabajo de tesis estudiamos el valor agregado (VA) de los modelos climáticos regionales (MCRs) en Sudamérica (SA) desde diferentes perspectivas y con diferentes metodologías. Nuestro objetivo principal fue identificar la señal del VA para obtener una comprensión más profunda de las fortalezas y debilidades de los MCRs en SA. A lo largo de la tesis, exploramos varios aspectos del VA y llegamos a las siguientes conclusiones:

6.1.1　Valor agregado en la climatología estacional

La primera pregunta que surge al estudiar el VA de los MCRs es si mejoran la representación del clima con respecto al Modelo Climático Global (MCG) o el reanálisis global utilizado como condición inicial y de borde. Por su mayor resolución, hay muchas razones para suponer que el modelo regional puede mejorar la simulación con respecto a su forzante global, como su mejor representación del forzante superficial, una mejor simulación de los procesos e interacciones regionales y un intervalo de tiempo más pequeño. Pero también hay muchas otras razones para creer que no: su incapacidad para simular escalas más grandes que su dominio limitado, las inconsistencias en la dinámica y la física entre el MCR y su forzante, el error propagado desde el MCG al MCR a través del condición lateral, entre otras.

　　Nuestra principal conclusión al analizar la literatura y de nuestra propia evaluación es que no hay una respuesta única a esta pregunta. A veces, el MCR agregará valor en comparación con su forzante, a veces no lo hará. El tema más importante aquí es identificar los factores clave a los que se atribuyen la mayoría de las señales de VA, donde estos factores pueden ser la variable, la región, la estadística, la temporada del año, el MCR, la condición de borde, entre otros. Igualmente, los resultados indican que la señal de VA es mayor para la temperatura superficial del aire que para la precipitación, debido a la sensibilidad de esta primera variable

al forzamiento superficial; y en las regiones donde los procesos regionales dominan sobre los forzantes remotos, como la circulación de verano en los trópicos.

6.1.2 Selección de la métrica correcta para la evaluación

No hay duda de que es muy importante evaluar si el MCR puede agregar valor en comparación con un MCG en las características del clima de gran escala, es decir, mediante la interpolación en la retícula más gruesa o mediante el promedio areal. Sin embargo, disminuir la resolución del MCR resulta en la pérdida de la principal potencial ventaja que este tiene: su capacidad para simular información de pequeña escala. Por lo tanto, si el MCG tiene una resolución mucho más gruesa que el MCR, entonces se recomienda una métrica que tenga en cuenta la escala espacial. En el segundo capítulo de la tesis, nos inspiramos en el trabajo de Kanamitsu and DeHaan (2011), que discute las posibles razones por las que el valor en un punto de retícula de un modelo climático es diferente de uno observado. Los autores llegaron a la conclusión de que las razones son cuatro: debido a la incertidumbre observada, la verdadera incapacidad del modelo para simular el clima, los errores de interpolación y el error de representatividad. Propusimos una manera de estimar la magnitud de cada fuente de error y extrajimos las siguientes conclusiones:

— La incertidumbre que surge de la dispersión entre bases observadas reticuladas de temperatura superficial del aire y la precipitación es pequeña. Sin embargo, encontramos que la incertidumbre es razonablemente alta en la temperatura superficial del aire sobre los Andes.

— El error de representatividad, es decir, el error asociado con el escalado de los datos observados en una retícula de resolución más gruesa, aumenta con la resolución, lo que significa que cuanto mayor sea la diferencia entre la resolución de la observación y la del MCG, mayor será este término. También es sensible a las características superficiales, siendo más grande sobre regiones de terreno complejo.

— El error de interpolación tiene la magnitud más baja, y su comportamiento es muy similar al error de representatividad.

— El error del modelo es mayor para la precipitación que para la temperatura del aire. Además, generalmente es el término más grande en comparación con los demás, ex-

cepto en regiones de terreno complejo donde las otras fuentes de error no son despreciables.

6.1.3 Identificando aquellas regiones donde las simulaciones de alta resolución tienen el potencial de agregar valor

En la última sección destacamos la importancia de tener en cuenta la variabilidad de pequeña escala de los MCRs. En ese sentido, una condición necesaria para que el MCR tenga el potencial de agregar valor (PAV) es que tanto las observaciones como los MCRs muestren una señal climática en aquellas escalas espaciales que pueden reproducirse explícitamente por el modelo regional, pero no por su forzante global de resolución más baja. Esta señal climática a escala regional se define como la señal de PAV. Una condición ligeramente más exigente es la capacidad de los MCRs para representar la variabilidad observada en escala regional.

Para la temperatura superficial del aire, seguimos la metodología propuesta por Di Luca et al. (2013a) y encontramos que la señal PAV más grande está asociada con características estacionarias. La señal se ubica en regiones de terreno complejo, que son la cordillera de los Andes y las tierras altas de Brasil, debido a un efecto de altitud que induce grandes gradientes horizontales medios entre pares de retículas adyacentes. La señal de PAV también se identificó en regiones costeras, debido al contraste térmico entre el continente y los océanos adyacentes. Es importante notar que esta es probablemente la razón por la cual los MCRs generalmente agregan valor en comparación con su forzante en la representación de la temperatura superficial del aire, especialmente en áreas costeras y de terreno complejo. La variación temporal de la temperatura superficial del aire a escala regional fue pequeña, y los modelos presentaron una gran dispersión entre sí al representar este tipo de variabilidad.

Para la precipitación, seguimos la metodología propuesta por Di Luca et al. (2012), y nos centramos en la variabilidad espacial regional de eventos extremos, representada como el percentil 95. La base TRMM_3B42 (Huffman et al., 2007) mostró poca sensibilidad espacial, identificando grandes diferencias entre puntos de retícula en todo el continente. Los MCRs presentaron una gran dispersión entre sí para representar la variabilidad espacial de las precipitaciones extremas, pero también tendieron a tener grandes valores de PAV en todo el continente, con las mayores intensidades de la señal PAV en la cordillera de los Andes.

6.1.4   Sensibilidad del modelo a una mayor resolución en la representación del clima

La principal motivación para usar un MCR es la posibilidad de integrarse a altas resoluciones. Por lo tanto, es importante comprender el papel que juega la resolución en la simulación del sistema climático. En esta tesis, realizamos dos tipos de experimentos de sensibilidad, uno centrado en el estudio del efecto del aumento de la resolución en la representación del Monzón Sudamericano y otro centrado en la comprensión del papel del clima regional en la simulación de la circulación extratropical.

El modelo RegCM4 mostró una respuesta positiva al aumento de la resolución al mejorar la simulación del Sistema Monzónico Sudamericano (SMSA). El modelo presenta un déficit en simular la intensidad de la lluvia convectiva durante la fase activa del SMSA, pero este sesgo seco se reduce cuando se aumenta la resolución. El aumento en la precipitación se debió en parte a un aumento en la convergencia de humedad en niveles bajos de la tropósfera. Además, la simulación de mayor resolución representó mejor las características de gran escala del monzón.

También estudiamos la influencia del clima regional sobre SA en la simulación de la circulación extratropical del hemisferio sur. Para esto, anidamos el MCG LMDZ a ERA-Interim y a una versión regional del mismo modelo pero con mayor resolución. Nuestros resultados mostraron que forzar el MCG con información climática regional influye positivamente en la representación de la circulación extratropical, especialmente durante el verano austral, al reducir el sesgo en la posición de la corriente en chorro en niveles altos. La mejora es causada por una mejor representación de los flujos transientes de calor y momento, junto con una mejor descripción en la latitud en donde el transporte de momento converge.

6.1.5   Observaciones finales

La tesis muestra que los MCRs agregan valor con respecto a su forzante global, pero solo en algunos aspectos del clima. El valor agregado se encuentra principalmente para la temperatura superficial del aire, ya que esta variable tiene marcadas características estacionarias regionales. La señal de VA más alta se puede encontrar en regiones de terreno complejo, como la cordillera de los Andes y las tierras altas de Brasil, y en las costas.

Los resultados son más complejos cuando se estudia la precipitación, y la respuesta dependerá de varios factores, como el MCR y su configuración física, la condición de borde, el dominio, la estación del año, entre otros. Sin embargo, nuestros resultados sugieren que un

aumento en la resolución tiene el potencial de mejorar la precipitación local en los trópicos y subtrópicos durante la fase activa del SMSA. Por otro lado, no se encontró valor agregado para la precipitación durante el invierno, probablemente porque se origina por sistemas frontales de escala sinóptica.

También encontramos que la información a escala regional sobre SA excita efectivamente la circulación extratropical en el hemisferio sur, especialmente durante el verano austral. La mejora está asociada a un mayor transporte de energía desde los trópicos a los subtrópicos impulsados por la corriente en chorro en niveles bajos, alias "low-level jet", que intensifica/desarrolla los ciclones en la parte oriental del continente. Esto excita positivamente las perturbaciones transientes en latitudes medias, y por lo tanto, reduce el sesgo medio en la posición de la corriente en chorro en la tropósfera superior.

Si bien esta tesis considera varios aspectos asociados con el VA de los MCRs, hay otros temas que quedaron por estudiar. Algunos de ellos se discuten a continuación.

6.2 Otros aspectos relevantes que no hemos considerado

6.2.1 Comparando la sensibilidad del modelo a la resolución y a diferentes configuraciones físicas

A pesar de haber encontrado que el modelo RegCM4 es sensible a la resolución, las diferencias entre las simulaciones fueron relativamente pequeñas. Lo mismo sucedió cuando se comparó el modelo LMDZ sin ningún forzante y forzado por información regional.

Creemos que los estudios de sensibilidad a diferentes configuraciones físicas asociadas con esquemas de superficie terrestre, esquemas de convección y esquemas de capa límite son muy importantes. En el marco del proyecto CREMA, se evaluó la sensibilidad de RegCM4 a diferentes configuraciones en la física del modelo, y los resultados sugieren que el modelo está fuertemente influenciado por la configuración elegida. Por lo tanto, creemos que es esencial continuar con este tipo de análisis para diferentes modelos regionales.

6.2.2 Ciclo diurno

La precipitación de verano en SA tropical muestra un máximo de lluvia por la tarde como consecuencia de la inestabilidad convectiva diurna. En el caso del sudeste de Sudamérica (SESA), el pico de precipitación se encuentra durante la noche y se asocia con sistemas con-

vectivos de mesoescala (SCM) que se propagan diurnamente hacia el este y se originan en los Andes en la tarde. Estos SCM deben su existencia al aire caliente y húmedo transportado por el low-level jet que, como sabemos, no está muy bien representado por los MCGs.

Creemos que es interesante estudiar el valor agregado de los MCRs en comparación con su forzante en la simulación del ciclo diurno en los trópicos y subtrópicos, especialmente en SESA. También es importante comprender la sensibilidad de la simulación del ciclo diurno a la resolución y la parametrización de la convección. Desafortunadamente, una gran limitación para esta evaluación es la falta de datos horaria en el portal CORDEX ESGF. Considerando que el futuro del modelado climático regional es simular explícitamente la convección, creemos que es fundamental incluir la mayor frecuencia posible en esta base de datos, al menos para las precipitaciones.

6.2.3 Cadena de comportamiento MCR-MCG

La evaluación del comportamiento en cadena MCR/MCG es fundamental para los estudios de cambio climático (Sørland et al., 2018). La información del MCR es generalmente utilizada por modelos de impacto, y aunque sabemos que el modelo representa bien el sistema climático cuando es forzado por un reanálisis, esta afirmación no es necesariamente cierta cuando es forzada por un MCG. Creemos que es necesario realizar una evaluación adicional sobre cómo los MCRs responden a diferentes condiciones de borde, e identificar aquellas regiones en el continente donde el forzante global tiene un efecto de primer orden en el MCR.

Por las razones descritas anteriormente, alentamos a la comunidad del modelado a llevar a cabo más experimentos de sensibilidad MCR/MCG. Un trabajo que aborda parcialmente esta cuestión es el de Solman (2016), quien evalúa simulaciones pertenecientes al Proyecto CLARIS-LPB. Solman documentó que los errores sistemáticos del modelo dependían más de los MCRs que de los MCGs que los conducen. Además, el experimento CREMA habilitó varias simulaciones del modelo RegCM4 impulsado por diferentes MCGs del CMIP5. Sin embargo, actualmente no hay una evaluación sobre el comportamiento MCR/MCG, ni tampoco la disponibilidad de simulaciones para realizar este tipo de análisis dentro del marco de CORDEX.

6.2.4 El potencial valor agregado en las proyecciones de cambio climático

Como sabemos, los MCRs se desarrollaron con el objetivo de generar información regional sobre el clima, no solo para el clima actual, sino también para proyecciones de cambio climático

(CC). Destacamos nuevamente la importancia de validar conjuntamente las simulaciones históricas de MCR/MCG, y agregamos la importancia de comparar las diferencias de proyección entre ambos. Por otro lado, en la literatura hay algunos trabajos que proponen una forma de estudiar el potencial VA de los MCRs en proyecciones climáticas futuras (Di Luca et al., 2013b, Racherla et al., 2012). Por ejemplo, Di Luca et al. (2013b) cuantifica el porcentaje regional de la señal de CC derivada del MCR y evalúa su importancia relativa en comparación con el porcentaje de CC asociado a la gran escala o en comparación a las estadísticas climáticas actuales. Racherla et al. (2012) explora si existe una correlación entre la calidad del clima histórico en una simulación regional y la calidad de la señal de CC.

6.3 Desafíos futuros

6.3.1 A nivel de proyectos: estudios piloto de CORDEX-FPS

Los estudios piloto de CORDEX Flagship (CORDEX-FPS) surgieron de la necesidad de desarrollar configuraciones experimentales más específicas que el protocolo experimental estándar propuesto por CORDEX. Estas configuraciones experimentales de FPS deberían permitir a las comunidades CORDEX abordar mejor muchos desafíos actuales, como una evaluación más rigurosa y cuantitativa del valor agregado de la reducción de escala regional, o una evaluación más amplia y más basada en procesos de técnicas y modelos de reducción de escala, entre otros. Actualmente hay varias configuraciones FPS aprobadas, pero probablemente la más desafiante es la que busca avanzar hacia simulaciones a largo plazo de alta resolución, que permitan la convección explícita en Europa y el Mediterráneo. Este proyecto de CORDEX-FPS recientemente lanzado se encuentra en su fase de prueba para crear el primer conjunto multimodelo de convección explícita que permita la investigación de fenómenos convectivos (Coppola et al., 2018). Para probar estos modelos se seleccionaron tres casos de precipitación extrema con el fin de obtener una primera visión del rendimiento del conjunto, y los resultados preliminares son alentadores.

En América del Sur, se está coordinando el FPS CORDEX-SESA, cuyo objetivo es estudiar procesos e interacciones a gran escala (procesos de convección, locales, regionales y remotos, incluido el comportamiento conjunto de los procesos) que resultan en eventos de precipitación extrema sobre el sudeste de Sudamérica. El proyecto también tiene como objetivo desarrollar información climática accionable a partir de múltiples fuentes (productos de re-

ducción de escala estadísticos y dinámicos) basada en la producción conjunta entre la comunidad de impacto y la comunidad de usuarios (Huth et al., 2017).

6.3.2 A nivel de modelado: hacia la zona gris

La resolución actual de las simulaciones climáticas varía de cientos a decenas de km, y se requieren parametrizaciones que representen los procesos físicos de escala menor. Durante las últimas décadas, ha habido avances considerables en el desarrollo de esquemas físicos para este rango de escalas espaciales que no son explícitamente simulados por los modelos. Sin embargo, si aumentamos la resolución a 1-10 km, ya no se requiere la parametrización de los procesos convectivos, pero surgen nuevos desafíos, como la necesidad de modelos no hidrostáticos con nuevos esquemas de parametrización (Sakradzija et al., 2016). El desarrollo de parametrizaciones adecuadas dentro de este rango de resoluciones, llamado "la zona gris", es el desafío actual para la Comunidad de Desarrollo de Modelos (Frassoni et al., 2018). A medida que los modelos han transicionado para simular explícitamente la convección profunda, se ha encontrado que es preferible la modificación del esquema de convección ya existente a simplemente desactivar este esquema (Stirling and Lock, 2017). El problema detrás es la imposibilidad de simular las conversiones de energía cinética a calor dentro de la nube, ya que el calor es la fuente que impulsa la dinámica de la nube.

Los expertos en el modelado de la zona gris sugieren que la mejor resolución para simular los procesos es de hasta 1 km, con la intención de simular los ascensos asociados a la convección profunda, pero surgen nuevos problemas en estas escalas debido a que importantes circulaciones dentro de la capa límite convectiva también entran en un régimen de zona gris. Dados los desafíos y costos computacionales involucrados en la ejecución de modelos dinámicos a escalas de convección explícita, actualmente se están realizando casos de prueba para proporcionar una primera evaluación de estas simulaciones (Prein et al., 2015). Sin embargo, las integraciones a escala climática y continental son actualmente inalcanzables y se esperan recién para las próximas décadas.

Los modelos de superficie terrestre también avanzan en la representación de la dinámica de la tierra, especialmente cuando se usan para proyecciones del cambio climático. Los modelos de tierra comenzaron como una condición de límite de los modelos atmosféricos y presentaban una vegetación estática. Estos modelos pronto evolucionaron para incluir vegetación dinámica, luego ecosistemas dinámicos (sucesión de plantas), y actualmente se están expandiendo a una componente compleja del sistema terrestre que simula ciclos biogeoquímicos

con fotosíntesis basada en CO2 en interacción con ecosistemas dinámicos que incluyen diferentes cultivos, aerosoles de polvo terrestre, entre otros conjuntos de datos terrestres.

6.3.3 A nivel social: estudios de impacto e información fácil para los usuarios

El cambio climático es ahora innegable y un riesgo para los sistemas humanos y naturales. La evaluación de los impactos, la adaptación, la vulnerabilidad y la forma en que puede reducirse y manejarse a través de la adaptación y la mitigación es imperativa.

El primer paso es identificar aquellas áreas que son localmente vulnerables y expuestas a eventos climáticos extremos, así como las respuestas de adaptación que se han producido hasta la fecha. Actualmente, hay un cambio gradual en la forma de abordar los riesgos de desastres, ya que combina el conocimiento científico de eventos extremos provenientes de especialistas en diferentes áreas, como meteorólogos, hidrólogos, ingenieros, antropólogos, geógrafos, entre otros, y el conocimiento local de los vecinos de las zonas más afectadas (Hidalgo et al., 2018). Este enfoque transdisciplinario, que involucra la participación de los tomadores de decisiones y la comunidad involucrada, ayuda a desarrollar una visión común de riesgo y permite estudios de impacto más orientados a los problemas a nivel local, junto con la coproducción de información fácil de usar (Vera, 2018).

En el contexto de áreas urbanas y rurales, el cambio climático afectará estas áreas con eventos cada vez más frecuentes y peligrosos. Por lo tanto, el siguiente paso es examinar los riesgos futuros y los beneficios potenciales en todos los sectores y regiones, destacando cuáles son las estrategias más importantes para reducir los riesgos mediante la mitigación y la adaptación.

Supplementary-Material
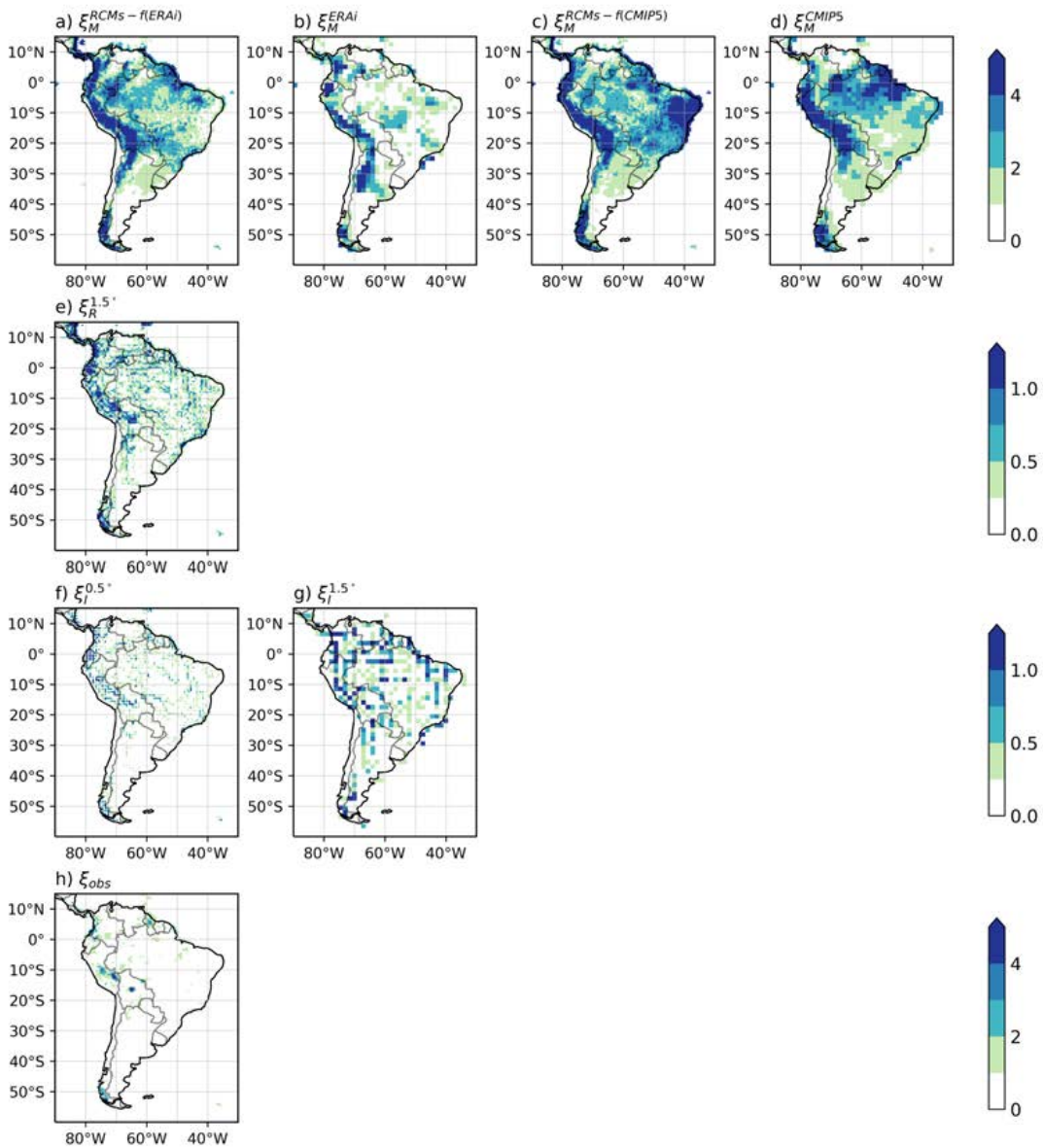
Fig. S2.1. Comparison of model error (top row), representativeness error (second row), interpolation error (third row) and observation uncertainty (bottom row) for summer precipitation climatology (mm/day). Representativeness error is calculated for a grid resolution of 1.5°x1.5° with respect to the original 0.5°x0.5° resolution. Interpolation error is calculated for a regular grid of 0.5°x0.5° using a phase shift of 0.25° and for a regular grid of 1.5°x1.5° with a phase shift of 0.75°.
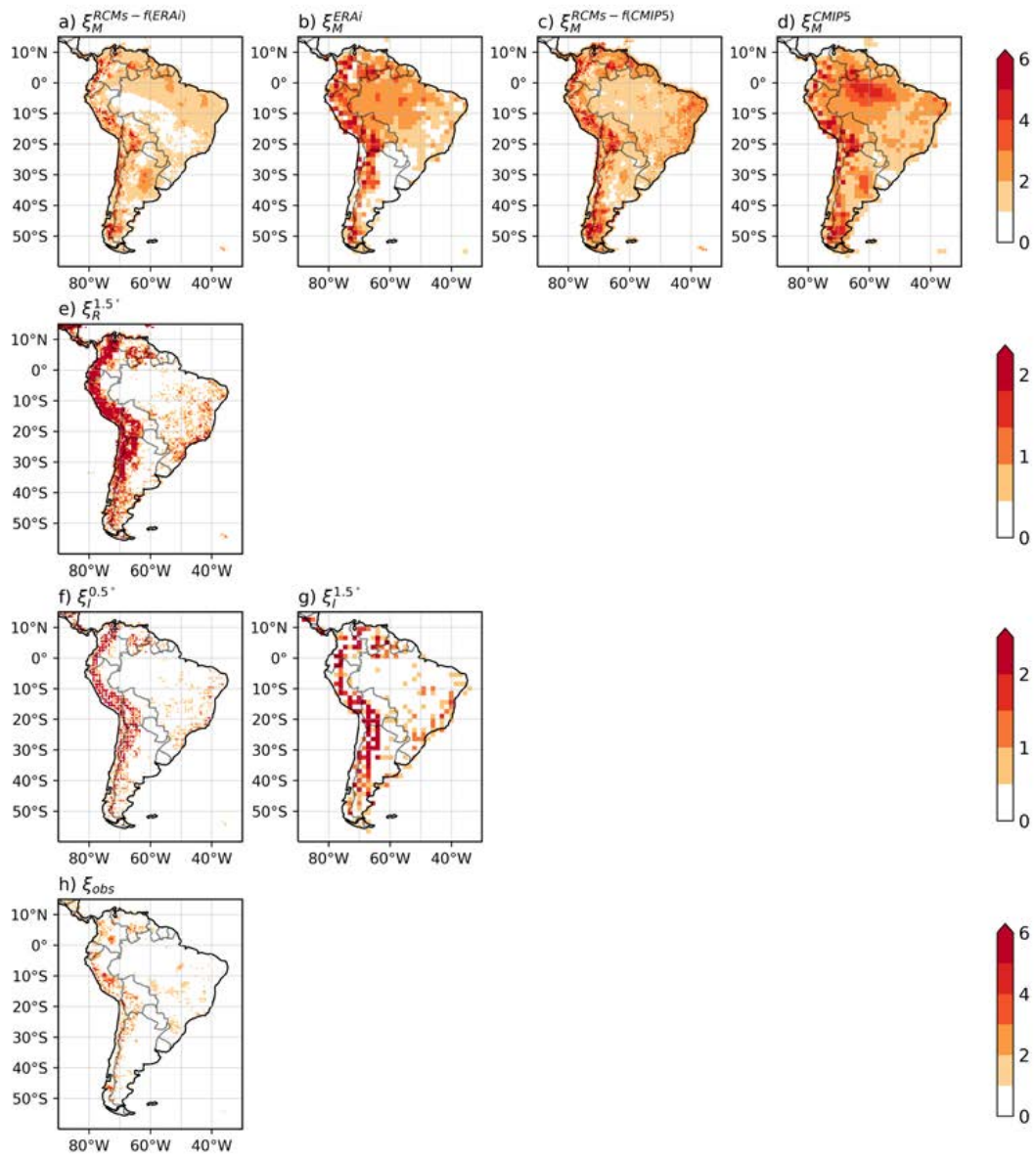
Fig. S2.2. Same as in Fig. S2.1 but for summer surface air temperature climatology (°C).
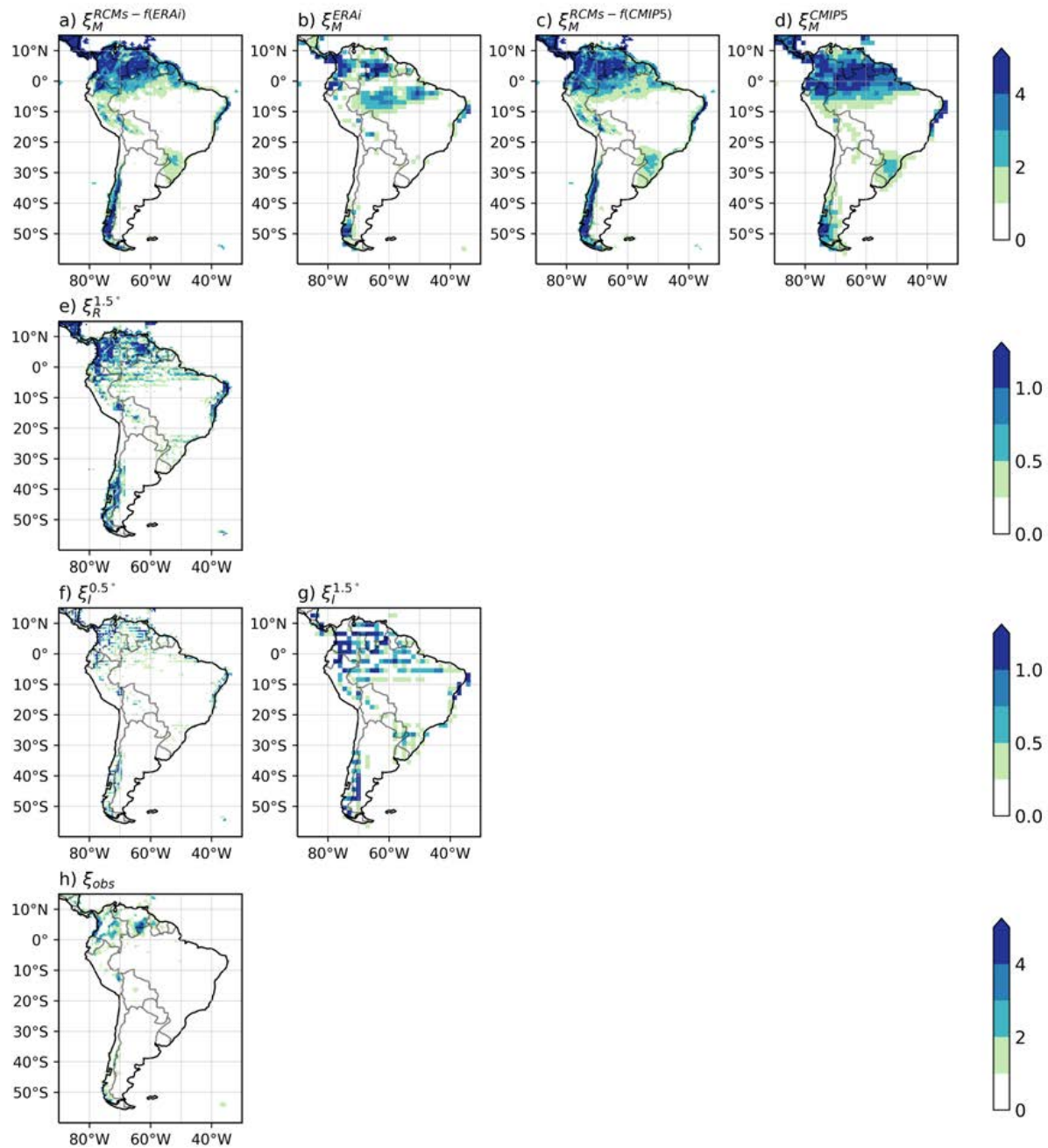
Fig. S2.3. Same as in Fig. S2.1 but for winter precipitation climatology (mm/day).
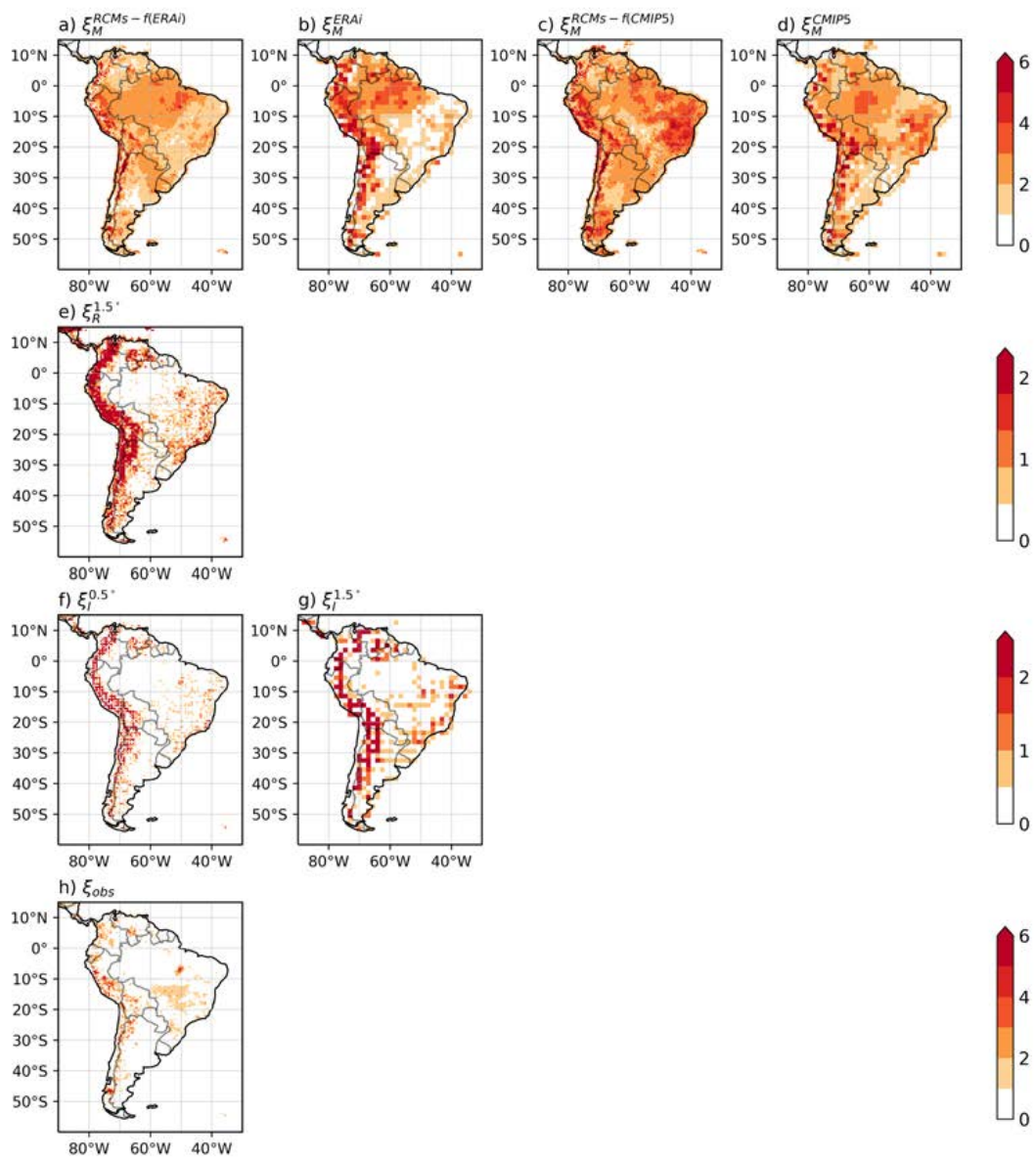
Fig. S2.4. Same as in Fig. S2.1 but for winter surface air temperature climatology (°C).
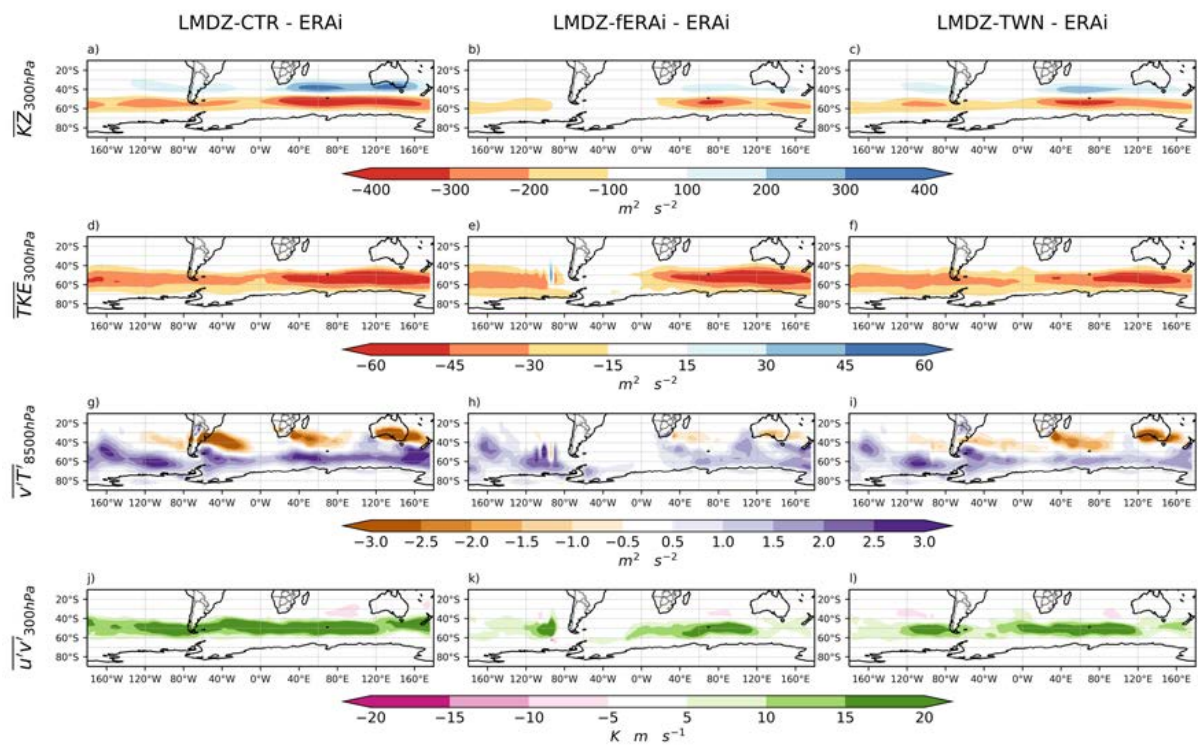
Fig. S5.1. Summer climatology biases of the zonal kinetic energy at 300 hPa (a-c), transient eddy kinetic energy at 300 hPa (d-f), transient meridional momentum flux at 300 hPa (g-i) and transient meridional heat flux at 850 hPa (j-l). The left to right panels display the biases of LMDZ-CTR, LMDZ-fERAi and LMDZ-TWN with ERAi.
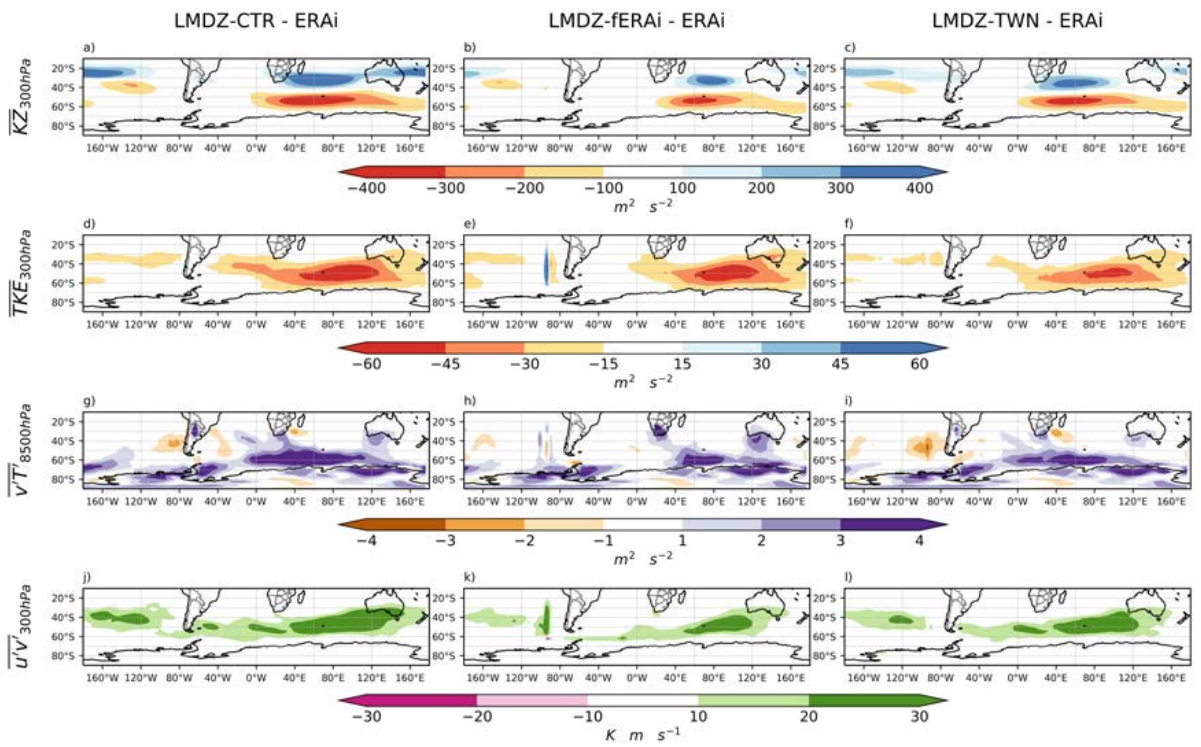
Fig. S5.2. Same as in Fig. S5.1 but for the winter season.

Bibliography

Abadi, A. M., Oglesby, R., Rowe, C., and Mawalagedara, R. (2018). Evaluation of GCMs historical simulations of monthly and seasonal climatology over Bolivia. *Climate Dynamics*, 51(1-2):733–754.

AghaKouchak, A., Behrangi, A., Sorooshian, S., Hsu, K., and Amitai, E. (2011). Evaluation of satellite-retrieved extreme precipitation rates across the central United States. *Journal of Geophysical Research*, 116(D2):D02115.

Anand, A., Mishra, S. K., Sahany, S., Bhowmick, M., Rawat, J. S., and Dash, S. K. (2018). Indian Summer Monsoon Simulations: Usefulness of Increasing Horizontal Resolution, Manual Tuning, and Semi-Automatic Tuning in Reducing Present-Day Model Biases. *Scientific Reports*, 8(1):3522.

Angélil, O., Stone, D., Perkins-Kirkpatrick, S., Alexander, L. V., Wehner, M., Shiogama, H., Wolski, P., Ciavarella, A., and Christidis, N. (2018). On the nonlinearity of spatial scales in extreme weather attribution statements. *Climate Dynamics*, 50(7-8):2739–2752.

Bacmeister, J. T., Wehner, M. F., Neale, R. B., Gettelman, A., Hannay, C., Lauritzen, P. H., Caron, J. M., and Truesdale, J. E. (2014). Exploratory High-Resolution Climate Simulations using the Community Atmosphere Model (CAM). *Journal of Climate*, 27(9):3073–3099.

Barros, V. R. and Doyle, M. E. (2018). Low-level circulation and precipitation simulated by CMIP5 GCMS over southeastern South America. *International Journal of Climatology*.

Berbery, E. H. and Barros, V. R. (2002). The Hydrologic Cycle of the La Plata Basin in South America. *Journal of Hydrometeorology*, 3(6):630–645.

Berckmans, J., Woollings, T., Demory, M.-E., Vidale, P.-L., and Roberts, M. (2013). Atmospheric blocking in a high resolution climate model: influences of mean state, orography and eddy forcing. *Atmospheric Science Letters*, 14(1):34–40.

Bettge, T. W. and Baumhefner, D. P. (1980). A Method to Decompose the Spatial Characteristics of Meteorological Variables within a Limited Domain. *Monthly Weather Review*, 108(7):843–854.

Bielli, S. and Laprise, R. (2006). A Methodology for the Regional-Scale-Decomposed Atmospheric Water Budget: Application to a Simulation of the Canadian Regional Climate Model Nested by NCEP–NCAR Reanalyses over North America. *Monthly Weather Review*, 134(3):854–873.

Bielli, S. and Laprise, R. (2007). Time mean and variability of the scale-decomposed atmospheric water budget in a 25-year simulation of the Canadian Regional Climate Model over North America. *Climate Dynamics*, 29(7-8):763–777.

Bonan, G. B., Lawrence, P. J., Oleson, K. W., Levis, S., Jung, M., Reichstein, M., Lawrence, D. M., and Swenson, S. C. (2011). Improving canopy processes in the Community Land Model version 4 (CLM4) using global flux fields empirically inferred from FLUXNET data. *Journal of Geophysical Research*, 116(G2):G02014.

Boulanger, J., Carril, A., and Sanchez, E. (2016). CLARIS-La Plata Basin: regional hydroclimate variability, uncertainties and climate change scenarios. *Climate Research*, 68(2-3):93–94.

Boville, B. A. (1991). Sensitivity of Simulated Climate to Model Resolution. *Journal of Climate*, 4(5):469–485.

Bracegirdle, T. J., Shuckburgh, E., Sallee, J.-B., Wang, Z., Meijers, A. J. S., Bruneau, N., Phillips, T., and Wilcox, L. J. (2013). Assessment of surface winds over the Atlantic, Indian, and Pacific Ocean sectors of the Southern Ocean in CMIP5 models: historical bias, forcing response, and state dependence. *Journal of Geophysical Research: Atmospheres*, 118(2):547–562.

Bresson, R. and Laprise, R. (2009). Scale-decomposed atmospheric water budget over North America as simulated by the Canadian Regional Climate Model for current and future climates. *Climate Dynamics*, 36(1-2):365–384.

Campetella, C. M. and Vera, C. S. (2002). The influence of the Andes mountains on the South American low-level flow. *Geophysical Research Letters*, 29(17):7–1.

Carril, A., Cavalcanti, I., Menéndez, C., Sörensson, A., López-Franca, N., Rivera, J., Robledo, F., Zaninelli, P., Ambrizzi, T., Penalba, O., da Rocha, R., Sánchez, E., Bettolli, M., Pessacg, N., Renom, M., Ruscica, R., Solman, S., Tencer, B., Grimm, A., Rusticucci, M., Cherchi, A., Tedeschi, R., and Zamboni, L. (2016). Extreme events in the La Plata basin: a retrospective analysis of what we have learned during CLARIS-LPB project. *Climate Research*, 68(2-3):95–116.

Carril, A. F., Menendez, C., Nunez, M., and Treut, H. L. (2002). Mean flow-transient perturbation interaction in the Southern Hemisphere: a simulation using a variable-resolution GCM. *Climate Dynamics*, 18(8):661–673.

Carril, A. F., Menéndez, C. G., Remedio, A. R. C., Robledo, F., Sörensson, A., Tencer, B., Boulanger, J.-P., de Castro, M., Jacob, D., Le Treut, H., Li, L. Z. X., Penalba, O., Pfeifer, S., Rusticucci, M., Salio, P., Samuelsson, P., Sanchez, E., and Zaninelli, P. (2012). Performance of a multi-RCM ensemble for South Eastern South America. *Climate Dynamics*, 39(12):2747–2768.

Carril, A. F. and Nuñez, M. N. (2000). La respuesta de la circulación atmosférica en el Hemisferio Sur ante cambios prescritos en la temperatura de la superficie del mar extratropical. *Atmósfera*, 13(1):39–51.

Casanueva, A., Kotlarski, S., Herrera, S., Fernández, J., Gutiérrez, J. M., Boberg, F., Colette, A., Christensen, O. B., Goergen, K., Jacob, D., Keuler, K., Nikulin, G., Teichmann, C., and Vautard, R. (2016). Daily precipitation statistics in a EURO-CORDEX RCM ensemble: added value of raw and bias-corrected high-resolution simulations. *Climate Dynamics*, 47(3-4):719–737.

Ceppi, P., Hwang, Y.-T., Frierson, D. M. W., and Hartmann, D. L. (2012). Southern Hemisphere jet latitude biases in CMIP5 models linked to shortwave cloud forcing. *Geophysical Research Letters*, 39(19):n/a–n/a.

Chan, S. C., Kendon, E. J., Fowler, H. J., Blenkinsop, S., Ferro, C. A. T., and Stephenson, D. B. (2013). Does increasing the spatial resolution of a regional climate model improve the simulated daily precipitation? *Climate Dynamics*, 41(5-6):1475–1495.

Chang, E. K. M., Guo, Y., and Xia, X. (2012). CMIP5 multimodel ensemble projection of storm track change under global warming. *Journal of Geophysical Research: Atmospheres*, 117(D23):n/a–n/a.

Chen, W., Jiang, Z., Li, L., and Yiou, P. (2010). Simulation of regional climate change under the IPCC A2 scenario in southeast China. *Climate Dynamics*, 36(3-4):491–507.

Chou, S. C., Bustamante, J. F., and Gomes, J. L. (2005). Evaluation of Eta Model seasonal precipitation forecasts over South America. *Nonlinear Processes in Geophysics*, 12(4):537–555.

Chou, S. C., Tanajura, C. A. S., Xue, Y., and Nobre, C. A. (2002). Validation of the coupled Eta/SSiB model over South America. *Journal of Geophysical Research*, 107(D20):8088.

Chylek, P., Li, J., Dubey, M. K., Wang, M., and Lesins, G. (2011). Observed and model simulated 20th century Arctic temperature variability: Canadian Earth System Model CanESM2. *Atmospheric Chemistry and Physics Discussions*, 11(8):22893–22907.

Collins, W. J., Bellouin, N., Doutriaux-Boucher, M., Gedney, N., Halloran, P., Hinton, T., Hughes, J., Jones, C. D., Joshi, M., Liddicoat, S., Martin, G., O 'connor, F., Rae, J., Senior, C., Sitch, S., Totterdell, I., Wiltshire, A., and Woodward, S. (2011). Geoscientific Model Development Development and evaluation of an Earth-System model – HadGEM2. *Geosci. Model Dev*, 4:1051–1075.

Coppola, E., Giorgi, F., Raffaele, F., Fuentes-Franco, R., Giuliani, G., LLopart-Pereira, M., Mamgain, A., Mariotti, L., Diro, G. T., and Torma, C. (2014). Present and future climatologies in the phase I CREMA experiment. *Climatic Change*, 125(1):23–38.

Coppola, E., Sobolowski, S., Pichelli, E., Raffaele, F., Ahrens, B., Anders, I., Ban, N., Bastin, S., Belda, M., Belusic, D., Caldas-Alvarez, A., Cardoso, R. M., Davolio, S., Dobler, A., Fernandez, J., Fita, L., Fumiere, Q., Giorgi, F., Goergen, K., Güttler, I., Halenka, T., Heinzeller, D., Hodnebrog, O., Jacob, D., Kartsios, S., Katragkou, E., Kendon, E., Khodayar, S., Kunstmann, H., Knist, S., Lavín-Gullón, A., Lind, P., Lorenz, T., Maraun, D., Marelle, L., van Meijgaard, E., Milovac, J., Myhre, G., Panitz, H.-J., Piazza, M., Raffa, M., Raub, T., Rockel, B., Schär, C., Sieck, K., Soares, P. M. M., Somot, S., Srnec, L., Stocchi, P., Tölle, M. H., Truhetz, H., Vautard, R., de Vries, H., and Warrach-Sagi, K. (2018). A first-of-its-kind multi-model convection permitting ensemble for investigating convective phenomena over Europe and the Mediterranean. *Climate Dynamics*, pages 1–32.

Curry, C. L., Tencer, B., Whan, K., Weaver, A. J., Giguère, M., and Wiebe, E. (2016). Searching for Added Value in Simulating Climate Extremes with a High-Resolution Regional Climate Model over Western Canada. *Atmosphere-Ocean*, pages 1–21.

Custodio, M. d. S., da Rocha, R. P., Ambrizzi, T., Vidale, P. L., and Demory, M.-E. (2017). Impact of increased horizontal resolution in coupled and atmosphere-only models of the HadGEM1 family upon the climate patterns of South America. *Climate Dynamics*, 48(9-10):3341–3364.

Custodio, M. d. S., da Rocha, R. P., and Vidale, P. L. (2012). Analysis of precipitation climatology simulated by high resolution coupled global models over the South America. *Hydrological Research Letters*, 6(0):92–97.

da Rocha, R., Cuadra, S., Reboita, M., Kruger, L., Ambrizzi, T., and Krusche, N. (2012). Effects of RegCM3 parameterizations on simulated rainy season over South America. *Climate Research*, 52:253–265.

da Rocha, R. P., Morales, C. A., Cuadra, S. V., and Ambrizzi, T. (2009). Precipitation diurnal cycle and summer climatology assessment over South America: An evaluation of Regional Climate Model version 3 simulations. *Journal of Geophysical Research*, 114(D10):D10108.

da Rocha, R. P., Reboita, M. S., Dutra, L. M. M., Llopart, M. P., and Coppola, E. (2014). Interannual variability associated with ENSO: present and future climate projections of RegCM4 for South America-CORDEX domain. *Climatic Change*, 125(1):95–109.

da Silva, A. E. and de Carvalho, L. M. V. (2007). Large-scale index for South America Monsoon (LISAM). *Atmospheric Science Letters*, 8(2):51–57.

Daubechies, I. (1988). Orthonormal bases of compactly supported wavelets. *Communications on Pure and Applied Mathematics*, 41(7):909–996.

De Haan, L. L., Kanamitsu, M., De Sales, F., and Sun, L. (2014). An evaluation of the seasonal added value of downscaling over the United States using new verification measures. *Theoretical and Applied Climatology*, 122(1-2):47–57.

De Sales, F. and Xue, Y. (2006). Investigation of seasonal prediction of the South American regional climate using the nested model system. *Journal of Geophysical Research*, 111(D20):D20107.

De Sales, F. and Xue, Y. (2011). Assessing the dynamic-downscaling ability over South America using the intensity-scale verification technique. *International Journal of Climatology*, 31(8):1205–1221.

Dee, D. P., Uppala, S. M., Simmons, A. J., Berrisford, P., Poli, P., Kobayashi, S., Andrae, U., Balmaseda, M. A., Balsamo, G., Bauer, P., Bechtold, P., Beljaars, A. C. M., van de Berg, L., Bidlot, J., Bormann, N., Delsol, C., Dragani, R., Fuentes, M., Geer, A. J., Haimberger, L., Healy, S. B., Hersbach, H., Hólm, E. V., Isaksen, L., Kållberg, P., Köhler, M., Matricardi, M., McNally, A. P., Monge-Sanz, B. M., Morcrette, J.-J., Park, B.-K., Peubey, C., de Rosnay, P., Tavolato, C., Thépaut, J.-N., and Vitart, F. (2011). The ERA-Interim reanalysis: configuration and performance of the data assimilation system. *Quarterly Journal of the Royal Meteorological Society*, 137(656):553–597.

Denis, B., Côté, J., Laprise, R., and Olume, V. (2002a). Spectral Decomposition of Two-Dimensional Atmospheric Fields on Limited-Area Domains Using the Discrete Cosine Transform (DCT). *Monthly Weather Review*, 130(7):1812–1829.

Denis, B., Laprise, R., Caya, D., and Côté, J. (2002b). Downscaling ability of one-way nested regional climate models: the Big-Brother Experiment. *Climate Dynamics*, 18(8):627–646.

Desrochers, P. R. and Yee, S. Y. K. (1999). Wavelet Applications for Mesocyclone Identification in Doppler Radar Observations. *Journal of Applied Meteorology*, 38(7):965–980.

Di Luca, A., Argüeso, D., Evans, J. P., de Elía, R., and Laprise, R. (2016). Quantifying the overall added value of dynamical downscaling and the contribution from different spatial scales. *Journal of Geophysical Research: Atmospheres*, 121(4):1575–1590.

Di Luca, A., de Elía, R., and Laprise, R. (2012). Potential for added value in precipitation simulated by high-resolution nested Regional Climate Models and observations. *Climate Dynamics*, 38(5-6):1229–1247.

Di Luca, A., de Elía, R., and Laprise, R. (2013a). Potential for added value in temperature simulated by high-resolution nested RCMs in present climate and in the climate change signal. *Climate Dynamics*, 40(1-2):443–464.

Di Luca, A., de Elía, R., and Laprise, R. (2013b). Potential for small scale added value of RCM's downscaled climate change signal. *Climate Dynamics*, 40(3-4):601–618.

Di Luca, A., de Elía, R., and Laprise, R. (2015). Challenges in the Quest for Added Value of Regional Climate Dynamical Downscaling. *Current Climate Change Reports*, 1(1):10–21.

Diaconescu, E. P., Gachon, P., and Laprise, R. (2015). On the Remapping Procedure of Daily Precipitation Statistics and Indices Used in Regional Climate Model Evaluation. *Journal of Hydrometeorology*, 16(6):2301–2310.

Dimitrijevic, M. and Laprise, R. (2005). Validation of the nesting technique in a regional climate model and sensitivity tests to the resolution of the lateral boundary conditions during summer. *Climate Dynamics*, 25(6):555–580.

Dirmeyer, P. A., Cash, B. A., Kinter, J. L., Jung, T., Marx, L., Satoh, M., Stan, C., Tomita, H., Towers, P., Wedi, N., Achuthavarier, D., Adams, J. M., Altshuler, E. L., Huang, B., Jin, E. K., and Manganello, J. (2012). Simulating the diurnal cycle of rainfall in global climate models: resolution versus parameterization. *Climate Dynamics*, 39(1-2):399–418.

Domingues, M. O., Mendes, O., and da Costa, A. M. (2005). On wavelet techniques in atmospheric sciences. *Advances in Space Research*, 35(5):831–842.

Dufresne, J.-L., Foujols, M.-A., Denvil, S., Caubel, A., Marti, O., Aumont, O., Balkanski, Y., Bekki, S., Bellenger, H., Benshila, R., Bony, S., Bopp, L., Braconnot, P., Brockmann, P., Cadule, P., Cheruy, F., Codron, F., Cozic, A., Cugnet, D., de Noblet, N., Duvel, J.-P., Ethé, C., Fairhead, L., Fichefet, T., Flavoni, S., Friedlingstein, P., Grandpeix, J.-Y., Guez, L., Guilyardi, E., Hauglustaine, D., Hourdin, F., Idelkadi, A., Ghattas, J., Joussaume, S., Kageyama, M., Krinner, G., Labetoulle, S., Lahellec, A., Lefebvre, M.-P.,

Lefevre, F., Levy, C., Li, Z. X., Lloyd, J., Lott, F., Madec, G., Mancip, M., Marchand, M., Masson, S., Meurdesoif, Y., Mignot, J., Musat, I., Parouty, S., Polcher, J., Rio, C., Schulz, M., Swingedouw, D., Szopa, S., Talandier, C., Terray, P., Viovy, N., and Vuichard, N. (2013). Climate change projections using the IPSL-CM5 Earth System Model: from CMIP3 to CMIP5. *Climate Dynamics*, 40(9-10):2123–2165.

Emanuel, K. A. (1991). A Scheme for Representing Cumulus Convection in Large-Scale Models. *Journal of the Atmospheric Sciences*, 48(21):2313–2329.

Erfanian, A. and Wang, G. (2018). Explicitly Accounting for the Role of Remote Oceans in Regional Climate Modeling of South America. *Journal of Advances in Modeling Earth Systems*.

Errico, R. M. (1985). Spectra Computed from a Limited Area Grid. *Monthly Weather Review*, 113(9):1554–1562.

Falco, M., Carril, A. F., Menéndez, C. G., Zaninelli, P. G., and Li, L. Z. (2018). Assessment of CORDEX simulations over South America: added value on seasonal climatology and resolution considerations. *Climate Dynamics*.

Fantini, A., Raffaele, F., Torma, C., Bacer, S., Coppola, E., Giorgi, F., Ahrens, B., Dubois, C., Sanchez, E., and Verdecchia, M. (2018). Assessment of multiple daily precipitation statistics in ERA-Interim driven Med-CORDEX and EURO-CORDEX experiments against high resolution observations. *Climate Dynamics*, 51(3):877–900.

Fernandez, J. P. R., Franchito, S. H., and Rao, V. B. (2006). Simulation of the summer circulation over South America by two regional climate models. Part I: Mean climatology. *Theoretical and Applied Climatology*, 86(1-4):247–260.

Feser, F. (2006). Enhanced Detectability of Added Value in Limited-Area Model Results Separated into Different Spatial Scales. *Monthly Weather Review*, 134(8):2180–2190.

Feser, F., Rockel, B., von Storch, H., Winterfeldt, J., and Zahn, M. (2011). Regional Climate Models Add Value to Global Model Data: A Review and Selected Examples. *Bulletin of the American Meteorological Society*, 92(9):1181–1192.

Feser, F. and von Storch, H. (2005). A Spatial Two-Dimensional Discrete Filter for Limited-Area-Model Evaluation Purposes. *Monthly Weather Review*, 133(6):1774–1786.

Figueroa, S. N., Satyamurty, P., and Da Silva Dias, P. L. (1995). Simulations of the Summer Circulation over the South American Region with an Eta Coordinate Model. *Journal of the Atmospheric Sciences*, 52(10):1573–1584.

Fotso-Nguemo, T. C., Vondou, D. A., Pokam, W. M., Djomou, Z. Y., Diallo, I., Haensler, A., Tchotchou, L. A. D., Kamsu-Tamo, P. H., Gaye, A. T., and Tchawoua, C. (2017). On the added value of the regional climate model REMO in the assessment of climate change signal over Central Africa. *Climate Dynamics*, 49(11-12):3813–3838.

Frassoni, A., Castilho, D., Rixen, M., Ramirez, E., De Mattos, J., Kubota, P., Calheiros, A., Reed, K., Da, M., Dias, S., Da, P., De Campos Velho, H., De Roode, S., Doblas-Reyes, F., Eiras, D., Ek, M., Figueroa, S., Forbes, R., Freitas, S., Grell, G., Herdies, D., Lauritzen, P., Machado, L., Manzi, A., Martins, G., Oliveira, G., Rosário, N., Sales, D., Wedi, N., and Yamada, B. (2018). Building the next generation of climate modelers: scale–aware physics 2 parameterization and the "Grey Zone" challenge. *Bulletin of the American Meteorological Society*.

Gan, M. A. and Rao, V. B. (1994). The Influence of the Andes Cordillera on Transient Disturbances. *Monthly Weather Review*, 122(6):1141–1157.

Gao, X., Xu, Y., Zhao, Z., Pal, J. S., and Giorgi, F. (2006). On the role of resolution and topography in the simulation of East Asia precipitation. *Theoretical and Applied Climatology*, 86(1-4):173–185.

Gao, Y., Leung, L. R., Zhao, C., and Hagos, S. (2017). Sensitivity of U.S. summer precipitation to model resolution and convective parameterizations across gray zone resolutions. *Journal of Geophysical Research: Atmospheres*, 122(5):2714–2733.

Garreaud, R. D., Vuille, M., Compagnucci, R., and Marengo, J. (2009). Present-day South American climate. *Palaeogeography, Palaeoclimatology, Palaeoecology*, 281(3-4):180–195.

Gibba, P., Sylla, M. B., Okogbue, E. C., Gaye, A. T., Nikiema, M., and Kebe, I. (2018). State-of-the-art climate modeling of extreme precipitation over Africa: analysis of CORDEX added-value over CMIP5. *Theoretical and Applied Climatology*, pages 1–17.

Gilleland, E., Ahijevych, D., Brown, B. G., Casati, B., Ebert, E. E., Gilleland, E., Ahijevych, D., Brown, B. G., Casati, B., and Ebert, E. E. (2009). Intercomparison of Spatial Forecast Verification Methods. *Weather and Forecasting*, 24(5):1416–1430.

Giorgi, F. (2002). Dependence of the surface climate interannual variability on spatial scale. *Geophysical Research Letters*, 29(23):2101.

Giorgi, F. (2006). Regional climate modeling: Status and perspectives. *Journal de Physique IV (Proceedings)*, 139(1):101–118.

Giorgi, F., Coppola, E., Raffaele, F., Diro, G. T., Fuentes-Franco, R., Giuliani, G., Mamgain, A., Llopart, M. P., Mariotti, L., and Torma, C. (2014). Changes in extremes and hydroclimatic regimes in the CREMA ensemble projections. *Climatic Change*, 125(1):39–51.

Giorgi, F., Coppola, E., Solmon, F., Mariotti, L., Sylla, M., Bi, X., Elguindi, N., Diro, G., Nair, V., Giuliani, G., Turuncoglu, U., Cozzini, S., Güttler, I., O'Brien, T., Tawfik, A., Shalaby, A., Zakey, A., Steiner, A., Stordal, F., Sloan, L., and Brankovic, C. (2012). RegCM4: model description and preliminary tests over multiple CORDEX domains. *Climate Research*, 52:7–29.

Giorgi, F. and Gutowski, W. J. (2015). Regional Dynamical Downscaling and the CORDEX Initiative. *Annual Review of Environment and Resources*, 40(1):467–490.

Giorgi, F. and Mearns, L. O. (1999). Introduction to special section- Regional climate modeling revisited in the issue illustrate a wide range of applications. *Journal of Geophysical Research: Atmospheres*, 104(98):6335–6352.

Gordon, C., Cooper, C., Senior, C. A., Banks, H., Gregory, J. M., Johns, T. C., Mitchell, J. F. B., and Wood, R. A. (2000). The simulation of SST, sea ice extents and ocean heat transports in a version of the Hadley Centre coupled model without flux adjustments. *Climate Dynamics*, 16(2-3):147–168.

Goubanova, K. and Li, L. (2007). Extremes in temperature and precipitation around the Mediterranean basin in an ensemble of future climate scenario simulations. *Global and Planetary Change*, 57(1-2):27–42.

Gozzo, L. F., da Rocha, R. P., Reboita, M. S., Sugahara, S., Gozzo, L. F., Rocha, R. P. d., Reboita, M. S., and Sugahara, S. (2014). Subtropical Cyclones over the Southwestern South Atlantic: Climatological Aspects and Case Study. *Journal of Climate*, 27(22):8543–8562.

Grise, K. M., Polvani, L. M., Grise, K. M., and Polvani, L. M. (2014). Southern Hemisphere Cloud–Dynamics Biases in CMIP5 Models and Their Implications for Climate Projections. *Journal of Climate*, 27(15):6074–6092.

Gulizia, C., Camilloni, I., and Doyle, M. (2013). Identification of the principal patterns of summer moisture transport in South America and their representation by WCRP/CMIP3 global climate models. *Theoretical and Applied Climatology*, 112(1-2):227–241.

Güttler, I., Stepanov, I., Branković, C., Nikulin, G., and Jones, C. (2015). Impact of Horizontal Resolution on Precipitation in Complex Orography Simulated by the Regional Climate Model RCA3*. *Monthly Weather Review*, 143(9):3610–3627.

Harzallah, A., Rocha de Aragao, J. O., and Sadourny, R. (1996). Interannual rainfall variability in Northeast Brazil: observation and model simulation. *International Journal of Climatology*, 16(8):861–878.

Hazeleger, W., Severijns, C., Semmler, T., Ştefănescu, S., Yang, S., Wang, X., Wyser, K., Dutra, E., Baldasano, J. M., and … (2010). EC-Earth: A Seamless Earth-System Prediction Approach in Action. *Bulletin of the American Meteorological Society*, 91(10):1357–1363.

Hidalgo, J., Lemonsu, A., and Masson, V. (2018). Between progress and obstacles in urban climate interdisciplinary studies and knowledge transfer to society. *Annals of the New York Academy of Sciences*.

Holtslag, A. A. M., De Bruijn, E. I. F., and Pan, H.-L. (1990). A High Resolution Air Mass Transformation Model for Short-Range Weather Forecasting. *Monthly Weather Review*, 118(8):1561–1575.

Hong, S.-Y. and Kanamitsu, M. (2014). Dynamical downscaling: Fundamental issues from an NWP point of view and recommendations. *Asia-Pacific Journal of Atmospheric Sciences*, 50(1):83–104.

Hoskins, B. J. and Hodges, K. I. (2005). A New Perspective on Southern Hemisphere Storm Tracks. *Journal of Climate*, 18(20):4108–4129.

Hourdin, F., Grandpeix, J.-Y., Rio, C., Bony, S., Jam, A., Cheruy, F., Rochetin, N., Fairhead, L., Idelkadi, A., Musat, I., Dufresne, J.-L., Lahellec, A., Lefebvre, M.-P., and Roehrig, R. (2012). LMDZ5B: the atmospheric component of the IPSL climate model with revisited parameterizations for clouds and convection. *Climate Dynamics*, 40(9-10):2193–2222.

Hourdin, F., Musat, I., Bony, S., Braconnot, P., Codron, F., Dufresne, J.-L., Fairhead, L., Filiberti, M.-A., Friedlingstein, P., Grandpeix, J.-Y., Krinner, G., LeVan, P., Li, Z.-X., and Lott, F. (2006). The LMDZ4 general circulation model: climate performance and sensitivity to parametrized physics with emphasis on tropical convection. *Climate Dynamics*, 27(7-8):787–813.

Hsu, P.-C. (2016). Global Monsoon in a Changing Climate. In de Carvalho, L. M. V. and Jones, C., editors, *The Monsoons and Climate Change*, pages 7–24. Springer.

Huffman, G. J., Bolvin, D. T., Nelkin, E. J., Wolff, D. B., Adler, R. F., Gu, G., Hong, Y., Bowman, K. P., and Stocker, E. F. (2007). The TRMM Multisatellite Precipitation Analysis (TMPA): Quasi-Global, Multiyear, Combined-Sensor Precipitation Estimates at Fine Scales. *Journal of Hydrometeorology*, 8(1):38–55.

Huth, R., Laura Bettolli, M., Solman, S., da Rocha, R. P., Llopart, M., Sin Chan, C., Machado, L., Cuadra, S. V., Doyle, M., Barreiro, M., Farneti, R., Gutierrez, J. M., and Bert, F. (2017). The South America CORDEX Flagship Pilot Study: Extreme precipitation events in Southeastern South America: a proposal for a better understanding and modeling. Technical report.

Inatsu, M. and Hoskins, B. J. (2004). The Zonal Asymmetry of the Southern Hemisphere Winter Storm Track. *Journal of Climate*, 17(24):4882–4892.

Inatsu, M. and Kimoto, M. (2009). A Scale Interaction Study on East Asian Cyclogenesis Using a General Circulation Model Coupled with an Interactively Nested Regional Model. *Monthly Weather Review*, 137(9):2851–2868.

Inatsu, M., Satake, Y., Kimoto, M., and Yasutomi, N. (2012). GCM Bias of the Western Pacific Summer Monsoon and Its Correction by Two-Way Nesting System. *Journal of the Meteorological Society of Japan. Ser. II*, 90B(0):1–10.

Insel, N., Poulsen, C. J., and Ehlers, T. a. (2010). Influence of the Andes Mountains on South American moisture transport, convection, and precipitation. *Climate Dynamics*, 35(7):1477–1492.

IPCC (2013). Climate Change 2013: The Physical Science Basis. Contribution of Working Group I to the Fifth Assessment Report of the Intergovernmental Panel on Climate Change. [Stocker, T.F., D. Qin, G.-K. Plattner, M. Tignor, S.K. Allen, J. Boschung, A. Nauels, Y. Xia. *Cambridge University Press*, page 1535 pp.

Iqbal, W., Leung, W., and Hannachi, A. (2018). Analysis of the variability of the North Atlantic eddy-driven jet stream in CMIP5. *Climate Dynamics*, 51:235–247.

Jacob, D., Elizalde, A., Haensler, A., Hagemann, S., Kumar, P., Podzun, R., Rechid, D., Remedio, A. R., Saeed, F., Sieck, K., Teichmann, C., and Wilhelm, C. (2012). Assessing the Transferability of the Regional Climate Model REMO to Different COordinated Regional Climate Downscaling EXperiment (CORDEX) Regions. *Atmosphere*, 3(4):181–199.

Jameson, L. and Waseda, T. (2000). Error Estimation Using Wavelet Analysis for Data Assimilation: EEWADAi*. *Journal of Atmospheric and Oceanic Technology*, 17(9):1235–1246.

Jin, E. K., Choi, I.-J., Kim, S.-Y., and Han, J.-Y. (2016). Impact of model resolution on the simulation of diurnal variations of precipitation over East Asia. *Journal of Geophysical Research: Atmospheres*, 121(4):1652–1670.

Jones, C. and Carvalho, L. M. V. (2013). Climate Change in the South American Monsoon System: Present Climate and CMIP5 Projections. *Journal of Climate*, 26(17):6660–6678.

Jung, T., Miller, M. J., Palmer, T. N., Towers, P., Wedi, N., Achuthavarier, D., Adams, J. M., Altshuler, E. L., Cash, B. a., Kinter, J. L., Marx, L., Stan, C., and Hodges, K. I. (2012). High-Resolution Global Climate

Simulations with the ECMWF Model in Project Athena: Experimental Design, Model Climate, and Seasonal Forecast Skill. *Journal of Climate*, 25(9):3155–3172.

Junquas, C., Li, L., Vera, C. S., Le Treut, H., and Takahashi, K. (2015). Influence of South America orography on summertime precipitation in Southeastern South America. *Climate Dynamics*.

Kalnay, E., Kanamitsu, M., Kistler, R., Collins, W., Deaven, D., Gandin, L., Iredell, M., Saha, S., White, G., Woollen, J., Zhu, Y., Leetmaa, A., Reynolds, R., Chelliah, M., Ebisuzaki, W., Higgins, W., Janowiak, J., Mo, K. C., Ropelewski, C., Wang, J., Jenne, R., and Joseph, D. (1996). The NCEP/NCAR 40-Year Reanalysis Project. *Bulletin of the American Meteorological Society*, 77(3):437–471.

Kanamitsu, M. and DeHaan, L. (2011). The Added Value Index: A new metric to quantify the added value of regional models. *Journal of Geophysical Research*, 116(D11):D11106.

Karmacharya, J., Jones, R., Moufouma-Okia, W., and New, M. (2017). Evaluation of the added value of a high-resolution regional climate model simulation of the South Asian summer monsoon climatology. *International Journal of Climatology*, 37(9):3630–3643.

Karmacharya, J., New, M., Jones, R., and Levine, R. (2016). Added value of a high-resolution regional climate model in simulation of intraseasonal variability of the South Asian summer monsoon. *International Journal of Climatology*.

Kerkhoff, C., Künsch, H. R., and Schär, C. (2014). Assessment of Bias Assumptions for Climate Models. *Journal of Climate*, 27(17):6799–6818.

Knippertz, P., Wernly, H., and Glaser, G. (2013). A Global Climatology of Tropical Moisture Exports. *Journal of Climate*, 26(10):3031–3045.

Kotlarski, S., Keuler, K., Christensen, O. B., Colette, A., Déqué, M., Gobiet, A., Goergen, K., Jacob, D., Lüthi, D., van Meijgaard, E., Nikulin, G., Schär, C., Teichmann, C., Vautard, R., Warrach-Sagi, K., and Wulfmeyer, V. (2014). Regional climate modeling on European scales: a joint standard evaluation of the EURO-CORDEX RCM ensemble. *Geoscientific Model Development*, 7(4):1297–1333.

Krüger, L. F., da Rocha, R. P., Reboita, M. S., and Ambrizzi, T. (2012). RegCM3 nested in HadAM3 scenarios A2 and B2: projected changes in extratropical cyclogenesis, temperature and precipitation over the South Atlantic Ocean. *Climatic Change*, 3-4(113):599 – 621.

Kupiainen, M., Jansson, C., Samuelsson, P., and Jones, C. (2014). Rossby Centre regional atmospheric model, RCA4, Rossby Center News Letter.

Laprise, R. (2003). Resolved Scales and Nonlinear Interactions in Limited-Area Models. *Journal of the Atmospheric Sciences*, 60(5):768–779.

Laprise, R. (2008). Regional climate modelling. *Journal of Computational Physics*, 227(7):3641–3666.

Lee, J.-W. and Hong, S.-Y. (2013). Potential for added value to downscaled climate extremes over Korea by increased resolution of a regional climate model. *Theoretical and Applied Climatology*, 117(3-4):667–677.

Lenters, J. D. and Cook, K. H. (1997). On the Origin of the Bolivian High and Related Circulation Features of the South American Climate. *Journal of the Atmospheric Sciences*, 54(5):656–678.

Lenz, C.-J., Früh, B., and Adalatpanah, F. D. (2017). Is there potential added value in COSMO–CLM forced by ERA reanalysis data? *Climate Dynamics*, 49(11-12):4061–4074.

Leung, L. R. and Qian, Y. (2003). The Sensitivity of Precipitation and Snowpack Simulations to Model Resolution via Nesting in Regions of Complex Terrain. *Journal of Hydrometeorology*, 4(6):1025–1043.

Liu, S., Xue, M., and Xu, Q. (2007). Using Wavelet Analysis to Detect Tornadoes from Doppler Radar Radial-Velocity Observations. *Journal of Atmospheric and Oceanic Technology*, 24(3):344–359.

Llopart, M., Coppola, E., Giorgi, F., da Rocha, R. P., and Cuadra, S. V. (2014). Climate change impact on precipitation for the Amazon and La Plata basins. *Climatic Change*, 125(1):111–125.

Llopart, M., da Rocha, R. P., Reboita, M., and Cuadra, S. (2017). Sensitivity of simulated South America climate to the land surface schemes in RegCM4. *Climate Dynamics*, pages 1–13.

Lo, J. C.-F., Yang, Z.-L., and Pielke, R. A. (2008). Assessment of three dynamical climate downscaling methods using the Weather Research and Forecasting (WRF) model. *Journal of Geophysical Research*, 113(D9):D09112.

López-Franca, N., Zaninelli, P., Carril, A., Menéndez, C., and Sánchez, E. (2016). Changes in temperature extremes for 21st century scenarios over South America derived from a multi-model ensemble of regional climate models. *Climate Research*, 68(2-3):151–167.

Lorenz, E. N. (1955). Available Potential Energy and the Maintenance of the General Circulation. *Tellus*, 7(2):157–167.

Lorenz, P. and Jacob, D. (2005). Influence of regional scale information on the global circulation: A two-way nesting climate simulation. *Geophysical Research Letters*, 32(18):n/a–n/a.

Lucas-Picher, P., Laprise, R., and Winger, K. (2016). Evidence of added value in North American regional climate model hindcast simulations using ever-increasing horizontal resolutions. *Climate Dynamics*, pages 1–23.

Madonna, E., Wernli, H., Joos, H., and Martius, O. (2014). Warm Conveyor Belts in the ERA-Interim Dataset (1979–2010). Part I: Climatology and Potential Vorticity Evolution. *Journal of Climate*, 27(1):3–26.

Mallat, S. G. (1989). A theory for multiresolution signal decomposition: the wavelet representation. *IEEE Transactions on Pattern Analysis and Machine Intelligence*, 11(7):674–693.

Maraun, D., Wetterhall, F., Ireson, A. M., Chandler, R. E., Kendon, E. J., Widmann, M., Brienen, S., Rust, H. W., Sauter, T., Themeßl, M., Venema, V. K. C., Chun, K. P., Goodess, C. M., Jones, R. G., Onof, C., Vrac, M., and Thiele-Eich, I. (2010). Precipitation downscaling under climate change: Recent developments to bridge the gap between dynamical models and the end user. *Reviews of Geophysics*, 48(3):RG3003.

Marengo, J. a., Ambrizzi, T., da Rocha, R. P., Alves, L. M., Cuadra, S. V., Valverde, M. C., Torres, R. R., Santos, D. C., and Ferraz, S. E. T. (2009). Future change of climate in South America in the late twenty-first century: intercomparison of scenarios from three regional climate models. *Climate Dynamics*, 35(6):1073–1097.

Marengo, J. A., Soares, W. R., Saulo, C., and Nicolini, M. (2004). Climatology of the Low-Level Jet East of the Andes as Derived from the NCEP–NCAR Reanalyses: Characteristics and Temporal Variability. *Journal of Climate*, 17(12):2261–2280.

Meehl, G. A., Covey, C., Taylor, K. E., Delworth, T., Stouffer, R. J., Latif, M., McAvaney, B., Mitchell, J. F. B., Meehl, G. A., Covey, C., Taylor, K. E., Delworth, T., Stouffer, R. J., Latif, M., McAvaney, B., and Mitchell, J. F. B. (2007). THE WCRP CMIP3 Multimodel Dataset: A New Era in Climate Change Research. *Bulletin of the American Meteorological Society*, 88(9):1383–1394.

Mendes, D., Souza, E. P., Trigo, I. F., and Miranda, P. M. A. (2007). On precursors of South American cyclogenesis. *Tellus A: Dynamic Meteorology and Oceanography*, 59(1):114–121.

Menéndez, C., Zaninelli, P., Carril, A., and Sánchez, E. (2016). Hydrological cycle, temperature, and land surface-atmosphere interaction in the La Plata Basin during summer: response to climate change. *Climate Research*, 68(2-3):231–241.

Menéndez, C. G., de Castro, M., Sorensson, A., and Boulanger, J. P. (2010). CLARIS Project: towards climate downscaling in South America. *Meteorologische Zeitschrift*, 19(4):357–362.

Menéndez, C. G., Saulo, A. C., and Li, Z.-X. (2001). Simulation of South American wintertime climate with a nesting system. *Climate Dynamics*, 17(2-3):219–231.

Mishra, S. K., Sahany, S., and Salunke, P. (2017). CMIP5 vs. CORDEX over the Indian region: how much do we benefit from dynamical downscaling? *Theoretical and Applied Climatology*, pages 1–9.

Misra, V., Dirmeyer, P. A., Kirtman, B. P., Juang, H. H., and Kanamitsu, M. (2002). Regional simulation of interannual variability over South America. *Journal of Geophysical Research*, 107(D20):8036.

Mizuta, R., Yoshimura, H., Murakami, H., Matsueda, M., Endo, H., Ose, T., Kamiguchi, K., Hosaka, M., Sugi, M., Yukimoto, S., Kusunoki, S., and Kitoh, A. (2012). Climate Simulations Using MRI-AGCM3.2 with 20-km Grid. *Journal of the Meteorological Society of Japan*, 90A(0):233–258.

Montini, T. and Jones, C. (2017). How well do modern reanalyses simulate the South America Low-Level Jet? ERI Summer Fellowship.

Müller, W. A., Jungclaus, J. H., Mauritsen, T., Baehr, J., Bittner, M., Budich, R., Bunzel, F., Esch, M., Ghosh, R., Haak, H., Ilyina, T., Kleine, T., Kornblueh, L., Li, H., Modali, K., Notz, D., Pohlmann, H., Roeckner, E., Stemmler, I., Tian, F., and Marotzke, J. (2018). A higher-resolution version of the Max Planck Institute Earth System Model (MPI-ESM 1.2-HR). *Journal of Advances in Modeling Earth Systems*.

National Geophysical Data Center (2006). 2-minute Gridded Global Relief Data (ETOPO2) v2.

New, M., Lister, D., Hulme, M., and Makin, I. (2002). A high-resolution data set of surface climate over global land areas. *Climate Research*, 21(1):1–25.

Nikulin, G., Jones, C., Giorgi, F., Asrar, G., Büchner, M., Cerezo-Mota, R., Christensen, O. B., Déqué, M., Fernandez, J., Hänsler, A., van Meijgaard, E., Samuelsson, P., Sylla, M. B., Sushama, L., Nikulin, G., Jones, C., Giorgi, F., Asrar, G., Büchner, M., Cerezo-Mota, R., Christensen, O. B., Déqué, M., Fernandez, J., Hänsler, A., Meijgaard, E. v., Samuelsson, P., Sylla, M. B., and Sushama, L. (2012). Precipitation Climatology in an Ensemble of CORDEX-Africa Regional Climate Simulations. *Journal of Climate*, 25(18):6057–6078.

Nobre, P., Moura, A. D., and Sun, L. (2001). Dynamical Downscaling of Seasonal Climate Prediction over Nordeste Brazil with ECHAM3 and NCEP's Regional Spectral Models at IRI. *Bulletin of the American Meteorological Society*, 82(12):2787–2796.

Nogués-Paegle, J., Mo, K. C., Nogués-Paegle, J., and Mo, K. C. (1997). Alternating Wet and Dry Conditions over South America during Summer. *Monthly Weather Review*, 125(2):279–291.

Panitz, H.-J., Dosio, A., Büchner, M., Lüthi, D., and Keuler, K. (2014). COSMO-CLM (CCLM) climate simulations over CORDEX-Africa domain: analysis of the ERA-Interim driven simulations at 0.44° and 0.22° resolution. *Climate Dynamics*, 42(11-12):3015–3038.

Panthou, G., Vrac, M., Drobinski, P., Bastin, S., and Li, L. (2018). Impact of model resolution and Mediterranean sea coupling on hydrometeorological extremes in RCMs in the frame of HyMeX and MED-CORDEX. *Climate Dynamics*, 51(3):915–932.

Parker, R. J., Reich, B. J., Sain, S. R., Parker, R. J., Reich, B. J., and Sain, S. R. (2015). A Multiresolution Approach to Estimating the Value Added by Regional Climate Models. *Journal of Climate*, 28(22):8873–8887.

Pesquero, J. F., Chou, S. C., Nobre, C. A., and Marengo, J. A. (2009). Climate downscaling over South America for 1961–1970 using the Eta Model. *Theoretical and Applied Climatology*, 99(1-2):75–93.

Pielke, R. A. and Wilby, R. L. (2012). Regional climate downscaling: What's the point? *Eos, Transactions American Geophysical Union*, 93(5):52–53.

Pithan, F., Shepherd, T. G., Zappa, G., and Sandu, I. (2016). Climate model biases in jet streams, blocking and storm tracks resulting from missing orographic drag. *Geophysical Research Letters*, 43(13):7231–7240.

Prein, A. F., Gobiet, A., Truhetz, H., Keuler, K., Goergen, K., Teichmann, C., Fox Maule, C., van Meijgaard, E., Déqué, M., Nikulin, G., Vautard, R., Colette, A., Kjellström, E., and Jacob, D. (2016). Precipitation in the EURO-CORDEX 0.11° and 0.44° simulations: high resolution, high benefits? *Climate Dynamics*, 46(1-2):383–412.

Prein, A. F., Langhans, W., Fosser, G., Ferrone, A., Ban, N., Goergen, K., Keller, M., Tölle, M., Gutjahr, O., Feser, F., Brisson, E., Kollet, S., Schmidli, J., van Lipzig, N. P. M., and Leung, R. (2015). A review on regional convection-permitting climate modeling: Demonstrations, prospects, and challenges. *Reviews of Geophysics*, 53(2):323–361.

Prömmel, K., Geyer, B., Jones, J. M., and Widmann, M. (2010). Evaluation of the skill and added value of a reanalysis-driven regional simulation for Alpine temperature. *International Journal of Climatology*, 30(5):760–773.

Pryor, S. C., Nikulin, G., and Jones, C. (2012). Influence of spatial resolution on regional climate model derived wind climates. *Journal of Geophysical Research: Atmospheres*, 117(D3):n/a–n/a.

Racherla, P. N., Shindell, D. T., and Faluvegi, G. S. (2012). The added value to global model projections of climate change by dynamical downscaling: A case study over the continental U.S. using the GISS-ModelE2 and WRF models. *Journal of Geophysical Research: Atmospheres*, 117(D20):n/a–n/a.

Raj, J., Bangalath, H. K., and Stenchikov, G. (2018). West African Monsoon: current state and future projections in a high-resolution AGCM. *Climate Dynamics*, pages 1–21.

Rauscher, S. A., Coppola, E., Piani, C., and Giorgi, F. (2010). Resolution effects on regional climate model simulations of seasonal precipitation over Europe. *Climate Dynamics*, 35(4):685–711.

Reboita, M., Fernandez, J., Pereira Llopart, M., Porfirio da Rocha, R., Albertani Pampuch, L., and Cruz, F. (2014a). Assessment of RegCM4.3 over the CORDEX South America domain: sensitivity analysis for physical parameterization schemes. *Climate Research*, 60(3):215–234.

Reboita, M. S., Amaro, T. R., and de Souza, M. R. (2018a). Winds: intensity and power density simulated by RegCM4 over South America in present and future climate. *Climate Dynamics*, 51(1-2):187–205.

Reboita, M. S., da Rocha, R. P., Ambrizzi, T., and Sugahara, S. (2010). South Atlantic Ocean cyclogenesis climatology simulated by regional climate model (RegCM3). *Climate Dynamics*, 35(7-8):1331–1347.

Reboita, M. S., da Rocha, R. P., de Souza, M. R., and Llopart, M. (2018b). Extratropical cyclones over the southwestern South Atlantic Ocean: HadGEM2-ES and RegCM4 projections. *International Journal of Climatology*, 38(6):2866–2879.

Reboita, M. S., da Rocha, R. P., Dias, C. G., Ynoue, R. Y., Dias, C., Gabriele, s., and Ynoue, R. Y. (2014b). Climate Projections for South America: RegCM3 Driven by HadCM3 and ECHAM5. *Advances in Meteorology*, 2014:1–17.

Rinke, A., Dethloff, K., Cassano, J. J., Christensen, J. H., Curry, J. A., Du, P., Girard, E., Haugen, J.-E., Jacob, D., Jones, C. G., Køltzow, M., Laprise, R., Lynch, A., Pfeifer, S., Serreze, M. C., Shaw, M. J., Tjernström, M., Wyser, K., and Žagar, M. (2006). Evaluation of an ensemble of Arctic regional climate models: spatiotemporal fields during the SHEBA year. *Climate Dynamics*, 26(5):459–472.

Roads, J., Chen, S., Cocke, S., Druyan, L., Fulakeza, M., LaRow, T., Lonergan, P., Qian, J., and Zebiak, S. (2003). International Research Institute/Applied Research Centers (IRI/ARCs) regional model intercomparison over South America. *Journal of Geophysical Research*, 108(D14):4425.

Rojas, M. (2006). Multiply Nested Regional Climate Simulation for Southern South America: Sensitivity to Model Resolution. *Monthly Weather Review*, 134(8):2208–2223.

Rojas, M. and Seth, A. (2003). Simulation and Sensitivity in a Nested Modeling System for South America. Part II: GCM Boundary Forcing. *Journal of Climate*, 16(15):2454–2471.

Rummukainen, M. (2016). Added value in regional climate modeling. *Wiley Interdisciplinary Reviews: Climate Change*, 7(1):145–159.

Rusticucci, M., Marengo, J., Penalba, O., and Renom, M. (2010). An intercomparison of model-simulated in extreme rainfall and temperature events during the last half of the twentieth century. Part 1: mean values and variability. *Climatic Change*, 98(3-4):493–508.

Sakaguchi, K., Leung, L. R., Zhao, C., Yang, Q., Lu, J., Hagos, S., Rauscher, S. A., Dong, L., Ringler, T. D., and Lauritzen, P. H. (2015). Exploring a Multiresolution Approach Using AMIP Simulations. *Journal of Climate*, 28(14):5549–5574.

Sakaguchi, K., Lu, J., Leung, L. R., Zhao, C., Li, Y., and Hagos, S. (2016). Sources and pathways of the upscale effects on the Southern Hemisphere jet in MPAS-CAM4 variable-resolution simulations. *Journal of Advances in Modeling Earth Systems*, 8(4):1786–1805.

Sakradzija, M., Seifert, A., and Dipankar, A. (2016). A stochastic scale-aware parameterization of shallow cumulus convection across the convective gray zone. *Journal of Advances in Modeling Earth Systems*, 8(2):786–812.

Salio, P., Nicolini, M., and Saulo, A. C. (2002). Chaco low-level jet events characterization during the austral summer season. *Journal of Geophysical Research*, 107(D24):4816.

Salio, P., Nicolini, M., and Zipser, E. J. (2007). Mesoscale Convective Systems over Southeastern South America and Their Relationship with the South American Low-Level Jet. *Monthly Weather Review*, 135(4):1290–1309.

Sanabria, A. L. and Carril, A. F. (2018). Maps of wind hazard over South Eastern South America considering climate change. *Climatic Change*, pages 1–13.

Sánchez, E., Solman, S., Remedio, A. R. C., Berbery, H., Samuelsson, P., Da Rocha, R. P., Mourão, C., Li, L., Marengo, J., de Castro, M., and Jacob, D. (2015). Regional climate modelling in CLARIS-LPB: a concerted approach towards twentyfirst century projections of regional temperature and precipitation over South America. *Climate Dynamics*, 45(7-8):2193–2212.

Scheel, M. L. M., Rohrer, M., Huggel, C., Santos Villar, D., Silvestre, E., and Huffman, G. J. (2011). Evaluation of TRMM Multi-satellite Precipitation Analysis (TMPA) performance in the Central Andes region and its dependency on spatial and temporal resolution. *Hydrology and Earth System Sciences*, 15(8):2649–2663.

Seluchi, M. E. and Marengo, J. A. (2000a). Tropical – Midlatitude exchange of air masses during summer and winter in South America: Climatic aspects and examples of intense events. *INTERNATIONAL JOURNAL OF CLIMATOLOGY Int . J . Climatol*, 20:1167–1190.

Seluchi, M. E. and Marengo, J. A. (2000b). TROPICAL – MIDLATITUDE EXCHANGE OF AIR MASSES DURING SUMMER AND WINTER IN SOUTH AMERICA: CLIMATIC ASPECTS AND EXAMPLES OF INTENSE EVENTS. *INTERNATIONAL JOURNAL OF CLIMATOLOGY Int. J. Climatol*, 20:1167–1190.

Seth, A., Rauscher, S. a., Camargo, S. J., Qian, J.-H., and Pal, J. S. (2007). RegCM3 regional climatologies for South America using reanalysis and ECHAM global model driving fields. *Climate Dynamics*, 28(5):461–480.

Seth, A. and Rojas, M. (2003). Simulation and Sensitivity in a Nested Modeling System for South America. Part I: Reanalyses Boundary Forcing. *Journal of Climate*, 16(15):2437–2453.

Shaffrey, L. C., Stevens, I., Norton, W. A., Roberts, M. J., Vidale, P. L., Harle, J. D., Jrrar, A., Stevens, D. P., Woodage, M. J., Demory, M. E., Donners, J., Clark, D. B., Clayton, A., Cole, J. W., Wilson, S. S., Connolley, W. M., Davies, T. M., Iwi, A. M., Johns, T. C., King, J. C., New, A. L., Slingo, J. M., Slingo, A., Steenman-Clark, L., and Martin, G. M. (2009). U.K. HiGEM: The New U.K. High-Resolution Global Environment Model—Model Description and Basic Evaluation. *Journal of Climate*, 22(8):1861–1896.

Shapiro, R., Force, A., and Field, L. G. H. (1970). Smoothing, filtering, and boundary effects. *Reviews of Geophysics*, 8(2):359.

Shaw, T. A., Baldwin, M., Barnes, E. A., Caballero, R., Garfinkel, C. I., Hwang, Y.-T., Li, C., O'Gorman, P. A., Rivière, G., Simpson, I. R., and Voigt, A. (2016). Storm track processes and the opposing influences of climate change. *Nature Geoscience*, 9(9):656–664.

Shi, Y., Wang, G., and Gao, X. (2018). Role of resolution in regional climate change projections over China. *Climate Dynamics*, 51(5-6):2375–2396.

Shuman, F. G. (1957). Numerical methods in weather prediction: II. Smoothing and filtering. *Monthly Weather Review*, 85(11):357–361.

Sifuzzaman, M., Islam, M. R., and Ali, M. Z. (2009). Application of Wavelet Transform and its Advantages Compared to Fourier Transform. *Journal of Physical Science*, 13:121–134.

Silvestri, G. and Vera, C. (2008). Evaluation of the WCRP-CMIP3 model simulations in the La Plata basin. *Meteorological Applications*, 15(4):497–502.

Sinclair, M. R. (1995). A Climatology of Cyclogenesis for the Southern Hemisphere. *Monthly Weather Review*, 123(6):1601–1619.

Singh, S., Ghosh, S., Sahana, A. S., Vittal, H., and Karmakar, S. (2016). Do dynamic regional models add value to the global model projections of Indian monsoon? *Climate Dynamics*, pages 1–23.

Sinha, P., Mohanty, U. C., Kar, S. C., Dash, S. K., and Kumari, S. (2013). Sensitivity of the GCM driven summer monsoon simulations to cumulus parameterization schemes in nested RegCM3. *Theoretical and Applied Climatology*, 112(1-2):285–306.

Skamarock, W. C. (2004). Evaluating Mesoscale NWP Models Using Kinetic Energy Spectra. *Monthly Weather Review*, 132(12):3019–3032.

Skamarock, W. C., Klemp, J. B., Dudhia, J., Gill, D. O., Barker, D. M., Wang, W., and Powers, J. G. (2005). A Description of the Advanced Research WRF Version 2.

Solman, S. A. (2016). Systematic temperature and precipitation biases in the CLARIS-LPB ensemble simulations over South America and possible implications for climate projections. *Climate Research*, 68(2-3):117–136.

Solman, S. A., Nuñez, M. N., and Cabré, M. F. (2008). Regional climate change experiments over southern South America. I: present climate. *Climate Dynamics*, 30(5):533–552.

Solman, S. A. and Pessacg, N. L. (2012). Regional climate simulations over South America: sensitivity to model physics and to the treatment of lateral boundary conditions using the MM5 model. *Climate Dynamics*, 38(1-2):281–300.

Solman, S. A., Sanchez, E., Samuelsson, P., da Rocha, R. P., Li, L., Marengo, J., Pessacg, N. L., Remedio, A. R. C., Chou, S. C., Berbery, H., Le Treut, H., de Castro, M., and Jacob, D. (2013). Evaluation of an ensemble of regional climate model simulations over South America driven by the ERA-Interim reanalysis: model performance and uncertainties. *Climate Dynamics*, 41(5-6):1139–1157.

Sörensson, A. A. and Menéndez, C. G. (2011). Summer soil-precipitation coupling in South America. *Tellus A*, 63(1):56–68.

Sörensson, A. A., Menéndez, C. G., Samuelsson, P., Willén, U., and Hansson, U. (2010). Soil-precipitation feedbacks during the South American Monsoon as simulated by a regional climate model. *Climatic Change*, 98(3-4):429–447.

Sørland, S. L., Schär, C., Lüthi, D., and Kjellström, E. (2018). Bias patterns and climate change signals in GCM-RCM model chains. *Environmental Research Letters*, 13(7):074017.

Stevens, B., Giorgetta, M., Esch, M., Mauritsen, T., Crueger, T., Rast, S., Salzmann, M., Schmidt, H., Bader, J. J., Block, K., Brokopf, R., Fast, I., Kinne, S., Kornblueh, L., Lohmann, U., Pincus, R., Reichler, T., and Roeckner, E. (2013). Atmospheric component of the MPI-M Earth System Model: ECHAM6. *Journal of Advances in Modeling Earth Systems*, 5(2):146–172.

Stirling, A. and Lock, S.-J. (2017). What have we learnt about the Grey Zone over the past decade? Technical report.

Su, F., Hong, Y., and Lettenmaier, D. P. (2008). Evaluation of TRMM Multisatellite Precipitation Analysis (TMPA) and Its Utility in Hydrologic Prediction in the La Plata Basin. *Journal of Hydrometeorology*, 9(4):622–640.

Taylor, K. E. (2001). Summarizing multiple aspects of model performance in a single diagram. *Journal of Geophysical Research: Atmospheres*, 106(D7):7183–7192.

Tian, B., Lee, H., Waliser, D. E., Ferraro, R., Kim, J., Case, J., Iguchi, T., Kemp, E., Wu, D., Putman, W., and Wang, W. (2017). Development of a Model Performance Metric and Its Application to Assess Summer Precipitation over the U.S. Great Plains in Downscaled Climate Simulations. *Journal of Hydrometeorology*, 18(10):2781–2799.

Torma, C., Giorgi, F., and Coppola, E. (2015). Added value of regional climate modeling over areas characterized by complex terrain-Precipitation over the Alps. *Journal of Geophysical Research: Atmospheres*, 120(9):3957–3972.

Trenberth, K. E. (1986). An Assessment of the Impact of Transient Eddies on the Zonal Flow during a Blocking Episode Using Localized Eliassen-Palm Flux Diagnostics. *Journal of the Atmospheric Sciences*, 43(19):2070–2087.

Trenberth, K. E. (1991). Storm Tracks in the Southern Hemisphere. *Journal of the Atmospheric Sciences*, 48(19):2159–2178.

Trenberth, K. E. and Stepaniak, D. P. (2003). Seamless Poleward Atmospheric Energy Transports and Implications for the Hadley Circulation. *Journal of Climate*, 16(22):3706–3722.

van Roosmalen, L., Christensen, J. H., Butts, M. B., Jensen, K. H., and Refsgaard, J. C. (2010). An inter-comparison of regional climate model data for hydrological impact studies in Denmark. *Journal of Hydrology*, 380(3-4):406–419.

Velasco, I. and Fritsch, J. M. (1987). Mesoscale convective complexes in the Americas. *Journal of Geophysical Research*, 92(D8):9591.

Veljovic, K., Rajkovic, B., Fennessy, M. J., Altshuler, E. L., and Mesinger, F. (2010). Regional climate modeling: Should one attempt improving on the large scales? Lateral boundary condition scheme: Any impact? *Meteorologische Zeitschrift*, 19(3):237–246.

Vera, C. (2018). Farmers transformed how we investigate climate. *Nature*, 562(7725):9–9.

Vera, C., Baez, J., Douglas, M., Emmanuel, C. B., Marengo, J., Meitin, J., Nicolini, M., Nogues-Paegle, J., Paegle, J., Penalba, O., Salio, P., Saulo, C., Silva Dias, M. A., Silva Dias, P., Zipser, E., Vera, C., Baez, J., Douglas, M., Emmanuel, C. B., Marengo, J., Meitin, J., Nicolini, M., Nogues-Paegle, J., Paegle, J., Penalba, O., Salio, P., Saulo, C., Dias, M. A. S., Dias, P. S., and Zipser, E. (2006a). The South American Low-Level Jet Experiment. *Bulletin of the American Meteorological Society*, 87(1):63–77.

Vera, C., Higgins, W., Amador, J., Ambrizzi, T., Garreaud, R., Gochis, D., Gutzler, D., Lettenmaier, D., Marengo, J., Mechoso, C. R., Nogues-Paegle, J., Dias, P. L. S., Zhang, C., Vera, C., Higgins, W., Amador, J., Ambrizzi, T., Garreaud, R., Gochis, D., Gutzler, D., Lettenmaier, D., Marengo, J., Mechoso, C. R., Nogues-Paegle, J., Dias, P. L. S., and Zhang, C. (2006b). Toward a Unified View of the American Monsoon Systems. *Journal of Climate*, 19(20):4977–5000.

Vernekar, A. D., Kirtman, B. P., Fennessy, M. J., Vernekar, A. D., Kirtman, B. P., and Fennessy, M. J. (2003). Low-Level Jets and Their Effects on the South American Summer Climate as Simulated by the NCEP Eta Model*. *Journal of Climate*, 16(2):297–311.

Walther, A., Jeong, J.-H., Nikulin, G., Jones, C., and Chen, D. (2013). Evaluation of the warm season diurnal cycle of precipitation over Sweden simulated by the Rossby Centre regional climate model RCA3. *Atmospheric Research*, 119:131–139.

Wang, B. and Ding, Q. (2006). Changes in global monsoon precipitation over the past 56 years. *Geophysical Research Letters*, 33(6):L06711.

Wang, B. and Ding, Q. (2008). Global monsoon: Dominant mode of annual variation in the tropics. *Dynamics of Atmospheres and Oceans*, 44(3-4):165–183.

Wang, J., Swati, F. N. U., Stein, M. L., and Kotamarthi, V. R. (2015). Model performance in spatiotemporal patterns of precipitation: New methods for identifying value added by a regional climate model. *Journal of Geophysical Research: Atmospheres*, 120(4):1239–1259.

Wilcox, L. J., Charlton-Perez, A. J., and Gray, L. J. (2012). Trends in Austral jet position in ensembles of high- and low-top CMIP5 models. *Journal of Geophysical Research: Atmospheres*, 117(D13):n/a–n/a.

Xie, P., Chen, M., and Shi, W. (2010). CPC unified gauge-based analysis of global daily precipitation. *American Meteorological Society*.

Yang, H., Jiang, Z., and Li, L. (2016). Biases and improvements in three dynamical downscaling climate simulations over China. *Climate Dynamics*, pages 1–17.

Yano, J.-I., Moncrieff, M. W., Wu, X., and Yamada, M. (2001). Wavelet Analysis of Simulated Tropical Convective Cloud Systems. Part I: Basic Analysis. *Journal of the Atmospheric Sciences*, 58(8):850–867.

Zaninelli, P. G., Carril, A. F., and Menéndez, C. G. (2015). Explorando temperaturas máximas y mínimas en diferentes reanálisis. Parte 1: campos medios estacionales. *Meteorologica*, 40(1):43–58.

Zaninelli, P. G., Menéndez, C. G., Falco, M., López-Franca, N., and Carril, A. F. (2018). Future hydroclimatological changes in South America based on an ensemble of regional climate models. *Climate Dynamics*.

Zappa, G., Shaffrey, L. C., Hodges, K. I., Sansom, P. G., and Stephenson, D. B. (2013). A Multimodel Assessment of Future Projections of North Atlantic and European Extratropical Cyclones in the CMIP5 Climate Models. *Journal of Climate*, 26(16):5846–5862.

Zazulie, N., Rusticucci, M., and Raga, G. B. (2017). Regional climate of the subtropical central Andes using high-resolution CMIP5 models—part I: past performance (1980-2005). *Climate Dynamics*, 49(11-12):3937–3957.

Zhou, J., Lau, K.-M., Zhou, J., and Lau, K.-M. (1998). Does a Monsoon Climate Exist over South America? *Journal of Climate*, 11(5):1020–1040.

Zhou, T. and Li, L. (2002). Simulation of the east asian summer monsoon using a variable resolution atmospheric GCM. *Climate Dynamics*, 19(2):167–180.